A MICROSTRUCTURAL KINEMATIC STUDY OF SELECTED SHEAR ZONES IN THE HARTBEES RIVER THRUST BELT, NORTHEASTERN NAMAQUA TECTONIC PROVINCE

Thesis submitted in fulfilment of the
requirements for the Degree of
MASTER OF SCIENCE
of Rhodes University,
Grahamstown

by

Christopher Jackson

November 1992

Abstract

The Hartbees River Thrust Belt (HRTB) is a 40-60 km wide, southwest-vergent zone of complex structure, lithostratigraphy and high-grade metamorphism in the northeastern part of the mid-Proterozoic Namaqua Tectonic Province. The HRTB comprises the boundary zone separating the Bushmanland and Gordonia Subprovinces of the Namaqua Province. A knowledge of the movement histories of major ductile shear zones within the HRTB is fundamental to understanding the tectonic development of the belt, and Namaqua tectogenesis as a whole. In spite of this, no detailed microstructural kinematic studies have been attempted and the movement histories and age relationships of these shear zones have not been described in detail.

This thesis represents a detailed microstructural kinematic study of a representative suite of orientated samples of mylonitic rocks, collected from five ductile shear zones within the HRTB. These shear zones include the Neusspruit Lineament, the Kakamas shear zone (KSZ), the Hugosput shear system (HSS), the Rozynenbosch-Ganzenmond shear zone (RGSZ) and the Graafwater shear system (GSS). Accepted modern methods of microstructural kinematic analysis were applied to samples of mylonite from these shear zones, in order to determine the precise orientation of the kinematic vectors, and the sense and relative ages of movements on each of the shear zones.

Shear sense criteria, including composite S-C planar fabrics and shear band foliations, asymmetrical porphyroclast systems, mica-fish, oblique grain-shape and subgrain fabrics, asymmetrical microfolds, and the displacement of fractured rigid grains, together with a well-developed mylonite elongation lineation, conclusively indicate that SSW-directed thrusting occurred along the HSS, RGSZ, GSS and possibly along the Neusspruit Lineament, while normal, top-to-NE movements occurred on the Neusspruit Lineament, KSZ and HSS. Rare transposition criteria, and textural and paragenetic contrasts between syn-kinematic fabrics, strongly suggest that the phase of normal, top-to-NE movement seen in the northeastern HRTB shear zones is younger than the more widespread top-to-SW thrusting event.

On the basis of mesoscopic structural criteria, SSW-directed thrusting is correlated with the D_2 deformation event in the HRTB. The mylonite zones have been refolded by ENE-SSW trending F_3 crossfolds, whose demonstrated coaxial relationship to the mylonite elongation lineation precluded reorientation of primary kinematic vectors. In the southwestern HRTB, primary thrust vectors have been reoriented by right-lateral, strike-slip shearing adjacent to the Pofadder Lineament during D_4. Simple shear dispersion of mylonite lineations related to normal movement, suggests that they too have been modified by D_4 shearing, and this constrains the timing of extensional movements to post-D_2 and pre- or syn-D_4.

Syn-kinematic mineral assemblages, rheological criteria and the annealing states of the mylonites, provide insight into the thermotectonic evolution of the shear zones. A model is proposed in which the movement histories of shear zones within the HRTB are explained in terms of a typical orogenic cycle, involving crustal thickening by thrusting during a compressional orogenic phase, followed by collapse of the thickened crust during an extensional taphrogenic phase.

Table of Contents

Abstract

Table of Contents I

List of Figures VI

List of Mineral Abbreviations VII

Acknowledgements VIII

Chapter 1. - Introduction 1

1.1 Background to study 1

1.2 Regional geological setting 2

1.2.1 The Bushmanland Subprovince 2

1.2.2 The Gordonia Subprovince 4

1.3 The study area 5

1.3.1 Lithostratigraphy 8

1.3.1.1 Pretectonic units 8

1.3.1.2 Syntectonic intrusive units 8

1.3.2 Structural synthesis 11

1.3.2.1 D_1 regional fabric forming event 11

1.3.2.2 D_2 folding and ductile shearing event 11

1.3.2.3 D_3 crossfolding event 12

1.3.2.4 D_4 transpressive event 13

1.3.3 Metamorphism 14

1.3.3.1 Granulite facies event 14

1.3.3.2 Amphibolite facies retrograde event 15

1.3.3.3 Granulite facies thermal event 16

1.3.3.4 Greenschist facies retrogression 16

1.4 Scope of the project 16

1.4.1 Motivation 17

1.4.2 Review of kinematic models for shear zones of the HRTB 17

1.4.2.1 The Neusspruit Lineament 17

1.4.2.2 The Kakamas shear zone 20

1.4.2.3 Shear zones of the southern HRTB 20

1.4.3 Aims of the project 23

Chapter 2. - Mylonites: Tectonic settings, terminology and methods of microstructural kinematic analysis 24

2.1 Ductile shear zones and mylonites 24

2.2 Tectonic settings of mylonitic rocks 24

2.3 Deformation mechanisms in crustal fault zones 26

2.4 Historical review of fault-rock classification 27

2.5 Microstructural kinematic analysis of ductile shear zones 31

2.5.1 Determination of displacement vectors and movement sense 31

2.5.1.1 Elongation lineations and the kinematic vector 31

2.5.2 Microstructural shear sense indicators 34

2.5.2.1 Asymmetrical porphyroclast systems and rolling structures 35

2.5.2.2 Pressure shadows 38

2.5.2.3 Spiralled inclusion fabrics 38

2.5.2.4 S-C composite planar fabrics and shear band foliations 39

2.5.2.5 Mica fish 42

2.5.2.6 Grain-shape and subgrain-shape fabrics 43

2.5.2.7 Asymmetrical microfolds 44

2.5.2.8 Displacement of fractured rigid grains 45

2.5.2.9 Crystallographic fabric asymmetry 46

2.6 Methods of microstructural kinematic analysis employed in this study 47

2.6.1 Selection of shear zones for analysis 47

2.6.2 Sample collection 47

2.6.3 Sample preparation 48

2.6.4 Movement sense determination 51

2.6.5 Confidence-index for microstructural kinematic interpretations 51

2.6.6 Calculation of kinematic vector means and the mean mylonite plane 52

2.6.7 Definition of the dip-slip to strike-slip ratio 53

2.6.8 Note on terrane nomenclature used in this study 53

Chapter 3. - The Neusspruit Lineament 54

3.1 Mesostructure 54

3.1.1 Neuspoort locality 54

3.1.1.1 Late extensional shear bands 56

3.1.2 Sonopeiland locality 57

3.2 Microstructure 58

3.2.1 Mylonitic feldspathic quartzite 58

3.2.1.1 Asymmetrical microstructures 59

3.2.1.2 Fry centre-to-centre fabric analysis 59

3.2.2 Quartz-feldspar mylonite gneiss 63

3.2.3 Biotite augen gneiss 64

3.2.4 Mylonitic amphibolite gneiss 64
3.2.5 Calc-silicate orthomylonite 65
3.2.5.1 R_f/ϕ fabric analysis 66
3.2.6 Retrograde rocks 69
3.3 Kinematic synthesis 69
3.3.1 P-T conditions of mylonitization 70
3.4 Discussion 71

Chapter 4. - The Kakamas Shear Zone 72
4.1 Mesostructure 72
4.1.1 Mesoscopic fabric elements 72
4.1.2 Brittle fault zone 73
4.2 Microstructure 74
4.2.1 Quartz-feldspar mylonite gneiss 74
4.2.2 Biotite augen gneiss (L>S tectonite) 76
4.2.3 Cataclasite 80
4.3 Kinematic synthesis 80
4.3.1 Estimation of the P-T conditions during transcurrent shearing 82
4.3.2 Implications of strain/stress induced myrmekite and sillimanite 83
4.4 Discussion 84

Chapter 5. - The Hugosput Shear System 86
5.1 Macrostructure 86
5.2 Mesostructure 88
5.2.1 Northern area 88
5.2.2 Central area 88
5.2.3 Southern area 89
5.3 Characteristic microstructures in mylonites from the HSS 89
5.3.1 Orthomylonites 90
5.3.2 Ultramylonites 91
5.3.3 K-feldspar-cordierite-quartz protomylonite 93
5.3.4 Asymmetrical microstructures 93
5.3.4.1 Northern area 93
5.3.4.2 Central area 94
5.3.4.3 Southern area 95
5.4 Kinematic synthesis 106
5.4.1 P-T conditions during mylonitization 107

Chapter 6. - The Rozynenbosch-Ganzenmond and Witvlei Shear Zones 109
6.1 Macrostructure 109
6.2 Sample localities 109
6.3 Mesostructure 111
6.3.1 Mylonite zones 111
6.3.1.1 Mylonite fabric elements 111
6.3.2 Sheath folds 113
6.3.3 Cataclastic zones 113
6.4 Microstructure 114
6.4.1 Rozynenbosch-Ganzenmond shear zone mylonitic microfabrics 114
6.4.2 Witvlei shear zone ultramylonitic microfabrics 115
6.4.3 Rozynenbosch-Ganzenmond shear zone cataclastic microstructures 115
6.5 Kinematic synthesis 124
6.5.1 Characterization of physical conditions and timing of deformation 124
6.6 Discussion 126

Chapter 7. - The Graafwater Shear System 127
7.1 Macrostructure 127
7.2 Sample localities 127
7.3 Mesostructure 129
7.3.1 Mylonite zones and mylonite fabric elements 129
7.3.1.1 Orientation of S_M fabrics 130
7.3.1.2 Orientation of L_M fabrics 131
7.3.2 Demonstration of folding of the mylonite zones 131
7.3.3 Demonstration of coaxiality of F_3 and L_M 131
7.4 Microstructure 133
7.4.1 Mylonitic microfabrics and microstructures 133
7.5 Kinematic synthesis 150
7.5.1 Modification of primary thrust vectors within the GSS 150
7.5.2 Characterization of the physical conditions of mylonitization 151
7.5.2.1 Rheological constraints 151
7.5.2.2 Paragenetic indicators 153
7.6 Discussion 153

Chapter 8. Discussion and conclusions 154
8.1 Discussion 1541
8.1.1 Overview 154
8.1.2 Dip-slip movements within the HRTB 154
8.1.2.1 Relative timing of dip-slip movements 155
8.1.3 Regional synopsis 157

8.1.3.1 Distribution and extent of extensional, top-to-NE shearing 159
8.1.3.2 Evidence for inversion tectonics 159
8.1.3.3 Spatial and temporal distribution of syn- to post-tectonic granitoids 160
8.1.3.4 Regional heterogeneity of thrusting trajectories 161
8.1.3.5 Relative orientation / evolution of L_M and S_M fabrics 163
8.1.4 Thermotectonic constraints on the evolution of the HRTB 167
8.1.4.1 Syn-kinematic parageneses 167
8.1.4.2 Rheological constraints 169
8.1.4.3 Degree of annealing 169
8.1.4.4 Strain regime 171
8.1.4.5 Implications of a metamorphic study in the northeastern HRTB 172
8.1.4.6 The significance of cataclastic rocks in the HRTB 173
8.2 Conclusion 1746
8.2.1 Kinematic model for the evolution of shear zones within the HRTB 174
8.2.2 Synopsis 178

References 180

Appendix i
Table 1: Neusspruit Lineament - microstructural summary ii
Table 2: Kakamas shear zone - microstructural summary iv
Table 3: Hugosput shear system - microstructural summary v
Table 4: Rozynenbosch-Ganzenmond shear zone - microstructural summary ix
Table 5: Graafwater shear system - microstructural summary ii

List of Figures

1. Tectonic subdivisions of the Namaqua Tectonic Province 3
2. Principal shear zones of the Hartbees River Thrust Belt 6
2B. Key to map areas of this investigation 7
3. Lithotectonic subdivisions of the southern Hartbees River Thrust Belt 9
4. Fault rock classification 28
5a. Asymmetrical porphyroclast systems 36
5b. S-C fabrics and shear band foliations 40
5c. Reverse and normal shear band crenulations 42
5d. Mica fish 43
5e. Oblique grain-shape and subgrain fabrics 43
5f. Asymmetrical microfolds 45
5g. Displacement of fractured rigid grains 46
6. Collection, sectioning and presentation of fabric data from orientated specimens 50
7. Kinematic synopsis of data from the Neusspruit Lineament and Kakamas Shear Zone . 55
8. Extensional shear bands, Neusspruit Lineament 56
9. Fry plot of quartz grains within mylonitic quartzite, Neuspoort, Neusspruit Lineament . 62
10. Sketches of selected kinematic indicators within Neusspruit Lineament tectonites 65
11. 2-D R_f/ϕ plots of deformed Grt-nodules from calc-silicate orthomylonite, Sonopeiland 68
12. Sketches of selected kinematic indicators within KSZ tectonites 76
13. Textural relationships and mineral equilibria within migmatitic augen gneisses, KSZ ... 78
14. Kinematic synoptic map of the HSS 87
15. Stereograms of L_M and S_M fabric data from the northern, central and southern HSS .. 88
16. Sketches of selected kinematic indicators within HSS mylonites 96
17. Photomicrographs of selected kinematic indicators within HSS mylonites 102
18. Photomicrographs of high-temperature microstructures within HSS tectonites 104
19. Kinematic synopsis of pooled microstructural and fabric data for HSS sample set 106
20. Kinematic synoptic maps of the RGSZ and WSZ 110
21. Stereogram of all RGSZ/WSZ L_M-S_M fabric data 112
22. Sketches of selected kinematic indicators within RGSZ and WSZ mylonites 117
23. Photomicrographs of selected kinematic indicators within RGSZ and WSZ mylonites 120
24. Kinematic synoptic map of GSS 128
25. Sketch illustrating penetrative L>S fabric development in banded biotite gneiss, GSS 130
26. Stereograms demonstrating F_3 folding of the GSS mylonite zones, and coaxiality of F_3 fold axes and L_M lineations 132
27. Sketches of selected kinematic indicators within GSS mylonites 138
28. Photomicrographs of selected kinematic indicators within GSS mylonites 146

29. Stereogram of all GSS L_M-S_M fabric data 151
30. Kinematic synoptic map of the HRTB 158
31. Triangular diagram illustrating relative orientation / evolution of L_M and S_M fabrics... 163
32. Diagram illustrating coaxial F_3 crossfolding of mylonite zones 165
33. Stereograms of reverse, normal and strike-slip mylonite elongation lineations 166
34. Schematic cross-sections illustrating a model for the development of the NE Namaqua Province 176

List of Mineral Abbreviations

And - andalusite
Ab - albite
Bt - biotite
Chl - chlorite
Crd - cordierite
Cte - calcite
Di - diopside
Ep - epidote
Fsp - feldspar
Grt - garnet
Hbl - hornblende
Kfs - K-feldspar
Lpd - lepidolite
Mc - microcline
Ms - muscovite
Mt - magnetite
Opx - orthopyroxene
Pl - plagioclase
Qtz - quartz
Sil - sillimanite
Sph - sphene
Spl - spinel
St - staurolite

Acknowledgements

Only through the selfless contribution of many people has this thesis been made possible and I wish to acknowledge my sincere appreciation for their guidance, support, understanding and patience. Special thanks go to Dr Rob Harris, who initially as a lecturer at U.C.T., then as an employer in the Precambrian Research Unit, and finally as a supervisor at Rhodes, contributed enormously to my development as a structural geologist. I thank him for his inspiration, encouragement and guidance through many difficult periods. Likewise, I have received considerable support, understanding and encouragement from Professor Roger Jacob, who, against all odds, revived my flagging motivation time-and-time again. Moreover, I thank him for much constructive criticism in his role as co-supervisor, and for arranging important financial assistance during a period of insolvency.

Thanks go to Professors John Moore, Julian Marsh and Hugh Eales, Drs Mark Von Veh, Johan Krynauw, Wolfgang Maier and Berndt Teigler, and Messrs Clyde Mallinson, Bruce Groenewald and Johan Steifenhofer for their encouragement and assistance in various ways. I thank my colleagues in the Antarctic Research Programme for their patience and empathy throughout the last year. I am extremely grateful to Lauren Friedrichs and Olive Anderson for their invaluable assistance with the drafting of some of the figures in this thesis (an unenviable task!). I thank Mrs Colleen Davies for her (intermittent) patience and adroit management of bureaucracy and bureaucrats.

I am disinclined to acknowledge exact gratitude to various unsavoury acquaintances, whose questionable contribution to this thesis may be measured in pints. I will not be specific, they know who they are! Finally, special thanks go to Joanne, who has been as much a victim of this thesis as I have. Without her patience, loyalty and support, I doubt whether this thesis could have been accomplished.

Chapter 1. - Introduction

1.1 Background to study

This thesis documents a detailed microstructural kinematic study of mylonitic and protomylonitic rocks from selected ductile shear zones in the northeastern segment of the Namaqua Tectonic Province. The shear zones under investigation occur principally between the towns of Kakamas and Kenhardt in the northern Cape Province, and represent tectonic discontinuities within the Hartbees River Thrust Belt (Harris, 1987, 1992), a 40 to 60 km wide zone marking the boundary between the Bushmanland and Gordonia subprovinces (Hartnady *et al.*, 1985).

Despite the fundamental importance of these shear zones to the tectonic evolution of the thrust belt and the Namaqua Province as a whole, their movement histories and relative ages remain poorly characterized. Categorization of the mylonite zones as reverse, normal, oblique or strike-slip shears is essential for kinematic reconstruction, and may only be achieved through the determination of the exact direction and sense of movement on the zones. Recent kinematic studies overseas have emphasized the potential of mylonite microstructures and microfabrics in constraining the movement histories of shear zones. In spite of this, the methods of microstructural kinematic analysis have been largely neglected in research into Namaqua tectogenesis. The aim of this project is to establish the exact nature of tectonic movements on selected shear zones of the Hartbees River Thrust Belt by means of detailed microstructural investigations.

Fieldwork was carried out in August 1989 and June 1990, and involved the collection of a representative suite of orientated samples of mylonite and protomylonite from 24 localities, on selected shear zones across the thrust belt. Measurements of the orientations of local mesoscopic mylonite fabrics were taken in the field to enable determination of the geometric relationships between these fabrics and internal microstructures. Microstructural fabric analyses and shear sense determinations were performed petrographically in order to establish the exact nature of tectonic movements on the shear zones. Based on the results of the microstructural kinematic analyses, reconstruction of the bulk movement history of shear zones within the Hartbees River Thrust Belt was undertaken.

1.2 Regional geological setting

The 1.3-1.0 Ga Namaqua Tectonic Province is an approximately 400km-wide belt of high-grade paragneiss, granulite, and granitoid rocks extending eastwards from the Atlantic coast for approximately 2000km around the southern margin of the Archaean-age Kaapvaal Craton, to Natal. The Province has been subdivided into the Richtersveld, Bushmanland and Gordonia Subprovinces in the west, and the Natal Subprovince in the east (Hartnady *et al.*, 1985). This thesis focusses on structures within the Bushmanland and Gordonia Subprovinces (Fig. 1), and in particular on the transitional zone separating these two Subprovinces i.e. the Hartbees River Thrust Belt (hereafter referred to as the HRTB) (Fig. 2). Separation of the two Subprovinces has in the past been proposed on the basis of their differing regional structural trends (Hartnady *et al.*, 1985). The Gordonia Subprovince has marked northwesterly regional structural trends in contrast to the generally east-west trends of Bushmanland. The nature of the tectonic boundary between the two Subprovinces has only recently been more clearly defined following regional mapping of the HRTB by Harris during 1983 to 1984. The exact boundary between the Bushmanland Subprovince and the Gordonia Subprovince has not been precisely defined, although the *Neusspruit Lineament* (Van Bever Donker, 1980, 1983; Stowe, 1988), the *Kakamas Shear Zone* (Joubert, 1978, 1986; Hartnady *et al.*, 1985, Stowe, 1986) and the *lowermost shear zone of the Hartbees River Thrust Belt* (Hartnady *et al.*, 1985; Joubert, 1986; Stowe, 1986) have all been targeted as potential geosutures (Fig. 2).

1.2.1 The Bushmanland Subprovince

The 1.7-1.0 Ga Bushmanland Subprovince comprises various high-grade, multiply-deformed para- and orthogneisses, charnockite and granitoids (Hartnady *et al.*, 1985). The subprovince is currently subdivided into the *Okiep Terrane* in the northwest, and the *Garies Terrane* in the southeast (Fig. 1) (Hartnady *et al.*, 1985). Only the easternmost portion of the *Garies Terrane* falls within the study area (Fig. 2), and is characterized by ENE-trending, dome and basin interference structures (Harris, 1988).

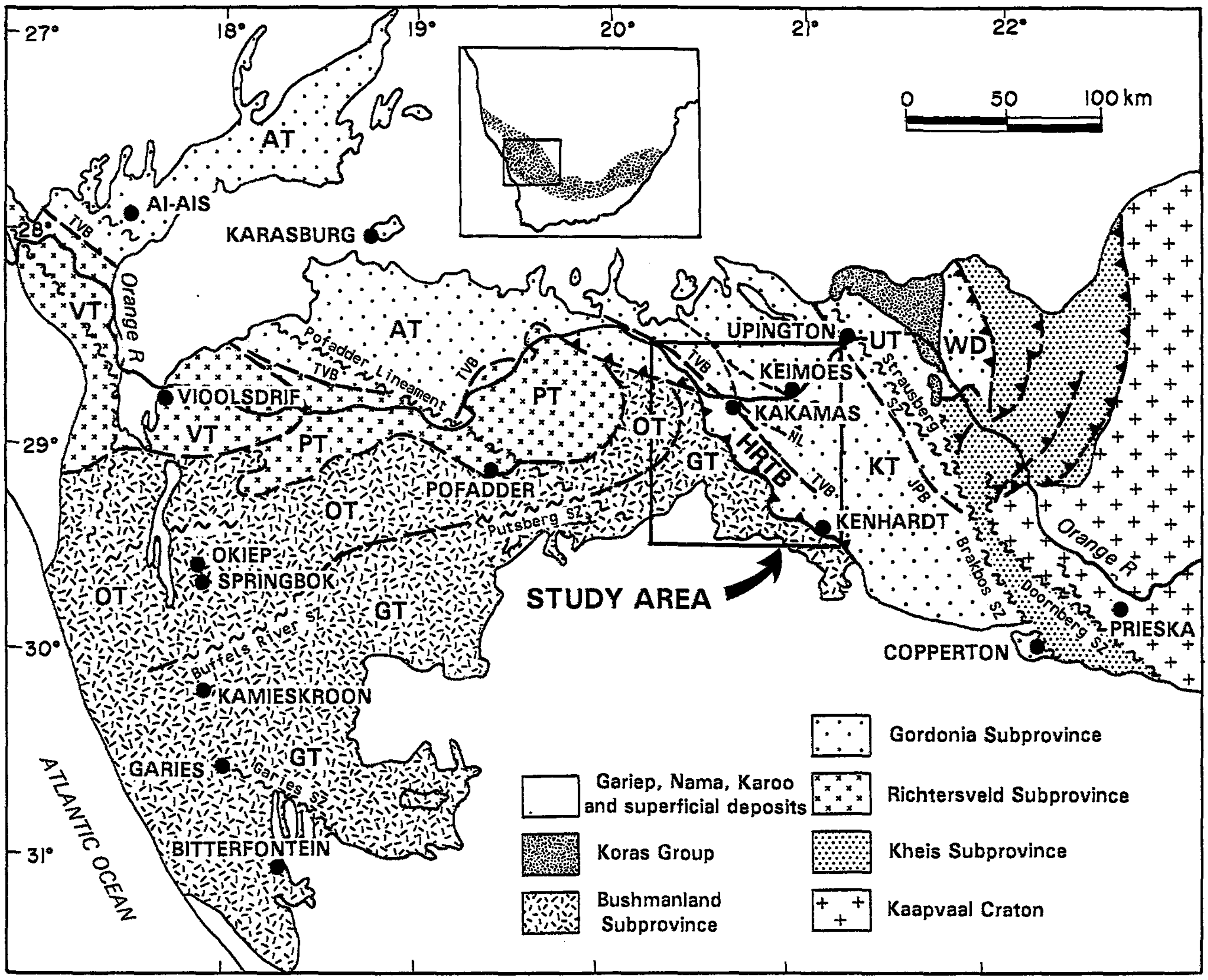

Figure 1. Tectonic subdivisions within the Gordonia, Bushmanland and Richtersveld Subprovinces of the Namaqua Tectonic Province (after Hartnady *et al.*, 1985; Joubert, 1986).

HRTB - Hartbees River Thrust Belt
KT - Kakamas Terrane
UT - Upington Terrane
WD - Wilgenhoutsdrif Formation
GT - Garies Terrane
OT - Okiep Terrane
VT - Vioolsdrif Terrane
PT - Pella Terrane
AT - Aus Terrane

TVB - Tantalite Valley Belt
NL - Neusspruit Lineament
JPB - Jannelsepan Belt

1.2.2 The Gordonia Subprovince

The 160km wide, northwest trending Gordonia Subprovince marks the transition from the *Namaqua Foreland* of folded and metamorphosed Kheis supercrustal rocks, to the *Namaqua Front*, a high-grade metamorphic / plutonic core complex, comprising a distinctive assemblage of metavolcanics, metasediments, high-grade gneisses, and late-tectonic plutons (Vajner, 1974 a, b, c, 1975; Stowe, 1983, 1986). Detailed structural studies (Vajner, 1974 a, b, c, 1975, 1978; Van Bever Donker, 1978, 1980; Van Zyl, 1981; and Stowe, 1979, 1980) in the Upington Geotraverse led to the subdivision of the Gordonia Belt into three northwest trending tectonic zones (Fig. 1) (Stowe, 1983, 1988):-

1) The 2.0 Ga *Upington Terrane* (zone "C" of Stowe, 1983) or the *Namaqua Foreland* is characterized by northeast-vergent structures, and marks the northeast margin of the Gordonia Subprovince, abutting against the Kaapvaal Craton and Early Proterozoic Kheis Belt (Fig. 1) (Hartnady *et al.*, 1985). The tectonic patterns of this boundary zone, between craton and mobile belt, are dominated by intense right-lateral shearing along the late northwest-trending Doornberg shear-system. The northeast margin of the Upington Terrane is marked by the *Jannelsepan Formation*, a suite of amphibolitic gneisses of calc-alkaline affinities (Geringer, 1979). The transition between the Upington Terrane and the Kakamas Terrane occurs abruptly across the *Straussberg-Trooilapspan shear zone*, an early steepened-up thrust, reactivated by later transcurrent shearing (Coward and Potgieter, 1983; Stowe, 1983, 1984, 1986). The Upington Terrane falls outside the area under investigation and consequently will not be discussed further.

2) The *Kakamas Terrane* (zone "B" of Stowe, 1983) or *Namaqua Front* lies northeast of the *Neusspruit Lineament* (Vajner and Jackson, 1974; Stowe, 1988) and contains the central high-grade plutonic core of the Gordonia Subprovince (Fig. 1 and 2). This zone comprises elongate, northwest-trending granitoid plutons of the 1.2-1.0 Ga *Keimoes Suite* (S.A.C.S., 1980), flanked on the southwest by, and containing vertical screens of, high-grade gneisses and metamorphosed supercrustal rocks of the *Korannaland Sequence* (S.A.C.S., 1980). This Sequence includes calc-silicate gneiss, micaceous quartzites and orthoquartzites, Mg-rich metapelites, and quartzo-feldspathic "pink-gneiss" (Von Backström, 1964;

Van Bever Donker, 1980). The most significant feature of the Kakamas Terrane is a central axis of high-grade gneiss, granulite, charnockite and late-tectonic granite, across which the steeply-dipping foliation has been compressed and arched in a right-lateral, transpressional shear regime (Stowe, 1986). The zone is characterized by steep fabric geometries associated with zones of intense transpressional shearing (Stowe, 1988).

3) The *Hartbees River Thrust Belt* in the southwest (Fig. 2 and 3) is dominated by south to southwest vergent folds and ductile thrusts (Harris, 1987; Stowe, 1988). Following regional mapping by Harris (1992), the HRTB became recognized as a structurally distinct tectozone or subterrane within the Gordonia subprovince (Stowe, 1988). Stowe (*op. cit.*) proposes that the provisional boundary between the HRTB and the Kakamas Terrane should be taken along the Neusspruit Lineament, which marks an abrupt transition in structural style, metamorphic grade and lithological continuity (Van Bever Donker, 1980, 1983). The southwestern boundary of the HRTB belt coincides with the proposed Gordonia-Bushmanland subprovince boundary (Hartnady, *et al.*, 1985; Joubert, 1986), and is positioned along the basal shear zone of the HRTB (Fig. 2). Further to the north the proposed subprovince boundary follows the Kakamas Shear Zone.

1.3 The study area

The study area overlaps the HRTB (Fig. 2), a 40 to 60 km wide, southwest-vergent zone of complex structure and lithostratigraphy along the western margin of the Gordonia Subprovince. The HRTB emerges from beneath Karoo cover southwest of the town of Kenhardt and extends northwestwards along the Hartbees and Orange Rivers for approximately 200km, before disappearing beneath Late Proterozoic Nama sediments east of Onseepkans. Joubert (1974a, 1978) first recorded the presence of thrusts in the zone south of Kakamas, and explained the fault pattern and associated structures of the HRTB in terms of convergent wrench-fault tectonics. Regional structural and lithological mapping of the southern HRTB was undertaken by Harris (1992), who established that the thrust zones and late-folds predate the transcurrent movements in eastern Namaqualand, and therefore could not have formed contemporaneously in a right-lateral transpressive regime (Harris, 1988). Furthermore the HRTB is dominated by down-dip elongation lineations more in keeping with compression than transpression (Harris, 1988; Stowe, 1988).

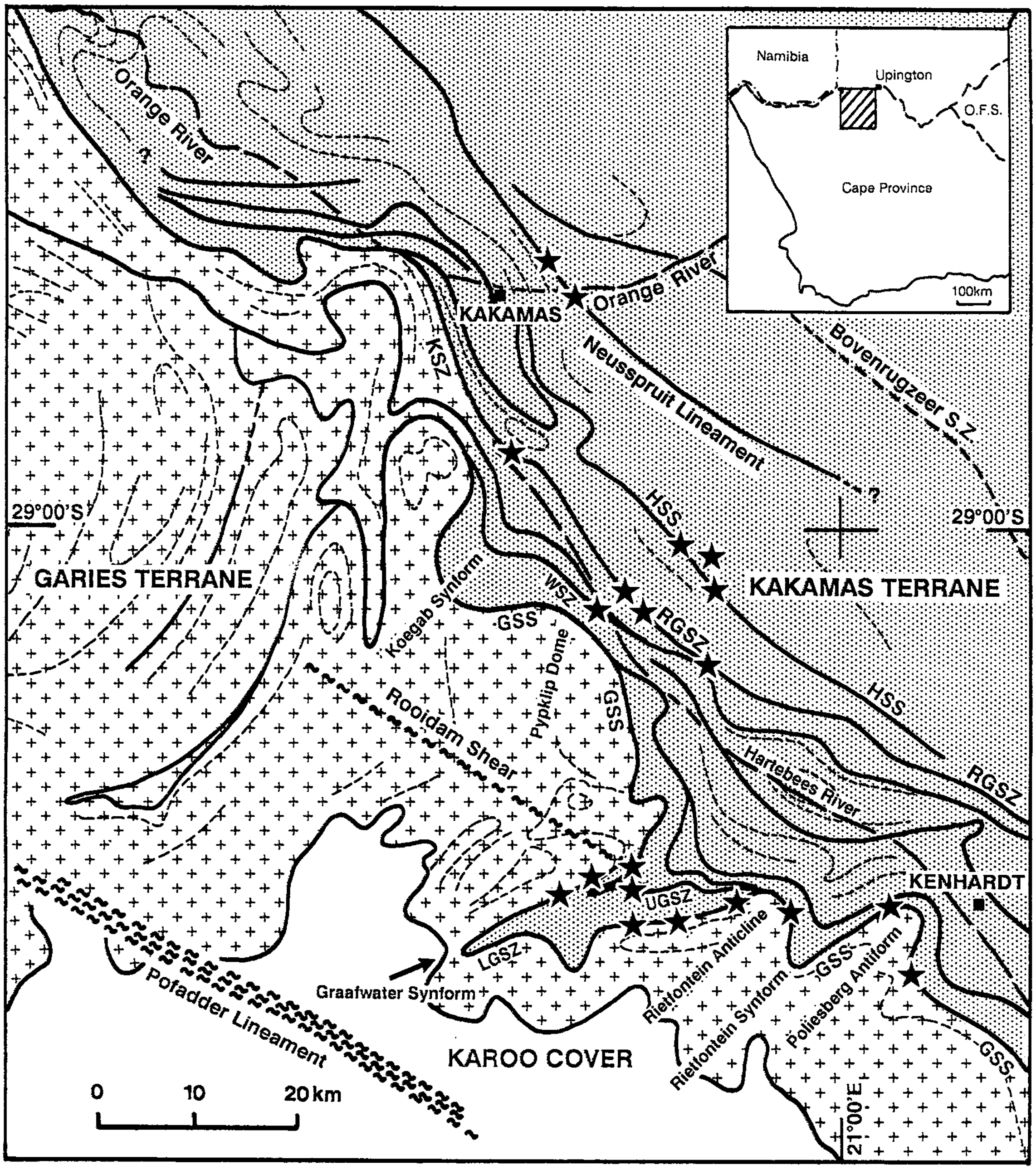

Figure 2. Map of the the principal ductile shear zones within the Hartbees River Thrust Belt (HRTB), modified after Harris (1992), and showing the proposed geoboundary between the ***Garies Terrane*** of the Bushmanland Subprovince, and the ***Kakamas Terrane*** of the Gordonia Subprovince (Hartnady ***et al.***, 1985; Joubert, 1986). Southwest of Kakamas the terrane boundary follows the Kakamas shear zone (**KSZ**), but further to the south it is taken along the basal mylonite zone of the Graafwater shear system (**GSS**). The HRTB as defined in this study is bounded by the Neusspruit Lineament in the northeast and the structurally lowermost shear zone of the GSS in the southwest. Other principal shear zones indicated include the Hugosput shear system (**HSS**), the Rozynenbosch-Ganzenmond shear zone (**RGSZ**), the Witvlei shear zone (**WSZ**), and the upper and lower Graafwater shear zones (**UGSZ** and **LGSZ**) in the south (Harris, 1992). The Rooidam Shear (Harris, 1992) and the Pofadder Lineament are late right-lateral strike-slip zones. The Pofadder Lineament may be traced below Karoo cover in the southwest of the map on the basis of its distinctive signature on aeromagnetic maps. Sampling localities for this study are indicated by stars.

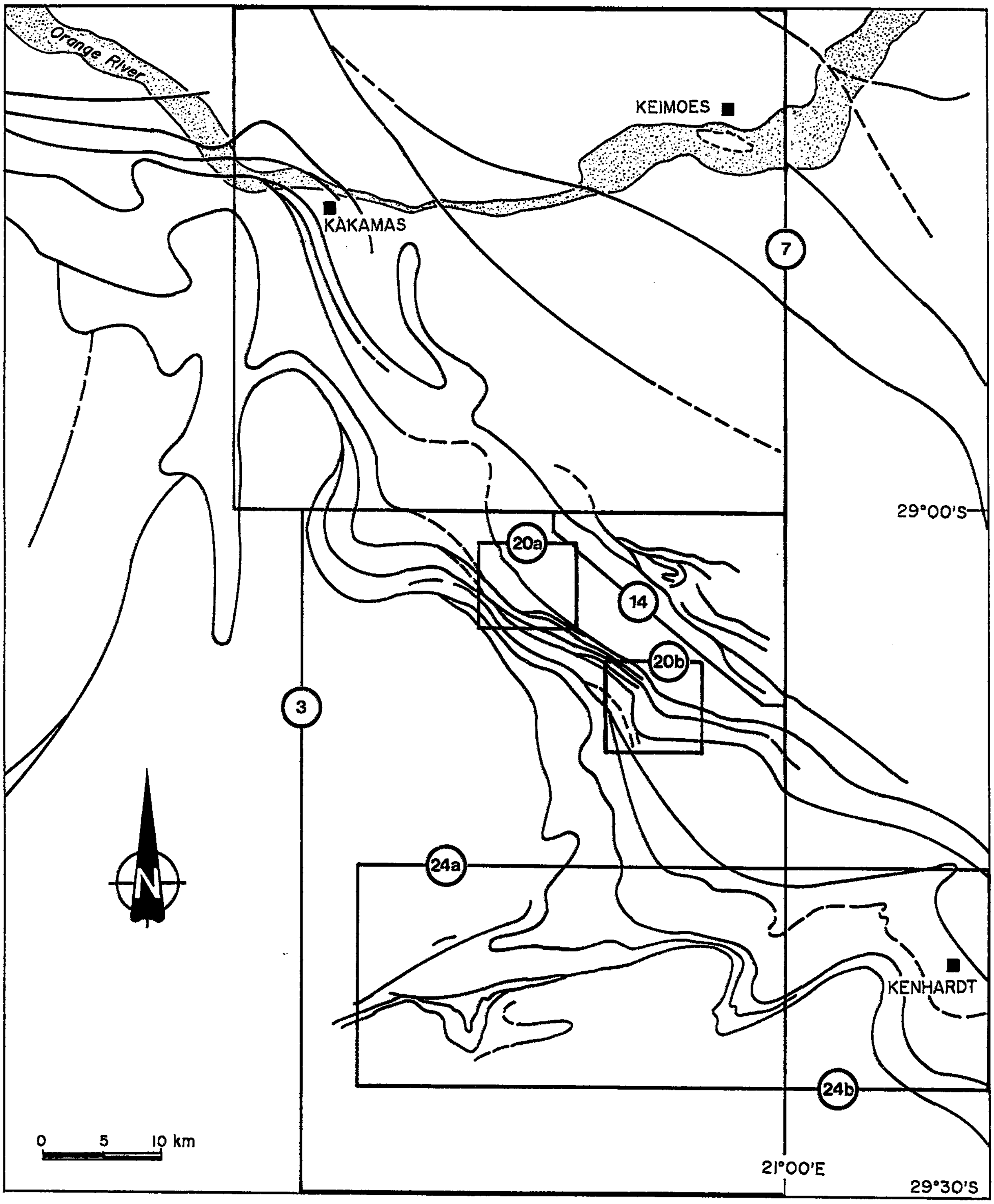

Figure 2B Key to the area maps contained in this thesis. Circled numbers indicate the Figure number for each map block.

1.3.1 Lithostratigraphy

Lithostratigraphic subdivisions within the southern HRTB are indicated on the map and legend of Fig. 3 (after Harris, 1992). For a more thorough review of the lithostratigraphy of the northern HRTB, readers are directed to Von Backström (1964) and Van Bever Donker (1980).

1.3.1.1 Pretectonic units

Harris (1992)) recognizes five pretectonic lithological components within the southern HRTB. At the structural base of the sequence are the regionally extensive *Leucocratic and Grey Granite-Migmatite Gneiss Complexes*, which together constitute probable basement to the overlying *Hartbees River Amphibolite-Gneiss Complex*. This latter unit is clearly visible on LANDSAT and MSS images, as dark sinuous bands tracing out the gross structure of the HRTB. Tectonic juxtaposition of the the above three units along major shear systems, resulted in a composite mixed syntectonic unit referred to as the *Vyfbeker Complex*. The *Bushmanland Sequence*, dominated by quartzo-feldspathic gneiss overlies the Hartbees River Amphibolite-Gneiss Complex. In the northeastern part of the HRTB (zone "A" of Stowe, 1983), high-grade supercrustal rocks of the *Korannaland Sequence* ($\geq$1.3 Ga) are interlayered with the early syn-tectonic (1.3-1.2 Ga), megacrystic *Riemvasmaak granite-gneiss* (Visser, 1984). Although tectonic basement / cover relationships have not yet been resolved, rocks of the Korannaland Sequence may represent lateral correlatives of the Bushmanland Sequence to the southwest (Stowe, 1986; Harris, 1990 *pers. comm.*).

1.3.1.2 Syntectonic intrusive rocks

Several syntectonic granitoid intrusive bodies are found in the HRTB, and these may be correlated to specific phases of deformation on the basis of fabrics and overprinting criteria. The age of granitic intrusives ranges from syn-D_1 through syn-D_4. Syn-D_1/early-D_2 intrusives in the southern HRTB are represented by quartz-feldspar-biotite augen gneisses (equivalent to the Riemvasmaak granite-gneiss in the northeast) and small gabbroic bodies. The principal syn-D_2 age intrusive in the southern HRTB is a large, weakly foliated leucogranite sheet containing xenolithic screens of biotite gneiss/schist, calc-silicate gneiss, amphibolite and quartzo-feldspathic gneiss, known collectively as the *Witvlei Migmatite Complex* (Harris, 1992).

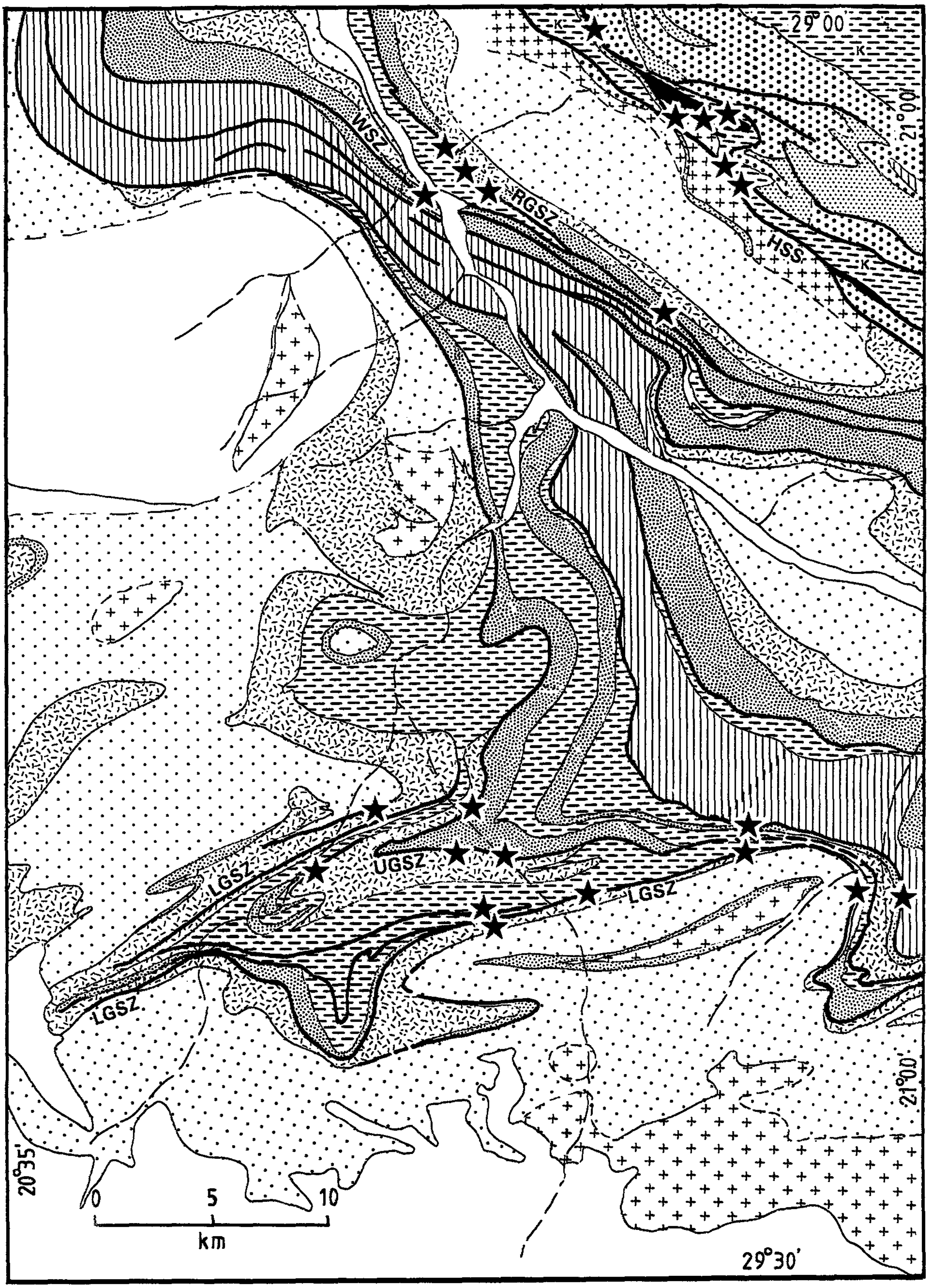

Figure 3. Lithotectonic subdivisions of the southern Hartbees River Thrust Belt (after Harris, 1992). Legend overleaf. Sampling localities for this study are indicated by stars. **HSS** = Hugosput shear system, **RGSZ** = Rozynenbosch-Ganzenmond shear zone, **WSZ** = Witvlei shear zone, **UGSZ** = upper Graafwater shear zone, **LGSZ** = lower Graafwater shear zone.

LITHOTECTONIC SUBDIVISIONS OF THE HARTBEES RIVER THRUST BELT

After Harris (1992)

KAROO ROCKS AND RECENT COVER

MYLONITE ZONE

PRETECTONIC UNITS

KORANNALAND SEQUENCE

SANDPUTS FORMATION
Calc-silicate mineral-bearing feldspathic quartzite

PIET ROOISBERG FORMATION
Kspar-qtz-cord-sill-bt gneiss
Calc-silicate gneiss
Qtz-feldspar gneiss

TOESLAAN FORMATION
Quartzo-feldspathic gneiss
locally with qtz-musc-sill nodules
Lenses of calc-silicate gneiss and amphibolite

BUSHMANLAND SEQUENCE
Predominantly quartzo-feldspathic gneiss
+- cordierite-anthophyllite gneiss, marble, amphibolite
and calc-silicate gneiss

TECTONIC IMBRICATION

HARTEBEES RIVER AMPHIBOLITE-GNEISS COMPLEX
Amphibolite gneiss +- calc-silicate gneiss +- marble-bands

GREY GRANITE-MIGMATITE GNEISS COMPLEX
Predominantly hornblende-bearing biotite-gneiss
biotite augen gneiss and K-fspar augen gneiss

LEUCOCRATIC GRANITE-MIGMATITE GNEISS COMPLEX
Migmatitic leucogneiss, pegmatoid and leuco-augen gneiss

SYNTECTONIC UNITS

SYN-D4 INTRUSIVES
Unfoliated granite and pegmatite

SYN-D3 INTRUSIVES
De Banken Granite
Uitsig Granite

SYN-D2 INTRUSIVES
Hugo's Put Potassic Charnokite

WITVLEI MIGMATITE COMPLEX
Poorly foliated sheet-like leucogranite
with xenolithic screens of:
Biotite gneiss / schist
calc-silicate gneiss
amphibolite
quartzo-feldspathic gneiss

VYFBEKER COMPLEX
Amphibolite, calc-silicate gneiss
Quartz-plagioclase+-hornblende gneiss
Marble (Wollastonite-calcite-quartz gneiss)
Grey augen gneiss
Leucocratic augen gneiss
Biotite-sillimanite-garnet gneiss
Minor Qtz-fsp gneiss

SYN-D1 - EARLY D2 INTRUSIVES
Pink-weathering qtz-fsp-bt augen gneiss
Gabbro

Syn-D_2 age potassic charnockite occurs in the Hugosput area, while the post-D_2 *Friersdale Charnockites* (S.A.C.S., 1980) straddle the Neusspruit Lineament in the north. Syn-D_3 intrusives include tonalite, granodiorite and granite, while syn-D_4 intrusives are represented by unfoliated granite and pegmatite.

The Proterozoic Namaqua rocks disappear under Palaeozoic Karoo cover in the extreme south and southwest of the HRTB.

1.3.2 Structural synthesis

A detailed description of the structural history of the entire Bushmanland-Gordonia region is beyond the scope of this chapter; however a summary of the sequence of structural events in the HRTB is imperative in order to assess the regional significance of this study. Harris (1987, 1988, 1992) recognizes four deformational events in the HRTB.

1.3.2.1 D_1 regional fabric forming event

The earliest recognisable deformation event in the HRTB (D_1) produced penetrative deformation fabrics in association with megascopic isoclinal, recumbent to reclined folds with limbs tens of kilometres in extent. No folds of this phase can be recognized in the HRTB, but repetitions in the stratigraphy endorse the existence of extensive F_1 fold-nappes. The regional D_1 fabrics include a penetrative mineral lineation (L_1) and gneissic banding in supercrustal rocks (S_1), and an augen elongation lineation (L_1) and augen foliation (S_1) in orthogneisses.

1.3.2.2 D_2 folding and ductile shearing event

D_2 was a continuous deformation event characterized by a phase of NNE to SSW directed compression, producing folds of varying style across the HRTB and culminating in strain localization along discrete ductile shear zones. The F_2 folds fold the regional L_1-S_1 fabrics and are therefore responsible for the local occurrence of S-SW plunging L_1 lineations within a regional lineation field dominated by NNE plunges (Harris, 1988, 1992). F_2 folds are the dominant macroscopic folds in the northeastern part of the HRTB, where they are characteristically tight, asymmetric plunging-inclined folds, overturned towards the SW and plunging to the SE or NW. They form elongate NW-trending, doubly-plunging structures resulting in closed outcrop patterns. Harris (1988, 1992) asserts that the double-plunge of these F_2 structures reflects primary non-cylindricity, related to rotation of the F_2 fold axes within the F_2 axial surfaces towards the NE-plunging kinematic vector of the contemporaneous shearing event. Towards the southwest of the HRTB the F_2 folds are less conspicuous, but occur as the open, upright, NW-trending component of the dome and basin structures typical of the Garies Terrane (Harris, 1988, 1992).

The D_2 ductile shear zones are discrete zones of strong refoliation, mylonitization and intense folding. They are defined by NW-trending zones of mylonitic rocks, characterized by intense L-S mylonite fabrics that rework the L_1-S_1 fabrics. The primary dip of the mylonite foliation (S_M) is towards the NE, and the mylonite elongation lineation (L_M) plunges approximately down-dip in almost all cases. This orthogonal relationship between L_M and the primary trend of the mylonite zones, together with the SW-vergence of the F_2 shear-related folds is suggestive of SW-directed thrusting during the D_2 ductile shearing event (Harris, 1988, 1992). Antiformal F_2 shear-related folds vary from mildly non-cylindrical folds with subhorizontal NW-SE plunging axes, to highly non-cylindrical sheath folds with axes plunging NE, parallel to the down-dip mylonite elongation lineation. The interposed synformal components are severely attenuated or sheared-out. Frequently the shear-planes are invaded by locally derived anatectic material, either pegmatite, or coarse-grained leucogranite (Stowe, 1988). *It is primarily with the D_2 ductile shear zones that this investigation is concerned, since most of the mylonite zones in the southern HRTB are of this generation.*

1.3.2.3 D_3 crossfolding event

The D_3 crossfolding event involved initial E to W directed compression, resulting in dome and basin structures in the southwest where F_3 interfered with open, upright F_2 folds, and in mild type-2 interference structures further north where F_3 interfered with tighter, overturned F_2 folds (Harris, 1992). The NNW to ENE trending F_3 folds are best developed in the southwest of the HRTB, becoming more open and less distinct towards the north and northeast. F_3 folds display a regional transition in axial trend from N-S in the northern part of the HRTB, to ENE-WSW in the south. Harris (1988, 1990, 1992) demonstrated that this change in the axial trend of F_3 folds is spatially related to the presence of D_4 right-lateral transcurrent shear zones.

F_3 folds are generally horizontal to plunging-upright or plunging-inclined, and their regional style is disharmonic. The regional disharmony of F_3 folds is particularly apparent across the syn-D_2 Witvlei leucogranite sheet, which may have functioned as a decoupling zone throughout D_2 and early D_3 (Harris, 1992). The D_2 mylonite zones, and consequently the S_M-L_M mylonite fabrics, are folded about the F_3 fold axes, confirming the temporal relationship between D_2 and D_3. D_3 produced local penetrative refoliation in the hinge regions of tight, mesoscopic to macroscopic folds, resulting in an intersection lineation, or a crenulation lineation in schistose lithologies (Harris, 1992).

1.3.2.4 D_4 transpressive event

The D_4 deformation phase involved protracted, right-lateral strike-slip shearing on WNW to ESE striking, near-vertical shear zones. Ductile shearing was initiated on the Pofadder Lineament (Toogood, 1976; Maclaren, 1984) and resulted in regional clockwise rotation, stretching and tightening of megascopic F_3 structures immediately adjacent to the Lineament, and rotation of the coaxial L_1 lineations (Harris, 1988, 1990). Localised shearing occurred on subsidiary ductile shears subparallel to the Pofadder Lineament. D_4 deformation was most intense along the southwestern margin of the HRTB, but is nevertheless detectable within the belt itself (Harris, 1992).

F_4 shear-related folds resulted from regional bending of large-scale D_3 structures. A single regional-scale fold occurs, related to rotation of structures in a broad belt marginal to the Pofadder Lineament. The F_4 folds are open and have WNW to ESE striking axial planes with fold axes plunging steeply to the northwest or southeast. The plunge of the F_4 folds is variable, and is controlled by the dip of the refolded F_3 fold limbs. No regional penetrative fabric is associated with the D_4 event, although penetrative mylonite fabrics are well-developed in discrete ductile shears associated with early D_4 strike-slip shearing. D_4 activity culminated in brittle faulting, also effecting right-lateral displacements.

Harris (1990, 1992) demonstrated that the reworking of F_3 folds by the D_4 shearing event occurred under conditions of elevated temperature (approximately 650°C), a finding which is in conflict with earlier interpretations (Joubert, 1974a, 1978; Van Bever Donker, 1980; Moore, 1989) which linked the regional metamorphic peak to the D_2/D_3 events, and characterized the post-D_3 events as retrogressive. The longevity of the D_4 shearing event finds its expression in the range of behavioural responses to progressive deformation. The style of deformation ranges from early ductile shearing with the formation of mylonitic rocks, to late brittle fracturing producing cataclasites (Maclaren, 1984). This suggests that the D_4 event was a continuous, protracted deformation phase accompanying uplift and unroofing of the Namaqua Metamorphic Complex.

The D_3 crossfolding phase coupled with subsequent reorientation during the D_4 shearing event, imparted a very irregular pattern to the HRTB. Moreover, the present orientation of the D_2 ductile shear zones is by no means primary. This has significant implications for any attempt at restoration of established kinematic vectors to their primary D_2 orientations.

1.3.3 Metamorphism

Rocks within the Kakamas Terrane and the HRTB of the Gordonia Subprovince have a high grade polymetamorphic history. Four metamorphic events have been recognized (Stowe, 1980; Van Bever Donker, 1980; Humphreys and Swartz, 1988; Waters, 1990).

1.3.3.1 Granulite facies event

Metapelitic gneisses, overlying the present Gordonia-Bushmanland boundary "thrusts" and west of the central core of late-tectonic charnockitic magmatism in the Kakamas Terrane (i.e. west of the Neusspruit Lineament), have Grt-Crd parageneses consistent with granulite facies metamorphism (Waters, 1990). This zone of granulite facies metamorphism within the HRTB is part of a broader northwest trending metamorphic belt, that is thought to reflect the Orange River orogeny at about 1750 Ma (Hartnady *et al.*, 1985). Rocks in the eastern Gordonia Subprovince experienced high grade metamorphism later than those to the west. Cornell *et al.* (1986)

propose an age of c. 1200 Ma for the early metamorphism of Areachap Group supercrustal rocks of eastern Gordonia. This early high grade metamorphic event may be correlated with the prograde M_1 event described by Van Bever Donker (1980) and Stowe (1980).

Humphreys and others (Humphreys and Swartz, 1988; Humphreys, 1990; Humphreys and Van Bever Donker, 1990) indicate that two broad subdivisions, based on metapelitic parageneses, are recognisable within the Kakamas Terrane. Within the HRTB, pelitic rocks contain granulite facies assemblages (Grt + Crd + Kfs + Sil ± Bt ± Spl ± Opx), while to the NE, across the Boven Rugzeer Shear Zone, pelitic schists contain relict assemblages and pseudomorphs of staurolite and andalusite in contact metamorphosed Spl-Crd rocks. The widespread preservation of relict staurolite and andalusite within pelites of the latter subdivision indicates that early low-pressure, prograde amphibolite facies metamorphism occurred over large areas of the eastern Namaqua Province. Fabric relationships indicate that early, low-pressure mineral growth was diachronous with respect to the D_2 deformation event.

1.3.3.2 Amphibolite facies retrograde event

The high grade rocks of the HRTB are retrogressively overprinted by the dominant (syn- to post-D_2) amphibolite-granulite facies event of the Bushmanland Subprovince. Within the metapelitic rocks of this zone, the early granulite Grt-Crd paragenesis is overprinted by the characteristic Bt-Crd-Sil amphibolite facies assemblage. Southwest of the HRTB, the amphibolite facies metamorphism increases in grade, finally attaining granulite facies in central Namaqualand (Waters, 1990). The age of this amphibolite-granulite facies metamorphic event (*the Namaqua thermal event*) in the Gordonia Subprovince is poorly constrained. In Bushmanland however, evidence exists for substantial mineral growth after D_2, with peak conditions persisting throughout D_3 and the emplacement of late-tectonic granites at c. 1150 Ma (Clifford *et al.*, 1975, 1981; Waters, 1989, 1990).

1.3.3.3 Granulite facies thermal event

Granulite facies metamorphism is recorded by rocks spatially associated with late-tectonic granite and charnockitic intrusives within the central magmatic core of the Kakamas Terrane. This metamorphic event may be correlated with the prograde M_2 event of Van Bever Donker (1980) and Stowe (1980). Typical products of this younger thermal metamorphic event are hornfelsic textured Grt-Crd-Sil gneisses locally termed "kinzigite" (Van Zyl, 1981), which often grade texturally into high-temperature mylonite zones (Waters, 1990). Emplacement ages of the late-tectonic intrusives are between 1.2 and 1.1 Ga (Botha *et al.*, 1976, 1979; Barton and Burger, 1983; Geringer *et al.*, 1988) and may be correlated with the high-grade regional event in the Bushmanland Subprovince (Waters, 1990).

1.3.3.4 Greenschist facies retrogression

Van Bever Donker (1980) and Stowe (1980) recognize a final regional retrogressive event (M_3) in the Gordonia Subprovince, that is most pronounced adjacent to the major strike-slip shear zones. Retrogressive parageneses include epidote-group minerals, chlorite and calcite.

1.4 Scope of the project

1.4.1 Motivation

Recent work in the Namaqua Province suggests that it comprises several potentially suspect lithotectonic terranes (Hartnady *et al.*, 1985; Joubert, 1986). Studies of the tectonic evolution of the Province have in the past focussed largely upon attempting to separate terranes on the basis of lithostratigraphic, geochronological and tectonic relationships. Rarely has the nature of possible terrane accretion processes, or mechanisms of tectonic juxtaposition of potential terranes been directly addressed. Current international research has shown that the mechanisms of terrane amalgamation, accretion or post-accretionary dispersion may be better understood by detailed examination of the zones along which tectonic juxtaposition has occurred (e.g. Takagi, 1986; Behrmann and Platt, 1982; Brown and Murphy, 1982; Simpson, 1984; Erdmer, 1985; Faure, 1985; Dietrich and Durney, 1986; Lagarde and Michard, 1986; Culshaw, 1987;

Edelman *et al.*, 1987; Lacassin, 1987; Maiver, 1987; Mawer and White, 1987; Hooper and Hatcher, 1988; Hansen, 1989; Carlson *et al.*, 1990; Cashman, 1990; Guerin *et al.*, 1990; Schulmann, 1990; Cluzel *et al.*, 1991; Crespo-Blanc, 1992).

A knowledge of the movement histories of major shear zones within the HRTB is fundamental to understanding the tectonic development of the belt, and the evolution of the Namaqua Province as a whole. Despite this fact, no precise kinematic studies have been undertaken, and the movement histories and age relationships of the shear zones have not been described in detail. Previous kinematic interpretations of the shear zones have relied largely upon analysis of neighbouring macroscopic structures (Joubert, 1978; Stowe, 1980, 1983, 1988; Harris, 1992), and differences in metamorphic grade across some of the shear zones (Van Bever Donker, 1980, 1983). These interpretations are often unexplicit, unqualified and ambiguous. Before a statement of the aims of this study, a short review of existing kinematic models for the principal shear zones of the HRTB is essential to fully appreciate the contention and ambiguity surrounding their movement histories.

1.4.2 Review of kinematic models for shear zones of the HRTB

1.4.2.1 The Neusspruit Lineament

The Neusspruit Lineament is a major northwest-trending, northeast-dipping structural discontinuity in the Gordonia Subprovince (Fig. 2). It has a pronounced topographic expression due to the presence of resistant mylonitic rocks, and is therefore highly visible on aerial photographs and LANDSAT imagery. Furthermore the lineament is notably conspicuous on aeromagnetic maps, endorsing the proposition that it represents a fundamental crustal discontinuity in the Namaqua Tectonic Province.

Vajner and Jackson (1974) first defined the Lineament and noted its importance in separating two distinct structural-metamorphic provinces. They observed that, northeast of the Lineament, low-medium grade (chlorite-zone) supercrustal rocks predominate (Poldervaart and Von Backström, 1949), but are absent southwest of the Lineament where metamorphic grades are high and pink gneisses are extensive. They found no evidence of tectonic movement on the Lineament. Van Bever Donker

(1980, 1983) however, proposes that the Lineament has been affected by horizontal shortening and crustal thickening, followed by wrench and block faulting.

Prior to D_3, horizontal shortening and crustal thickening dominated, with 74% shortening attained alongside the Lineament (Van Bever Donker, 1983). Considerable flattening during D_2 resulted in the tightening up of structures adjacent to the Lineament, and intense refoliation parallel to it, producing the mylonitic quartz-mica schists of the Neusberg range and ribbon-mylonites within the Riemvasmaak gneisses (Van Bever Donker, 1983). The pronounced aeromagnetic signature of the Lineament suggests that shortening during D_2 was partially accommodated by westward directed overthrusting, resulting in a thickened crust to the east of the Lineament (Van Bever Donker, 1980). Post D_2 and post D_3 right-lateral wrench faulting was invoked by Van Bever Donker (1980) to explain an apparent mismatch in the orientation of F_2 axial planes across the Lineament. Van Bever Donker (1980) calculated strike-displacements of up to 16.5km for the Lineament.

Van Bever Donker (1980, 1983) censured the low-grade proposed by Vajner and Jackson (1974) for supercrustal rocks northeast of the Lineament, but conceded that the Lineament marks a fundamental transition in metamorphic conditions. East of the Lineament both M_1 and M_2 mineral parageneses are recorded, while west of the Lineament the M_2 metamorphism is absent. M_3 retrograde parageneses occur on both sides of the Lineament. Parageneses west of the Lineament indicate PT conditions of at least 660°C and 5kb, while those east of the Lineament indicate conditions lower than 495-565°C and 2kb (Van Bever Donker, 1980). From this, assuming a constant regional geothermal gradient, Van Bever Donker (1980, 1983) inferred depths of approximately 18km west of the Lineament, and 8-13km east of the Lineament. The exposure of rocks of different metamorphic grade along the Lineament is thus explained by 5-10km of normal vertical movement after the D_2 event.

Stowe (1980, 1983) carried out displacement estimates for the Neusspruit Lineament based on the Ramsay and Graham (1970) method, using pre-existing foliations, and extended his studies to a 3-D solution in order to consider both horizontal and vertical displacements. A right-lateral strike-slip movement of between 8.3km and 10.5km, and a normal dip-slip movement of between 11.5km and 12.5km were obtained. Stowe (1980) noted that the calculated slip directions in the shear zone margins are generally subhorizontal, while in the centres they are subvertical. This is interpreted as indicative of a transition from predominantly wrench tectonics at an early stage, to vertical "graben and arch" tectonics as the ductility decreased and the shear zone narrowed (Stowe, 1980).

Stowe (1980, 1983) considered the right-lateral shearing episode as principally or wholly post-D_2, and probably post-D_3 since F_3 fold structures are reorientated adjacent to the transcurrent shear zones.

Van Bever Donker (1980) suggested that the Neusspruit Lineament represents a fundamental crustal discontinuity that has been active over a protracted period of geological time. He proposed that the present shear zone may have followed an older syndepositional fault, and that block faulting may have initiated prior to D_2. Furthermore, the occurrence of the Friersdale charnockitic adamellite on both sides of the Lineament suggests that the shear zone played a significant role in the emplacement of granitoids, and must have been deeply rooted to enable the upward passage of magma. Based on these observations, Van Bever Donker (1983) proposed that the Neusspruit Lineament represents a potential boundary between the the Namaqua Metamorphic Complex and the Namaqua Front (Kakamas Terrane).

Stowe (1988) noted a transition in structural style from predominantly "steep" structural domains northeast of the Lineament, to "recumbent" domains characteristic of the northern HRTB, southwest of the Lineament. Based on this, and taking into account the inadequacies of the currently accepted Bushmanland-Gordonia Subprovince geoboundary in fulfilling tectonostratigraphic preconditions (Harris, 1987, 1988), Stowe (*op. cit.*) proposed that the Neusspruit Lineament should mark the provisional southwestern margin of the Kakamas Terrane.

1.4.2.2 The Kakamas shear zone

Pretorius (1974), first defined the line of the northwest-trending Kakamas Fault in an interpretation of gravity data along the boundary between the Kaapvaal and "Sonama" Provinces. Joubert (1974a, 1978) corroborated the existence of this fault, and went on to describe the associated fault/shear zone pattern south of Kakamas in terms of a transpressive tectonic model.

Van Bever Donker (1980) noted that the Kakamas Shear Zone (hereafter referred to as the KSZ) is discernible on aeromagnetic maps as a "quiet-low", and in the field is defined by a number of narrow, parallel zones, characterized by porphyroblastesis, piedmontite enrichment, silicification, and locally by late tourmalinization. Petrographic work by Van Bever Donker (1980) revealed that some of the fault-rocks are brecciated, and comprise angular clasts of quartz and feldspar set in a finely recrystallized, glassy matrix. Van Bever Donker attributed the grain refinement evident in the matrix to dynamic recrystallization. Other coarsely recrystallized rocks display late growth of piedmontite often in association with silicification.

Van Bever Donker (1980) proposed that right-lateral transcurrent shearing is indicated by the sense with which secondary faults branch sigmoidally into the KSZ. Joubert (1978) described a similar fault branch-pattern from the southern continuation of the zone. Although Van Bever Donker (1980) contended that no structures are visibly "dragged" into the zone, Stowe (1980, 1983) performed displacement estimates based on the Ramsay and Graham (1970) method. He calculated a right-lateral strike-slip displacement of 11.3km with a 4.5km vertical thrust component. In addition, he estimated 3.2km left-lateral strike-slip displacement and 2.2km vertical thrust displacement for what he termed the Kakamas "late fracture".

1.4.2.3 Shear zones of the southern HRTB

Joubert (1978) examined the "fault-zones" of the southern HRTB and concluded on the basis of the vergence of shear related folds, and drag adjacent to the "faults", that movement along the principal, NW-trending, vertical zones has been right-lateral since the earliest deformational events. Based on the mixed fault-rock assemblages comprising both mylonites and cataclasites, and on the fault-rock parageneses which include both high-grade (sillimanite) and retrograde (chlorite, epidote, piedmontite, calcite) minerals, Joubert (1978) concluded that "fracturing" occurred over a relatively long period of time. Joubert (1978) conceded that folds associated with northerly-dipping "faults" indicate reverse movement with SW-directed overthrusting. Joubert (1978) described a pattern of subsidiary reverse faults branching off major, NW-striking, vertical faults characterized by right-lateral strike-slip movement. Additionally, Joubert (1974b) related the variable geometry of F_3 folds to formation within a right-lateral strike-slip regime. Joubert (1978) proposed that this structural association is typical of convergent wrench faulting (transpression), and is comparable to model strike-slip zones such as the San Gabriel fault zone (Wilcox *et al.*, 1973).

Following mapping and detailed geometrical analysis of the southern HRTB, Harris (1988) invalidated the wrench-tectonic model as envisaged by Joubert (1974a, 1978) for coeval development of the F_3 folds, thrust zones and right-lateral strike-slip zones in the HRTB. Harris (1988) contested that the F_3 folds existed prior to right-lateral shearing, and that the NW-striking thrust zones are even older, since they are demonstrably folded by the F_3 folds. Instead, Harris (1988) envisaged a sequence of events involving folding and thrusting during a compressional deformation phase (D_2), followed by a cross-folding event (F_3), and culminating in reorientation of structures due to right-lateral shearing within broad belts alongside the WNW-striking Pofadder Lineament and its subsidiary shears (D_4).

Based on the overall southwest vergence of F_2 shear-related folds, the sense of displacement of the S_1 foliation across the shear zones, and the ubiquitous down-dip mylonite elongation lineation within the shear zones, Harris (1992) indicates that the principal mylonite zones of the southern HRTB are indeed D_2 thrust faults with hangingwall movements towards the southwest. His kinematic interpretation encompasses the Hugosput shear system (hereafter referred to as HSS), the Rozynenbosch-Ganzenmond shear zone (hereafter referred to as RGSZ), the Witvlei shear zone (hereafter referred to as WSZ), and upper and lower Graafwater shear zones (hereafter referred to as the UGSZ and the LGSZ respectively, or collectively as the GSS: Graafwater Shear System.

New (1987), performed a microstructural, strain and kinematic analysis of a section across the HRTB, situated on the farm Witvlei. His study section included all of the mylonite zones in the footwall of the RGSZ, from the WSZ in the east, to the northwestern extension of the Graafwater shear zone in the west. Although principally an exercise in strain analysis, microstructural kinematic analysis was performed on a few oriented specimens from the WSZ, the GSZ, and a "paper" mylonite zone within the main body of the Witvlei Migmatite Complex. Shear sense determined from asymmetric fabrics and microstructures within the mylonites, indicate that movement was oblique reverse consistent with south-directed overthrusting. Based on observed fabric parageneses and the variable mechanical response of different feldspar mineral species to deformation, New (1987) proposed two thermally distinct thrusting events: An early shearing event, associated with injection of voluminous leucogranite, produced high-temperature (upper amphibolite facies) mylonites in major D_2 thrust zones within a compressive tectonic environment. Subordinate shearing on narrower thrust surfaces produced low-temperature (middle greenschist facies) mylonites in response to regional transpression during the right-lateral D_4 strike-slip event.

The Rozynenbosch-Ganzenmond shear zone

On the basis of the southwest vergence of F_2 folds, and the rotation of F_2 fold axes towards parallelism with ubiquitous down-dip, NNE-plunging, mylonite elongation lineations, Harris (1992) interprets the RGSZ as a D_2 thrust zone characterized by SSW directed overthrusting. Harris (1992) maintains that the presence of numerous silicified breccia zones and late fractures along the RGSZ, is evidence for potential reactivation of the RGSZ as a right-lateral strike-slip fault during late-D_4.

The Hugosput shear system

Despite the fact that the mylonite zones of the HSS are characterized by a ubiquitous down-dip mylonite elongation lineation in keeping with dip-slip movement, researchers from the Geological Survey of South Africa (M.J. Slabbert and H.F.G. Moen, *pers. comm. to* R.W. Harris, 1988) recognize the principal HSZ as a strike-slip zone. Harris (1992) interprets the HSS as a D_2 thrust zone with NE over SW displacement, purely on the basis of the down-dip orientation of the mylonite elongation lineation.

1.4.3 Aims of the project

The primary objective of this investigation is to produce a kinematically sensible movement history for each of the the principal shear zone systems of the HRTB, using modern methods of microstructural kinematic analysis. This requires determination of the precise orientation of the bulk kinematic vector, and the sense and relative ages of movements on each shear zone. Questions to be addressed will include the following:

1) Do the shear zones reflect only thrust, normal or strike-slip shear displacements, or have they experienced prolonged histories with sporadic reactivation events, each having a unique transport vector and shear sense?

2) Is the complete movement history of a shear zone recorded by microstructural indicators preserved within mylonites, or do later events overprint and totally obliterate earlier microfabrics?

3) What are the age relationships between the shear zones and other structural features within the HRTB? Have the shear zones been folded by later deformation events? These questions are important in the interpretation of the tectonic evolution of the HRTB, and the Namaqua Province as a whole.

4) Does the degree of coeval mylonitization vary spatially across the HRTB? If so, can inferences be made with respect to the three-dimensional geometry of the HRTB?

5) How reliable are microstructural kinematic and petrofabric techniques when applied to kinematic analysis of mylonites and protomylonites in high grade metamorphic terrains? Do the results of this study affirm the need for continued microstructural kinematic analyses of shear zones in the Namaqua Tectonic Province?

Modern techniques of microstructural kinematic analysis of ductile shear zones have been employed in this study. Consequently before describing methodology specific to this study, a historical review of literature pertaining to ductile shear zones, mylonite terminology, and accepted procedure in microstructural kinematic studies, is appropriate. This review is presented in the following chapter, in which the methods used in this study are also outlined.

Chapter 2. - Mylonites: Tectonic settings, terminology and methods of microstructural kinematic analysis

2.1 Ductile shear zones and mylonites

Deep level, ductile shear zones occur as broad planar zones of inhomogeneous deformation, dominated by crystal-plastic processes and characterized by mylonite and mylonitic rocks. They represent zones of dominantly simple shear (non-coaxial) deformation which wholly, or partially, accommodate imposed regional or local strains, which adjacent country rocks cannot accommodate by bulk deformation (White *et al.*, 1980). Ductile shear zones are thought to develop when the strain hardening capacity of the host lithology is exceeded, and their appearance reflects the onset of strain softening processes (Cobbold, 1977). Consequently shear zones represent areas dominated by strain softening processes, the extent of which is determined by the mechanical properties of the rock-type which develops within the shear zone. White *et al.* (1980) regard mylonite as the material instrumental in the strain softening process, and define it as *"the rock produced in a ductile shear, or fault zone and which allows the zone to accommodate the imposed strain rate by dominantly ductile processes".*

2.2 Tectonic settings of mylonitic rocks

Ductile shear zones and mylonitic rocks occur within rocks of all ages from most tectonic settings, and are common along convergent and transform plate boundaries as well as intercratonic regions.

At *continent-ocean plate boundaries* where active subduction occurs, mylonite zones may develop along the subduction zone (Monsen and Aalto, 1980; Ellis, 1986; Meneilly and Storey, 1986; Hansen, 1989, 1992 a and b) or within the mountain belts formed alongside the subduction zone (Ross, 1973; Brown and Murphy, 1982). Intense zones of ductile shearing characterized by mylonitic rocks are frequently developed along continent-ocean plate boundaries where obduction has occurred, e.g. St. Anthony

Complex, Newfoundland (Jamieson and Strong, 1981) and the Schistes Lustre's nappe in the French-Italian Alps and Corsica (Malavieille and Etchecopar, 1981; Mattauer *et al.*, 1981). However, the most frequently documented occurrences of mylonite zones are at *convergent plate boundaries* formed by the *collision of two continental plates*. Mylonites have been extensively described within major ductile thrusts and strike-slip zones of almost every orogenic belt in the world, and occurrences are far too numerous to list individually.

Mylonitic and cataclastic rocks are common along *transform plate boundaries* and two transform faults in particular are well documented: the San Andreas Fault, California (Waters and Campbell, 1935; Higgins, 1971; Sylvester and Smith, 1976) and the Alpine Fault, South Island, New Zealand (Higgins, 1971; White and White, 1983).

Mylonitic rocks also occur at *intercratonic boundaries* within plate interiors, for example in *Cordilleran metamorphic core complexes*. Such complexes are common in the western United States and form by major crustal *extension* (Davis, 1983; Malavieille, 1987; Lister and Davis, 1989; Reynolds and Lister, 1990). Mylonitic rocks within metamorphic core complexes occur below major, shallow-dipping detachment faults, and are the result of ductile deformation in crustal-scale extensional shear zones (e.g. Davis, 1983). Mylonitic rocks within western North American Cordilleran Core Complexes have been documented from the central Mojave Desert (Bartley and Fletcher, 1990), the Coyote (Davis *et al.*, 1987) and Whipple Mountains of California (Davis *et al.*, 1986); the South Mountains, Arizona (Davis *et al.*, 1986); and the Ruby and Snake Ranges, Nevada (Miller *et al.*, 1983; Bartley and Wernicke, 1984; Lee *et al.*, 1987). Mylonites have also been documented in the Paparoa Metamorphic Core Complex of New Zealand (Tulloch, 1989), and within a late Variscan metamorphic core complex in the Southern Massif Central, France (Echtler and Malavieille, 1990).

Mylonitic rocks indicating *extensional deformation* have also been recorded within *collisional orogenic belts* e.g. within the Rombak Window in the northern Norwegian Caledonides (Cashman, 1990), the Tauern Window of the eastern Alps (Selverstone, 1988), and within Variscan crust in the French Pyrenees (de Saint Blanquat *et al.*, 1990) and French Massif Central (Echtler and Malavieille, 1990; Malavieille *et al.*, 1990). Cashman (1990) considers extension to be due to flexing of a crystalline thrust sheet over a ramp in an underlying detachment, whereas Malavieille *et al.*, (1990) and Selverstone (1988) relate extension to the collapse and unroofing of orogenically thickened crust.

Cataclasites and mylonites occur along *allochtonous terrane boundaries* in the *North American Cordillera* e.g. within parts of the Nitsulin, Anvil and Simpson allochthons (Erdmer, 1985), and along the Teslin suture zone, Yukon (Hansen, 1989; 1990, 1992 a and b). In *Japan*, Faure (1985) and Takagi (1986) have described the microstructures of mylonitic rocks along the *Median Tectonic Line* (MTL).

2.3 Deformation mechanisms in crustal fault zones

In the conceptual model of Sibson (1977, 1983) for fault zones developed in continental crust of predominantly quartzo-feldspathic composition, faults are considered to have three main depth horizons, each characterized by unique deformation mechanisms and consequently unique fault rock assemblages. At shallow depths (0-7km) cataclastic rocks are produced in response to brittle deformation mechanisms. At depths between 7 and 15km both brittle and crystal-plastic deformation occur resulting in cataclastic and mylonitic rocks (*the brittle-ductile transition zone*), while at depths exceeding 15km mylonites and ultramylonites are produced in ductile shear zones characterized by predominantly crystal-plastic deformation.

In cataclasites grain-size reduction occurs by fracturing and crushing, with subsequent deformation dominated by the sliding and rotation of fragments. In mylonites grain refinement occurs by recrystallization or neomineralization, with subsequent deformation occurring through crystal-plastic mechanisms (White *et al.*, 1980; Tullis *et al.*, 1982). This distinction is for an ideal monomineralic rock but is applicable to polymineralic rocks if the behaviour of the matrix alone is considered. In a mylonite the matrix deforms by crystal-plastic processes, whereas in a cataclasite the matrix deforms by frictional sliding and rigid body rotation of the fragments (White *et al.*, 1980).

Subsidiary brittle deformation commonly accompanies mylonitization, resulting in grain refinement of a small proportion of relatively rigid grains (e.g. feldspar) in the rock by brittle fracturing (Mitra, 1978). However the main stress-supporting minerals in the rock deform by crystal-plastic processes, involving the migration of dislocations and other lattice defects through the grains, without fracturing of the grains themselves.

In quartzo-feldspathic crustal rocks, feldspar remains the relatively rigid mineral down to about 18km depth (T=450°C ± 50°C) (Sibson, 1977, 1983; Mitra, 1978), but, if it constitutes a minor portion of the rock, ductile behaviour of the accompanying quartz can occur at temperatures above 300°C ± 50°C (Tullis and Yund, 1977; Sibson, 1983). The mylonite produced is a high-strength tectonite, with a pronounced S-fabric (planar fabric), and commonly with a well-developed L-fabric (linear fabric) in response to intense mineral elongation (Simpson, 1986a).

2.4 Historical review of fault-rock classification

Over the years complex and frequently ambiguous classification schemes and terminology have evolved for mylonite and associated fault rocks. This is due partially to the rapid advances made in the understanding of physical processes operating in brittle and ductile fault zones. Overextended and ill-defined usage of traditional definitions and nomenclature is inappropriate when seen in the light of these modern conceptual advances.

Charles Lapworth (1885) first used the term mylonite ("milled" rock) to describe a fine-grained, well-laminated rock at Eriboll in the Moine Thrust zone of the Scottish Highlands. This original definition implied that mylonites were the products of low-temperature, high-pressure clastic milling and breakage, a view that has persisted until recently. The recrystallized texture exhibited by mylonite was attributed to subsequent post-tectonic grain growth of the fragmented material (Waters and Campbell, 1935; Higgins, 1971). To explain the presence of large, apparently undeformed porphyroclasts, extensive grain growth was invoked. Consequently complex classification schemes and terminology evolved, based on the relative amount of "milling" (cataclasis) and grain growth (Higgins, 1971; Zeck, 1974). Higgins' (1971) scheme omits important modern distinctions between brittle microcracking and ductile grain-size reduction processes, while Zeck's (1974) scheme is simply too complex for general applications (Wise *et al.*, 1984). Only recently have microstructural, petrofabric and Transmission Electron Microscopy (TEM) studies shown that the observed recrystallization is synkinematic, and that mylonites are the products of ductile flow and crystal-plastic grain-size reduction (Bell and Etheridge, 1973; White, 1973; Lister *et al.*, 1977). These studies have resulted in considerable simplification of mylonite terminology, and have enabled clearer divisions to be drawn between cataclasites and mylonites (White, 1976, 1982; Sibson, 1977; Hatcher, 1978; Takagi, 1986). Despite these advances, the need for a precise and generally acceptable definitive scheme for fault-related rocks was clear. Following the 1981 Penrose Conference on mylonites, in which the inadequacies of existing terminologies were examined (Tullis *et al.*, 1982), Wise *et al.* (1984) proposed an updated, simplified conceptual framework in which common terminology and mechanisms are accommodated. This scheme is based upon a rate-of-strain versus rate-of-recovery diagram (Fig. 4), to which the products of brittle and ductile deformation along faults are related. Elements of the systems of Higgins (1971), Sibson (1977), Hatcher (1978) and particulary that of White (1982) form the foundation of this framework. Terminology and classification criteria used in this thesis are those outlined by Wise *et al.* (*op cit.*).

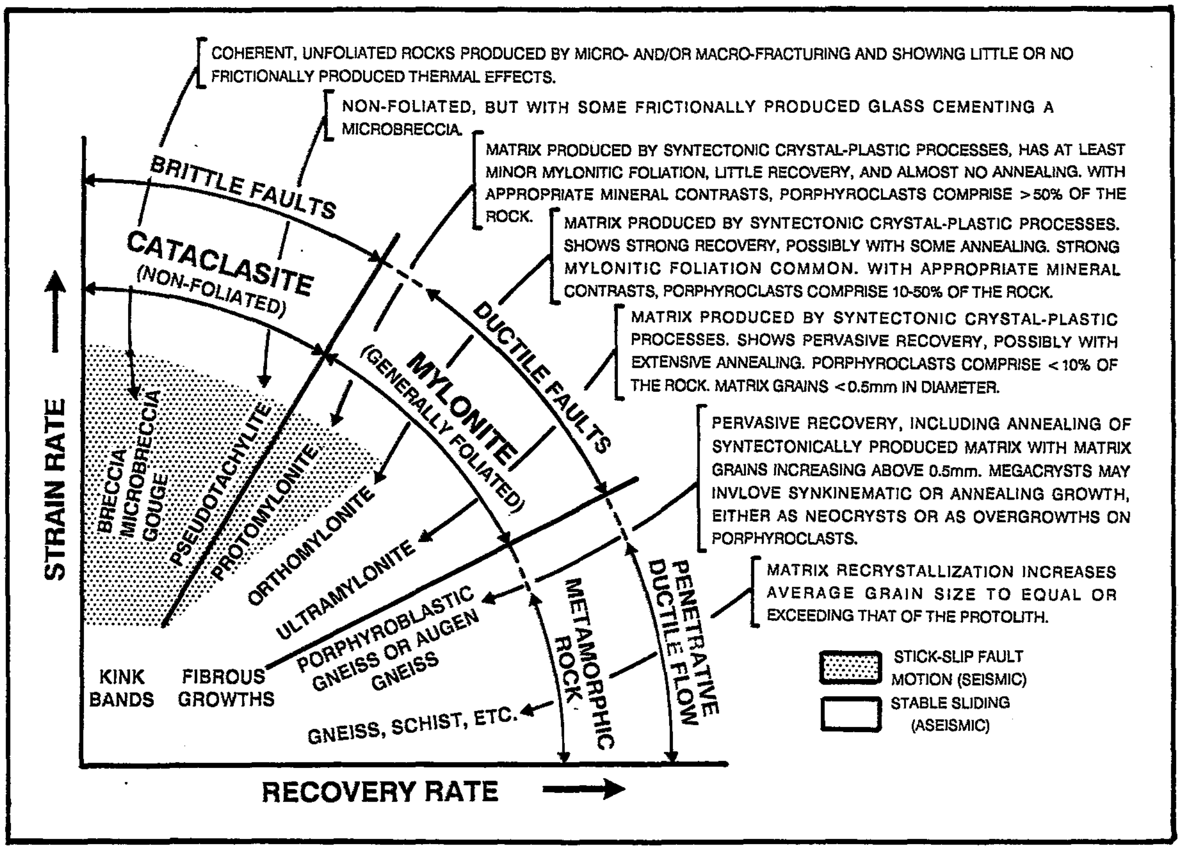

Figure 4. Fault rock classification (after Wise *et al.*, 1984). See text for explanation.

Wise *et al.* (1984), note that the texture of fault-related rocks is determined largely by competition between the strain rate and the recovery / recrystallization rate (rates are variable depending upon composition, grain size, temperature, fluids and the stress field). High strain rates at subdued temperatures, with little or no recovery, produce cataclastic rocks. Ordinary metamorphic rocks are produced when recovery / recrystallization processes dominate, regardless of large strain magnitudes. Between these two extremes is a spectrum of ductile to brittle behavioural responses with associated fault rock types.

Cataclasite series

According to Wise *et al.* (1984), cataclasites are fault rocks generated by brittle faulting at high rates of strain, and are characterized by lack of foliation with minor or no evidence of frictionally generated thermal changes. An increasing extent of microfracturing across and within grains results in the series breccia → microbreccia → fault-gouge. During rapid fault motion, microbrecciation accompanied by localised frictional heating and melting may occur. Injection of fragmentary and melted material into opened spaces, followed by quenching produces *pseudotachylite; "a highly strained but nonfoliated breccia formed from the clast-laden melt and lithified with minor amounts of glass"* (Wise *et al.*, *op cit.*; see also Wenk, 1978; Maddock, 1983)

Mylonite series

Mylonites occur when relatively high strain rates are coupled with appreciable recovery rates. The mylonite suite is characterized by a mylonitic foliation or fluxion banding developed subparallel to planes of maximum shear strain. Grain size dimunition occurs by syntectonic recrystallization associated with ductile strain or crystal-plastic processes (Bell and Etheridge, 1973; Hatcher, 1978). Large grains or crystals contained within the foliation are termed *"megacrysts."* Those formed by grain growth are termed *"porphyroblasts"*, while relict megacrysts, partially destroyed by either fragmentation or crystal plastic processes, are termed *"porphyroclasts."*

Wise *et al.* (1984) define mylonite as a general term for *"coherent rocks with at least microscopic foliation, with or without porphyroclasts, characterized by intense syntectonic crystal-plastic grain-size reduction of the country rock to an average diameter less than 0.5mm, and invariably showing at least minor syntectonic recovery / recrystallization"*.

The mylonite suite is divided into the series protomylonite → orthomylonite → ultramylonite with increasing degree of recovery and annealing processes, grain-size dimunition, foliation development, and decreasing proportion of survivor megacrysts. For fault rocks with monomineralic protoliths (e.g. quartzites and marbles) unlikely to yield megacrysts, classification according to a porphyroclast criterion is impossible. In these cases the modifier *"mylonitic"* is used e.g. mylonitic quartzite. In addition, the prefix qualifiers *"proto-"*, *"ortho-"* and *"ultra-"* are used when the degree of recovery and recrystallization is demonstrated e.g. protomylonitic quartzite.

Porphyroblastic gneiss and augen gneiss

At high recovery rates, syntectonic crystal growth processes dominate. The matrix becomes increasingly coarser grained, and porphyroblasts and augen form by the rapid growth of neocrysts, or by overgrowths of new mineral material about relict megacrysts. A megacrystic rock in which the matrix grain size exceeds 0.5 - 1.0 mm is termed a porphyroblastic gneiss or an augen gneiss, depending on the nature of its megacrysts. The traditional term *blastomylonite* is avoided because of confusion arising from differing applications of the term in the past.

The Wise *et al.* (1984) classification scheme (Fig. 4) does not offer a term for a coarse-grained fault rock produced by neocryst growth, which is devoid of megacrysts. For the purposes of this thesis the term *mylonite gneiss* (Sibson, 1977; Takagi, 1986) will be used to categorise these fault rocks.

2.5 Microstructural kinematic analysis of ductile shear zones

In the last decade considerable attention has been focussed internationally on the use of microstructures and microfabrics in mylonites and related rocks to determine the nature of deformation and the sense of shear within ductile shear zones. Integration of microstructural investigations of shear zones into regional deformation studies has helped characterize the types of strain path involved, and constrain both the movement directions and tectonic models.

2.5.1 Determination of displacement vectors and movement sense

Determination of relative displacement vectors for shallow fault zones (and sometimes ductile shear zones) across which dissimilar lithologies are juxtaposed, is a relatively simple procedure (e.g. Wheeler, 1987). Even at depth or within isotropic rock bodies, where unequivocal offset marker-layers are not always present, determination of displacement and shear sense is possible by examination of the angular relationship between the shear zone boundary and the foliation developed within the shear zone (Ramsay and Graham, 1970; Ramsay, 1980). However within wide shear zones and mylonite belts of regional significance, determination of the shear zone boundaries may not be possible, and where unequivocal field evidence is lacking, other criteria must be found to determine movement sense and direction.

2.5.1.1 Elongation lineations and the kinematic vector

Within a ductile shear zone, movement occurs in a zone of finite thickness by progressive simple shear (Ramsay and Graham, 1970; Ramsay, 1980). Total finite shear strain may reach very high values. Simple shearing leads to the progressive approach of the XY plane of the finite strain ellipsoid towards the shear plane, and the progressive approach of the principal extension axis (X) towards the movement direction (Ramsay and Graham, 1970; Ramsay, 1980). At high shear strains ($\tau \geq 10$), the XY plane of the finite strain ellipsoid coincides with the shear plane, and the extension axis (X) will parallel the movement direction (Simpson, 1986a). Commonly, penetrative LS-tectonite fabrics are developed, of which the planar element, represented by a schistosity or mylonite foliation, coincides with the XY plane and the linear element, represented by a mylonite elongation lineation, is parallel to the X axis (Fig. 6; Ramsay, 1980). Consequently, since shear strains characterize ductile shear zones, modern kinematic studies assume that the mylonite elongation lineation approximates the kinematic vector (e.g. Bryant and Reed, 1969; Escher and Watterson, 1974; Rhodes and Gayer, 1977; Williams, 1978; Brun and Burg, 1982; Coward *et al.*, 1982; Shackleton and Ries, 1984; Brunel, 1986; Coward and Ries, 1986; Ratschbacher, 1986; Ridley, 1986; Lacassin, 1987; 1989; Hansen, 1989, Merle *et al.*, 1989; Platt *et al.*, 1989).

Ductile thrusts and extensional fault zones are defined by movements orthogonal to the strike of their plane of shearing. Mylonite elongation lineations should therefore plunge down-dip within the shear plane. Conversely, strike-slip shear zones are defined by movements parallel to the strike of their shear planes, resulting in subhorizontal mylonite elongation lineations trending parallel to their strike.

Transverse stretching lineation patterns perpendicular to the regional trend are characteristic of many thrust belts, and have been described from the Scottish and Scandinavian Caledonides (Rhodes and Gayer, 1977; Williams, 1978), the Appalachians (Bryant and Reed, 1969), the Alpine orogenic belt (Malavielle and Etchecopar, 1981; Mattauer *et al.*, 1981; Brun and Burg, 1985; Lacassin, 1987, 1989), and the Himalayas (Coward *et al.*, 1982; Brunel, 1986). Similar lineation patterns have been described from metamorphic core complexes of southeastern Arizona and southern California (Davis, 1987; Bartley and Fletcher, 1990; Guérin *et al.*, 1990), where they are ascribed to extensional tectonics. Longitudinal lineation patterns parallel to the regional trend are characteristic of strike-slip orogens that often form at the post-collisional stage within orogenic belts (Shackleton and Ries, 1984). Examples of longitudinal stretching lineation patterns are found within the axial zone of the Variscan fold belt of western Europe (Brun and Burg, 1982; Shackleton and Ries, 1984), within the Caledonides of northwestern Europe (Harland, 1971), and within the Crystalline Core of the North Cascades, Washington (Brown and Talbot, 1989).

Shackleton and Ries (1984) demonstrated that stretching lineation patterns in many orogenic belts are approximately coincident with the known or inferred directions of relative plate motions. Although this simple relationship is generally faithful, locally and regionally anomalous lineation patterns do occur and these must be accounted for:-

- Brunel (1986) showed that stretch trajectories normal to the Main Central Thrust in the Himalayas describe a radial pattern, which implies that local motion does not always correspond to the average plate convergence.

- Ridley (1986) indicates that a wrench shear strain may be induced in a thrust belt if gradients in shear strain rate exist normal to the movement direction. This wrench shear strain will have the same movement direction as the thrusting, but occurs on a shear plane at right-angles to the thrust plane. The net strain is a shear strain on an inclined shear plane, which in rocks with a strong planar anisotropy may produce stretching lineations (and folds) significantly oblique to the movement direction. A possible example of this is found on Syros, Greece, where arcuate patterns of stretching lineations are developed in quartz-mica schists within a deep-level, ductile thrust belt (Ridley, 1982, 1986). Rattey and Sanderson (1982) explain similar oblique fold and lineation patterns within a thrust belt in southwestern Cornwall in terms of development within zones of differential movement within thrust sheets.

- Brun and Burg (1982) note that stretch trajectories within the Ibero-Armorican arc (France), are roughly parallel to the trend of the belt on a macroscopic scale, but become significantly oblique to this trend towards the base of each nappe. This pattern is explained by a simple shear model which combines two orthogonal thrusting and wrenching components. The increasingly oblique/transverse lineations near the basal surfaces of each nappe reflect progressive rotation of the wrench-associated longitudinal lineations towards the thrust vector in response to the intensifying thrust component. The observed strain pattern results from a corner effect produced at the intersection of a transcurrent shear zone (transform fault) and a thrust zone (convergence zone).

- The orientation of stretching lineations within transpressive shear belts is dependent on the ratio of pure shear (horizontal shortening and vertical extension) to simple shear (wrenching, strike-slip shear) (Sanderson and Marchini, 1984). Where wrenching dominates, lineations will be subhorizontal and subparallel to the wrench shear direction. Where wrenching is subordinate, lineations are steeper and more oblique to the trend of the belt. Sanderson and Marchini (1984) indicate that an important consequence of transpression characterized by crustal shortening and wrenching, is crustal thickening and uplift. Sheared and compressed material in the zone between two laterally and convergently slipping blocks will rise and flow over the tops of the blocks on oblique thrusts (Sanderson and Marchini, 1984; Ratschbacher, 1986). If one of the rigid blocks is depressed as a result of subduction / underthrusting, outward directed thrusting could be mainly single-sided (Sylvester and Smith, 1976). Ratschbacher (1986) uses an analogous transpressive model to explain the kinematic evolution of the Austro-Alpine cover nappes. Stretching lineations within the cover nappes indicate the transport direction of the oblique, transpression-related thrust sheets, suggesting that the kinematic history was not one of simple orthogonal convergence (Ratschbacher, 1986).

2.5.2 Microstructural shear sense indicators

Mylonitic rocks, which generally form within non-coaxial strain regimes (progressive simple shear), frequently contain asymmetrical microstructures and fabrics which preserve important information about the rotational component (vorticity) of the deformation. Extensive experimental modelling and research into the morphology and evolution of these microstructures and fabrics has yielded a set of "kinematic", "vorticity" or shear sense indicators that may be used with confidence to determine the sense of movement within ductile shear zones (Simpson and Schmid, 1983; Simpson, 1986b).

The set of currently accepted microstructural shear sense indicators include:-

(1) Asymmetrical porphyroclast systems and rolling structures;

(2) Pressure shadows;

(3) Spiralled inclusion fabrics;

(4) S-C fabrics and shear band foliations;

(5) Mica fish;

(6) Oblique grain-shape and subgrain-shape fabrics;

(7) Asymmetrical microfolds;

(8) Displacement of fractured rigid grains;

(9) Crystallographic preferred orientations.

In attempting to determine shear sense, and where possible the amount of shear, it is crucial to have a correctly oriented section plane. Observations are carried out on planes cut parallel to the X-axis of the finite strain ellipsoid (generally defined by the macroscopic elongation lineation) and normal to the XY-plane (generally defined by the macroscopic foliation) (Simpson and Schmid, 1983; Simpson, 1986b). The plane examined in thin-section or in outcrop surface is therefore the XZ-plane, where X, Y and Z are the principal axes of the finite strain ellipsoid ($X \geq Y \geq Z$; Ramsay and Graham, 1970; Ramsay, 1980). Oblique cuts will yield an unreliable estimate of the amount of shear, and a false impression of the shear sense.

A short review of the types of currently accepted kinematic indicators is necessary to fully appreciate the textures and microstructures illustrated and described in this thesis (Fig. 5 a to g).

2.5.2.1 Asymmetrical porphyroclast systems and rolling structures

Mylonites commonly contain relict megacrysts (porphyroclasts) of relatively rigid minerals that form augen-structures in a finer-grained, foliated matrix. Porphyroclasts frequently exhibit narrow, flattened mantles and elongate tails of either dynamically recrystallized or reaction softened material.

Two basic types of *tailed* porphyroclast systems, both exhibiting monoclinic symmetry with respect to a central reference plane (which contains the symmetry axis of the grain and the stretching axis), may be used as shear sense indicators. They are known as σ- and δ-types depending on the geometry of their tails (Passchier and Simpson, 1986; Simpson, 1986b).

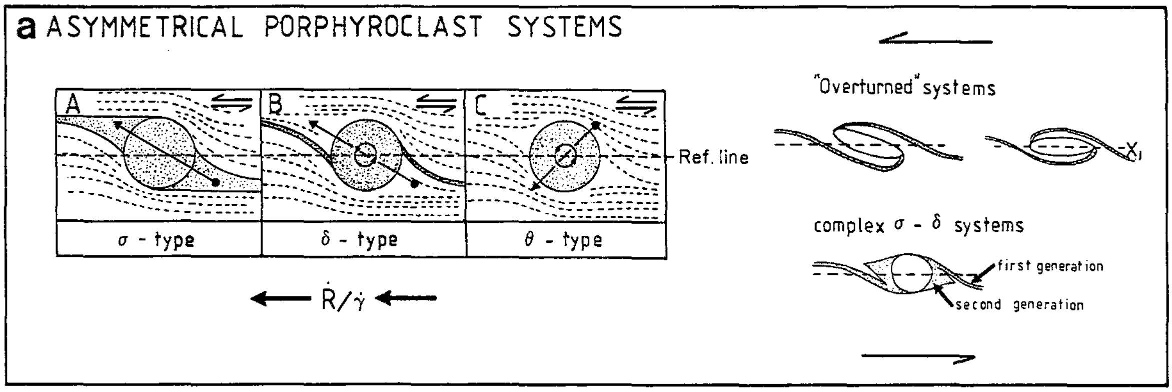

Figure 5a. Asymmetrical porphyroclast systems (after Simpson and Schmid, 1983; Passchier and Simpson, 1986; Simpson, 1986b; Hooper and Hatcher, 1988). $\dot{R}$ is the recrystallization rate, $\dot{\gamma}$ is the shear strain rate. See text for explanation.

σ-Type porphyroclast systems (A of Fig. 5a) are characterized by wedge-shaped recrystallized tails whose median lines lie on opposite sides of the reference plane at all points. The side nearest the reference plane characteristically has concave curvature whilst that farthest away is planar. σ-Types are subdivided into σ_a-types, where the porphyroclast system is isolated in a relatively homogeneous matrix, and σ_b-types where the porphyroclast system occurs in association with a shear band foliation (Passchier and Simpson, 1986; Simpson, 1986b). σ_b-Type systems are commonly feldspars associated with S-C quartz-feldspar mylonites (e.g. Berthé *et al.*, 1979). σ_b systems have planar surfaces along C-planes and tend to occur in clusters. σ-Type porphyroclast systems are thought to form at relatively low shear strains, where the rate of dynamic recrystallization ($\dot{R}$) of the porphyroclast mineral is high with respect to the shear strain rate ($\dot{\gamma}$) in the rock (Passchier and Simpson, 1986).

δ-Type porphyroclast systems or "rolling structures" (Van Den Driessche and Brun, 1987), have narrow recrystallized tails whose median lines cross the reference plane adjacent to the central porphyroclast (B of Fig. 5a). Their tails are generally thinner and longer than those of σ-types, and are characteristiclly bent with embayments of matrix material adjacent to the clast (Passchier and Simpson, 1986; Simpson, 1986b). δ-Type porphyroclast systems occur in fine grained, highly strained mylonites where the recrystallization rate ($\dot{R}$) of the porphyroclast is relatively low with respect to the shear strain rate ($\dot{\gamma}$) (Passchier and Simpson, 1986). Their geometry results from the drag of the spinning clast on the developing tails.

Based on studies of granitoid mylonites from the Grenville Province, Mawer (1987) demonstrated that δ-type porphyroclasts may develop from σ-type porphyroclasts, through a decrease in the porphyroclast aspect ratio due to dynamic recrystallization with subsequent porphyroclast rotation. Complex σ-δ type porphyroclast systems (Fig. 5a) characterized by two generations of tails, are thought to result from fluctuating $\dot{R}/\dot{\gamma}$ (Passchier and Simpson, 1986). Overturned porphyroclast systems are characterized by elongate tails which spiral around a commonly elongate central clast (Fig. 5a). Elongate or elliptical clasts tend to lie with their long axes at a low-angle to the shear plane for much of the deformation history. As deformation progresses, these clasts eventually accelerate and "flip over" to enter a new cycle of slow rotation, producing an overturned system (Passchier and Simpson, 1986).

The shear sense of σ- and δ-type porphyroclast systems can be determined by the direction in which the tails on opposite sides of the central clast *"step up"* across the reference plane. This is easily resolved provided the tails are relatively long and become parallel to the reference plane at some distance from the central clast. Where tails are short, the characteristic morphology of the systems may enable the shear sense to be determined (Passchier and Simpson, 1986; Simpson, 1986b). It should be noted that *S-shaped* σ-type asymmetry indicates the same shear sense as *Z-shaped* δ-type asymmetry (and vice versa; as indicated in Fig. 5a where a Z-shaped σ-type system (A) and a S-shaped δ-type system (B) indicate left-lateral shear sense). Without this awareness and the ability to recognize δ-type porphyroclast systems, misinterpretation of shear sense is highly likely.

A third type of asymmetrical porphyroclast system has recently been documented following a study by Hooper and Hatcher (1988) of mylonites from the Towaliga fault zone of central Georgia (C of Fig. 5a). These systems are termed Θ-type porphyroclast systems and do not possess visible tails. They do however display distinctive asymmetrical perturbations of the matrix about the central clast, resulting from "piling up" of the matrix during non-coaxial deformation (Hooper and Hatcher, 1988). The asymmetrical distribution of the perturbed zones on opposite sides of the porphyroclast may be used to determine the shear sense. A line linking the perturbed zones across the central clast will *"step down"* in the shear direction (Hooper and Hatcher, 1988). These systems are valuable vorticity indicators in mylonites where tailed systems are relatively rare, and where local interclast interference and matrix flow-field perturbations are such that very few tailed systems yield an unequivocal shear sense (Hooper and Hatcher, 1988). Θ-type systems typically develop in advanced stages of mylonitization, when ductility contrasts are large and $\dot{R}/\dot{\gamma}$ ratios are low.

2.5.2.2 Pressure shadows

In many cases when porphyroclasts remain rigid, pressure shadows (*"beards"*) of a different mineral phase (e.g. quartz) develop in low strain domains adjacent to the porphyroclast with a geometry that is identical to σ_a-type porphyroclast systems. Within these pressure shadow systems, the long axes of the quartz fibres track the incremental elongation direction through the deformation history of the rock. The sense of the rotational component of the strain path can therefore be easily determined (Ramsay and Huber, 1983; Simpson, 1986b; Etchecopar and Malavieille, 1987).

2.5.2.3 Spiralled inclusion fabrics

The traditional interpretation of spiralled inclusion trails in syntectonic porphyroblasts as evidence for porphyroblast rotation (e.g. Spry, 1963; Powell and Treagus, 1967, 1970; Rosenveld, 1970; Schoneveld, 1977; Olesen, 1982) has been brought into contention following a publication by Bell and Rubenbach, (1983) and subsequent publications by Bell and other workers (Bell, 1985, 1986; Bell *et al.*, 1986, 1989, 1992, 1992; Vernon, 1988; Bell and Johnson, 1989, 1990, 1992; Johnson, 1990; Bell and Hayward, 1991; Hayward, 1992). These researchers argue that porphyroblasts (or any rigid object), and especially equidimensional porphyroblasts (e.g. garnets), do not rotate relative to geographical coordinates during non-coaxial ductile deformation. Instead, progressive foliation transposition and/or shearing, produce changes in orientation of the external fabric with respect to the growing porphyroblast. This results in an spiral-shaped inclusion fabric which has an opposite sense of rotation to that determined by assuming that the porphyroblast rotated. Furthermore it has recently become apparent that porphyroblasts grow much faster than previously realized ($<10^5$ years), and therefore develop extremely rapidly with respect to progressive deformation (Cashman and Ferry, 1988; Walther and Wood, 1984). This has the important implication that many spiralled inclusion fabrics probably represent overgrowths onto syntectonic crenulation patterns (Barker, 1990, p96). Consequently it is apparent that the reliability of spiralled inclusion fabrics as kinematic indicators is in doubt, and their use is not recommended until the current controversy is resolved.

Although it is beyond the scope of this thesis to review or resolve aspects of the present debate regarding rotation (e.g. Passchier *et al.*, 1992) or non-rotation (e.g. Bell *et al.*, 1992; Bell and Johnson, 1992) of rigid objects during non-coaxial ductile deformation, it is necessary to define the author's stance with regard to the dispute since aspects of the contention bear directly on the interpretation of microstructures encountered in mylonites of the HRTB. For the purposes of interpretation of contentious microstructures such as δ- and Θ-type porphyroclast systems ("rolling structures") I have through an "intuitive prejudice" (see Bell and Johnson, 1990) taken the position of the rotational school. My conviction in no way denies the possibility that these structures formed by non-rotation, *and more importantly it does not influence the overall shear sense derived from the microstructure* (no porphyroblasts containing spiralled inclusion fabrics were encountered in this study).

2.5.2.4 S-C composite planar fabrics and shear band foliations

Mylonites and phyllonites (mylonitic rocks rich in phyllosilicates) that have been deformed by intense, non-coaxial shearing commonly display two fabrics that are demonstrably synchronous (e.g. Berthé *et al.*, 1979; Jegouzo, 1980; Lister and Snoke, 1984; Mawer and White, 1987; Vauchez, 1987). These composite planar fabrics are known as *S-C fabrics* and comprise C- (cisaillement: French for shear) surfaces subparallel to the shear zone margin, and S- (schistosité: French for foliation) surfaces oblique to this (Berthé *et al.*, 1979; Simpson and Schmid, 1983) (Fig. 5b). The S-surfaces are related to the accumulation of finite strain and correspond to the flattening (XY) plane of the finite strain ellipsoid (Ramsay and Graham, 1970; Berthé *et al.*, 1979; Ramsay, 1980; Lister and Snoke, 1984). The C-surfaces are related to localized high shear strains, and are discrete slip surfaces coinciding with the flow plane of simple shear (Simpson and Schmid, 1983; Lister and Snoke, 1984; Simpson, 1986b).

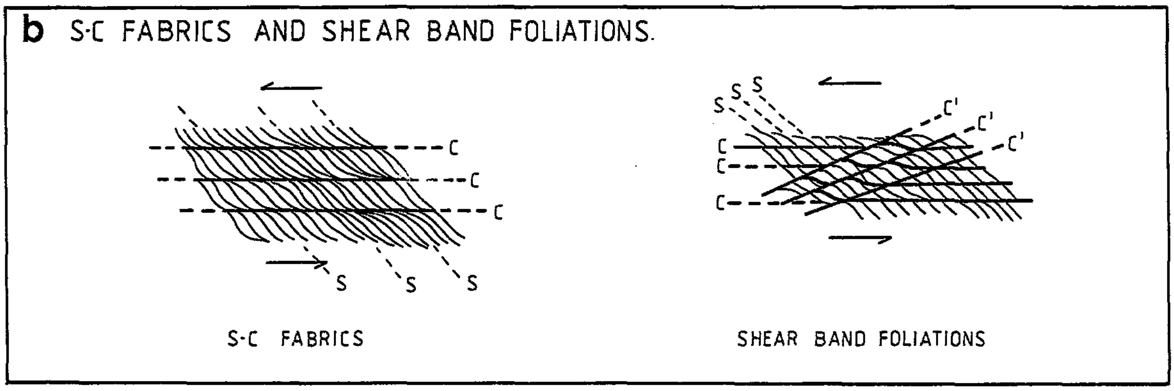

Figure 5b. S-C fabrics and shear band foliations (after Berthé *et al.*, 1979; Simpson and Schmid, 1983; Lister and Snoke, 1984; Simpson, 1986b). See text for explanation.

The S-fabric develops at an angle (α) of about 45° to the C-fabric, but rotates towards sub-parallelism with the C-plane as shearing progresses (Berthé *et al.*, 1979; Ramsay and Graham, 1970; Ramsay, 1980; Simpson, 1984). The density of C-surfaces increases with decreasing α (Berthé *et al.*, 1979; Simpson, 1984). At high shear strains ($\gamma > 10$) the S-surfaces and C-surfaces coincide, resulting in an ultramylonite with a single planar fabric (CS-surfaces) (Berthé *et al.*, 1979; Simpson, 1986b).

S-surfaces curve sigmoidally into the C-surfaces (commonly with an associated reduction in grain size), so that the acute angle between the two surfaces defines the shear sense (White *et al.*, 1980; Simpson and Schmid, 1983; Simpson, 1986b). Intersection lines of S- and C-surfaces are invariably sub-perpendicular to the elongation lineation in the rock, and maximum shear sense information is obtained by viewing samples or outcrops down the S-C intersection lines (Simpson, 1986b).

The relatively simple geometry of S-C fabrics is frequently complicated by secondary planar fabrics developed later in the deformation history. These are commonly antithetic to the orientation of the S-surfaces, and are usually more pronounced (Fig. 5b). They are known as *C'-fabrics* (Ponce de Leon and Choukroune, 1980) or *extensional crenulation cleavages* (Platt, 1979; Platt and Vissers, 1980; Platt, 1984), and are thought to result from heterogeneous strain concentrations at a late stage during mylonitization (Berthé *et al.*, 1979, White *et al.*, 1980; Weijermars and Rondeel, 1984). C'-fabrics characteristically exhibit a consistent angular relationship to the shear zone boundaries and rotated early foliations (Weijermars and Rondeel, 1984). Within thrust zones, C'-surfaces characteristically dip towards the foreland, and are therefore useful for determination of the bulk transport vector (Barker, 1990). Shear sense is determined in the same way as for S-C fabrics.

The term *shear band* or *shear band foliation*, is used to define very small-scale, discrete, highly-sheared surfaces within mylonitic rocks, that deflect some pre-existing planar anisotropy (White *et al.*, 1980; Simpson, 1986b). The term is applicable to both C- and C'-surfaces and does not imply a specific orientation. Simpson (1986b) suggests that the term be used as a general description whenever the relative ages of the two foliations is ambiguous, or when one foliation is demonstrably of a different origin. Several models have been proposed for the development of shear band foliations based on their orientation with respect to the shear zone boundaries and finite strain axes, and the relative ages of the shear bands and the deflected planar fabric (Berthé *et al.*, 1979; Platt, 1979; Platt and Vissers, 1980; Platt, 1984; Vernon *et al.*, 1983; Lister and Snoke, 1984; Shimamoto, 1989). A complete review of these models is beyond the scope of this summary, and interested readers are referred to the publications cited above.

Conjugate sets of shear bands with opposing sets of shear occasionally occur within mylonite zones and are thought to indicate a strong component of coaxial flattening across the zone (Platt and Vissers, 1980). However, Harris and Cobbold (1984), using a plasticine model, demonstrated that conjugate systems may occur in simple shear if sliding occurs along foliation planes.

Dennis and Secor (1987) documented two sets of oblique crenulations associated with a major dextral shear zone within the Southern Appalachian Piedmont. These crenulations are called *normal- and reverse-slip crenulations* (hereafter referred to as NSC and RSC; Fig. 5c) and form in response to slip on along preexisting foliation planes (Dennis and Secor, 1987). Using a mathematical model supported by examples and data from the Irmo shear zone, Dennis and Secor (*op cit.*) demonstrated that NSC and RSC serve to maintain the initial thickness of the shear zone, by compensating for displacement components of foliation slip normal to the bulk movement direction of the zone. NSC are analogous to the S-C fabrics (Berthé *et al.*, 1979; Simpson and Schmid, 1983; Lister and Snoke, 1984), shear bands (White *et al.*, 1980), and extensional crenulation cleavage (Platt, 1979; Platt and Vissers, 1980) described above. RSC occur as rootless, intrafolial folds of foliation contained within lens shaped pods with the same vergence as the main shear zone (Fig. 5c). NSC and RSC form as a result of slip along foliation orientated at a clockwise and counter-clockwise acute angle respectively to the displacement direction (Fig. 5c; Dennis and Secor, 1987). NSC and RSC are reliable shear sense indicators as a result of their unique morphology, and consistent geometrical relationship with respect to the folia along which slip is inferred.

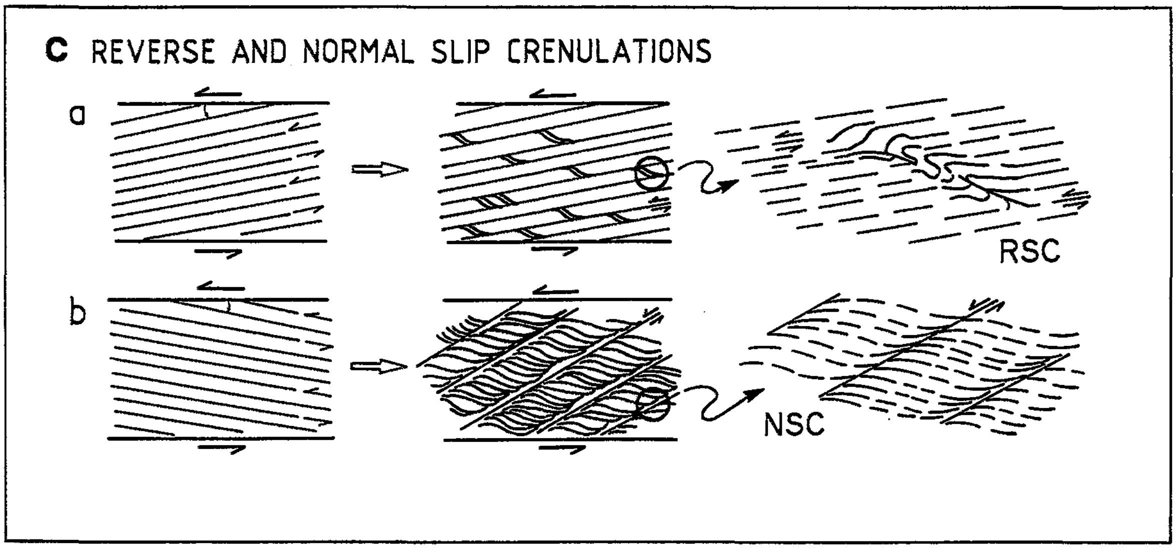

Figure 5c. Stylized sketch showing the development of (a) reverse slip crenulations (**RSC**) and (b) normal slip crenulations (**NSC**) (after Dennis and Secor, 1987). See text for explanation.

2.5.2.5 Mica fish

Lozenge-shaped "mica fish" (Fig. 5d) are common in phyllonites and S-C mylonites, and result from the deformation of large porphyroclasts, or early porphyroblasts of mica, through a combination of brittle and crystal-plastic processes (Eisbacher, 1970; Lister and Snoke, 1984). The asymmetrical geometry of mica fish, with (001) planes oriented at a low-angle to the main mylonite foliation (facing the incremental shortening direction), and with elongate recrystallized tails of fine-grained mica extended parallel to the flow plane, is consistent with that of σ-type porphyroclast systems (Simpson, 1986b). Shear sense is determined in the same way as for σ-type porphyroclast systems. Mica fish are often linked by their recrystallized tails, resulting in a stair-stepping geometry (Lister and Snoke, 1984). The "fish" step-up in the direction of shear. Multiplication of mica-fish occurs by a process of fragmentation and dispersion of large early micas (Lister and Snoke, 1984).

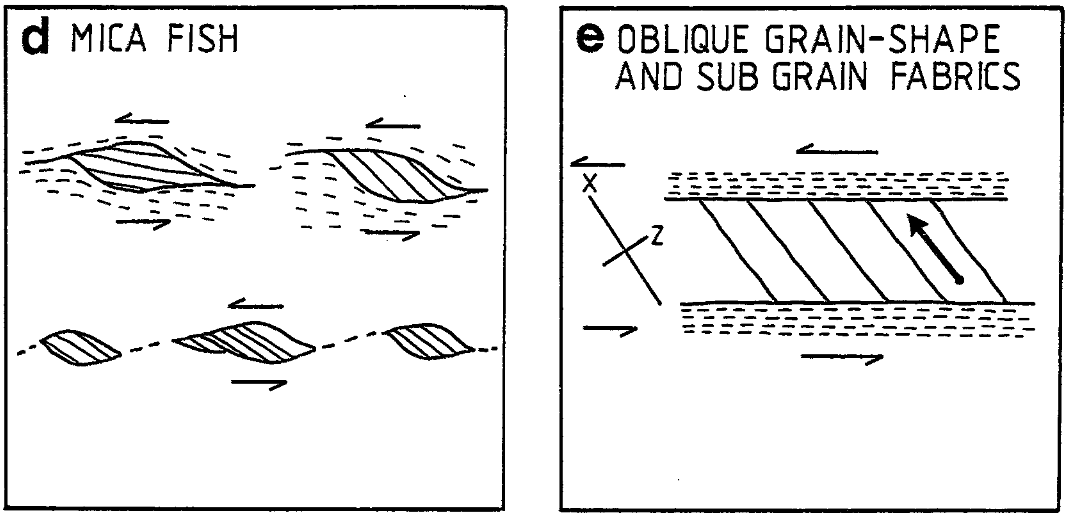

Figure 5 d and e. (d) Mica fish (after Lister and Snoke, 1984; Barker, 1990). Note the stair-stepping geometry of the linked mica fish in the lower illustration. See text for explanation.
(e) Oblique grain-shape and subgrain fabrics (after Simpson and Schmid, 1983; Simpson, 1986b). **X** and **Z** indicate the major and minor axes of the incremental strain ellipsoid respectively. See text for explanation.

2.5.2.6 Grain-shape and subgrain-shape fabrics

Within monomineralic bands in quartzo-feldspathic mylonites and highly sheared carbonate rocks, a secondary fabric, inclined obliquely to the main foliation, is commonly observed (e.g. Brunel, 1980; Schmid *et al.*, 1981, 1987; Law *et al.*, 1984, 1986, 1990; Lister and Snoke, 1984; Culshaw, 1987). This secondary fabric is usually observable only in thin section, and is defined by elongate recrystallized grains and subgrains. Recrystallization processes, involving grain boundary migration and the progressive rotation of subgrains, coupled with strain-induced slip of lattice dislocations during crystal-plastic deformation, produce elongate new grains aligned with their long-axes parallel to the incremental stretching direction (Simpson, 1986b). The acute angle formed by the intersection of the secondary fabric and the main foliation points in the shear direction (Fig. 5e).

These secondary shape-fabrics are thought to form late during progressive shearing, and consequently are only reliable kinematic indicators for the final increment of deformation (Simpson and Schmid, 1983; Simpson, 1986b). Furthermore, grain-shape and subgrain-shape preferred orientations are easily reset by subsequent folding events (Simpson, 1986b). Therefore, shear sense determinations made using these secondary fabrics should be evaluated with caution.

Within mylonitic rocks with a high content of evenly dispersed, fine-grained mica, a further type of secondary foliation may develop where reorientation of mica flakes occurs such that their (001) planes face the direction of maximum incremental shortening. Provided the rock has a relatively uniform grain size and few porphyroclasts, the secondary mica (001) foliation will have a regular orientation that reflects the overall movement sense for the final stages of deformation (Simpson, 1986b).

Throughout this study grain shape fabrics are commonly referred to as *dimensional preferred orientations*, which is usually abbreviated to DPO's.

2.5.2.7 Asymmetrical microfolds

Local perturbations in the flow regime in mylonites may amplify into asymmetric microfolds whose vergence is consistent with the sense of shear of the mylonite zone (Fig. 5f) (Simpson, 1986b). However, it is important to remember that late-stage folding of mylonitic layering is not the only mechanism that may result in asymmetrical microfolds. Discordant dykelets, having an initial oblique orientation with respect to the shear zone margins, will become folded in such a way that asymmetrical parasitic microfolds displaying the incorrect vergence may develop (for full treatment of this problem see Simpson, 1986b). Consequently, unless the relationship of the folded layering to the shear zone flow-plane is known, shear sense determinations using asymmetrical microfolds should be treated with caution.

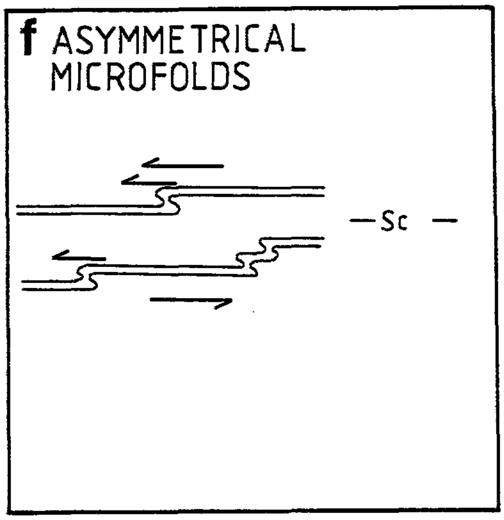

Figure 5f. Asymmetrical microfolds (after Simpson, 1986b). See text for explanation.

2.5.2.8 Displacement of fractured rigid grains

Rigid minerals (e.g. feldspar) in a deforming ductile matrix are often unable to accommodate strain by crystal-plastic mechanisms and instead undergo brittle fracturing. The fractures may initate and propogate through the grain, as extension fractures along the XY plane of the bulk strain ellipsoid, or along specific crystallographic planes (Simpson, 1986b). Consequently the fractures will have a variable initial fracture angle (α) with respect to the flow plane (Fig. 5g). As shear deformation proceeds the rigid grain will rotate, and the presence of fractures allows the grain to extend along the flow direction. The sense of offset along internal microfaults produced in this manner, will depend on the initial fracture angle (α) and the amount of rotation (Fig. 5g):

- At low α values with respect to the flow plane (0-35°, 165-180°), "detachment" or "thrust" type microfaults result, with offsets synthetic with the bulk shear sense of the shear zone (Fig. 5g a and b).

- At intermediate to high values of α with respect to the flow plane (45-135°), high angle reverse, and more commonly, high angle normal microfaults will result, with offsets *antithetic* to the bulk shear sense (c of Fig. 5g, and stage 1 of d of Fig. 5g).

- Those fractures that initiate at a fairly high α value with respect to the flow plane (45-90°), could conceivably rotate through 45° into a low angle orientation and change their sense of offset from antithetic to synthetic (d of Fig. 5g - stages 2 and 3).

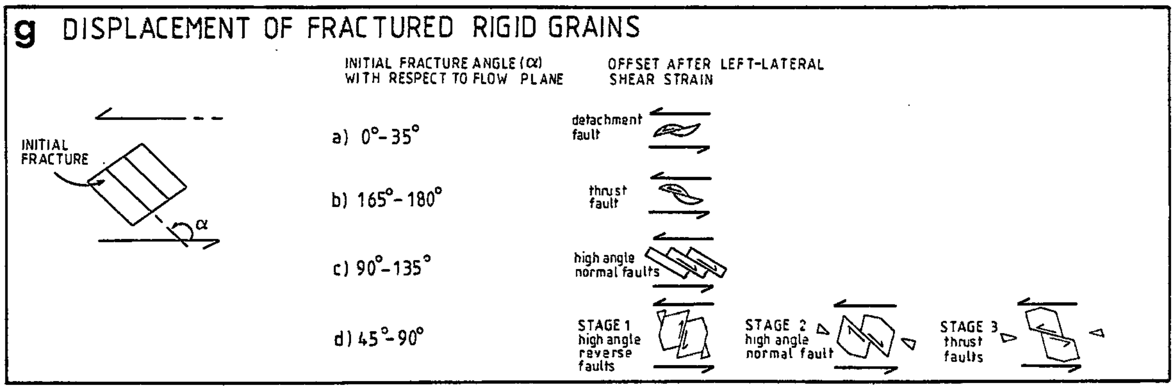

Figure 5g. Displacement of fractured rigid grains (after Simpson, 1986b). See text for explanation.

Thus, Simpson (1986b) recommends that only those offset fractures that either have high-angles (45-135°), or very low-angles (<20° or >165°) to the flow plane, should be used.

2.5.2.9 Crystallographic fabric asymmetry

Many minerals (e.g. quartz, calcite, olivine) develop strong crystallographic or lattice preferred orientations (LPO) in highly deformed mylonitic rocks. Following early work by Nicolas *et al.* (1971) on peridotites, many workers have analysed LPO when studying the kinematics of ductile deformation. In particular, the asymmetry of quartz c-axes with respect to the macroscopic fabric axes of shear zones has been extensively researched and discussed (e.g. Carreras *et al.*, 1977; Lister and Price, 1978; Lister and Williams, 1979; Brunel, 1980; White *et al.*, 1980; Lister and Hobbs, 1980; Behrmann and Platt, 1982; Lister and Dornsiepen, 1982; Passchier, 1983; Simpson and Schmid, 1983; Lister and Snoke, 1984; Vissers, 1989; Law *et al.*, 1990; Ralser, 1990).

Etchecopar and Vasseur (1987) note that the obliquity of LPO in olivine with respect to macroscopic fabric elements, reflects rotational deformation and may be used to determine shear sense. Wenk *et al.* (1987) describe how LPO in calcite marbles can be used to determine shear sense, to estimate finite strain, and to differentiate between pure and simple shear.

In recent years it has become common practice to study quartz c-axis fabrics when interpreting the shear sense in mylonite zones (e.g. Watts and Williams, 1979; Evans and White, 1984; Law *et al.*, 1984, 1986; Kelley and Powell, 1985, Brunel, 1986; Culshaw, 1987; Lacassin, 1987; Vauchez and Brunel, 1988; Hansen, 1989; Gibson, 1990; Schulmann, 1990). A full treatment of the use of asymmetric quartz c-axis patterns as a kinematic indicator is beyond the scope of this chapter, and the reader is referred to the above publications.

Kinematic studies reliant on analysis of quartz c-axis patterns make use of a computer assisted texture goniometer, since manual measurement using a universal stage is an extremely time-consuming procedure. Noting this, in addition to the potential for ambiguity arising from sampling local zones of heterogeneous strain, Simpson (1986b) suggests that the technique is perhaps "best left as a last resort". Lack of ready access to a sophisticated analytical instrument precluded the use of quartz c-axes as a kinematic indicator in this investigation.

2.6 Methods of microstructural kinematic analysis employed in this study

2.6.1 Selection of shear zones for analysis

Isolation of shear zones for examination was performed on the basis of their relative importance as potential terrane boundaries. Consequently shear zones chosen for analysis include the Neusspruit Lineament, the Kakamas Shear Zone (KSZ), the Rozynenbosch-Ganzenmond Shear Zone (RGSZ), and selected shear zones of the Hugosput Shear System (HSS) and the Graafwater Shear System (GSS).

2.6.2 Sample collection

A representative suite of 62 orientated samples of protomylonite, mylonite, ultramylonite, mylonite gneiss, porphyroblastic gneiss and augen gneiss were collected from several localities on the selected shear zones of the HRTB. Sample localities were selected on the basis of good exposure of mylonitic rocks. Sample localities are indicated in Figure 2 and Figure 3.

Selection of representative specimens, containing kinematically useful fabrics and microstructures, was often frustrated in the field by the extremely fine-grained nature of the mylonites. Wherever possible, samples were collected from mylonitic layers characterized by extreme ductility contrasts between component mineral species, as this property promotes the development of indicator fabrics. This property is best expressed in quartzo-feldspathic lithologies, and consequently the suite of samples is dominated by quartz-feldspar mylonites. Quartz-deficient amphibolitic protoliths lack the ductility contrast required for production of strong indicator fabrics, and so relatively few of these were collected. Care was taken in the sampling procedure to avoid zones disrupted by minor folding or late brittle fractures, in order to circumvent problems related to local reorientation of the mylonite fabrics .

At each sample station the orientation of the local mylonite linear (L_M) and planar (S_M) fabrics were recorded, to enable determination of geometric relationships between these fabrics and internal microstructures. Specimens were orientated by marking a strike-arrow and dip-tick on the exposed upper mylonite foliation surface, whilst the specimen was still in its correct outcrop position and attitude (Fig. 6a). Dip amount was measured, and strike and dip values were recorded both on the sample and in the field notebook. For consistency, a right-hand convention between the strike and dip direction was adopted. In instances where the mylonite elongation lineation was not discernible within exposed foliation surfaces, measurement of the L_M fabric orientation was accomplished during the sample-sectioning stage.

2.6.3 Sample preparation

Oriented thin-sections and polished slabs of the samples comprise the raw-material for microstructural kinematic analysis. Sections were carefully selected to maximise the kinematic information to be gained from individual samples. To enable accurate three-dimensional reconstruction of directional fabric shape and finite strain data, three mutually-perpendicular oriented sections were cut from each sample. The three sections have a systematic geometrical relationship to penetrative mylonite fabric elements, and consequently to the strain axes of the finite strain ellipsoid.

a) XZ- sample section: parallel to the mylonite elongation lineation (L_M) and normal to the principal mylonite foliation (S_M),

b) YZ (or YZ') - sample section: normal to both L_M and S_M,

c) XY (or X'Y) - sample section: within the S_M plane.

The use of X, Y and Z above refers to an orthogonal reference system that is defined as the Z axis being perpendicular to the principal mylonitic foliation (S_M), and the Y axis lying within the plane of S_M and perpendicular to the mylonite elongation lineation (L_M = X) . This coordinate system does not implicitly assume a parallelism with the principal axes of the finite strain ellipsoid, since the principal mylonite foliation may be represented by either cissaillement (C) or schistosity (S) surfaces (Berthé *et al.*, 1979), depending on the relative intensity of these composite planar fabrics. For the case of S_M represented by the schistosity, the X, Y and Z coordinate axes coincide with the finite strain ellipsoid axes, and the sample sections approximate the three principal planes of the finite strain ellipsoid (XY, XZ and YZ) (Ramsay and Graham, 1970). For S_M represented by the cissaillement, the X, Y and Z coordinate axes *do not coincide exactly with the finite strain axes*, and only the XZ sample section corresponds to a principal plane of the finite strain ellipsoid. The remaining two sample sections are denoted X'Y and YZ' and reflect oblique cuts through the finite strain ellipsoid, containing the intermediate (Y) and minimum (Z) finite strain axes respectively.

Figure 6b illustrates the geometric relationships between the three orthogonal sections of the orientated specimen, typical internal mylonitic fabric elements and micostructures, and the principal axes of the finite strain ellipsoid (X, Y and Z). Typical fabric elements of HRTB mylonites include a composite S-C planar fabric preserved within the XZ section, a principal mylonitic foliation S_M (in this case corresponding to the cissaillement of the S-C fabric, and coplanar with the X'Y section), and a mylonite elongation lineation L_M within the S_M plane. Figure 6c is a stereographic representation of the geometric relationships between the typical mylonite L_M and S_M fabrics, and the three orthogonal sections prepared from the oriented specimen. The kinematic vector coincides with L_M, and is represented by a split-circle which describes the inferred movement sense. In the example shown (Fig. 6), movement sense is oblique reverse, with hangingwall movement towards the south.

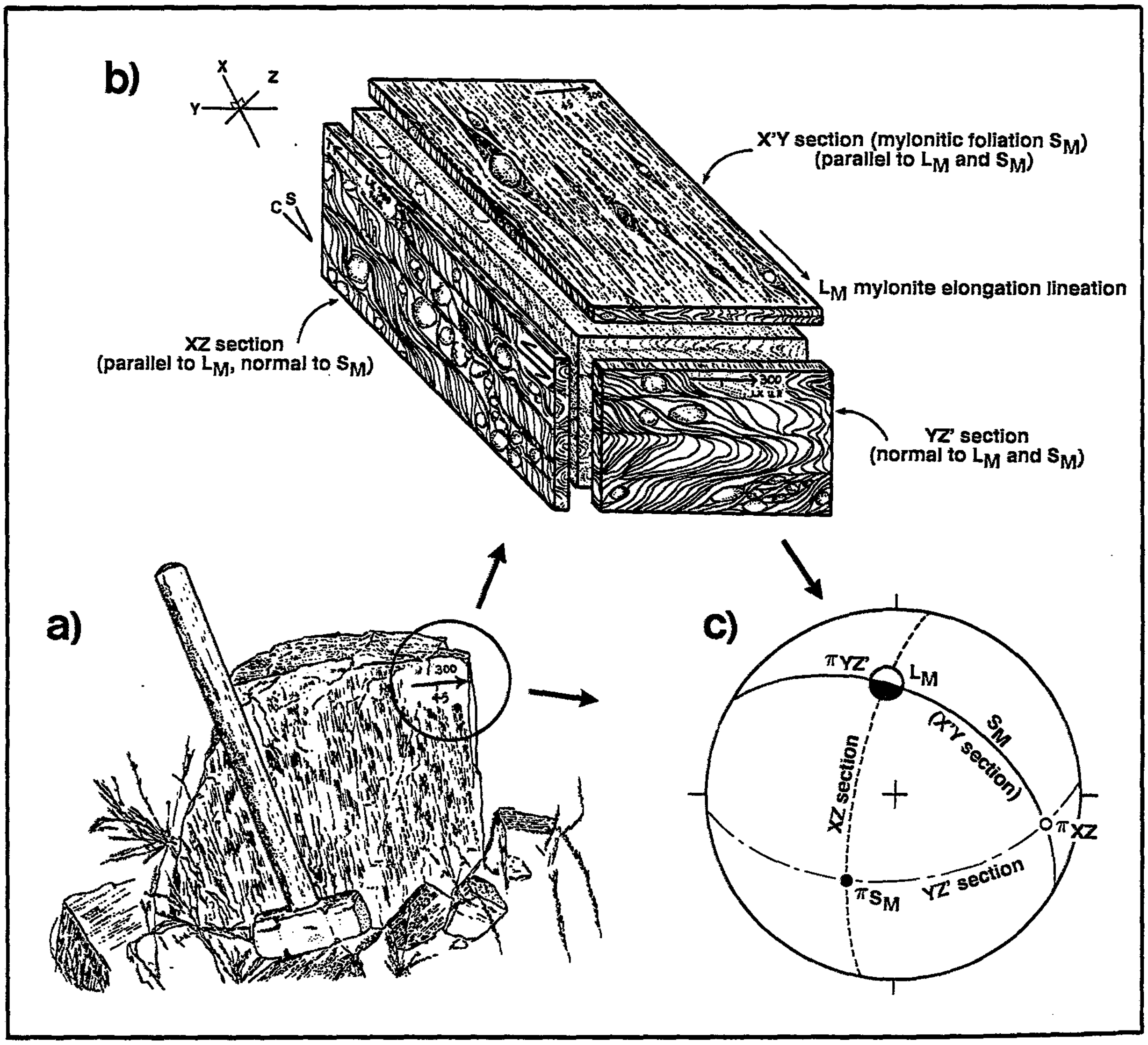

Figure 6. (a) Sketch illustrating the collection of an oriented specimen of mylonite from an outcrop exhibiting a pronounced down-dip mylonite elongation lineation. (b) Stylized block diagram illustrating the geometric relationships between the three orthogonal sections of the oriented specimen, typical internal mylonitic fabric-elements and microstructures, and the principal axes of the finite strain ellipsoid (X, Y and Z). Shear sense determinations are always made within XZ-sections (parallel to L_M, normal to S_M) since oblique cuts will give a false impression of the shear sense (Simpson and Schmid, 1983). (c) Stereographic representation of the geometric relationship between the typical mesoscopic mylonite fabric elements (S_M and L_M) measured in the field, and the three orthogonal sections prepared from the oriented specimen (shown in (b)). The filled and open circles represent poles to S_M (X'Y section) and the XZ section respectively. The large split circle symbol indicates the orientation of L_M, and therefore the kinematic vector. Movement sense determined from the XZ section is indicated by means of a half-filled circle, the filled part of the circle signifying the down-dropped side.

2.6.4 Movement sense determination

Sections cut parallel to the mylonite elongation lineation (L_M) and normal to the mylonite foliation (S_M), represent the XZ-plane of the local finite strain ellipsoid (Ramsay and Graham, 1970; Ramsay, 1980). These sections (hereafter referred to as XZ-sections) represent an observation plane that contains the movement direction and is perpendicular to the movement plane. Consequently XZ-sections yield the greatest, and most reliable, kinematic information. Oblique cuts were avoided, as they give an unreliable assessment of the amount of shear that has taken place, and can give a false impression of the shear sense. For all samples, XZ-sections were examined for microstructural shear sense indicators using conventional petrographic techniques, and where possible the movement sense was determined.

Cognizance of the effect that optical systems in various petrographic microscopes may have on altering the orientation and symmetry of the image at the objective, is essential to avoid misinterpretation of shear sense. Most microscope optics perform a left-right reversal, such that left-lateral asymmetry in the object translates to right-lateral asymmetry in the objective image, and vice versa. Furthermore, some microscopes rotate the plane of the image through a complimentary angle so that the object appears inverted. Consequently it is necessary to establish the exact optical translation for a particular microscope, and then apply the reverse translation as a correction during determination of asymmetry, vorticity or shear sense.

2.6.5 Confidence-index for microstructural kinematic interpretations

Microstructural kinematic analysis is by nature a rather subjective undertaking, and consequently problems relating to quantification and objectivity frequently arise. To begin with, some microstructural indicator types are more consistently interpretable than others. Furthermore many lithologies do not develop or preserve microstructures that are useful for kinematic analysis. Ductile shear zones usually have complex strain histories and movements may persist over prolonged periods. This may result in cryptic resetting and overprinting of kinematic fabrics. Also ductile shear zones are generally wide, and mylonites may develop in a variety of lithologies having different mechanical properties. Thus the potential for lithologically controlled strain-localization is great. All these factors may result in incorrect or ambiguous kinematic interpretations. To overcome these problems a numerical system has been devised for this study, based on a similar system proposed by Hansen (1989), which provides a measure of confidence for the kinematic interpretation made at single, one sample stations.

The kinematic confidence-index (hereafter referred to as KCI) is based on:

- the indicator type,
- the clarity and intensity of development of the indicator fabric,
- the variety of independent indicators that are preserved within samples from a single sample station.

The confidence-index ranges from 0 to 3. A rating of 0 indicates that no kinematic interpretation was possible. A rating of 1 indicates a potentially ambiguous interpretation, 2 a moderately reliable interpretation, and 3 a trustworthy interpretation.

The purpose of the system is not to provide an absolute confidence scale that can be used objectively by a number of independent researchers, but rather to establish a statistic whereby the author could compare the quality of his own kinematic interpretations across the study area.

2.6.6 Calculation of kinematic vector means and the mean mylonite plane

To minimize the effects of localized refolding of the mylonite zones, the mylonite fabric orientation data from each sample locality were pooled for sample areas of limited strike extent, and analysed independently. For each sample area with multiple L_M and S_M fabric orientation data, a computer program (VSTAT) was used to define the populations in terms of various vector statistical parameters, determined by eigenvalue analysis (Charlesworth *et al.*, 1976; Woodcock, 1977). Within each sampling area the computed hemispherical vector mean of the L_M orientation data was taken as representative of the orientation of the kinematic vector. The S_M orientation data populations for each sampling area were tested for folding using vector statistical procedures, and where appropriate, best-fit fold axes were computed. If the sampling area proved to be unaffected by folding, a hemispherical vector mean orientation for the S_M plane was determined.

2.6.7 Definition of the dip-slip to strike-slip ratio

Dip-slip ductile shear zones are characterized by down-dip elongation, while strike-parallel elongation is characteristic of strike-slip zones (Ramsay and Graham, 1970). A ratio ds:ss, expressing the degree of obliquity of the mylonite elongation lineation (L_M) with respect to the strike of the mylonite foliation (S_M), is used in this study to characterize the relative dominance of either dip-slip or strike-slip movements within the mylonite plane. The ds:ss ratio is calculated as follows:-

$$ds:ss = \tan (\text{rake of } L_M \text{ in } S_M \text{ plane})$$

- For dip-slip dominated shear zones: $1 < ds:ss < \text{infinity}$;
- For strike-slip dominated shear zones: $0 \leq ds:ss < 1$;
- When dip-slip component = strike-slip component: $ds:ss = 1$.

2.6.8 Note on terrane nomenclature used in this study

Explanation of tectonostratigraphic terrane nomenclature and terminology used in this thesis is necessary to avoid the inherent pitfalls of overextended, unselective and ill-defined usage (see Hudson, 1987; Dover, 1990; Sengör, 1991). Where possible, generalized terrane terminology is avoided, and instead use is made of well-established tectonic and stratigraphic vocabulary by which specific geological entities and situations can be more precisely defined. To avoid confusion regarding the existing terrane nomenclature employed in northeastern Namaqualand, I have adopted the current terrane names and subdivisions *in a purely descriptive sense*. Where existing terrane designations are used in this thesis, *no genetic implication is intended*, and the author *does not necessarily support the terrane status nor the proposed origins of these crustal fragments as envisioned or implied by previous workers.*

Chapter 3. - The Neusspruit Lineament

Twelve oriented samples of mylonite, mylonite gneiss and augen gneiss were collected from two localities on the Lineament in the Kakamas area. Sample localities are indicated in Figure 1 and 7.

At *Neuspoort*, 12km east of Kakamas on the Upington road, two oriented samples of orthomylonitic feldspathic quartzite (*Goedehoop Formation*) were collected away from zones of late extensional shear deformation. A single oriented sample of magnetite-bearing, mylonitic amphibolite gneiss was collected from the *Puntsit Formation*, structurally underlying the *Goedehoop Formation* quartzites at the same locality.

The second sample locality is situated approximately 15km southeast of Neuspoort, near *Sonopeiland* on the south bank of the Orange River. Eight oriented samples of mylonitic calc-silicate, amphibolite, quartzo-feldspathic gneiss and biotite augen gneiss were collected at this locality.

3.1 Mesostructure

3.1.1 Neuspoort locality

At Neuspoort, orthomylonitic quartzites are developed within rocks of the *Goedehoop Formation*. L_M-S_M mylonite fabrics are distinct within the orthomylonitic quartzites, and the penetrative S_M fabric imparts a highly-foliated, "platy" character to the rocks, as described by previous workers (e.g. Van Bever Donker 1980, 1983). The mylonite elongation lineation L_M, defined by stretched quartz ribbons and streaks of phyllosilicates, plunges down-dip by 50° within the NE-dipping S_M plane (rake of L_M in foliation = 85°, ds:ss = 11.4). No evidence of strike-parallel elongation was observed at this locality.

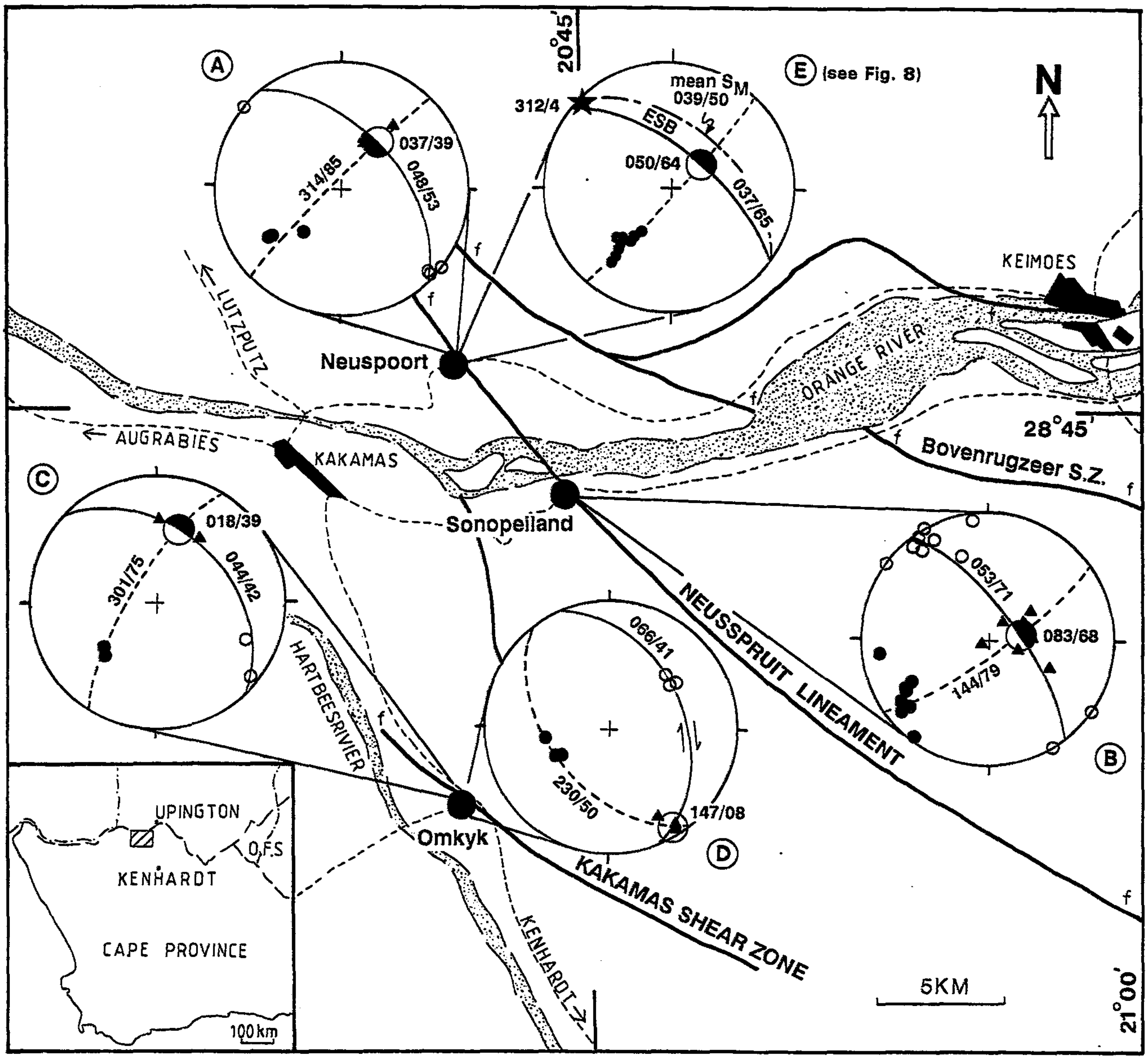

Figure 7. Compilation of kinematic interpretations of microstructural and mesostructural data from the Neuspoort and Sonopeiland localities on the Neusspruit Lineament, and from the Omkyk locality on the Kakamas Shear Zone. Lower-hemisphere stereoprojections show poles to mylonitic foliation (solid circles), poles to XZ sections (open circles) and mylonite elongation lineations (solid triangles). Mean S_M planes are shown as solid great-circles, and mean XZ sections are shown as dashed great-circles. Calculated kinematic vectors with relative dip-slip component of shear are indicated by large split-circle symbols; filled half marks down-dropped side. Shear arrows indicate the sense of relative strike-slip translation. Stereogram E shows structural and fabric data adjacent to, and within an ESB at Neuspoort. Filled circles indicate poles to S_M, and the dashed great-circle indicates the computed best-fit girdle to the planar dispersion of S_M poles. The statistical shear band crenulation axis is indicated by the star. The inferred kinematic vector is indicated by the split-circle; filled half marks down-dropped side.

3.1.1.1 Late extensional shear bands

At Neuspoort, widely-spaced extensional shear bands (ESB) are observed cross-cutting and disrupting the well-developed L_M-S_M fabrics within the orthomylonitic quartzites. Figure 8b is a schematic three-dimensional diagram, illustrating the in-situ geometry of these structures. Fabric and structural data from a single shear band are presented stereographically in Figure 8a.

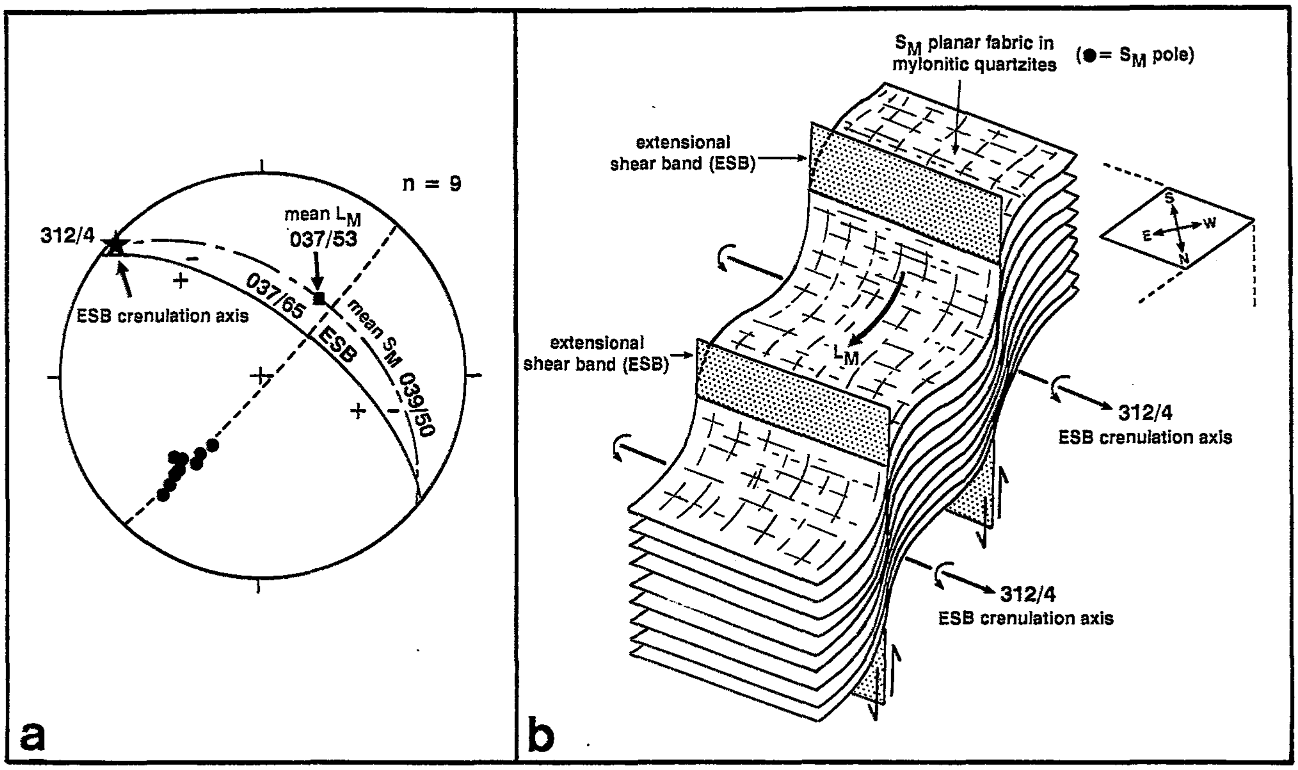

Figure 8. (a) Stereographic projection of structural and fabric data adjacent to, and within an extensional shear band (**ESB**) at Neuspoort, Neusspruit Lineament. Filled circles indicate poles to S_M, and the dashed great circle indicates the computed best-fit girdle to the planar dispersion of S_M poles. The statistical shear band crenulation axis and the mean L_M are indicated by the filled star and square respectively. The angle between the mean S_M plane and the ESB is 15°. Relative movement on the ESB is indicated by means of + and - symbols, signifying the up-thrown and down-thrown sides respectively. (b) Schematic diagram illustrating the disruption of L_M-S_M fabrics within mylonitic quartzites by late extensional shear bands (**ESB**) at Neuspoort. Sigmoidal deflection of S_M about subhorizontal crenulation axes is consistent with normal (NE-side down), dip-slip movement along the shear bands. Scale is arbitrary and angular relationships are approximate.

The shear bands occur as discrete, decimetre-scale planar crenulations, striking parallel to the local S_M fabric but dipping more steeply (65°) to the NE. The angle between the enveloping surface of the S_M foliation (which approximates the average S_M plane) and the shear bands is approximately 15°. The separation between individual shear bands varies from a few metres to tens of metres.

The L_M-S_M fabrics are sigmoidally deflected across the shear band boundaries, rotating about sub-horizontal crenulation axes (313/04). *Normal, NE-side down, dip-slip movement* is indicated by clockwise rotation of the S_M fabric about the gently-plunging crenulation axes as viewed down the plunge of the crenulation axes (Fig. 8b).

Normal displacements associated with crenulation slip within individual shear bands are in the order of a few tens of centimetres. Consequently, crenulation is not penetrative at a mesoscopic scale, and reorientation of L_M-S_M fabrics is restricted to zones immediately adjacent to the shear bands. The S_M foliation planes between widely-spaced crenulation surfaces are not back-rotated. Although the shear bands represent zones of high shear strain, no penetrative transposition of the older L_M-S_M fabrics is evident at a mesoscopic scale.

The attitude of, and sense of movement on, the shear bands at Neuspoort is highly consistent, and no conjugate sets were observed. Their discordant nature, and the fact that they deform the L_M-S_M fabrics indicate that they developed late within, or subsequent to, the mylonite fabric-forming event.

3.1.2 Sonopeiland locality

At this locality shearing has occurred along the contact between the skarn-like *Puntsit Formation* calc-silicate gneisses and pink *Riemvasmaak granite-gneiss*. Recrystallization of the pink quartzo-feldspathic gneisses has produced an extremely resistant lithology that forms a pronounced topographic ridge along the Lineament. Although penetrative L-S fabrics are widespread within the quartzo-feldspathic rocks at Sonopeiland, true mylonites characterized by grain-size dimunition are not encountered. Instead coarser-grained mylonite gneisses predominate. Mylonitic fluxion textures occur within calc-silicate mylonite gneisses, while intense flow-folding and boudinage of internal calc-silicate layers is common within marble bands.

At *Sonopeiland*, L_M plunges towards the E (083/68), within the steep NE-dipping S_M plane (053/71). The L_M fabric attitude therefore clearly reflects down-dip elongation (ds:ss = 4.7), and no evidence pointing to strike-parallel elongation was observed.

3.2 Microstructure

The following section documents the characteristic microstructures and microfabrics exhibited by tectonites of the Neusspruit Lineament. A more comprehensive microtextural review of individual samples is presented in Table 1 of the Appendix.

3.2.1 Mylonitic feldspathic quartzite

Textures exhibited by the mylonitic quartzites indicate dynamic recrystallization in response to plastic deformation. The mylonitic foliation (S_M) is defined in XZ-sections by a dimensional preferred orientation of elongate quartz-grains and a strong (001) preferred orientation of white mica parallel to L_M.

Bands of recrystallized quartz grains having matching crystallographic orientations occur subparallel to L_M, and are suggestive of recrystallized quartz ribbons. These coarsely recrystallized "ghost" ribbons attain shape aspects in excess of 20:1. Quartz grain shapes are typically globular or tabular (mean maximum dimension 0.3mm) with irregular and serrate boundaries. Internal strain features are widespread, and include marked undulose extinction, deformation bands and subgrains. Typical "mortar-structures" of small high-angle subgrains and new grains, are developed about the margins of larger strained grains. New grains show little evidence of post-crystalline strain and extinction is sharp, or only very weakly undulatory. "Protected" quartz grains enclosed within feldspar grains display very weak undulose extinction and no internal substructure. The inclusion of small micas within some quartz-grains is evidence for strain-driven grain boundary migration (Evans and White, 1984).

Feldspar grains are generally small in size (<0.2mm), and display strain features consistent with plastic deformation. Bending of twin-planes, mechanical twinning, kink bands, deformation bands and undulatory extinction are common. Brittle deformation features are absent. Feldspar grain shapes are typically globular or tabular with curved or straight edges.

3.2.1.1 Asymmetrical microstructures

The absence of obvious asymmetrical microstructures within these rocks precluded direct movement sense determination. However, vague monoclinic shape asymmetry of the recrystallized quartz grains, and oblique development of subgrains and deformation bands, are suggestive of reverse, NE-side up, movement. This observation prompted further microfabric analysis with the aim of resolving the shear sense potentially recorded by the quartz mylonites. A semi-quantitative Fry centre-to-centre fabric analysis (Fry, 1979) was performed on quartz grains and subgrains, in order to establish the shape-fabric and orientation of quartz in these samples, and hence the movement sense of the zone.

3.2.1.2 Fry centre-to-centre fabric analysis

Fry (1979) proposed a method of finite strain measurement based upon the spatial relationships between passive, spherical or ellipsoidal objects (marker grains etc.) in a rock. In the Fry (1979) method, the relative positions of adjacent grains are directly plotted by sequentially superimposing the origin of an overlay over each grain centre and recording the locations of all adjacent grain-centres as points. In many strained grain aggregates, these points define an elliptical void and parallel ring of high point-density around the overlay origin. For homogeneously deformed populations of originally statistically-uniform centres, the ellipticity and orientation of the elliptical void correspond directly to those of the finite strain ellipse (Fry, 1979; Hanna and Fry, 1979).

Objectives

The Fry (1979) method was employed for fabric analysis of quartz in the orthomylonitic quartzites due to the speed and simplicity of the analytical process, and the ease of interpretation. The purpose of this fabric analysis was not to obtain an absolute measurement of finite strain exhibited by quartz grains in the mylonite, but rather to estimate the mean shape-aspect of quartz within each of three orthogonal sample sections. It was hoped that the orientation of the strain ellipse obtained for XZ-sections would reflect a subtle shape-fabric asymmetry, and hence indicate the movement sense.

Sample preparation

Three orthogonal section planes were chosen for analysis: The first coplanar with S_M (XY-section), the second parallel to L_M and orthogonal to S_M (XZ-section), and the third orthogonal to both L_M and S_M (YZ-section). Several crossed-polar photomicrographs were taken of random portions of each section plane, and the trace of L_M-S_M fabric elements were recorded on each photograph. Identification and isolation of feldspar and white mica grains on the photograph enabled their exclusion from the marker-grain population. This was done to avoid interference from mineral grain populations of differing mechanical properties.

Analytical procedure

For each section, quartz grain boundaries were traced off the photomicrographs onto a transparent plastic overlay. The centre of each grain was then located using the method outlined by Odling (1984) for a strain analysis of quartz aggregates from the Loch Tollie gneisses, NW Scotland. According to this method, the long axis of each grain is determined and its maximum length halved. The maximum width normal to the long axis is drawn at this point, and the grain-centre is located at the mid-point of the width chord. This method was employed to avoid subjectivity in the location of grain-centres.

For each section, the grain-centres were then digitised, and the resulting coordinate sets analysed using the computer program INSTRAIN 2.5 (copyright 1987-89 Eric Erslev, Colorado State University), which uses the Fry (1979) method to produce two-dimensional all-object-object separation plots. Several photomicrographs were analysed from each sample section to circumvent errors related to strain heterogeneity. In this manner, two-dimensional Fry plots were obtained for each of the three sample sections. The orientation (ϕ,Θ,α) and ellipticity (E) of the finite strain ellipses were measured manually from each plot, and mean vector azimuths and vector magnitudes of the ellipse axes (Potter and Pettijohn, 1977) were calculated for each sample section.

Results

In the following tabulation ϕ and Θ are angles measured in a clockwise direction from the S_M trace to the long axis of the strain ellipse, within the XZ and YZ sections respectively (XZ sections viewed towards the NW, YZ sections viewed down the plunge of L_M). α is an angle measured in a clockwise direction from the strike-line of the S_M plane to the long axis of the strain ellipse within XY sections.

XZ section

SAMPLE	ϕ	E
CJS1XZ1	11	2.00
CJS1XZ2	5	1.64
CJS1XZ3	173	1.75
CJS1XZ4	30	1.40
CJS1XZ5	36	2.10
mean	15	1.71

YZ section

SAMPLE	Θ	E
CJS1YZ1	19	1.56
CJS1YZ2	3	1.06
CJS1YZ3	0	1.17
CJS1YZ4	175	1.16
mean	5	1.22

XY section

SAMPLE	α	E
CJS1XY1	79	2.00
CJS1XY2	64	1.10
CJS1XY3	76	1.75
mean	75	1.61

Discussion of results

Despite the advanced state of recrystallization in the orthomylonitic quartzites, the results of the Fry fabric analysis were consistent with field observations. Within the foliation plane (XY section) the long axis of the calculated strain ellipse (E = 1.61; α = 75°) is sub-parallel to the measured lineation (rake in S_M = 80°), indicating that L_M is indeed a quartz elongation lineation. Some degree of flattening subparallel to S_M is indicated by the strain ellipse (E = 1.22; Θ = 5°) for YZ sections, while greatest extension occurs in XZ sections (strain ellipse E = 1.71; ϕ = 15°). Low maximum finite strains are attributed to the advanced state of dynamic recrystallization.

The applicability of the technique in the evaluation of subtle fabric anisotropies is evident in XZ sections (Fig. 9). For these sections an average strain ellipse was obtained (E = 1.71) with its long-axis inclined at 15° clockwise to the trace of S_M. The obliquity of this strain ellipse reflects a cryptic, inclined, secondary quartz grain-shape foliation (S_s), defined by elongate, dynamically recrystallized grains and subgrains.

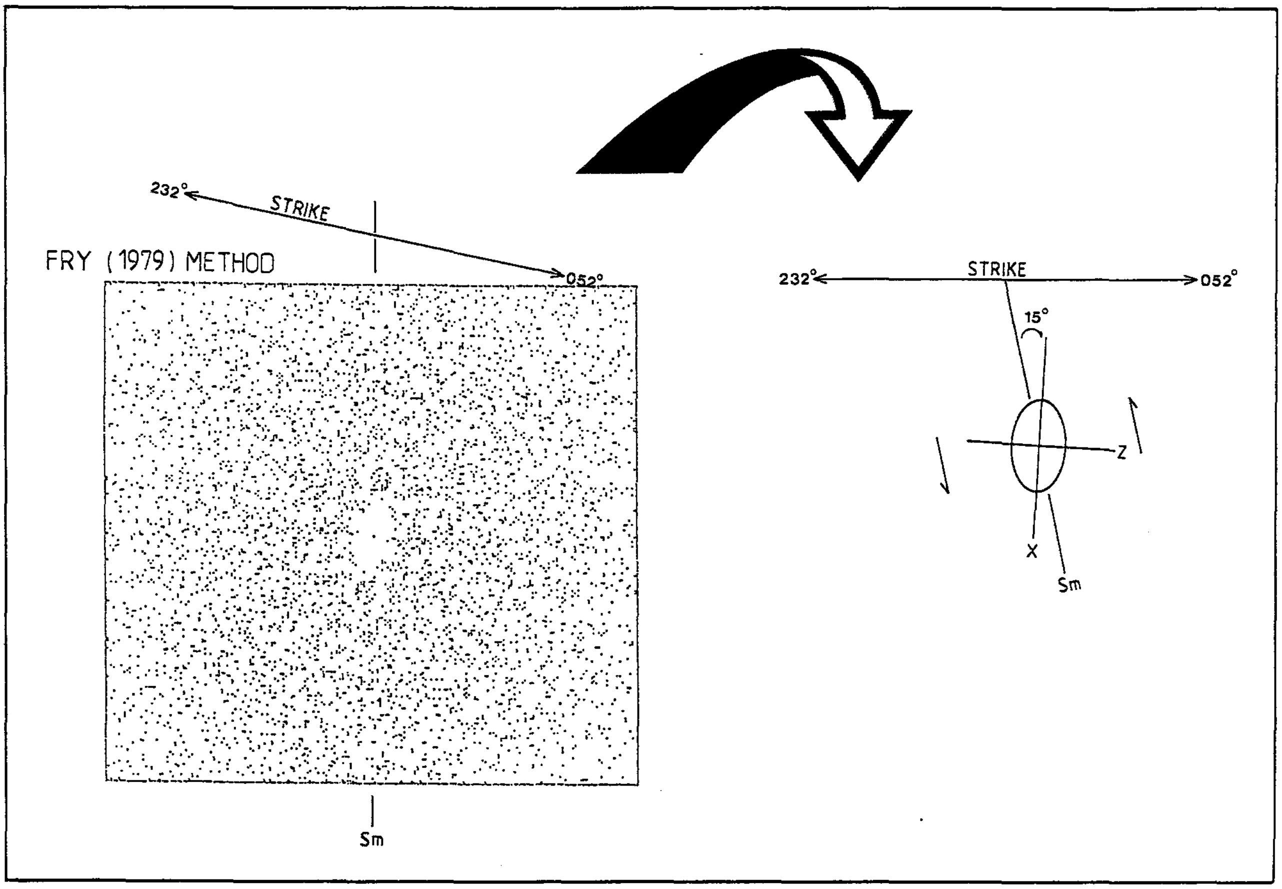

Figure 9. Computer-generated, two-dimensional Fry all-object-object separations plot of 194 centres of quartz grains within the XZ-section of a mylonitic quartzite (sample CJS/1), Neuspoort, Neusspruit Lineament. Look-direction is NW. The elliptical void and parallel ring of high point-density about the plot-origin define a finite strain ellipse (E = 1.71) inclined at 15° to the mylonitic foliation (S_M). This strain-ellipse reflects the shape-fabric of a cryptic, inclined secondary quartz foliation. The clockwise obliquity of the finite stretching axis (X) with respect to S_M is consistent with reverse (top to SW), dip-slip movement sense. The Fry plot was generated using the computer program INSTRAIN 2.5 (copyright 1987-1989 Eric Erslev, Colorado State University).

The orientation and ellipticity of the calculated finite strain ellipse (within XZ sections) should correspond to those of the incremental strain ellipse during the final increment of penetrative, progressive shear deformation (Brunel, 1980). The S_M plane coincides with the plane of finite flattening within the bulk rock, while the inclined S_s plane reflects the orientation of the flattening plane during the final penetrative strain increment (Simpson and Schmid, 1983; Simpson, 1986b).

The obliquity of S_s with respect to the macroscopic foliation S_M (indicated by the acute clockwise inclination of the calculated finite strain ellipse to the bulk flattening plane, defined by S_M - Fig. 9) is consistent with a penetrative strain increment in response to *reverse, top to SW,* shearing. Since quartz deformation fabrics are highly sensitive to any changes in the kinematic framework (Simpson, 1986b), this result is only likely to reflect the strain state during the final stages of *penetrative* ductile deformation.

After reviewing current literature it is apparent that the usefulness of the Fry fabric analysis technique in highlighting subtle fabric anisotropies for shear sense evaluation has been overlooked. Bouchez (1977) outlines a conceptually similar technique for the determination of shear sense, using the angular distribution of quartz subgrain boundary traces. The results of the Fry analysis conducted on Neusspruit samples, illustrate the potentially valuable role this technique can play in the determination of movement sense in quartz mylonites.

3.2.2 Quartz-feldspar mylonite gneiss

Quartzo-feldspathic tectonites at Sonopeiland are well-foliated mylonite gneisses, exhibiting textures consistent with extensive post-tectonic recovery and annealing grain growth. These mylonite gneisses comprise inequigranular polygonal mosaics of quartz and feldspar, with a strong grain-shape alignment defining the foliation. Highly-elongate, coarsely-recrystallized, ribbon aggregates of quartz surround finer-grained domains of quartz and feldspar (QF domains). The shape-aspects of the quartz ribbon aggregates often exceed 20:1, and individual quartz grains may attain 8mm in long dimension.

Grain shapes of quartz and feldspar are rectangular to globular polygonal, and grain boundaries are curved or straight. 120° triple junctions are common. Grain size is highly variable, but generally exceeds 0.2mm in the QF domains.

Weak undulatory extinction and poorly developed crystal substructure indicate that post-crystalline strain has been minimal. Textural equilibration has obliterated earlier, potentially useful microfabrics in these rocks, and consequently no kinematic interpretation could be made.

3.2.3 Biotite augen gneiss

Coarse-grained biotite augen gneiss layers occur within the quartz-feldspar mylonite gneiss at Sonopeiland. Where observed, the monoclinic symmetry of feldspar augen in XZ-planes indicated a *normal, NE-side down, sense of shear*. Due to the isolated nature of augen gneiss outcrops at this locality, low confidence is given to this kinematic interpretation.

Within a single highly-altered specimen of augen gneiss, chlorite pressure shadow beards developed asymmetrically about saussuritized plagioclase porphyroclasts indicate *normal, NE-side down, movement sense* (Fig. 10a).

3.2.4 Mylonitic amphibolite gneiss

Mylonitic amphibolite gneisses at Neuspoort and Sonopeiland are well-foliated rocks with strong stretching fabrics defined by the parallel alignment of elongate green-brown hornblende. Amphibole-rich layers alternate with plagioclase-rich domains and define a crude compositional layering. In XZ sections, strong elongation of amphiboles and magnetite aggregates occurs parallel to L_M, and amphibole shape-aspects may exceed 7:1. Plagioclase-rich domains are characterized by equigranular polygonal aggregates consistent with near-complete recovery.

Weakly-developed, asymmetric quartz-feldspar pressure shadows developed about elongate magnetite aggregates display ambiguous shear sense relationships in XZ sections. No kinematic interpretation could be made from these indeterminate shear sense indicators.

3.2.5 Calc-silicate orthomylonite

Calc-silicate orthomylonite from Sonopeiland (sample CJS/6) exhibits a well-developed fluxion banding defined by a compositional layering of calc-silicate minerals (Di-Pl-Sph-Qtz ± scapolite). Synkinematic andradite-garnet poikiloblasts (2-7mm in diameter), rimmed by diopside - feldspar ± calcite coronas, are dispersed throughout the rock as irregular clustered aggregates, enveloped by the mylonitic fluxion foliation. Asymmetric disruption of the fluxion foliation about the garnet poikiloblasts in XZ sections is consistent with *normal, NE-side down,* shear sense (Fig. 10b). These well-developed systems display a consistent sense of shear in all XZ sections, and highest confidence is credited to their kinematic interpretation.

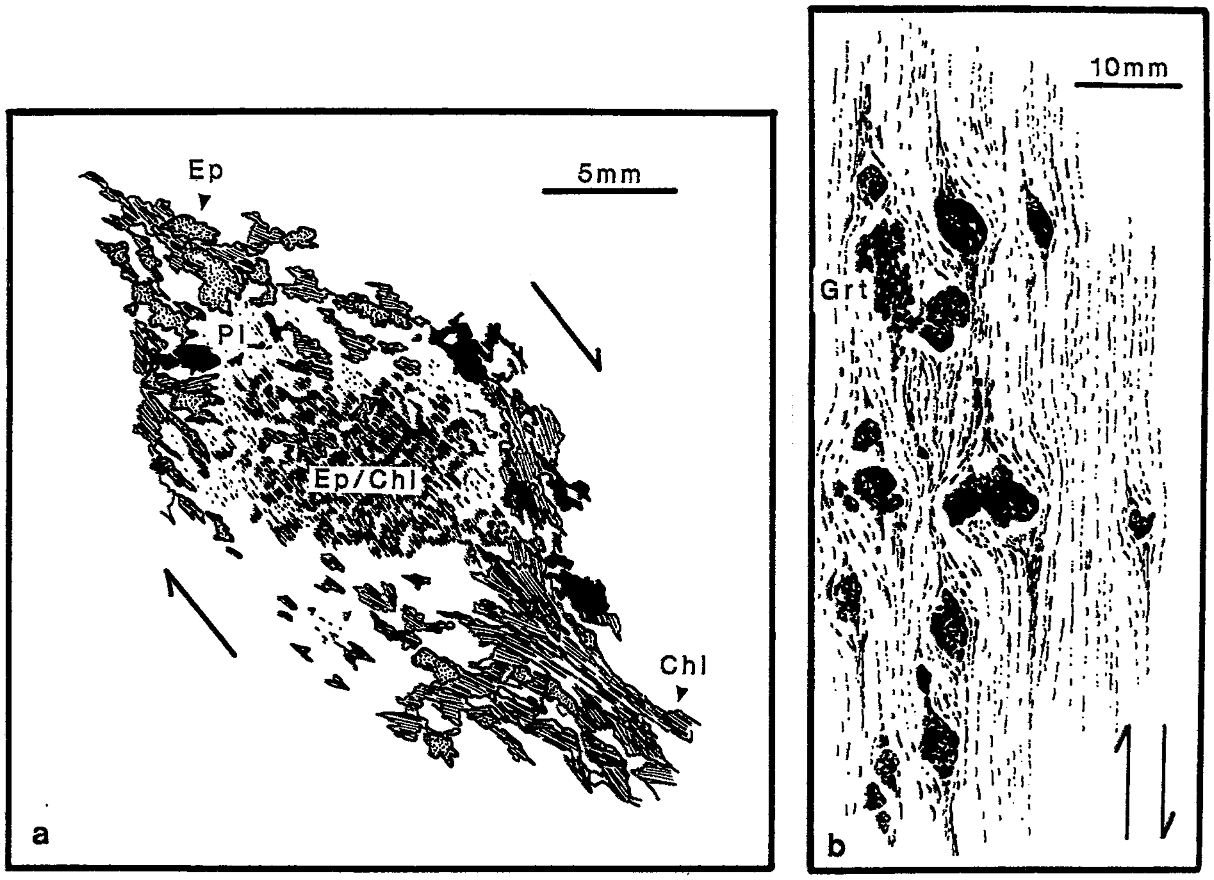

Figure 10. Examples of kinematic indicators developed within mylonitic rocks from the Neusspruit Lineament. All sketches made from XZ-sections. Look direction is NW. Angle of dip approximate.

(a) Asymmetric beard-like clusters of new chlorite developed in pressure-shadow domains about an extensively saussuritized plagioclase porphyroclast, within highly altered feldspathic augen gneiss, Sonopeiland locality. The central plagioclase porphyroclast displays a fine-grained replacement intergrowth of epidote and chlorite. The asymmetrical distribution of the new chlorite "beards" is consistent with normal (top-to-NE) movement sense (sample CJS/8).

(b) Disruption of the mylonite foliation about σ-type andradite-garnet poikiloblasts within a calc-silicate orthomylonite, Sonopeiland locality. The "stair-stepping" geometry of asymmetric tails, and the perturbation of the mylonite foliation about the poikiloblasts, indicate NE-side down movement sense (sample CJS/6).

Poikiloblastic andradite aggregates together with their diopside - feldspar ± calcite coronas define elongate ellipsoidal nodules. A semi-quantitative R_f/ϕ fabric analysis technique (Ramsay and Huber, 1983) was applied to these deformed garnet nodules, to test their shape-fabric for purposes of comparison with the Fry fabric analysis of quartz in the Neuspoort orthomylonitic quartzites. Again the purpose of the analysis was not to obtain an absolute measurement of finite strain in the nodules, but rather to estimate their mean shape aspect in each of the three sample sections, and to determine the relationship between the calculated shape-aspect of the nodules and penetrative mylonitic fabric elements.

3.2.5.1 R_f/ϕ fabric analysis

Ramsay (1967) outlined a graphical method to determine the finite strain ellipse on a plane section from homogeneously deformed elliptical markers (R_f/ϕ_f diagram technique). Subsequently, the method has been further developed and applied to naturally deformed rocks by Dunnet (1969), Dunnet and Siddans (1971), Elliot (1970), Matthews *et al.* (1974), Shimamoto and Ikeda (1976), Lisle (1977, 1979), Peach and Lisle (1979) and Lisle *et al.* (1983). A comprehensive review of the methods of R_f/ϕ strain analysis is presented by Paterson (1983), and Ramsay and Huber (1983).

The following fabric analysis utilized the computer programmes RPHIN and THETA (Von Veh and Hartnady, 1983), which are based on a FORTRAN IV programme written by Peach and Lisle (1979) for estimating the tectonic strain using deformed elliptical markers. RPHIN calculates the axial ratios (R_f), long axis orientations (ϕ), axis lengths and ellipse centroid positions of digitized elliptical objects. An option is included for the plotting of R_f/ϕ scatter diagrams. THETA calculates the vector mean of ϕ_f values, the median ϕ direction, the strain ratio and a range of acceptable strain values. The markers are "unstrained" perpendicular to the median direction, and the undeformed marker orientations (Θ) are grouped into classes and tested for randomness using a Chi-square test. This procedure is repeated using incrementally changed reciprocal strain ratios, and the lowest Chi-square value is taken as the strain ratio (Peach and Lisle, 1979).

Sample preparation

The sample was cut into three portions (XY,XZ,and YZ section portions) and serial sectioning, parallel to either the XY, XZ or YZ section planes, was performed at approximately 10mm intervals across each portion. After sectioning, the slices were coated with a clear vinyl aerosol spray to provide visual contrast between the deformed nodules and the matrix. Both sides of the section slices were used for the analysis, and the ellipse shape and orientation data for the slices were pooled for each of the three section sets. This procedure was necessary in order to maximise the data from each section set, as the specimen was relatively small. The number of nodules analysed in XY, XZ, and YZ section sets were 181, 350, and 256 respectively. Davidson (1983) notes that a minimum of 100 markers per plane gives accurate and reproducible results in this type of analysis.

Analytical procedure

The shapes of deformed nodules were traced onto clear plastic film, and their long and short axes located using the method of Odling (1984) (see section 3.2.1.2). The end-points of the long and short axes were digitised, and the axial ratios (R_f), long axis orientations (ϕ), axes lengths and ellipse centroid positions are calculated using the computer program RPHIN. R_f/ϕ scatter diagrams for each of the three section planes were produced using RPHIN and THETA.

Discussion of results

Two dimensional R_f/ϕ scatter plots for the XY, XZ and YZ section planes are presented in Figure 11 a, b and c respectively. Within the foliation plane (Fig. 11a), the angle between the measured mylonite lineation (L_M) and the calculated value of mean-ϕ is 4°. This result demonstrates that the L_M fabric element is a penetrative elongation lineation. Furthermore, the 79° rake-angle of mean-ϕ within the foliation plane is consistent with down-dip elongation (ds:ss = 5.60). Greatest stretching (R_s = 2.234) is measured in the XZ section (Fig. 11b), where the counterclockwise angle from the S_M trace to the calculated value mean-ϕ is 3°. Flattening parallel to S_M is indicated by the the finite strain (R_s = 1.608) in the YZ section (Fig. 11c).

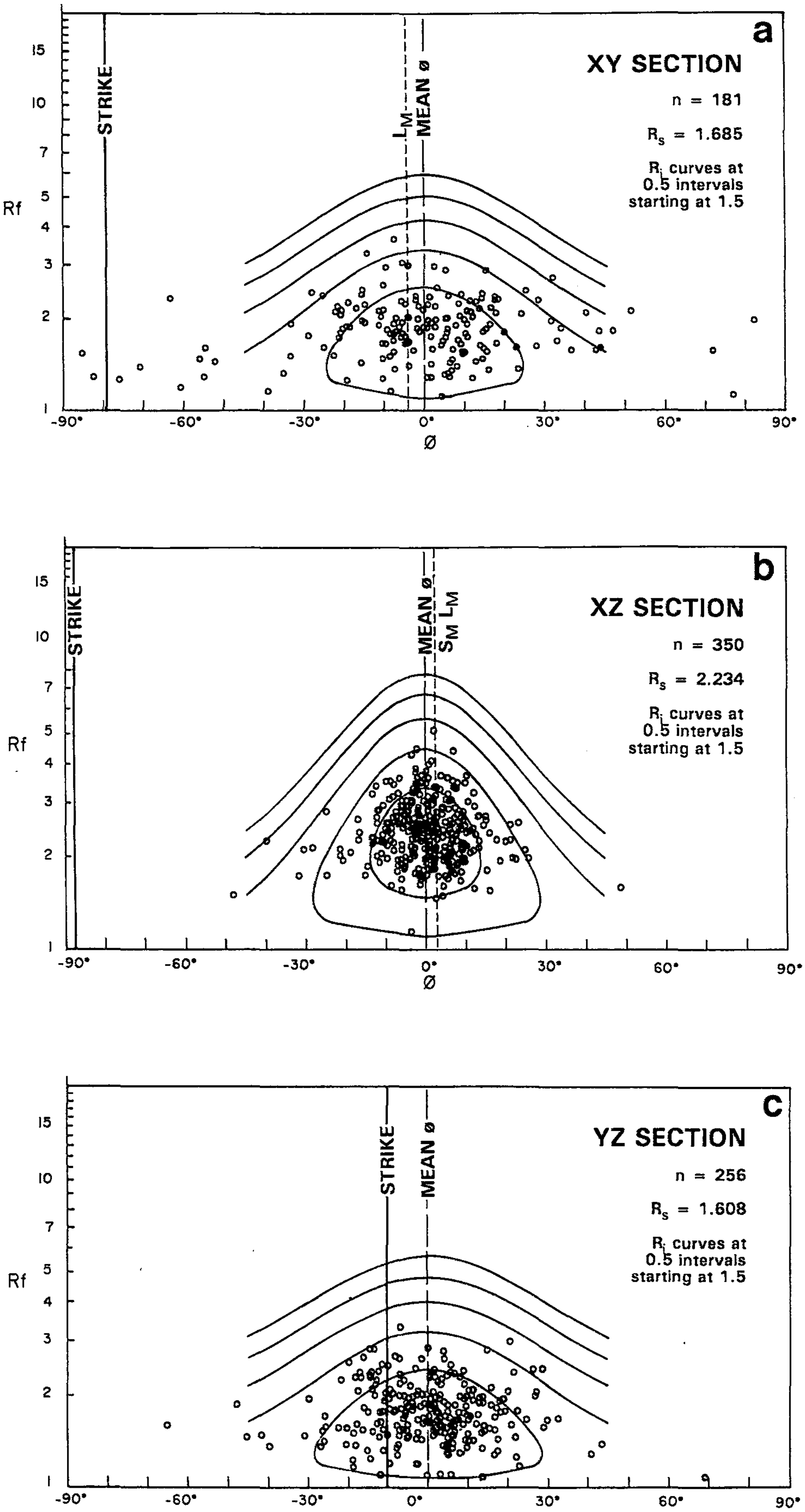

Figure 11. Two-dimensional R_f/ϕ plots for (a) XY sections, (b) XZ sections, and (c) YZ sections of deformed garnet nodules from a calc-silicate orthomylonite (sample CJS/6), Sonopeiland locality, Neusspruit Lineament. See text for explanation.

Although finite strain values obtained in this analysis are higher compared to those obtained by the Fry-analysis, maximum finite strains remain relatively low. This is interpreted as a consequence of a high viscosity contrast existing between the cohesive, competent garnet aggregates and an incompetent matrix which accommodated a higher degree of strain.

3.2.6 Retrograde rocks

A significant feature of several specimens collected at the Sonopeiland locality is low-temperature mineral assemblages consistent with pervasive secondary alteration. Epidote, chlorite and calcite are the principal retrograde minerals. Within some calc-silicate rocks early tectonite fabrics are completely obliterated by pervasive epidotization, precluding kinematic interpretation. Within altered augen gneisses, feldspars are sericitized and saussuritized, and early biotite is replaced by chlorite.

3.3 Kinematic synthesis

Stereograms A and B of Figure 7 provide a synopsis of mylonite fabric orientation data, calculated kinematic vectors and movement sense determinations, for the Neusspoort and Sonopeiland sample sets. Structural and fabric orientation data from a single extensional shear band at Neuspoort are presented in stereogram E of Figure 7 (see also Fig. 8a).

Microstructural kinematic indicators preserved within tectonites from two localities on the Neusspruit Lineament provide evidence for both reverse and normal movement. At the Neusspoort locality, a Fry centre-to-centre fabric analysis of mylonitic quartzite revealed a subtle, oblique quartz grain shape fabric consistent with *reverse (top to SW) movement sense*. At the Sonopeiland locality, asymmetric andradite porphyroblasts within calc-silicate orthomylonite (Fig. 10b), and asymmetrical chlorite pressure shadows about feldspar augen within altered augen gneisses (Fig. 10a), indicate *normal (top to ENE) movement sense*. Calculated kinematic vectors for the Neuspoort and Sonopeiland localities, plunge 037/53 and 083/68 respectively.

On a mesoscopic scale, late shear bands characterized by *normal (NE-side down) displacements*, deform the L_M-S_M fabrics in mylonitic quartzites at the Neuspoort locality (Fig. 8). Assuming that deformation within the shear band boundaries approximated simple shear, movement will have occurred in a direction normal to the vorticity vector (Passchier, 1988) represented by the subhorizontal crenulation axis. Based on this assumption a kinematic vector plunging 050/64 is calculated.

3.3.1 P-T conditions of mylonitization

Mineral assemblages defining the mylonite fabrics within the Neusspruit samples do not allow accurate assessment of the P-T conditions at the time of shearing.

The presence of occasional "pinhead" garnets, and patches of sillimanite needles aligned parallel to L_M within the orthomylonitic quartzites at Neusspoort, suggests that high-temperature conditions prevailed during penetrative mylonite fabric formation. This proposition cannot exclude the possibility that the sillimanite needles were rotated into parallelism with L_M without recrystallization or re-equilibration, and do not reflect growth during shearing.

The absence of accurate data on the chemical composition of individual minerals defining the mylonitic fluxion banding in calc-silicate mylonite gneisses at Sonopeiland, precluded accurate determination of metamorphic conditions during normal sense shearing. P-T stability fields of calc-silicate mineral assemblages are strongly dependent on the composition of the metamorphic fluid, which would have been highly variable in an open shear zone system.

Pervasive alteration and replacement of syn-kinematic mineral parageneses by low-grade hydrated minerals within some samples from Sonopeiland, suggests that the Lineament acted as a channel for fluids during retrogression. Early deformation fabrics and microstructures are passively pseudomorphed or overprinted by retrograde minerals, and no microstructural criteria pointing to active tectonism during low-temperature retrograde metamorphism are in evidence.

Textures within quartzo-feldspathic mylonite gneisses from Sonopeiland are consistent with extensive post-tectonic recovery and annealing grain growth. Textural re-equilibration may have been facilitated by high-temperatures associated with emplacement of late charnockitic bodies to the east of the the Lineament e.g. Friersdale Charnockite (Von Backström, 1964).

3.4 Discussion

The relative ages of normal and reverse ductile shearing events recorded by microstructures and fabrics within the Neusspruit sample set are unclear. However, disruption of mylonite fabrics by extensional shear bands within quartzites at Neuspoort, is compelling evidence that ductile shear deformation on the Lineament culminated with normal movement localized within discrete zones of high shear strain. Oblique quartz grain-shape fabrics, consistent with reverse movement sense, are preserved in orthomylonitic quartzites within domains of lower strain away from these late shear bands. This is significant since quartz deformation fabrics usually reflect the last increment of progressive shear deformation, and are easily reset by subsequent deformation (Brunel, 1980; Simpson and Schmid, 1983; Simpson, 1986b). This incongruous relationship may be an artifact of the scale at which the extensional shear bands are penetrative. The spaced shear bands do not transpose the L_M-S_M mylonite fabrics at a mesoscopic scale, and it is likely that penetrative modification of the oblique quartz deformation fabrics by crystal-plastic strain was restricted to narrow domains centered on the crenulations. To resolve this apparent incongruity, detailed investigation of quartz deformation fabrics within, and immediately adjacent to the extensional shear bands is required.

Chapter 4. - The Kakamas Shear Zone

4.1 Mesostructure

Two samples of quartz-feldspar mylonite gneiss and three samples of biotite augen gneiss were collected from a single 100m, strike-perpendicular transect across the Kakamas Shear Zone (hereafter referred to as the KSZ). The transect is located on the farm Omkyk, approximately 800m southeast of the intersection of the Kakamas-Kenhardt road and the Kakamas-Loeriesfontein road (Fig. 2 and 7).

At Omkyk the KSZ follows the contact between augen gneisses of the *Kenhardt Migmatite Formation* (name not yet approved by S.A.C.S.), and the quartzo-feldspathic *Riemvasmaak gneiss* (Geringer, 1973). Tectonites within the zone of ductile shearing on Omkyk are typically medium to coarse grained, with well-developed L-S fabrics. They exhibit textures characteristic of porphyroblastic gneisses, augen gneisses and mylonite gneisses. True fine-grained mylonites are scarce, and are only encountered in narrow (<1 - 10 cm), diffuse bands.

4.1.1 Mesoscopic fabric elements

At the Omkyk locality, the orientation and type of ductile deformation fabrics occurring within the Riemvasmaak gneisses differ significantly from those developed within augen gneisses of the Kenhardt Migmatite Formation. The most conspicuous difference is reflected by the plunge of the elongation lineation. Stretching lineations within the Riemvasmaak gneisses plunge down-dip, while those within tectonites of the Kenhardt Migmatite Formation are subparallel to the strike. For purposes of discrimination in the following discussion, the dip-slip and strike-slip elongation lineations will be referred to as L_{ds} and L_{ss} respectively.

The Riemvasmaak gneisses exhibit a well-developed penetrative foliation (S_M) defined by elongate, flattened quartz and feldspar mineral aggregates, monomineralic quartz stringers, and preferred alignment of biotite flakes. Small (1-4 mm diam.) feldspar porphyroclasts occur infrequently within discrete layers, characterized by a fluxion foliation subparallel to S_M.

S_M dips at 42° towards the ENE. L_{ds} plunges NNE within foliation surfaces, and is defined by elongate quartz ribbons and aligned biotite flakes. Down-dip elongation is indicated by ds:ss = 2.82 (rake of L_{ds} in S_M = 71°).

The biotite augen gneisses at Omkyk are coarsely crystalline tectonites, characterized by penetrative L>S fabrics. A strongly penetrative stretching lineation (L_{ss}) is defined by elongate, flattened rods of granular feldspar and quartz, and lenticular aggregates of biotite. A weak foliation is defined by a crude compositional layering, comprising leucocratic bands of flattened quartz-feldspar rods, alternating with anastomosing, melanocratic biotite-rich layers. Relict feldspar megacrysts (augen) are elongated parallel to L_{ss}, and are enveloped by quartz-feldspar domains. S_M dips at 41° to the NE, while L_{ss} plunges very shallowly (<10°) towards the SE. Strike-parallel elongation is indicated by ds:ss = 0.18 (rake of L_{ss} in S_M = 10°).

The orientation of mesoscopic fabric elements within the quartz-feldspar mylonite gneiss and the biotite augen gneiss at Omkyk, are represented stereographically in C and D of Figure 7 respectively.

4.1.2 Brittle fault zone

A narrow (<10m wide), brecciated fault zone occurs parallel to, and 250m to the west of, the principal zone of ductile shearing at Omkyk (in line with the easternmost outbuildings of the Omkyk homestead). The breccia zone has slight positive topographic expression as a result of silicification. Localised piedmontite enrichment imparts a reddish colouring to the outcrop. Intense fracturing is evident on all scales, and vein infillings of quartz or epidote are common. Angular clasts of disrupted protomylonite and mylonite, and sub-angular clasts of reworked cataclasite occur in a fine-grained, dark-grey matrix. Occasionally the fine-grained matrix is supplanted by coarse-grained recrystallized quartz. Clast size is extremely variable ranging from sub-millimetre fragments through to decimetre size "blocks". The internal structure of the breccia is chaotic. No dimensional preferred orientation of clasts is observed, and fabrics are random.

Brittle comminution and fragmentation are suggested by the angular shape of the mylonite clasts. The co-inclusion of mylonite and cataclasite series clasts testifies to the protracted, polyphase nature of movements on the fault zone.

A single unorientated sample (sample KSZ) of cataclasite was collected from the brittle fault zone at the Omkyk locality for the purposes of microstructural investigation.

4.2 Microstructure

A comprehensive summary of microstructural development within individual samples from the KSZ sample set is presented in Table 2 of the Appendix. The following section documents characteristic textures and microfabrics exhibited by sheared rocks of the KSZ.

4.2.1 Quartz-feldspar mylonite gneiss

The variable recovery / recrystallization state of quartz within the quartz-feldspar mylonite gneiss defines two basic textural types. Both textural types may be present within the same sample, occurring as microstructurally distinct domains:-

(1) Textural domains of partial recrystallization and incomplete recovery/annealing, are characterized by a strong quartz grain shape orientation defined by strained, irregular quartz-aggregates and coarser, relict ("ghost") quartz-ribbons, elongated parallel to L_{ds}. The irregular quartz-aggregates and "ghost" quartz-ribbons have undergone partial dynamic recrystallization: Quartz grains are typically globular or elongate-irregular in shape, with curved or serrated boundaries. Grain-size varies from <0.1mm to 1.5mm, averaging about 0.6mm (long-axis). Quartz grains exhibit moderate to strong undulose extinction and substructure is significantly developed. Deformation bands and deformation lamellae are widespread, and subgrain development is locally well-advanced. Polyhedral strain-free neoblasts occur along grain boundaries of the larger highly-strained grains. Relict microcline and plagioclase megacrysts occur within coarsely-recrystallized, elongate quartz-feldspar aggregates. They range in size from 0.1mm to 6mm and are commonly sub-ovoid in shape. The megacrysts display strain features consistent with both plastic and brittle deformation: Extension cracks, microfaults and healed fractures occur together with bent twin-planes, mechanical twins, deformation lamellae, kink bands, and undulose extinction. The clasts are often partially, or wholly pseudomorphed by coarsely recrystallized, "strain-free" feldspar aggregates.

(2) Textural domains of complete recrystallization, pervasive recovery and extensive annealing, are characterized by equigranular polygonal mosaics of quartz and feldspar grains, exhibiting a weak dimensional preferred orientation and showing little evidence of internal strain. Quartz grain-size decreases in these zones to an average of 0.1mm. Rectangular and polygonal grain shapes dominate, and grain boundaries are characteristically curved or straight with 120° triple junctions. Indicators of post-crystalline strain are scarce. Grain substructure is notably absent or only poorly developed. Extinction is sharp or occasionally weakly undulose, while deformation bands, deformation lamellae and subgrains are uncommon. Biotite growth is common in the polygonal textural domains and a strong mica (001) preferred orientation is developed parallel to S_M. The biotite flakes display an affinity for grain boundaries within the polygonal quartz-feldspar mosaics.

Asymmetrical microstructures

Asymmetrical microstructures useful for shear sense determination are scarce in the quartz-feldspar mylonite gneisses. Within type (1) domains, deformation bands and elongate subgrains inclined to the margins of recrystallizing quartz ribbons, suggest that an oblique quartz microfabric may be present. Although only weakly-developed and often ambiguous, the prevalent monoclinic shape symmetry of these microstructures reflects probable *reverse, top to SSW, shearing*. Extremely low-confidence is assigned to this kinematic interpretation ($0<KCI<1$). Recovery and annealing processes are responsible for textural re-equilibration within type (2) domains, rendering them unsuitable for shear sense determination.

Within discrete fluxion foliated layers, coarsely recystallized quartz ribbons link with mantle structures surrounding relict feldspar clasts to form asymmetric σ-type porphyroclast systems (Fig. 12b). Although these systems may be totally recrystallized internally, their original shape is preserved, and *normal, top to NNE, movement sense* is indicated. Because of the advanced state of static recrystallization of these porphyroclast systems, polished slabs offer the best medium for shear sense determinations (clast-mantle-tail geometrical relationships are more easily distinguished). In view of the consistency of asymmetry exhibited by these porphyroclast systems, moderate confidence is placed in this movement sense determination ($KCI=2$).

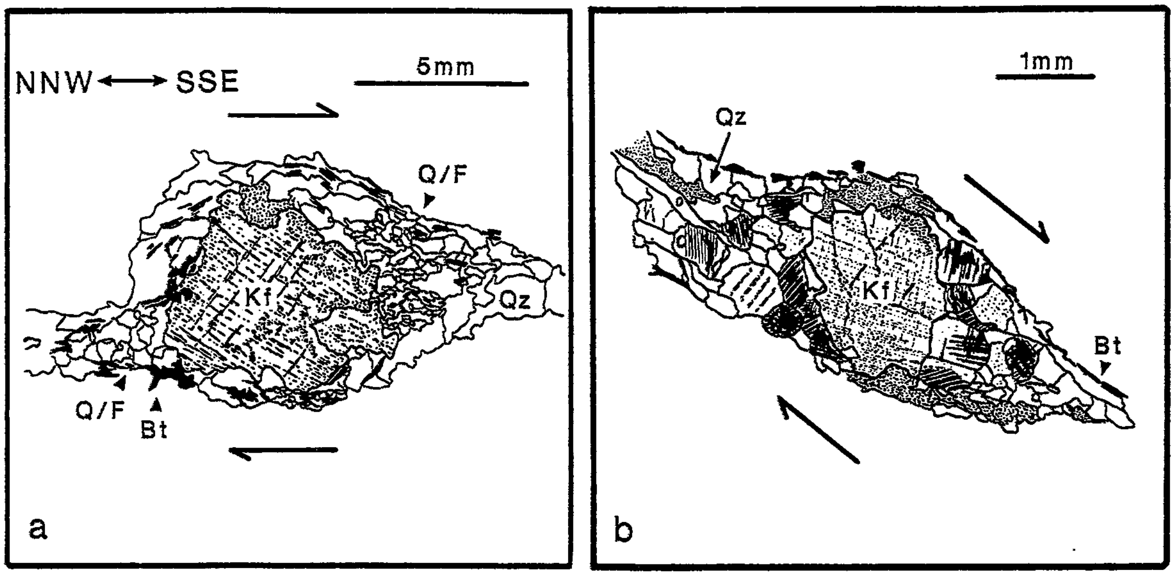

Figure 12. Examples of kinematic indicators within augen gneisses and mylonite gneisses from the Kakamas Shear Zone. All sketches made from XZ-sections. Look-direction is virtually down-dip for (a) and NW for (b).
(a) Resistant K-feldspar megacryst (**Kf**) wrapped by ribbons of ductilely-deformed, polycrystalline quartz (**Qz**), occurring within biotite augen gneiss. Asymmetric tails of recrystallized quartz and feldspar (**Q/F**) are developed in pressure shadow domains adjacent to the central clast. A distinct grain-size contrast exists between the refined, dynamically recrystallized pressure shadows, and the coarser quartz-ribbon mantle material. The asymmetry of pressure shadow development is consistent with SSE-directed, right-lateral, strike-slip shearing (sample CJS/12).
(b) Statically recrystallized, asymmetric σ-type porphyroclast system. Coarsely-recrystallized quartz ribbons and biotite trains define the boundaries of the pre-existing dynamically recrystallized tails. The relict central K-feldspar clast (**Kf**) is mantled by annealing overgrowths comprising coarsely recrystallized twinned microcline aggregates. Asymmetry of the system is consistent with normal, top-to-NE, dip-slip movement sense (sample CJS/10).

4.2.2 Biotite augen gneiss (L>S tectonite)

Dynamic recrystallization and annealing grain growth (or static recrystallization) have texturally overprinted microstructures in these rocks leaving only patchy relicts of the earlier augen fabrics. Textural relationships within the L>S-tectonites are typical of porphyroblastic gneisses and augen gneisses.

Within XZ-sections, millimetre-scale, feldspar-rich compositional bands are defined by elongate, relict K-feldspar augen, oriented sub-parallel to L_{SS}, enveloped by domains comprising coarsely-recrystallized, subpolygonal mosaics of quartz and feldspar. Coarsely-recrystallized remnants of elongate quartz ribbons occur within these bands, and are oriented parallel to the subhorizontal L_{SS} lineation. The feldspathic bands alternate with finer-grained, biotite-rich layers.

Occasional relict feldspar clasts (augen) are mantled by neoblasts. These mantle structures link with quartz-feldspar compositional bands to form vague porphyroclast systems. Broad quartz-feldspar pressure shadows are distributed asymmetrically about feldspar porphyroclasts. The pressure shadows are usually wholly recrystallized, yet remain texturally distinct from recrystallized mantle and compositional band material (Fig. 12a). The pressure shadow domains are generally finer-grained than their enveloping mantles. Myrmekite is common within the rims of relict, recrystallizing K-feldspar augen, and shows an affinity for the long sides of elongate augen that parallel L_{ss}. Patches of fibrolitic sillimanite occur at sites of high-stress at the contact points between abutting feldspar augen, and along their margins. Myrmekitic intergrowths and felted aggregates of acicular sillimanite occasionally coincide within feldspar megacrysts.

Planar domains characterized by finer-grained, recrystallized mineral mosaics occur along the margins of the coarsely-recrystallized, feldspathic compositional bands, and may represent surfaces of localized high shear strain. These surfaces are characterized by sheaves of recrystallized biotite, irregular aggregates of highly-pinitized cordierite, occasional "atoll-type" (Bard, 1986) garnet aggregates, and discontinuous lens-like mats of fibrolitic sillimanite needles, displaying a strong dimensional preferred orientation parallel to L_{ss}. Relict feldspar porphyroclast systems, including their recrystallized mantles and pressure shadows, are frequently enveloped by the biotite-sillimanite-cordierite-garnet bearing layers. Within these layers cordierite and garnet are often found partially rimmed by selvages of biotite flakes, and cordierite grain-aggregates are transected by anastomosing folia of fibrous sillimanite (Fig. 13 a and b).

Within the augen gneisses, relict feldspar clasts exhibit deformation microstructures consistent with crystal-plastic strain. Strain shadows, deformation twins and kink-bands are ubiquitous. Twin-planes within microcline and plagioclase grains are often bent or distorted. Quartz-ribbon aggregates are coarsely-recrystallized, and display little evidence of internal strain other than moderate undulose extinction. Biotite is completely recrystallized, with (001) planes generally aligned parallel to L_{ss}. Very minor retrogression of biotite to chlorite occurs locally.

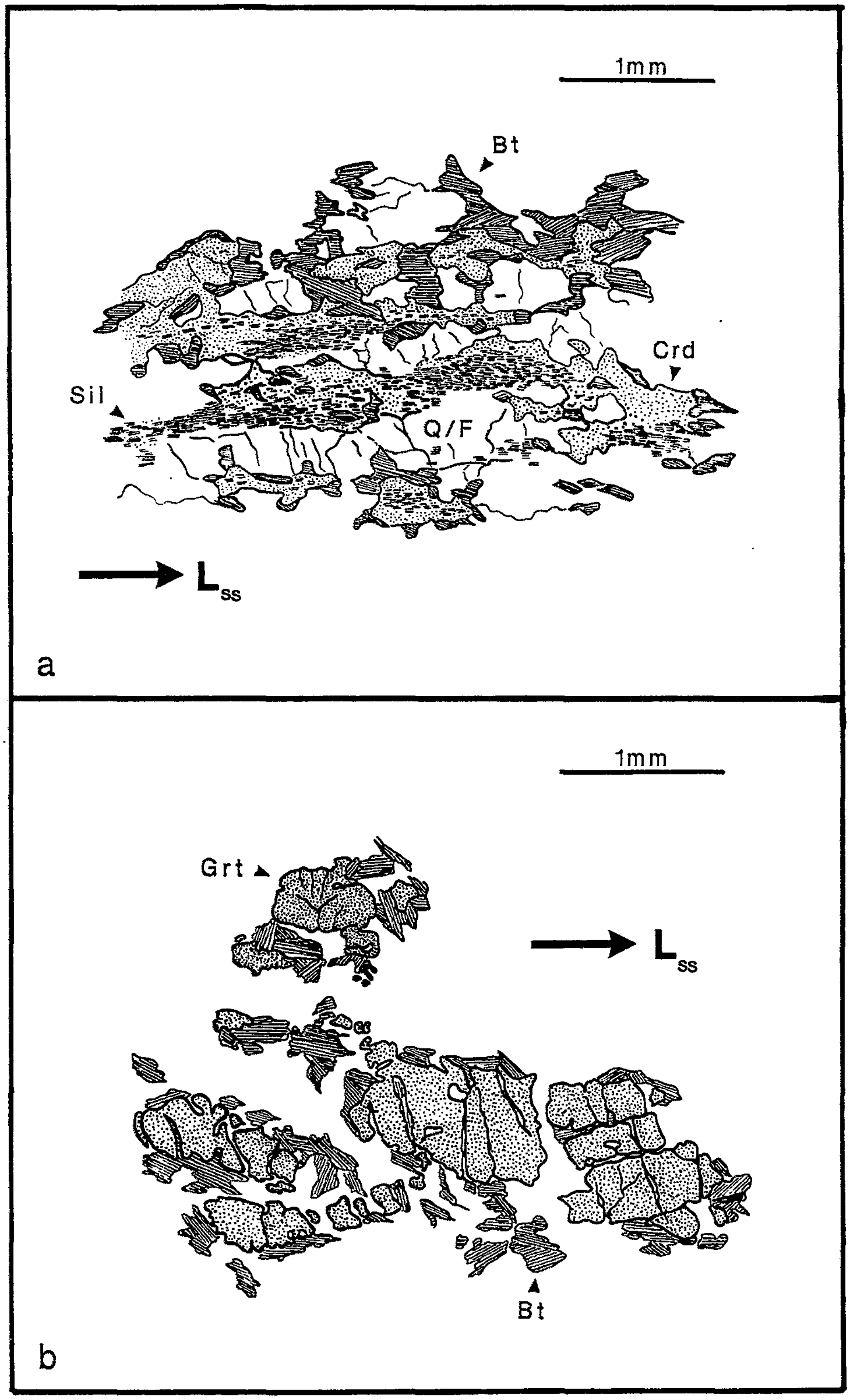

Figure 13 a and b. Textural relationships indicating metastable phase equilibria preserved in the margins of sheared and stretched leucosomes within the migmatitic augen gneisses, Kakamas Shear Zone. Sketches drawn from XZ-sections. Trend of the strike-subparallel elongation lineation (L_{ss}) is indicated.

(a) Elongate aggregates of pinitized cordierite, partially rimmed by biotite selveges, and shot-through by fibrous mats of sillimanite needles (sample CJS/12).

(b) Sheaves of biotite partially rimming poikiloblastic garnet aggregates (sample CJS/12).

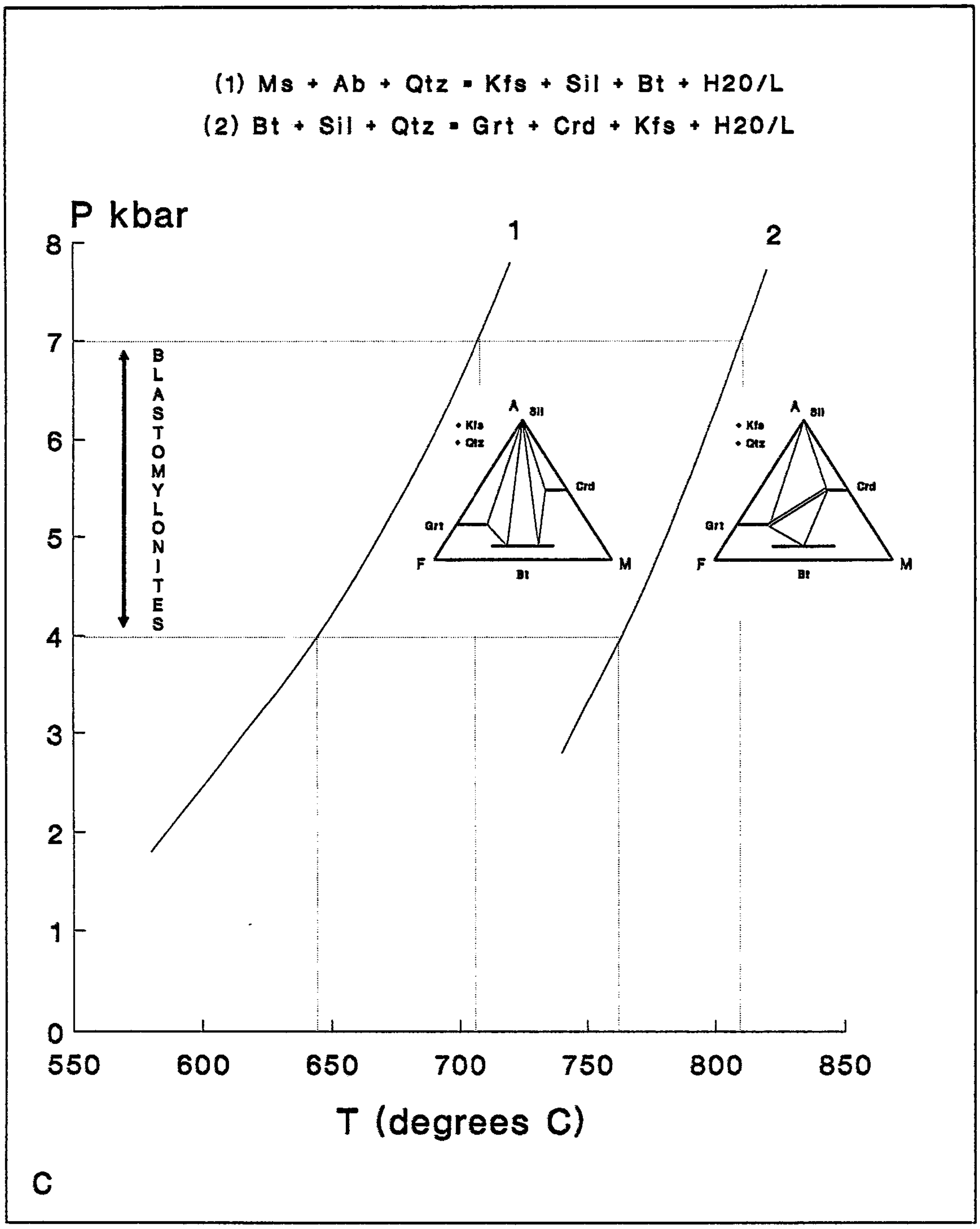

Figure 13c. P-T diagram illustrating phase equilibria for metapelitic rocks (after Thompson, 1982). Univariant reaction curves 1 and 2 represent the muscovite-out and sillimanite-out isograds. Textural relationships illustrated in Figure 13 a and b are consistent with the breakdown of Grt and Crd, to Bt and Sil, and are represented by reaction curve 2. The absence of Ms, and the assemblage Qtz + Kfs + Pl + Bt ± Sil ± Grt, within the augen gneisses, constrains metamorphic conditions during strike-slip shearing to the P-T space between reaction curves 1 and 2. The 4-7kb pressure range indicated, is representative of the generation-depths required for the formation of the "blastomylonitic" textures observed within the augen gneisses (Sibson, 1986). This pressure range and the above assemblage, require lower-limit temperatures of 650°C at 4kb, or 720°C at 7kb, during the right-lateral, strike-slip shearing. The term "blastomylonite" is used here to indicate fault rocks characterized by coarse grain-size resulting from extensive syntectonic or post-tectonic grain growth, and hence encompasses porphyroblastic, augen and mylonite gneisses.

Asymmetrical microstructures

Weakly-asymmetric σ-type feldspar porphyroclast systems (augen structures) and the stair-stepping geometry of "ghost" pressure shadows developed about some feldspar augen (Fig. 12a), indicate that the movement was *right-lateral, transcurrent, directed towards the SSE*. Although texturally cryptic, the inferred movement sense is invariable for all systems examined in both thin-section and on polished slabs. Consequently moderate confidence is placed in this kinematic interpretation (KCI = 2).

4.2.3 Cataclasite

The cataclasite displays textures consistent with a silicified microbreccia: Angular to subangular clasts of partially to wholly recrystallized, foliated mylonite and unfoliated reworked cataclasite are set in a fine-grained granoblastic matrix, comprising neoblasts of predominantly quartz, with lesser feldspar and dispersed sericite needles. Fine-grained epidote and chlorite aggregates occur in patches throughout the matrix, and are found partially or wholly replacing and pseudomorphing the clasts. Internal structure is random and several generations of crosscutting fractures occur on a variety of scales, affecting only minor displacements. Fractures commonly host coarse-grained, crystal-fibre infillings of quartz and coarse epidote.

4.3 Kinematic synthesis

Stereograms C and D of Figure 7 provide a synopsis of mylonite fabric orientation data, calculated kinematic vectors and movement sense determinations, for the quartz-feldspar mylonite gneiss and augen gneiss, respectively, from the Omkyk locality. Fabrics and microstructures preserved within ductile tectonites from a single transect of the KSZ, provide evidence for two distinct ductile shearing events.

1) Within quartz-feldspar mylonite gneisses, down-dip elongation lineations (L_{ds}) and σ-type porphyroclast systems within fluxion bands, indicate *normal (top to NNE)* dip-slip *movement, parallel to a kinematic vector orientated 018/39* (stereogram C, Fig. 7). Potential reverse movement

indicated by weak quartz deformation fabrics in sample CJS/9, is excluded from this discussion because of the general unreliability of quartz deformation fabrics, and the extremely low KCI assigned to this shear sense interpretation.

2) Subhorizontal elongation lineations (L_{ss}) and asymmetrical augen structures within biotite augen gneisses, are consistent with *right-lateral, strike-slip movement along a vector orientated 147/08* (stereogram D, Fig. 7).

No progressive change in orientation of the elongation lineation was observed along the transect, and the transition from down-dip to strike-parallel lineations occurs abruptly across the contact between the mylonite gneisses and the augen gneisses. Therefore it is unlikely that these two kinematic vectors are coeval, and that their difference in orientation reflects progressive rotation states of a single pre-existing lineation in response to a transverse shear strain gradient during later shearing*. Instead, the two kinematic vectors must be considered temporally distinct and representative of unique shearing events on the KSZ. Isolation of a fault block (shear lozenge) bearing an early kinematic signature, from penetrative ductile deformation during a later shearing event, could prevent transposition of the early vector, and might account for the preservation of two distinct movement vectors along this sampling transect.

It was not possible to constrain the *relative* timing of dip-slip and strike-slip shearing events on the basis of kinematic mineral assemblages or from microstructural criteria.

* Note that this interpretation differs significantly with an alternative hypothesis presented in (2) of section 8.1.3.4 and section 8.1.3.5. Neither interpretation is satisfactorily supported by the available data, nor is one model favoured above the other.

4.3.1 Estimation of the P-T conditions during transcurrent shearing

Mineral fabric and textural relationships within the augen gneisses allow a preliminary estimation of the metamorphic conditions at the time of strike-slip shearing.

Within the augen gneisses (L>S tectonite) sheaves of sillimanite and biotite locally define the L_{ss} elongation lineation (section 4.2.2 and Fig. 13a). Furthermore, localised disequilibrium textures (Fig. 13 a and b) along shear surfaces (S_M) are consistent with the retrograde reaction:

garnet + cordierite + K-feldspar + H_2O/L → biotite + sillimanite + quartz;

reflecting high-temperature retrogression of granulite facies dehydration products (Holdaway and Lee, 1977; Thompson, 1982). This reaction typically marks the upper amphibolite (Bt + Sil + Qtz) subfacies - granulite (Grt + Crd + Kfs) subfacies transition (reaction curve 2 of Fig. 13c) for metapelitic rocks.

Whether the sillimanite fibres and biotite sheaves locally defining L_{ss}, grew parallel to the elongation direction during shearing, or were passively rotated towards it, is unclear. However, the localised occurrence of sillimanite along inferred shear surfaces suggests that sillimanite growth was syn-kinematic with respect to the development of L_{ss} and S_M fabrics. No evidence pointing to sillimanite instability was found. Biotite flakes are unbent and display no internal strain features, reflecting post-kinematic static recrystallization.

Shear surfaces may have acted as fluid-pathways, promoting high-temperature retrogression, resulting in the development of biotite and sillimanite at the expense of garnet, cordierite and K-feldspar along the margins of sheared neosome material in the deformed migmatitic gneiss.

The absence of muscovite, and the stable coexistence of quartz, K-feldspar and sillimanite, is consistent with amphibolite facies metamorphism and constrains PT conditions of metamorphism to the P-T space between the continuous reaction curves 1 and 2 of Fig. 13c. Assuming that the porphyroblastic gneiss / augen gneiss was generated within a typical 15-25km [4-7kb] depth range (Sibson, 1986), and following mineral equilibria established by Thompson (1982), lower-limit temperatures of between 640°C and 710°C are prescribed for the strike-slip shearing event recorded by the penetrative L>S tectonite fabrics.

Harris (1990) describes equivalent textural relationships in quartzo-feldspathic gneisses within the zone of stretching adjacent to the Pofadder Lineament. He notes that the elongation lineation within these rocks is locally defined by sheaves of sillimanite, indicating temperatures within the sillimanite-almandine-orthoclase subfacies (approximately 650°C) during the D_4 right-lateral shearing event.

Bard (1986, p204-205) describes similar textures in a biotite-sillimanite bearing gneiss from Sierra Morena, Spain. He notes that this fabric relationship is relatively common in anatectic catametamorphic zones, where ductile shearing accompanied metamorphism and anatexis. Under these conditions shear planes may present favourable nucleation sites for fibrolite formed by mass transfer of aluminium, silica, and alkali (particularly K_2O).

4.3.2 Implications of strain/stress induced myrmekite and sillimanite

The development of myrmekite and/or fibrolitic sillimanite at sites of high shear strain and/or stress within the rims of K-feldspar megacrysts, and at contact-points between abutting porphyroclasts, indicates that high-temperatures accompanied penetrative fabric development in the augen gneisses. Simpson (1985) and Simpson and Wintsch (1989) documented occurrences of deformation-induced myrmekite within amphibolite facies mylonite and lineated gneiss from the Eastern Peninsula Ranges mylonite zone (EPRMZ), California, and the Hope Valley Shear Zone (HVSZ), Connecticut. Average minimum and maximum temperatures during deformation of 495-540°C (at 4-5kb; middle amphibolite facies) and 440-445°C, have been calculated for the EPRMZ and HVSZ respectively (Simpson and Wintsch, 1989). La Tour and Barnett (1987) described deformation-induced myrmekite within mylonitic granitic rocks of the Idaho Batholith, and indicated that deformation temperatures were in the range 500-600°C (at 4.5kb). Wintsch and Andrews (1988) estimate temperatures of 700°C (at 5kb) for stress-induced replacement of feldspar and biotite by fibrolitic sillimanite within a deformed pegmatitic dyke near Centerbrook, Connecticut.

Development of subgrains within K-feldspar and plagioclase in the augen gneisses are consistent with their deformation by recrystallization-accommodated dislocation creep (White, 1975; Tullis and Yund, 1985, 1987). This mechanism is prevalent in feldspars deformed at middle to upper amphibolite grade (Tullis and Yund, 1987).

4.4 Discussion

Textural relationships within the ductile tectonites of KSZ are consistent with significant static recrystallization and annealing grain growth. No true mylonite microtextures are present, but larger mylonite microstructures e.g. porphyroclast systems, retain their shapes and are recognizable despite the degree of recovery. The asymmetry of internal microstructures and the intensity of penetrative fabric development (particularly in the augen gneisses), are indicative of their formation under conditions of non-coaxial, high-temperature, *ductile* deformation. Three conceivable scenarios account for the microtextural state of KSZ tectonites:-

1) Shear deformation occurred during the prograde metamorphic path, and mylonitic textures annealed following cessation of deformation.

2) Shear deformation occurred at elevated temperatures coinciding with, or closely following the metamorphic peak in the area. At high recovery rates and low strain rates, penetrative ductile flow produced tectonites characterized by coarse grain-size and pervasive recovery.

3) Shear deformation and mylonitization was followed by emplacement of bodies of Friersdale charnockite to the east and southeast of the Omkyk locality, which elevated temperatures, causing widespread textural re-equilibration within KSZ tectonites.

If, as Stowe (1983, 1986) and Van Bever Donker (1980) suggest, the age of right-lateral, strike-slip shearing on the KSZ is partially, or wholly post-D_3, then the previous characterization of post-D_3 events as retrogressive (with respect to M_2) and low-grade (Joubert, 1974a, 1978; Van Bever Donker, 1980; Moore, 1989) is in conflict with the high-temperature, "blastomylonitic" fabrics of the augen gneisses. Mineral parageneses and textural relationships within KSZ tectonites, clearly indicate that right-lateral, transcurrent shearing on the KSZ, with associated development of penetrative stretching fabrics (L_{ds}) within migmatitic augen gneisses, occurred at elevated temperatures. Earlier interpretations correlating the metamorphic thermal peak with D_2/D_3 are called into question, and the persistence of elevated temperatures well into the D_4, right-lateral transcurrent shearing event seems probable (see also Harris, 1990, 1992).

Brittle reactivation, associated with low-temperature hydrothermal alteration and pervasive silicification, appears to have occurred late in the deformation history of the KSZ, producing true cataclasites and crush breccias. *Episodic* seismic strain rates within a prolonged, high-temperature aseismic shearing event *is not* a conceivable mechanism for generating these cataclasites, in view of their association with low-temperature hydrated minerals, and the absence of overprinting of random fabrics by a second generation of continuous mylonitic fabrics.

Chapter 5. - The Hugosput Shear System

5.1 Macrostructure

The Hugosput Shear System (hereafter referred to as the HSS) is a 7km wide, northwest-trending belt of anastomosing ductile shear zones characterized by intense mylonitization (Fig. 2 and 14). Protoliths for the mylonitic rocks include Korannaland Sequence quartzo-feldspathic gneisses, aluminous gneisses, calc-silicate gneisses, amphibolite gneisses, and feldspathic quartzites. Small, contorted lens-like bodies of potassic charnockite occur in the central part of the HSS and are intimately associated with the mylonite zones. A single lens of potassic charnockite occurs in the southern part of the HSS. The contact relationships of the potassic charnockite and the Korannaland Sequence rocks are obscured by the high degree of shearing that has occurred. Harris (*pers. comm.*, 1989; 1990) suggests that the charnockitic bodies may represent up-thrusted slices of older, deeper-level crustal material, that have been dispersed laterally by later, right-lateral transcurrent movement on the mylonite zones.

Fifteen samples of protomylonite, orthomylonite and ultramylonite, dominated by quartzo-feldspathic mineralogies, were collected from three selected localities on the HSS. Three samples were obtained from the northern extension of the HSS on the farm Koegab 59 (locality A, Fig. 14), eight from the central portion on the farm Rozynenbosch 104 (locality B, Fig. 14), and three from the south-central extension on the farm Pypklip 105 (locality C, Fig. 14). Kinematic analyses of the three sampling areas were performed independently in order to minimize the effects of localized refolding and movement partitioning along strike.

Figure 14. (overleaf) Compilation of kinematic interpretations of fabric orientation and microstructural data of samples from the northern (A), central (B) and southern (C) areas of the Hugosput Shear System. Sample localities are labelled and are indicated on the map by KCl symbols. Lower-hemisphere stereoprojections (1 to 6) show the orientation of poles to S_M (solid circles), poles to XZ sections (open circles), and L_M lineations (solid triangles). Mean S_M planes and XZ sections are shown as solid and dashed great-circles respectively. Calculated kinematic vectors with relative dip-slip component of shear are indicated by large split-circle symbols; filled half marks down-dropped side.

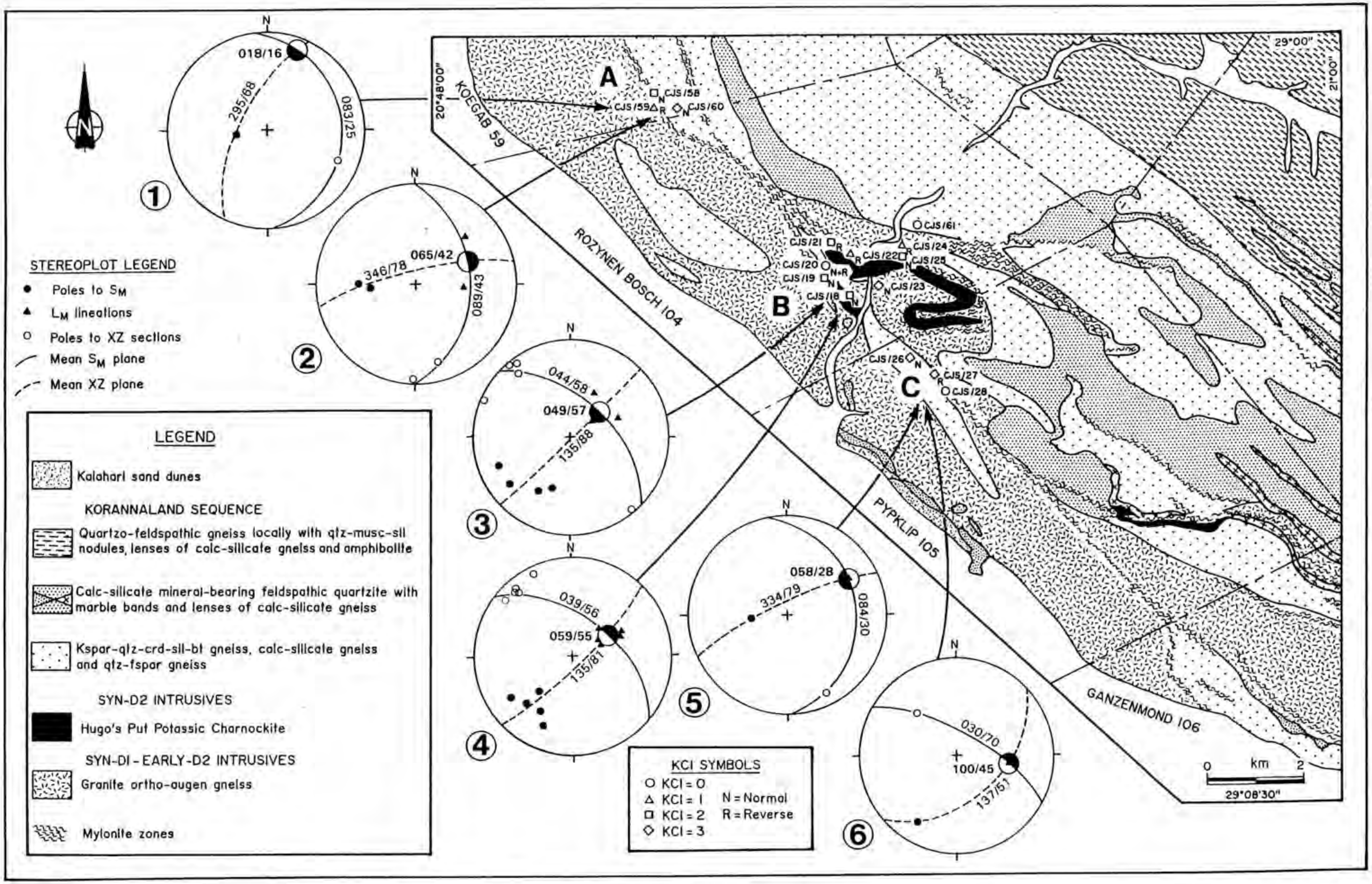
A
B
C
CJS/58
CJS/59
CJS/60
CJS/61
CJS/18
CJS/19
CJS/20
CJS/21
CJS/22
CJS/23
CJS/24
CJS/25
CJS/26
CJS/27
CJS/28
KOEGAB 59
ROZYNEN BOSCH 104
PYPKLIP 105
GANZENMOND 106
20°48'00"
29°00"
21°00"
29°08'30"
0 km 2
N
018/16
295/68
083/25
065/42
346/78
089/43
044/58
049/57
135/88
039/56
059/55
135/81
058/28
334/79
084/30
030/70
100/45
137/51
STEREOPLOT LEGEND
Poles to S_M
L_M lineations
Poles to XZ sections
Mean S_M plane
Mean XZ plane
LEGEND
Kalahari sand dunes
KORANNALAND SEQUENCE
Quartzo-feldspathic gneiss locally with qtz-musc-sil nodules, lenses of calc-silicate gneiss and amphibolite
Calc-silicate mineral-bearing feldspathic quartzite with marble bands and lenses of calc-silicate gneiss
Kspar-qtz-crd-sil-bt gneiss, calc-silicate gneiss and qtz-fspar gneiss
SYN-D2 INTRUSIVES
Hugo's Put Potassic Charnockite
SYN-D1 - EARLY-D2 INTRUSIVES
Granite ortho-augen gneiss
Mylonite zones
KCI SYMBOLS
KCI = 0
KCI = 1
KCI = 2
KCI = 3
N = Normal
R = Reverse

5.2 Mesostructure

The orientation of mylonite fabric elements within the northern, central and southern sampling areas are shown on stereograms A, B and C of Figure 15 respectively. Combined fabric orientation data for the whole HSS sample set are shown in Figure 19.

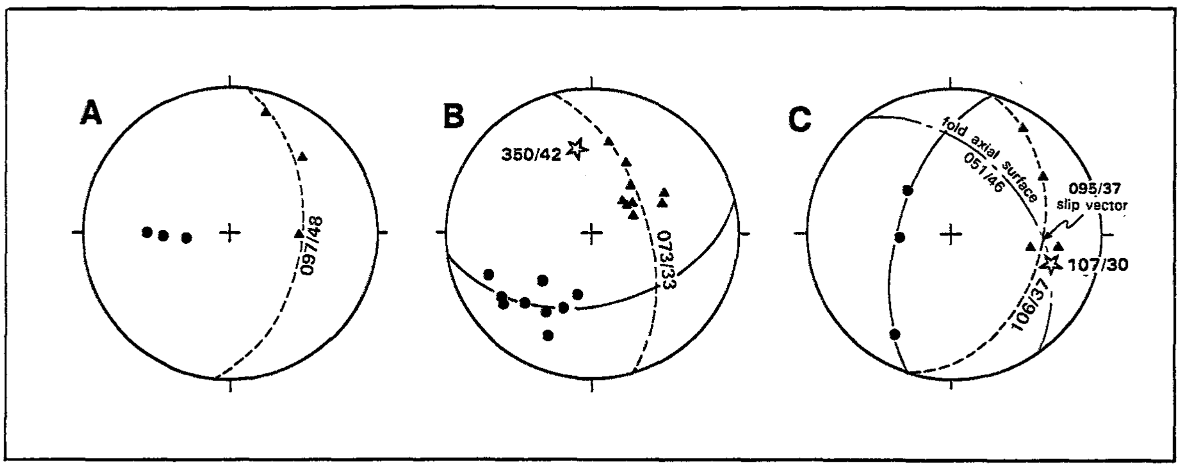

Figure 15. Lower-hemisphere, equal-area stereograms illustrating the orientation of mylonite fabric elements within the northern (A), central (B), and southern (C) sampling areas of the HSS. L_M lineations and poles to S_M foliations are indicted by triangle and circle symbols respectively. Stars denote statistical fold axes for each sampling area (calculated using S_M data). Solid and dashed great-circles indicate computed best-fit girdles to the planar dispersion of S_M poles and L_M lineations respectively. See text for explanation.

5.2.1 Northern area

The mylonite zone sampled on the northern extension of the HSS is characterized by quartzo-feldspathic orthomylonites with well-developed L-S fabrics. At the sample locality, S_M dips at 37° to the E, while the orientation of L_M is variable, and a range in trends from NNE to E is observed (stereogram A, Fig. 15). NNE-trending lineations are characterized by shallow plunges, and plunges become increasingly steep with more easterly trends (ds/ss = 0.34 - 4.70, rake of L_M in S_M = 19-78°).

5.2.2 Central area

Within the central area several subsidiary splays were sampled adjacent to the central mass of potassic charnockite. The attitude of S_M within the central area is variable and reflects the divergence of subsidiary splays from the principal NW-SE trending mylonite zone. Subsidiary splays strike E-W and dip at 35-45° towards the N. Broad synformal warping of the mylonite zone about a moderately plunging, NNW-trending (350/42) F_3 fold axis may also explain the variable orientation of S_M (see stereogram B of Fig. 15. and the map of Fig. 14), but this explanation is not favoured since no sympathetic folding of lithological contacts is observed. Harris (*pers. comm.*, 1991) finds no evidence of megascopic F_3 structures in the Hugosput area, but notes that metre-scale, minor N-NE plunging cross-folds are widespread, and these he correlates with D_3. Throughout the central area the orientation of L_M is down-dip (ds/ss = 2.05 - 28.64, rake of L_M in S_M = 64-88°), with plunges varying from moderate towards the NNE, to slightly steeper towards the NE.

5.2.3 Southern area

Samples from the southern area were collected around a broad, plunging-inclined, monoclinal flexure in the basal mylonite zone of the HSS. The calculated fold axis for this fold is 107/30 (stereogram C, Fig. 15). This minor fold displays Z-vergence, consistent with an origin by right-lateral transcurrent shearing of post-mylonite fabric age. This is corroborated by the great-circle distribution of dispersed L_M lineations (106/37) which is diagnostic of a shear-folding mechanism (Hobbs *et al.*, 1976). For ideal shear-folding, the intersection of the lineation dispersion plane (dashed-line, Fig. 15C) and the plane of shearing (parallel to the axial plane of the fold) gives the slip-direction. The intersection of the reconstructed axial surface of this fold (051/46) and the lineation dispersion plane (106/37) yields a slip vector of 095/37.

5.3 Characteristic microstructures in mylonites from the HSS

A comprehensive microtextural review of individual samples is presented in Table 3 of the Appendix. Selected sketches and photomicrographs of microtextures exhibited by HSS mylonites are presented in Figures 16, 17 and 18.

Quartz-feldspar orthomylonites and ultramylonites from the HSS are characterized by textures indicating uniformly strong recovery, commonly with extensive annealing. The size and abundance of feldspar porphyroclast systems is variable, as well as the relative proportions of component mineral species (particularly micas), the degree of quartz-ribbon development, and the grain-size of the matrix.

5.3.1 Orthomylonites

The orthomylonites are typically porphyroclastic, with a well-developed fluxion foliation (S_M), defined by highly-elongated and flattened quartz-ribbon aggregates, and millimetre to centimetre scale compositional banding. Some samples display a strong preferred alignment of magnetite and mica (001) platelets parallel to S_M.

Feldspar (K-feldspar, microcline and plagioclase) porphyroclasts are ubiquitous and σ (Fig. 16 a, f, g, h, n and r, Fig. 17 a and b),δ (Fig. 16 b, d and e) and complex σ-δ type systems (Fig. 16 c and l) are represented. In porphryroclast-rich orthomylonites, σ_b type porphyroclasts are observed in weak S-C fabric configurations (Fig. 16 g, h and r). Porphyroclast size is extremely variable and ranges from 0.2mm to 4mm. Porphyroclasts are frequently concentrated in discrete layers parallel to S_M, but may also be dispersed within a fine to medium-grained matrix, showing strong recovery and moderate annealing.

Feldspar porphyroclast systems commonly comprise a central highly-strained, relict feldspar megacryst, surrounded by a mantle of smaller recrystallized grains and subgrains, which merges with asymmetric tails of recrystallized feldspar. The recrystallized tails and mantles are commonly enveloped and "armoured" by quartz ribbon-aggregates, which preserve the shape of the porphyroclast system despite a high degree of recrystallization (e.g. Fig. 16f). Myrmekite is sometimes developed at the interface between recrystallized mantle material and the relict clast (Fig. 18a). Some feldspar megacrysts are completely recrystallized, forming coarse-grained polygonal aggregates which remain texturally distinct from mantle and matrix material.

The matrix is composed of recrystallized aggregates of microcline (K-feldspar), plagioclase, quartz and chlorite (after biotite), whose relative proportions define the compositional banding (Fig. 17c). Matrix grain-size is variable ($<$0.1-0.3 mm) and is determined largely by the relative proportions of quartz and feldspar; feldspar-rich domains are generally finer-grained than quartz-rich domains. Quartz and feldspar grain-shapes are globular to tabular, with curved or straight grain boundaries. Serrate grain boundaries are extremely uncommon. Most matrix grains show evidence of internal strain, including deformation twinning and undulatory extinction.

Highly-elongate quartz-ribbons are widespread, comprising strain-free aggregates with high-angle grain-boundaries, suggesting that quartz is almost completely recrystallized and recovered. The "pinning" of quartz grain-boundaries by micas, opaques and recrystallized feldspar grains, aligned along the edges of the ribbons, preserves their smooth outlines. Feldspar porphyroclast systems are frequently concentrated along bands containing abundant quartz-ribbons.

Orthomylonites from the northern area show a greater degree of recovery and annealing grain-growth than do those from the central and southern areas

5.3.2 Ultramylonites

The ultramylonites comprise a very fine-grained matrix (<0.1mm) of recrystallized quartz, feldspar, micas (usually biotite or chlorite) and opaque minerals, containing relatively few feldspar porphyroclasts. The matrix comprises >90% of the rock. Variations in the relative proportions of quartz, feldspar and (particularly) micas in the matrix, define a millimetre-scale, compositional fluxion banding (S_M) (e.g. Fig. 17c). Matrix grain-size is determined largely by the volume density of micas, indicating that inclusion inhibition was an active process during matrix recrystallization and grain growth (Hobbs *et al.*, 1976). The result is a series of planar domains of different matrix grain-size and mica-content, with mica-rich compositional bands tending to be finer-grained than mica-poor bands (e.g. Fig. 17d).

Within some ultramylonites, fine-grained micas display a strong (001) alignment, inclined obliquely to S_M (Fig. 16 i and j, Fig. 17 c and d). Opaque mineral grains occur in trains along discrete planes parallel to S_M (Fig. 16 i and j), but are also dispersed within the mica-rich layers, where they exhibit a weak oblique shape-fabric which parallels the oblique mica (001) alignment. Within mica-rich porphyroclastic ultramylonites (e.g. sample CJS/26), disruption and deflection of the mica preferred-orientation fabric occurs around feldspar porphyroclasts (Fig. 16 m, o and p, Fig. 17e).

Porphyroclasts within the ultramylonites are generally small ($<$2mm) and are composed of K-feldspar, microcline and plagioclase, which show evidence of intracrystalline ductility (Fig. 18b). Asymmetrical porphyroclast systems include σ (Fig. 16 k), δ (Fig. 16m, Fig. 17e), complex σ-δ, and tailess Θ types (Fig. 16 o and p). Porphyroclast shapes are generally spheroidal to ellipsoidal, but may be extremely elongate attaining shape-aspects of 5:1 (sample CJS/26). Most elongate porphyroclasts are orientated with their long-axes parallel to the flow plane, resulting in flat-geometry σ-type systems. However, a few tabular feldspar porphyroclasts occur as "rolling structures" (δ- and tailess Θ-type systems) at high-angle to the flow plane (Fig. 16o and Fig. 17e). This conflicts with the finding of Passchier and Simpson (1986) that δ-type systems only occur around equidimensional or very slightly elongate porphyroclasts. Porphyroclast-matrix interfaces are generally sharp, although some clasts are enclosed by narrow mantles of polygonal neoblasts. The grain-size of the recrystallized mantles generally exceeds that of the matrix. The relict feldspar clasts often exhibit strain features consistent with strong ductile deformation. Undulatory extinction, deformation twins, bent twin lamellae and kink bands are ubiquitous.

Relict quartz ribbon-aggregates are a volumetrically minor component of some ultramylonites, where they help define S_M. The ribbon-aggregates are generally more attenuated and discontinuous than those in the orthomylonites. Ribbon-matrix interfaces are "pinned" by micas, feldspars and opaque mineral grains, aligned along the margins of the ribbon-aggregates. The ribbon-aggregates are always more coarsely-recrystallized than the matrix, and exhibit high-angle grain-boundaries consistent with complete recovery.

Recovery within HSS ultramylonites is pervasive and annealing textures are locally well-developed. Quartz-rich ultramylonites (sample CJS/22) and ultramylonitic quartzites (sample CJS/28) in particular, exhibit equilibrium textures consistent with significant static annealing. Within the ultramylonitic quartzite, polygonization is complete, and sub-rectangular, strain-free quartz-grains form composite S_M-parallel ribbons separated by linear trains of opaque minerals (Fig. 18c).

5.3.3 K-feldspar-cordierite-quartz protomylonite

A single sample (CJS/24) of Kfs-Crd-Qtz protomylonite was collected from a zone of sheared aluminous gneisses within the central area. The protomylonite is weakly-foliated, comprising domains of fractured K-feldspar and cordierite, interspersed with irregular bands or lozenge-shaped domains of ductilely deformed quartz. The Kfs-Crd domains are characterized by subparallel arrays of grain-scale tension fractures aligned perpendicular to the protomylonitic foliation. Tension fractures are infilled by magnetite (Fig. 17h). Quartz-domains reflect typical intermediate products of dynamic recrystallization, in which coarse, relict, monocrystalline quartz-ribbons (1-3 mm - long-dimension), displaying undulatory extinction, deformation bands and subgrains, are almost completely modified to polycrystalline aggregates of fine-grained neoblasts (<0.2 mm) with dentate grain-boundaries.

The Kfs-Crd domains are disrupted by anastomosing microshears, subparallel to S_M, defined by sheaves of fibrolitic sillimanite. Locally, the fibrolitic microshears isolate and enclose irregular cordierite porphyroclasts, resulting in indistinct σ_b-type systems with weak S-C fabric configurations (Fig. 17 g and h). Isolated σ_a-type cordierite porphyroclasts with asymmetrical fibrolitic tails occur in the quartz-domains (Fig. 17 g and h). Cordierite porphyroclasts often contain inclusion trails of acicular and prismatic sillimanite, and are pinitized along healed intergranular fractures (Fig. 17g). Deformation twins are common within cordierite grains.

Fibrolitic sillimanite forms narrow (<0.1mm) reaction rims around cordierite (and sometimes K-feldspar) porphyroclasts. Biotite occurs as reaction rims around magnetite grains, and in low-strain domains, such as within boudin-necks and pressure shadow tails adjacent to feldspar and cordierite porphyroclasts (Fig. 17 g and h). Intergrowths of biotite and fibrolitic sillimanite occur locally.

5.3.4 Asymmetrical microstructures

5.3.4.1 Northern area

Asymmetrical feldspar porphyroclast systems provide the most useful kinematic information in orthomylonites from the northern area. Both σ, δ and complex σ-δ types are represented. Due to the advanced recovery state of these rocks, these systems are best observed in polished rock sections. Although texturally cryptic, the asymmetrical shapes of recrystallized porphyroclast systems are often outlined in thin-section by enveloping quartz ribbon-aggregates, or by deflection of micas in the matrix. Asymmetrical pressure-shadow "beards" of chlorite are developed about some feldspar porphyroclasts (Fig. 16a).

Sketches of selected asymmetrical porphyroclast systems within northern area tectonites are illustrated in Figure 16 (a) to (f), and Figure 17 (a) and (b). These σ, δ and complex σ-δ porphyroclast systems provide evidence for both normal (top to NNE) and reverse (top to SSW) movement sense. Porphyroclast systems indicating reverse movement (Fig. 16d) are generally more weakly-developed than those indicating normal movement (Fig. 16 a-c, e-f), and are only encountered in a single sample (CJS/59), characterized by a shallow, NNE-plunging L_M.

5.3.4.2 Central area

Kinematic indicators within the central area attest to both reverse (NE-side up) and normal (NE-side down) movement corroborating the results of shear sense determinations for the northern area samples. σ and δ porphyroclast systems and oblique mica (001) fabrics proved the most useful kinematic indicators within mylonites of the central area (Fig. 16 g-l and n).

Most samples preserve a variety of indicators that prescribe a consistent shear sense (either normal *or* reverse movement). Within these samples there is generally no relationship between the precribed shear sense and the type, or intensity of development, of the indicator fabric/microstructure. Only one ultramylonite sample (CJS/20) contains asymmetrical microstructures indicating opposing shear sense within the same section. A weakly-developed oblique chlorite (001) fabric and the antithetic stacking of opaque mineral platelets indicate normal (top to ENE) movement (Fig. 16j), whilst well-developed σ (Fig. 16k) and δ feldspar porphyroclasts indicate reverse (top to WSW) movement.

5.3.4.3 Southern area

Asymmetrical microstructures indicating both normal (top to E) and reverse (top to SW) movement sense are preserved within mylonites from the southern area. σ (Fig. 17 g and h), δ (Fig. 16m and 17e), tailess Θ porphyroclast systems (Fig. 16 o and p), and oblique biotite (001) and magnetite DPO fabrics (Fig. 17 c and d), preserved within an orthomylonite-ultramylonite specimen (sample CJS/26) indicate that movement was *normal (top to E)*. *Reverse (top to SW)* movement sense is indicated by the stair-stepping geometry of σ_a porphyroclasts (Fig. 17 g and h), the S-C fabric configuration of σ_b porphyroclasts (Fig. 17 g, h and r), rare δ porphyroclasts, and the rotation of fractured feldspar porphyroclast fragments (Fig. 16q and 17f). Highest confidence (KCI=3) is assigned to both these shear sense interpretations.

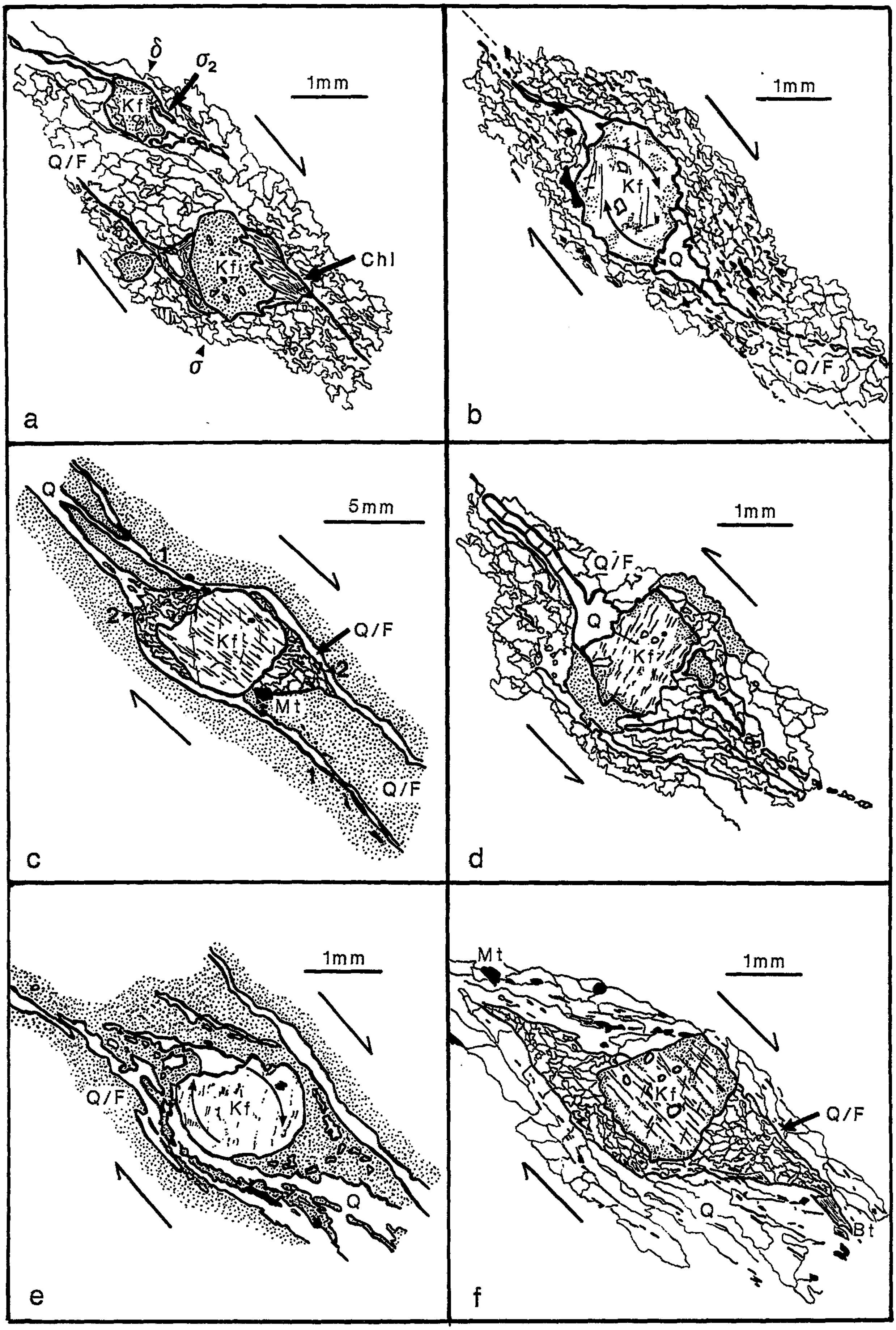
δ
σ2
1mm
Kf
Q/F
Kf
Chl
σ
a
1mm
Kf
Q
Q/F
b
Q
5mm
1
2
Kf
Q/F
2
Mt
1
Q/F
c
1mm
Q/F
Q
Kf
d
1mm
Q/F
Kf
Q
e
Mt
1mm
Kf
Q/F
Q
Bt
f

Figure 16. (previous page) (a)-(f) Examples of asymmetrical porphyroclast systems within quartz-feldspar orthomylonites from the northern area, Hugosput Shear System (HSS). All sketches made from XZ-sections, viewed towards the NW and maintaining the correct dip sense. Dip angles are not true.

(a) σ_a-type K-feldspar porphyroclast system (**Kf**) with dynamically recrystallized tails of feldspar and new chlorite (**Chl**) in a quartz-rich matrix (**Q/F**), indicating normal (top-to-NNE) movement sense. A smaller relict δ-type porphyroclast with elongate, boudinaged tails of partially recrystallized quartz and a single incipient, second generation σ-type tail of reaction-softened feldspar (σ_2). Both systems are consistent with normal, NNE-side down, movement sense (sample CJS/58).

(b) K-feldspar δ-type system with characteristically long, curved tails of recrystallized quartz which traverse the symmetry axis of the system (dashed-line). The tails become boudinaged at some distance away from the central clast. Normal, NNE-side down, movement sense is indicated (sample CJS/58).

(c) Complex σ-δ system developed about a K-feldspar porphyroclast in a quartz-rich quartzo-feldspathic matrix. Normal, NNE-side down, movement sense is indicated. First generation (δ-type) tails (**1**) are defined by narrow, elongate recrystallized quartz-ribbons (**Q**) extending away from the quartz-rich grain mantle. Second generation (σ-type) tails (**2**) comprise more distinct, asymmetrical pressure-shadow domains of recrystallized quartz and feldspar, mantled and armoured by ribbon-like quartz which extends away from the apex of the pressure-shadow "beards", parallel to the flow plane (sample CJS/60).

(d) δ-Type K-feldspar porphyroclast partially obscured by annealing grain overgrowths. Adjacent to the central clast the tails comprise reaction softened clast-derived material. Tail extensions are defined by recrystallized ribbon-like quartz that has been partially consumed by the recrystallizing quartz-rich matrix. Tail asymmetry is consistent with reverse (top-to-SSW) sense of shearing (sample CJS/59).

(e) δ-Type K-feldspar porphyroclast with tails of recrystallized quartz set in a quartz-feldspar matrix. Normal (top-to-NNE) vorticity is indicated (sample CJS/60).

(f) Asymmetric, highly-recrystallized quartz-feldspar pressure-shadow "beards" developed in a σ-type feldspar porphyroclast system. Grain size dimunition has accompanied pervasive recrystallization within the strain-shadow domains. Pressure shadow "beards" are mantled and armoured by coarse-grained quartz-ribbons. Shear sense is normal (top-to-NNE) (sample CJS/60).

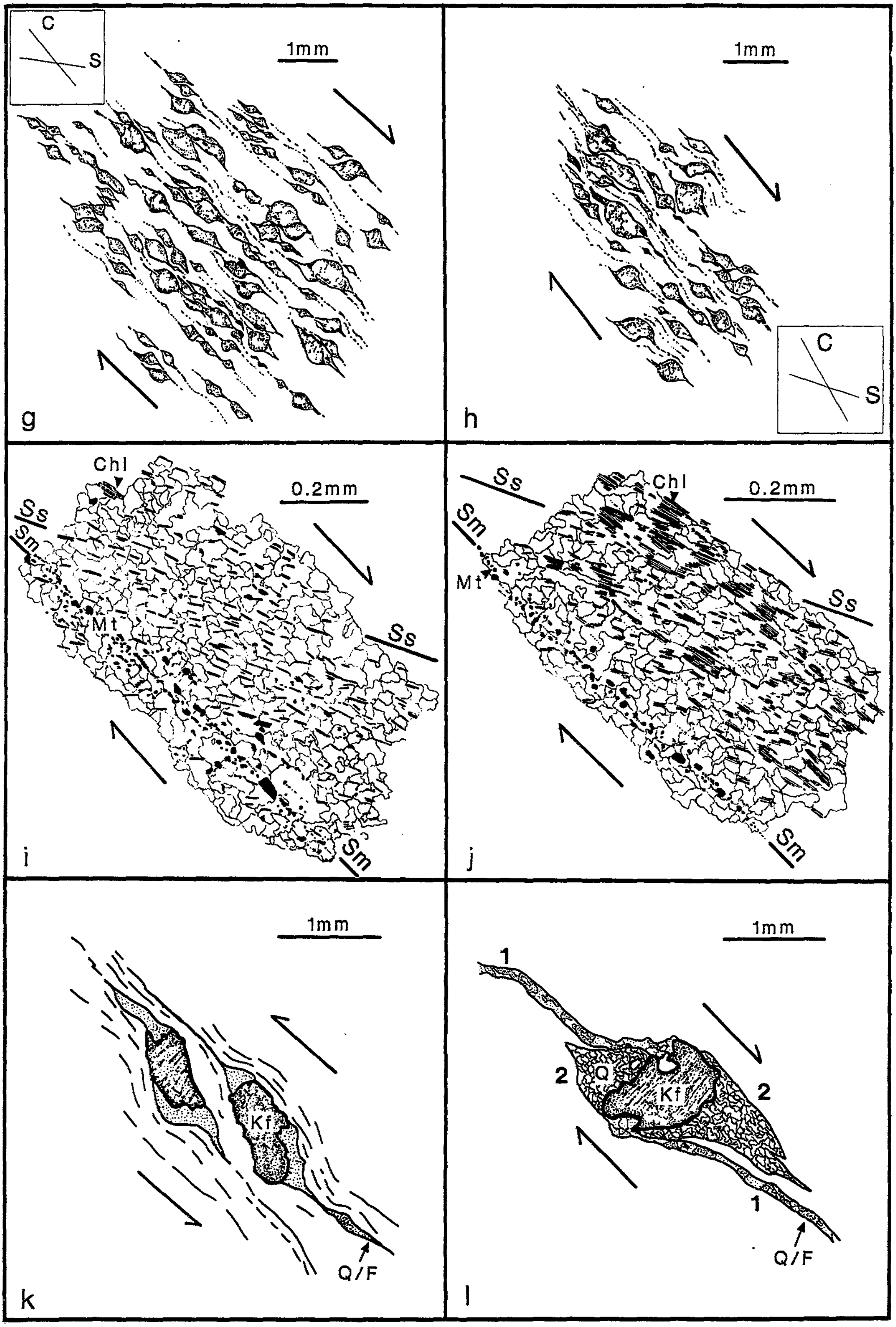
C
S
1mm
g
1mm
C
S
h
Chl
0.2mm
Ss
Sm
Mt
Ss
Sm
i
Ss
Chl
0.2mm
Sm
Mt
Ss
Sm
j
1mm
Kf
Q/F
k
1mm
1
2
Q
Kf
2
1
Q/F
l

Figure 16. (continued) Selected kinematic indicators within tectonite samples from the central area (i, j, k and l) and southern area (g and h) of the HSS. All sketches made from XZ-sections, viewed towards the NW and maintaining the correct dip sense. Dip angles are not true.

(g) and (h) Typical retort (sigmoidal) shaped feldspar augen in weak S-C fabric configuration within a quartz-feldspar orthomylonite. Shear band development is highly localized and impersistent. Note the typical "stair-stepping" geometry of augen linked by recrystallized tails. Tails trend subparallel to C-surfaces and step-up in the direction of shear. Normal, NE-side down, shear sense is indicated (sample CJS/19).

(i) and (j) Chlorite (001) preferred orientation in quartz-feldspar ultramylonites, defining a secondary fabric ($\mathbf{S_s}$) oblique to the mylonite compositional layering ($\mathbf{S_m}$). S_m defined by trains of opaque mineral grains (**Mt**), and by regular variations in the grain-size of recrystallized quartz. The sense of obliquity of S_s with respect to S_m indicates normal, NE-side down, movement sense and presumably reflects a late increment of deformation (sample CJS/18 and CJS/20).

(k) σ-Type K-feldspar porphyroclasts with asymmetric tails of recrystallized quartz and feldspar, indicating reverse, NE-side up, movement sense. Quartz-feldspar ultramylonite (sample CJS/20).

(l) Complex σ-δ system developed about a K-feldspar porphyroclast within quartz-feldspar orthomylonite. Embayments are developed at the rim of the clast where the "roots" of first generation (δ-type) polycrystalline tails (**1**) have consumed reaction softened clast material. Broader second generation (σ-type) tails (**2**) have developed in pressure shadow domains adjacent to the central clast, and comprise equigranular, structureless quartz. Normal, NE-side down, shear sense is indicated (sample CJS/21).

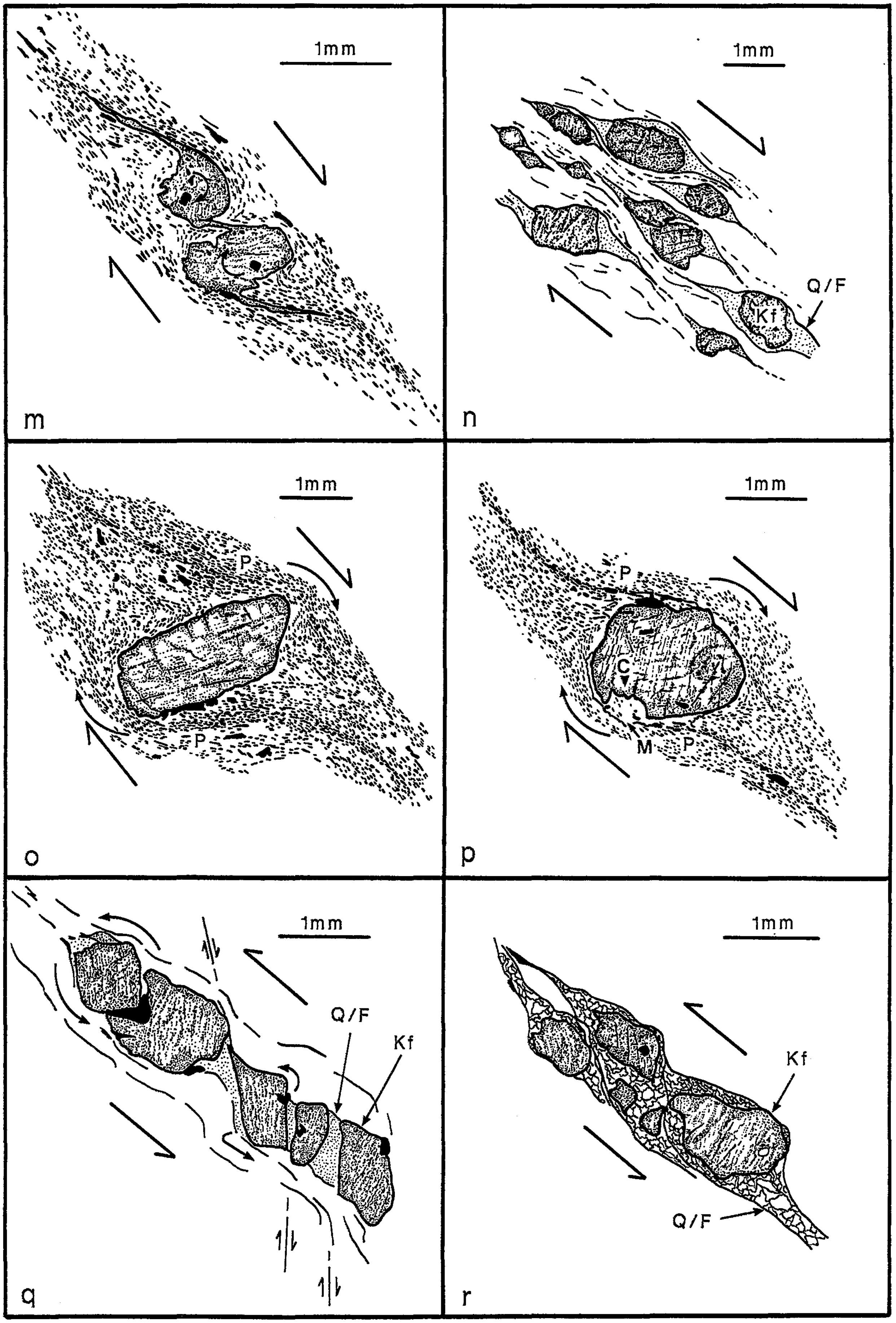
1mm
m
1mm
Q/F
Kf
n
1mm
P
P
o
1mm
P
C
M
P
p
1mm
Q/F
Kf
q
1mm
Kf
Q/F
r

Figure 16. (continued) Selected kinematic indicators within tectonite samples from the central area (n) and southern area (m, o, p, q and r) of the HSS. All sketches made from XZ-sections, viewed towards the NW and maintaining the correct dip sense. Dip angles are not true.

(m) Linked δ-type K-feldspar porphyroclast systems disrupting biotite-rich matrix within quartz-feldspar ultramylonite. Clockwise (normal, NE-side down) vorticity is indicated. Trailing edges of the rotating clasts drag the matrix into parallelism with their recrystallizing tails, while the leading edges cause distortion of the matrix ahead of the clast (sample CJS/26).

(n) Asymmetric σ-type K-feldspar porphyroclasts, with mantles and tails of recrystallized quartz and feldspar, within quartz-feldspar orthomylonite. The stair-stepping geometry of the systems is consistent with normal, NE-side down, movement sense (sample CJS/23).

(o) Elongate, tailless Θ-type K-feldspar porphyroclast system disrupting biotite-rich matrix in quartz-feldspar ultramylonite. Biotite-rich matrix material, flowing around the rotating clast during non-coaxial deformation, has piled-up on opposite sides of the clast, creating a paired set of perturbed zones (**P**) which are asymmetrically distributed about the central clast. Shear sense is indicated by the direction in which the perturbed zones step-down across the clast. Normal, NE-side down, movement sense is prescribed (sample CJS/26).

(p) Disruption of biotite-rich matrix about an equidimensional, tailless Θ-type porphyroclast system within quartz-feldspar ultramylonite. Normal, NE-side down, shear sense is indicated. Paired corrosion embayments (**C**) and partial myrmekitic mantles (**M**) are asymmetrically developed about the central K-feldspar clast at sites facing the inferred incremental shortening direction. This phenomenon reflects the preferential localization of the myrmekite replacement reaction at high-pressure sites on the clast rim, in response to the extra strain energy at these sites (Simpson and Wintsch, 1989) (sample CJS/26).

(q) Brittle microfractures and pull-apart structures developed within a formerly contiguous K-feldspar porphyroclast in a ductile quartz-rich matrix. High-angle antithetic microfaults, asymmetrical quartz-feldspar boudin-necks and the anticlockwise rotation of individual fragments are consistent with reverse, NNE-side up, shear sense. Quartz-feldspar orthomylonite (sample CJS/27).

(r) σ_b-Type K-feldspar porphyroclast systems mantled by dynamically recrystallized quartz and feldspar, and enclosed within a quartz-rich matrix. The sigmoidal geometry of deflected mantle material indicates reverse, NNE-side up, movement sense (sample CJS/27).

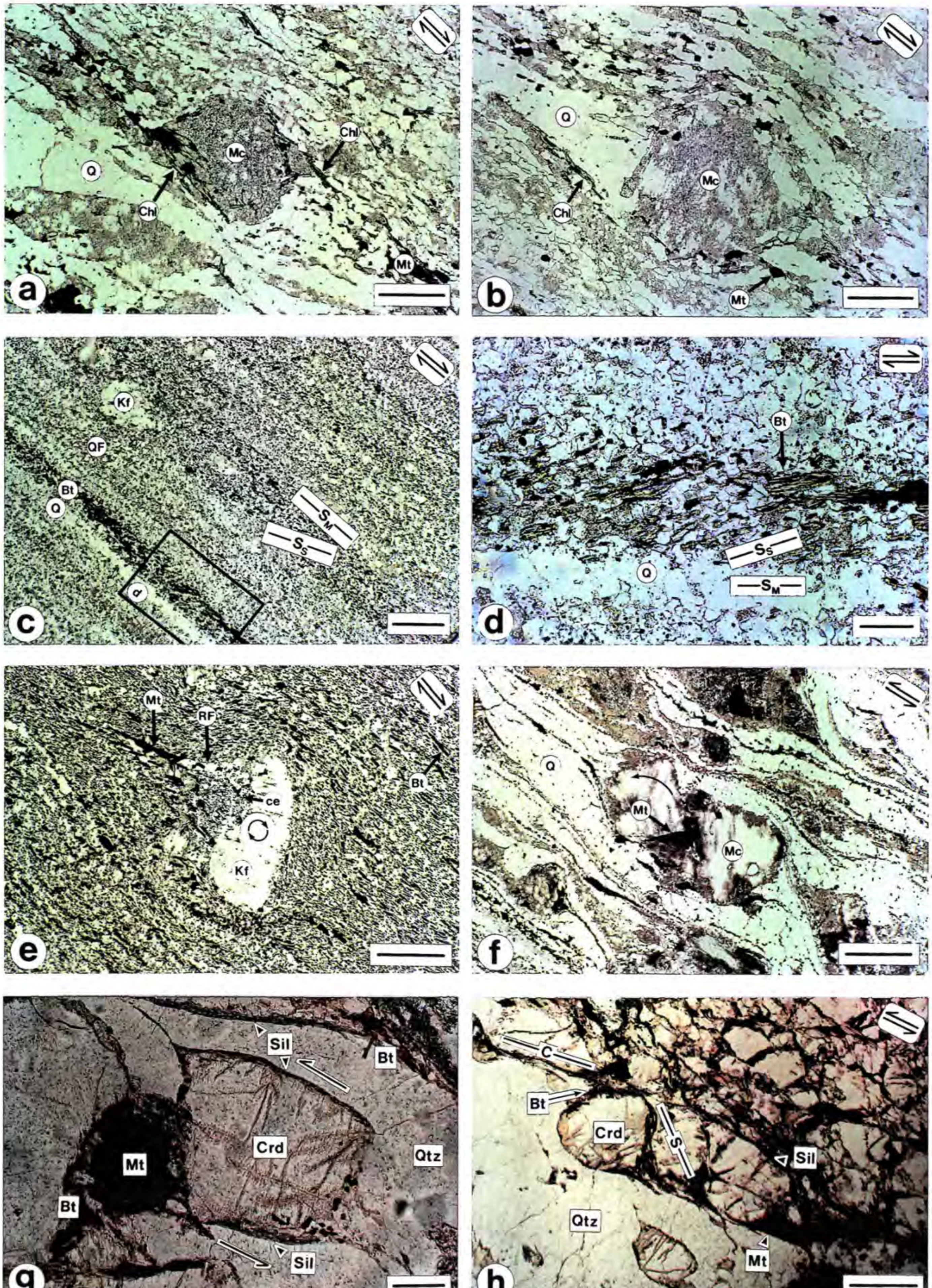
Q
Chl
Mc
Chl
Mt
a
Q
Chl
Mc
Mt
b
Kf
QF
Bt
Q
d
S_M
S_S
c
Bt
S_S
Q
S_M
d
Mt
RF
ce
Kf
Bt
e
Q
Mt
Mc
f
Sil
Bt
Mt
Crd
Qtz
Bt
Sil
g
C
Bt
Crd
S
Sil
Qtz
Mt
h

Figure 17. (previous page) Photomicrographs of selected kinematic indicators preserved within mylonitic tectonites from the northern area (a and b), southern area (c to f) and central area of the Hugosput Shear System. All are XZ-sections, viewed towards the NW and maintaining the correct dip sense. Dip angles are not true. PPL. Scale bars for (a), (b), (e), (f), (h) = 0.5mm; (c) = 1mm; (d), (g) = 0.1mm.

(a) Microcline σ_a porphyroclast system with secondary chlorite (**Chl**) and opaque oxides (**Mt**) within pressure-shadow tails, quartz-feldspar orthomylonite. The stair-stepping geometry of the pressure-shadow tails indicates normal (top-to-NNE) movement sense (sample CJS/58).

(b) Microcline σ_a porphyroclast system (**Mc**) partially mantled and armoured by ribbon-like quartz (**Q**), quartz-feldspar orthomylonite. The asymmetrical distribution of elongate quartz-ribbons adjacent to the central clast is consistent with normal (top-to-NNE) movement sense (sample CJS/58).

(c) Biotite (001) preferred orientation (**Bt**) defining an oblique secondary foliation (S_S), within a quartz-feldspar ortho/ultramylonite. The principal mylonite foliation (S_M) is defined by a crude compositional layering. Normal (top-to-NE) shear sense is indicated by the obliquity of S_S with respect to S_M (sample CJS/26).

(d) Magnified view of a portion of (c), illustrating the oblique inclination of biotite (001) planes within a micaceous layer. A neighbouring recrystallized quartz-ribbon (**Q**) is parallel to S_M. Shear sense is normal (top-to-NE) (sample CJS/26).

(e) K-feldspar δ-type porphyroclast system disrupting a biotite-rich matrix within quartz-feldspar ultramylonite. A corrosion embayment (**ce**) has developed at the rim of the central clast, where the "root" of a recrystallized feldspar tail (**RF**) has consumed reaction softened clast material. Elongate grains of magnetite (**Mt**) occur within the recrystallized tails. The clockwise vorticity of the system indicates normal (top-to-NE) movement sense (sample CJS/26).

(f) Detail of a portion of the microstructure illustrated in Figure 15q. Brittle fracture of a microcline porphyroclast (**Mc**), with counter-clockwise rotation of a component fragment indicating reverse (top-to-SSW) movement sense. The void created by reorientation of the fragment has been filled by opaque oxides (**Mt**) (sample CJS/27).

(g) Cordierite σ_a-type porphyroclast system (**Crd**) with asymmetrical fibrolite (**Sil**) tails, within K-feldspar-cordierite-quartz protomylonite. The central cordierite porphyroclast has a narrow reaction rim of sillimanite and is pinitized along healed intergranular fractures. An irregular magnetite grain-aggregate (**Mt**), rimmed by biotite (**Bt**), occupies a low-strain domain between neighbouring cordierite porphyroclasts. Intergrowths of biotite and fibrolitic sillimanite occur along the margins of polycrystalline quartz ribbons (**Qtz**). The asymmetry of the porphyroclast system indicates reverse, NE-side up, movement sense (sample CJS/24).

(h) Cordierite σ_b-type porphyroclast systems in a S-C fabric configuration, within K-feldspar-cordierite-quartz protomylonite. S and C surfaces are defined by sheaves of fibrolitic sillimanite. Biotite and magnetite occur within asymmetrical pressure shadow domains adjacent to the porphyroclasts. Magnetite occupies subparallel, intergranular tension fractures in the upper right-hand portion of the photomicrograph. Movement sense is reverse, NE-side up (sample CJS/24).

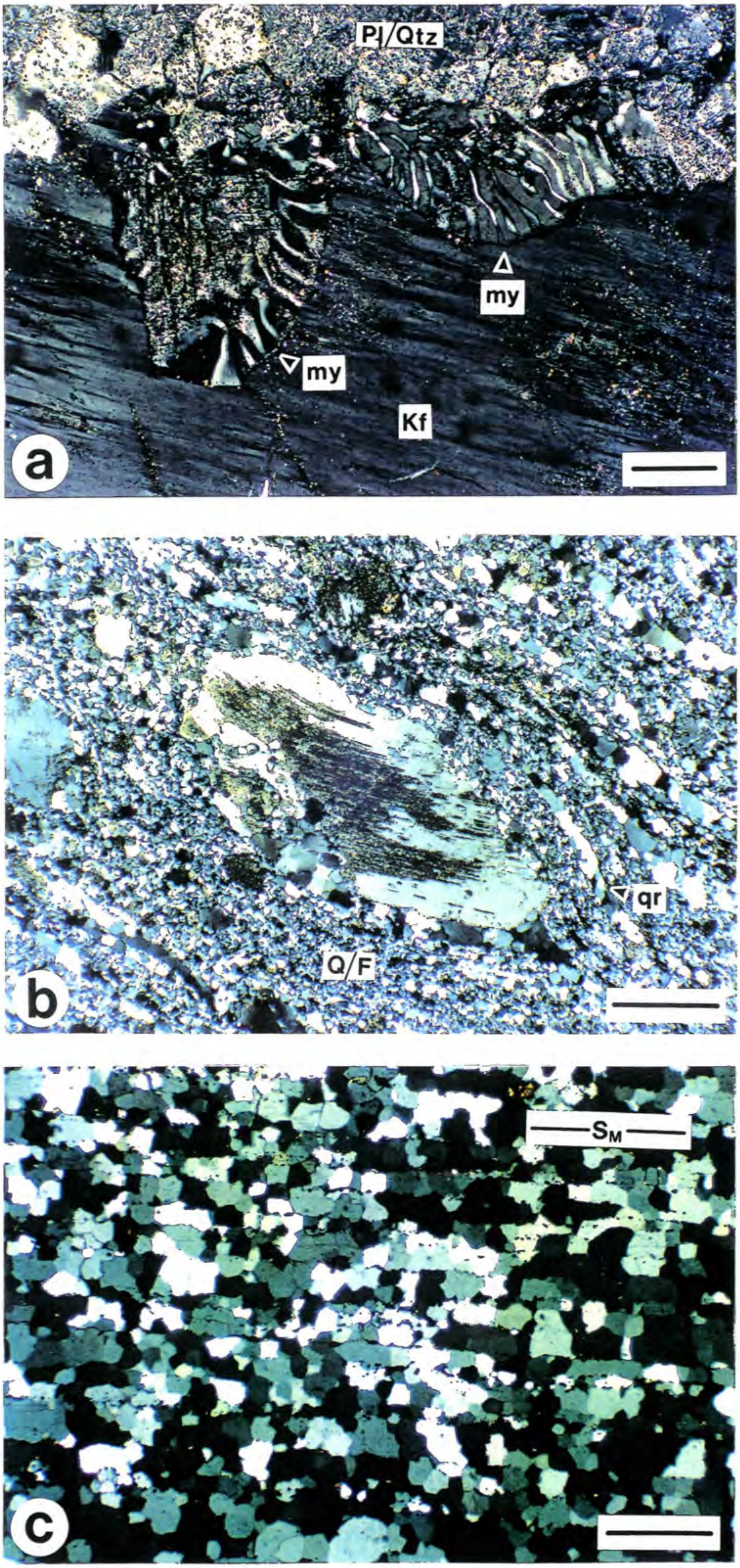
Pl/Qtz
my
my
Kf
a
qr
Q/F
b
SM
c

Figure 18. (previous page) Crossed-polar photomicrographs of microstructures within HSS tectonites indicative of high-temperature deformation and recovery. All are XZ-sections. Scale bars for (a) = 0.1mm; (b) and (c) = 0.5mm.

(a) Bulbous lobes of myrmekite (**my**), comprising vermicular oligoclase-quartz symplectite, formed along the margin of a relict K-feldspar porphyroclast (**Kf**) within quartz-feldspar orthomylonite, northern area, HSS (sample CJS/59). The vermicular myrmekite passes into fine-grained, recrystallized aggregates of plagioclase and quartz (**Pl/Qtz**) in the matrix.

(b) Plastically deformed feldspar porphyroclast surrounded by a fine-grained, dynamically recystallized quartz-feldspar matrix (**QF**), within an ultramylonite from the central area, HSS (sample CJS/21). Feldspar grain shows evidence of lattice bending. Note the highly-elongate, monomineralic quartz ribbon-aggregates (**qr**) wrapping around the porphyroclast.

(c) Equilibrium texture within quartz ultramylonite, southern area, HSS (sample CJS/28), showing composite S_M-parallel ribbons of polygonized quartz separated by linear trains of opaque minerals. Note that the quartz grains are relatively strain free.

5.4 Kinematic synthesis

Stereograms A (1 and 2), B (3 and 4) and C (5 and 6) of Figure 14 provide a synopsis of mylonite fabric orientation data, and movement sense determinations, for the northern, central and southern sampling areas of the HSS. Microstructures and microfabrics preserved within mylonites from all three sample domains preserve microstructural evidence for two ductile movements:

1) Reverse (top to SW) movement

2) Normal (top to ENE) movement

The pooled fabric orientation data and mean kinematic vectors for samples preserving the normal and reverse movement histories are presented in Fig. 19 a and b respectively. Although poorly constrained by the data, those samples preserving microstructures reflecting reverse movement are generally characterized by shallower, more northerly-plunging lineations, while those preserving the normal movement history are characterized by slightly steeper, more easterly-plunging lineations. Although this pattern is extremely vague and considerable overlap occurs between normal and reverse lineation populations, their statistical mean orientations are significantly different. The calculated kinematic vectors for the normal and reverse shear components are 066/52 and 045/47 respectively.

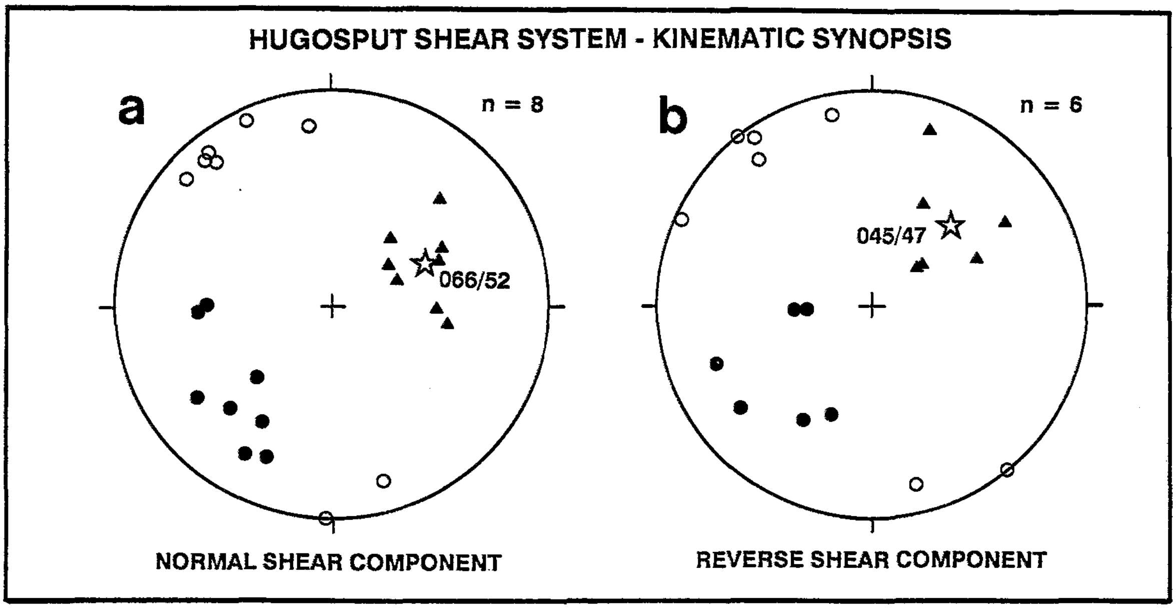

Figure 19. Kinematic synopsis of HSS microstructural and fabric data reflecting normal (a) and reverse (b) movement components. Solid and open circles indicate poles to S_M foliations and XZ sections respectively. L_M lineations are denoted by triangles. The calculated kinematic vectors for the two movement episodes are indicated by stars.

Unequivocal evidence for the relative age of the shearing events is not forthcoming. However the coexistence within a single sample (CJS/20) of weakly-developed mica (001) fabrics indicating normal movement, with well-developed porphyroclast systems consistent with reverse movement, *suggests* that normal movement occurred later than reverse movement. This follows from the fact that grain-shape alignments are particularly susceptible to changes in the kinematic framework, and are easily modified by subsequent deformation (Brunel, 1980; Simpson and Schmid, 1983; Simpson, 1986b). Consequently it is highly unlikely that an early oblique mica (001) fabric could have remained unmodified by the high shear strains required to produce porphyroclast systems.

5.4.1 P-T conditions during mylonitization

Since the bulk of the HSS sample set comprises quartzo-feldspathic mylonites containing synkinematic mineral assemblages stable over a wide range of metamorphic conditions, unequivocal correlation of the reverse and normal shearing episodes with established metamorphic events was not possible. However within the sheared aluminous gneisses, the development of protomylonitic foliation is associated with the retrogression of granulite facies metapelitic assemblages. Textural relationships described in 5.3.3 show that the development of sillimanite, biotite and magnetite occurs within syn-shearing microstructures, including protomylonitic shear planes, porphyroclast tails and tension fractures (Fig. 17 g and h). Furthermore, replacement microtextures are consistent with syn-kinematic formation of the above retrograde assemblage at the expense of cordierite and K-feldspar. This retrograde reaction might be expressed as follows:

cordierite + K-feldspar + H_2O/L → sillimanite + biotite + magnetite + quartz

The favoured preservation of the older, high-temperature assemblage is attributed to the absence of free-water under high-grade conditions. Inclusion trails of prismatic sillimanite within cordierite porphyroclasts may represent relics of the earlier prograde metamorphic path. Asymmetrical cordierite porphyroclast systems within the sheared aluminous gneiss, indicate that the formation of the protomylonitic fabric is related to reverse (top to SW) shearing. Consequently, reverse movement on the HSS appears to coincide with retrogression from granulite facies to upper-amphibolite facies.

The absence of useful mineral assemblages within mylonites preserving normal movement history, precluded P-T definition of this event.

The degree of recovery and annealing exhibited by HSS mylonites is variable, yet shows no systematic variation between mylonites representing products of normal shearing and those produced by reverse shearing. Recovery is generally well-advanced in all orthomylonites and ultramylonites, but their annealing state is inconsistent, and appears to be controlled largely by compositional differences. Quartz-rich, mica-deficient mylonites generally exhibit textures consistent with significant static recrystallization. In contrast, feldspathic, micaceous mylonites are usually finer-grained and are not significantly annealed. This may reflect the inhibition of annealing grain-growth by abundant fine-grained micas and opaques.

Chapter 6. - The Rozynenbosch-Ganzenmond and Witvlei Shear Zones

6.1 Macrostructure

The Rozynenbosch-Ganzenmond shear zone (RGSZ) and the Witvlei shear zone (WSZ) are the northeasternmost mylonite zones in the northwest-trending belt of ductile shear zones that comprise the central core of the HRTB (Fig. 2 and 3). The RGSZ outcrops east of the Hartbees River and strikes subparallel to it, merging with the WSZ on the farm Pypklip 105 before folding gently about a synformal F_3 fold axis on Ganzenmond 106 into a more easterly orientation. In the north, the WSZ is folded openly about the F_3 Pypklip dome, and more tightly about the neighbouring F_3 Koegab synform (Fig. 2).

6.2 Sample localities

Sample localities for the RGSZ and the WSZ are indicated on maps (a) and (b) of Figure 20.

Eight oriented specimens of quartz-feldspar protomylonite and orthomylonite were collected from four sampling localities (A,B,D, and F) along the RGSZ, on the farms Rozynenbosch 104, Pypklip 105 and Ganzenmond 106. This sample set was supplemented by an additional five oriented specimens of mylonitic and cataclastic rocks, collected by Harris (1992) from a single sample locality (C) on Rozynenbosch 104. Accurate L_M fabric orientation data was not available for locality C.

Although the WSZ was not originally targeted for investigation in this project, a single locality (E of Fig. 20a) on the farm Witvlei (103) was visited and an oriented sample of quartz-epidote ultramylonite (CJS/56) was collected.

Kinematic analyses of samples from the six localities were performed independently to minimise the effects of refolding of the mylonite zones.

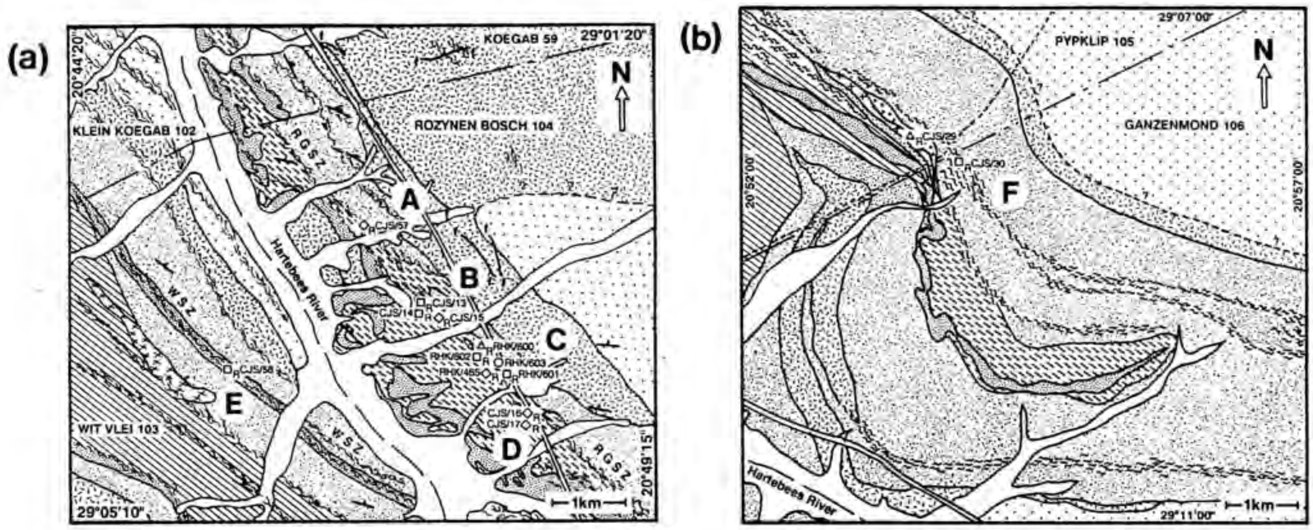
(a)
KOEGAB 59
29°01'20"
20°44'20"
N
KLEIN KOEGAB 102
ROZYNEN BOSCH 104
RGSZ
A
CJS/57
B
CJS/13
CJS/14
CJS/15
Hartebees River
C
RHK/600
RHK/602
RHK/603
RHK/465
RHK/601
WSZ
CJS/58
E
WIT VLEI 103
CJS/16
CJS/17
D
WSZ
RGSZ
1km
20°49'15"
29°05'10"
(b)
29°07'00"
PYPKLIP 105
N
GANZENMOND 106
CJS/29
CJS/30
20°52'00"
20°57'00"
F
Hartebees River
29°11'00"
1km

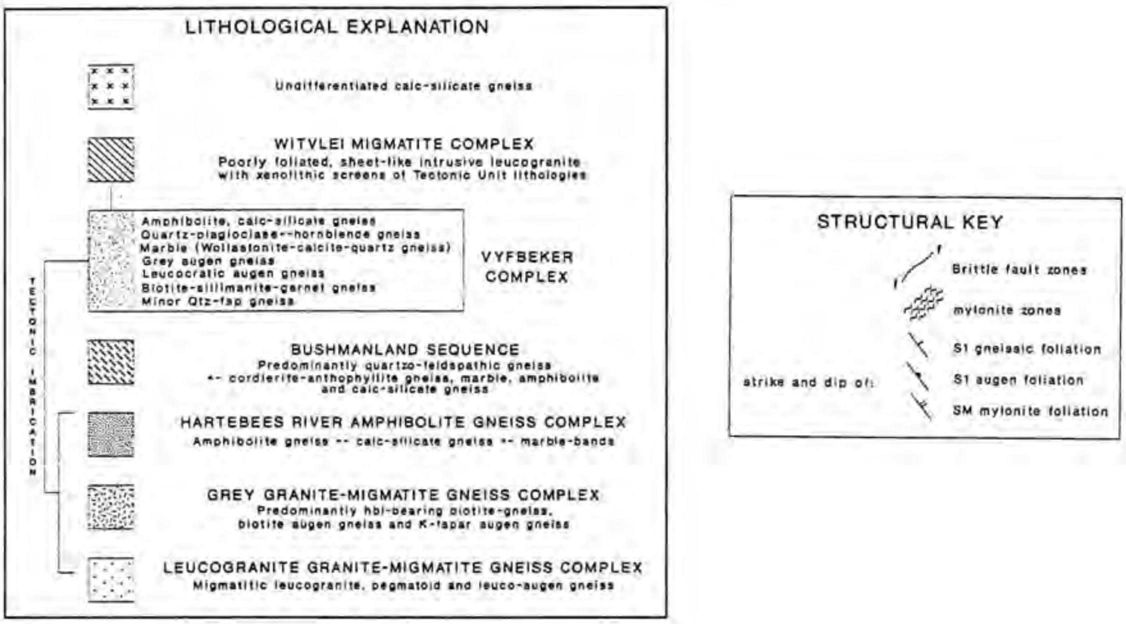
LITHOLOGICAL EXPLANATION
Undifferentiated calc-silicate gneiss
WITVLEI MIGMATITE COMPLEX
Poorly foliated, sheet-like intrusive leucogranite with xenolithic screens of Tectonic Unit lithologies
Amphibolite, calc-silicate gneiss
Quartz-plagioclase--hornblende gneiss
Marble (Wollastonite-calcite-quartz gneiss)
Grey augen gneiss
Leucocratic augen gneiss
Biotite-sillimanite-garnet gneiss
Minor Qtz-fsp gneiss
VYFBEKER COMPLEX
TECTONIC IMBRICATION
BUSHMANLAND SEQUENCE
Predominantly quartzo-feldspathic gneiss +- cordierite-anthophyllite gneiss, marble, amphibolite and calc-silicate gneiss
HARTEBEES RIVER AMPHIBOLITE GNEISS COMPLEX
Amphibolite gneiss -- calc-silicate gneiss -- marble-bands
GREY GRANITE-MIGMATITE GNEISS COMPLEX
Predominantly hbl-bearing biotite-gneiss, biotite augen gneiss and K-fspar augen gneiss
LEUCOGRANITE GRANITE-MIGMATITE GNEISS COMPLEX
Migmatitic leucogranite, pegmatoid and leuco-augen gneiss
STRUCTURAL KEY
Brittle fault zones
mylonite zones
strike and dip of:
S1 gneissic foliation
S1 augen foliation
SM mylonite foliation

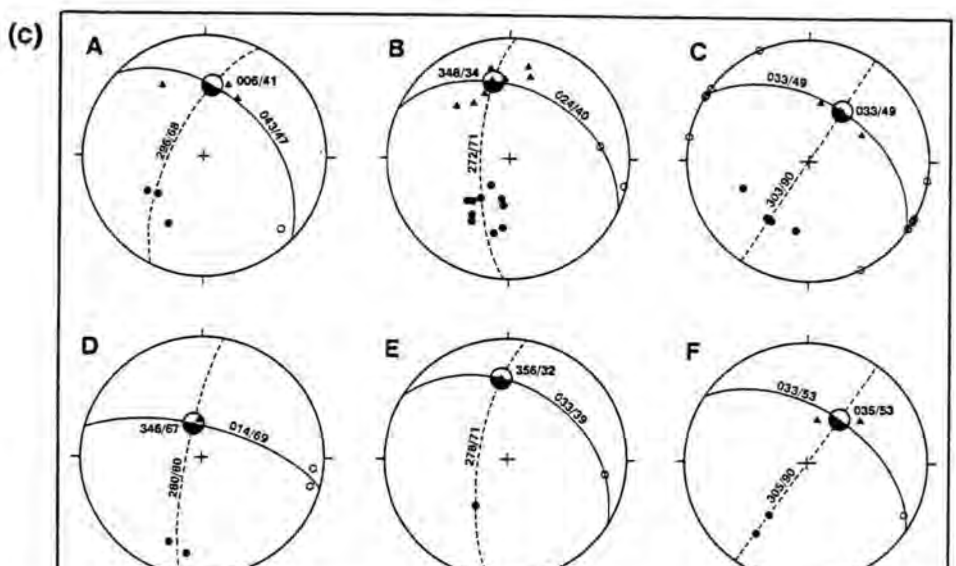
(c)
A
006/41
043/47
286/88
B
348/34
024/40
272/71
C
033/49
033/49
303/90
D
346/67
014/69
280/80
E
356/32
033/39
278/71
F
033/53
035/53
305/90

Figure 20. (previous page) (a and b) Lithotectonic maps of portions of the RGSZ and WSZ (modified after Harris, 1992), showing the six sampling areas (A to F). Individual sample localities are labelled and indicated on the maps by KCI symbols:-

○ KCI = 0
△ KCI = 1
□ KCI = 2
◇ KCI = 3

subscript R = relative reverse movement sense
subscript N = relative normal movement sense

(c) Lower-hemisphere stereprojections of fabric orientation and microstructural data for each of the sampling areas. Poles to S_M foliations and XZ sections are indicated by the filled and open circle symbols respectively. L_M lineations are indicated by triangles. Calculated kinematic vectors are indicated by large split-circle symbols: filled half marks down-dropped side.

6.3 Mesostructure

6.3.1 Mylonite zones

The Rozynenbosch-Ganzenmond and Witvlei shear zones comprise anastomosing zones of intense ductile deformation, characterized by mylonitic rocks exhibiting penetrative L-S tectonite fabrics. The width of individual mylonite zones is highly variable, but in general the mylonitic cores of the principal shear zones are a few tens of metres wide. The mylonite zones usually conform to the regional structural trend, but are locally discordant with respect to lithological contacts. The degree of mylonitization is typically determined by the protolith, and the best-developed mylonites occur within quartzose and quartzo-feldspathic lithologies. Quartz-rich protoliths include biotite-bearing augen gneiss of the *Grey Granite-Migmatite Gneiss Complex*, and quartzo-feldspathic gneisses of the *Bushmanland Sequence*.

6.3.1.1 Mylonite fabric elements

In outcrop RGSZ/WSZ mylonitic rocks exhibit a well-developed penetrative mylonitic foliation (S_M) containing a prominent mylonite elongation lineation (L_M). Locally, two or more composite planar fabrics (i.e. S-C or S-C-C') are developed, and in such cases, the principal S_M fabric usually approximates the shear plane (cisaillement).

The orientation of RGSZ/WSZ mylonite fabric elements (S_M and L_M) in each of six sampling localities are indicated stereographically in Figure 20c. The combined S_M and L_M fabric orientation data for all RGSZ and WSZ sampling localities are presented in stereograms (a) and (b) of Figure 21.

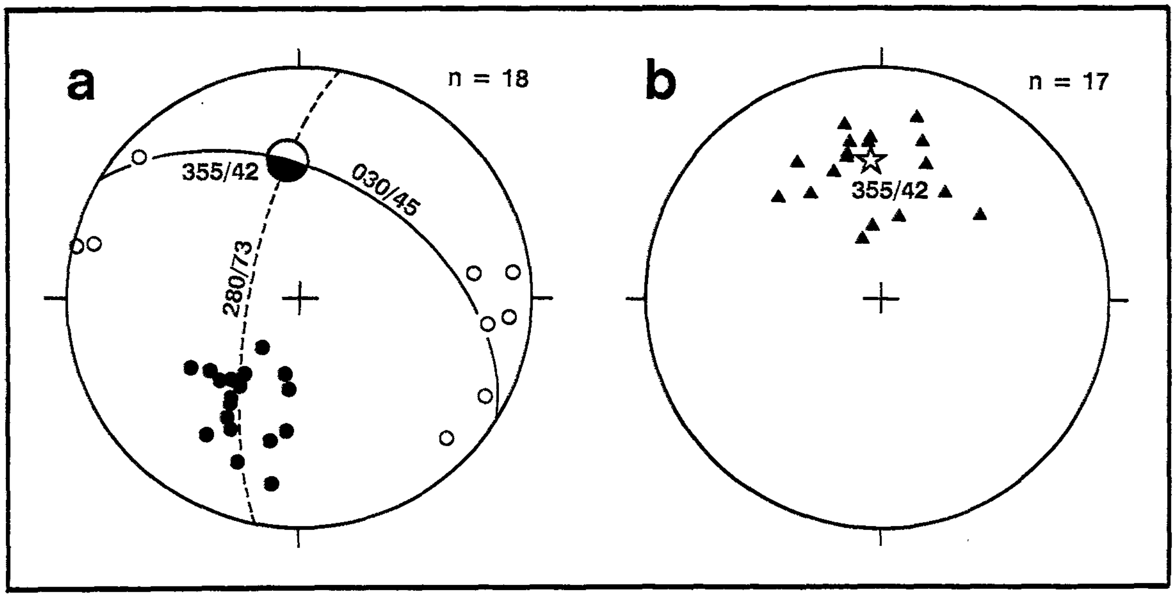

Figure 21. Microstructural and fabric data for all RGSZ/WSZ samples. Stereogram (a) shows poles to S_M foliations (solid circles) and XZ sections (open circles). The mean S_M plane and XZ section are indicated by the solid and dashed great-circles respectively. The calculated kinematic vector is indicated by a large split-circle symbol; filled-half marks down-dropped side. Stereogram (b) shows L_M lineations, with the L_M vector mean indicated by a star symbol.

The orientation of the planar mylonitic fabric (S_M) within the six RGSZ and WSZ sampling localities is remarkably consistent. S_M dips towards the NE at 40°-50° except where local steepening of the mylonite zone occurs within locality D. The orientation of L_M within the mylonite plane is more variable. L_M lineations in the five northern areas (A,B,C,D and E) generally plunge towards the N-NNW at between between 30° and 40°. Steeper plunges reflect local steepening of the mylonite plane e.g. locality D. NE-plunging L_M lineations in locality C reflect incomplete fabric orientation data for the RHK sample set, and are not reliable (the orientation of L_M was not recorded on the processed thin-sections, and for the purpose of movement sense determinations it was necessary to assume the plunge of L_M to be exactly down-dip in each case). Shear sense determinations for this locality are however dependable, since the plunge of L_M in this area is characteristically down-dip (*pers. comm.* R.W. Harris, 1990). The oblique N-NNW-plunges of L_M seen in the northern areas (ds:ss = 1.88, rake of L_M in S_M = 62°; Fig.

20c, stereograms a, b, d and e), are supplanted by NE down-dip plunges in the southeast (ds:ss = 57.29, rake of L_M in S_M = 89°; Fig. 20c, stereogram f). At locality F, L_M plunges down-dip towards 035°. Possible explanations for this variation in the orientation of the stretching direction along the RGSZ are considered in section 6.4.4.

6.3.2 Sheath-folds

An intensely sheared and contorted band of interlayered dolomite and calc-silicate gneiss occurs a few metres above the WSZ sample locality in area E. This outcrop exhibits numerous minor sheath folds and highly non-cylindrical folds of varying amplitude (5 - 30 cm). The folds are commonly asymmetrical, with curved fold axes which lie within the plane of the mean mylonite foliation (S_M) and plunge oblique or parallel to the mylonite elongation lineation (L_M) (Fig. 32 of New, 1987; Fig. 26 I and J in Appendix 3 of Harris, 1992). When viewed in sections normal to L_M, the folded S_M surface traces out characteristic eye-like structures.

6.3.3 Cataclastic zones

On the farm Rozynenbosch 104 brittle reworking of mylonitic rocks is evident within discrete, concordant decimetre-scale bands, characterized by random-fabric cataclasites (silicified microbreccias) and retrogressive greenschist facies parageneses. A single specimen of cataclasite from area C (RHK-603) was examined petrographically to determine its microstructural relationship to the mylonitic rocks (section 6.4.3).

Other broad (2 - 10 m wide) zones of intense fracturing, brecciation, silicification and retrograde alteration, were observed on the northern part of Rozynenbosch 104. These zones, although impersistent along strike, are mostly subparallel to the main zone of mylonitization. Clasts of reworked mylonitic rocks are frequently observed within the silicified breccias.

6.4 Microstructure

The following section documents the characteristic microstructures and microfabrics exhibited by sheared rocks of the RGSZ and WSZ. A more comprehensive microtextural review of individual samples is presented in Table 4 of the Appendix.

6.4.1 Rozynenbosch-Ganzenmond Shear Zone mylonitic microfabrics

S-C composite planar fabrics and asymmetrical porphyroclast sytems

Quartzo-feldspathic mylonitic rocks of the RGSZ are characterized by well-developed, composite planar microfabrics (Fig. 22 a-h and 23 a-f). Early, incomplete S-C fabrics are ubiquitous in quartz-feldspar tectonites, and are frequently overprinted locally by brittle C' shear band sets (Fig. 23g). Feldspar porphyroclasts, enveloped by polycrystalline quartz-ribbons, adopt typical σ_b-system configurations with recrystallized tails parallel to C, and axes of elongation parallel to S (e.g. Fig. 22 b, c and g, Fig. 23 a, b and f). Cisaillement surfaces are defined by highly-recrystallized quartz-ribbons and planar domains of recrystallized micas (biotite, sericite and secondary chlorite), oxides and feldspar. No variation in mica parageneses or equilibria is observed between C and S surfaces, suggesting that development of these fabrics was approximately synchronous. The mean angle between S and C planes is 33° ($S\hat{}C = 32.68 \pm 7.26°$; n = 93).

Quartz grain and subgrain shape-fabrics

Within elongate lenses of polycrystalline quartz, subgrain development and neocrystallization is advanced, and secondary quartz grain-shape fabrics commonly evolve parallel to S (Fig. 23 i and j). Local reorientation of quartz grain / subgrain shape fabrics occurs within quartz-ribbons adjacent to cross-cutting C' surfaces.

Displacement of fractured and bent feldspar porphyroclasts

Many feldspar porphyroclasts (commonly relict grains of microcline microperthite) have undergone brittle fracture, commonly with subsequent ductile bending and reorientation of the component fragments (Fig. 22i). Intrusion of plastically deformed quartz into dilation cracks within fractured feldspar clasts is common.

Semi-brittle - brittle C' microfaults

Locally, secondary, discordant C' shear surface sets overprint the composite S-C fabrics at a high angle (C^C' = 50-75°), effecting millimetre-scale synthetic displacements (Fig. 22e and 23g). Quartz-ribbons, feldspathic compositional layers and individual feldspar porphroclasts are abruptly truncated and offset by C' microfaults with very limited ductile reorientation (Fig. 22e).

6.4.2 Witvlei Shear Zone ultramylonitic microfabrics

In thin-section the quartz-epidote ultramylonite from the WSZ is uniformly fine-grained, and comprises a wholly recrystallized mosaic of quartz and epidote grains, exhibiting irregular grain boundaries and well-developed crystal substructure. Grain-size variation is from 0.1 to 0.4 mm (maximum dimension). The principal shear surfaces (C = S_M) are defined by trains of extremely fine-grained, recrystallized epidote parallel to the flow plane, and also by coarser-grained quartz-rich compositional layers. Both quartz and epidote exhibit strong preferred grain / subgrain shape alignments, which define an oblique secondary fabric (S), inclined at approximately 30° to C (Fig. 22j and 23k).

6.4.3 Rozynenbosch-Ganzenmond Shear Zone cataclastic microstructures

A single oriented sample of quartz-feldspar microbreccia (RHK/603) was collected from a narrow band on the farm Rozynenbosch 104. This coherent, highly-fractured fault-rock contains fragments of mylonite in which earlier (ductile) asymmetric planar fabrics and microstructures are preserved. The mylonitic fragments show a tendency to fracture and shatter parallel to their elongation direction. A pervasive network of irregular fractures and brittle slip-surfaces, commonly hosting secondary chlorite, epidote and calcite, are transposed upon the early mylonitic fabrics. Based on overprinting relationships, three phases of fracturing are recognized and may be correlated with a paragenetic sequence of secondary mineralisation.

1) Early slip surfaces are generally parallel to planar fabrics in the mylonitic fragments, and are defined by fine-grained chloritic intergrowths.

2) Second generation fractures and dilational jogs occur at a high-angle to the mylonitic planar fabrics, and host angular fragments of reworked mylonite in an epidote-rich matrix.

3) Third generation fractures are subparallel to (2) and contain coarse-grained calcite and subordinate epidote.

A small degree of mismatch in mylonitic fabrics across fractures, and extension microfracturing normal to the long-axis of fragments indicates limited cataclastic flow within the microbreccia matrix. No consistently interpretable movement sense was established, and flow appears to have been chaotic.

Pervasive, low-temperature hydrothermal alteration and silicification are evident in isolated patches.

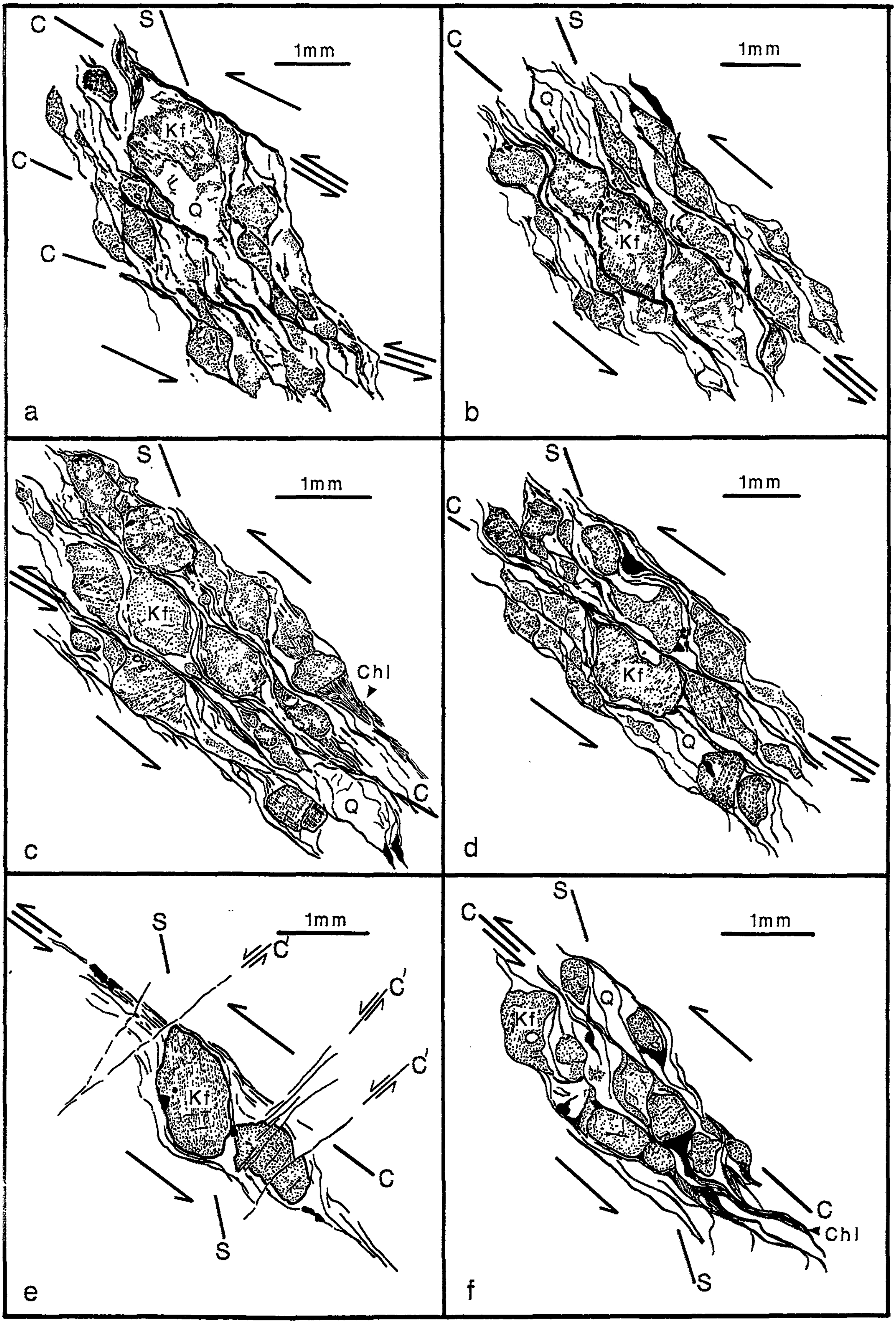
C
S
1mm
Kf
C
Q
C
a
C
S
1mm
Q
Kf
b
S
1mm
Kf
Chl
Q
C
c
S
C
1mm
Kf
Q
d
S
1mm
C'
C'
C'
Kf
C
S
e
S
C
1mm
Kf
Q
C
Chl
S
f

Figure 22. (previous page) Examples of kinematic indicators within mylonitic rocks, Rozynenbosch-Ganzenmond Shear Zone and Witvlei Shear Zone. All sketches made from XZ-sections. Look direction is NW. Angle of dip approximate.

S-C composite planar fabrics within quartz-feldspar protomylonite (a and d) and orthomylonite (b, c, d and f) indicating reverse (top-to-SW/SSW) movement sense. S-planes are defined by subparallel alignment of quartz ribbons, feldspar σ_b porphyroclast aggregates and chlorite (001) planes. C-planes are defined by reoriented, highly-recrystallized quartz ribbons and domains of recrystallized white mica, chlorite and feldspar. Oxides resulting from the breakdown of biotite are common along shear surfaces. S-surfaces have a sigmoidal geometry and anastomose in and out of the C-surfaces. (a) sample CJS/13, (b and c) sample CJS/15, (d) sample CJS/16, and (f) sample CJS/17).

(e) Brittle micro-shears (**C'**) overprinting and disrupting feldspar σ_b porphyroclast systems in typical S-C fabric configuration within a quartz-feldspar orthomylonite. C'-shear surfaces have the same shear sense as the principal C-planes. S-C fabric vergence relationships are consistent with reverse (top-to-SW/SSW) movement (sample CJS/16).

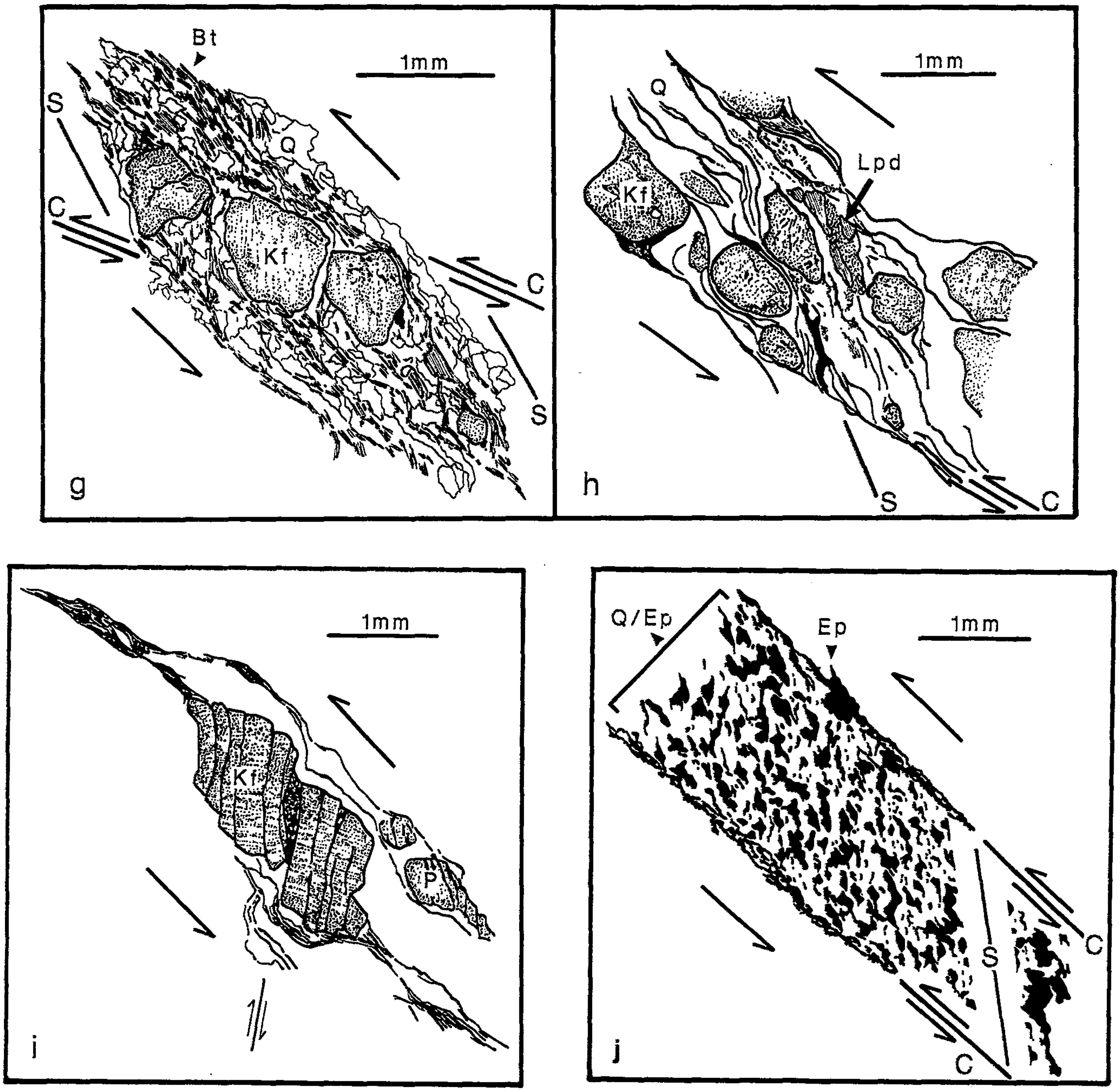

Figure 22. (continued) (g) Asymmetric K-feldspar augen within a quartz-feldspar-biotite augen gneiss, displaying weak S-C fabric geometry consistent with reverse (top-to-SW/SSW) movement. S-surfaces are defined by the subparallel alignment of elongate quartz grains, and a (001) preferred orientation of biotite flakes which wrap around feldspar augen and are deflected sigmoidally into the C-surfaces. C-surfaces are defined by trains of biotite flakes and elongate tails of dynamically recrystallized feldspar adjacent to augen structures (sample RHK/602).

(h) σ_b Feldspar porphyroclast aggregates and highly-altered white mica fish (lepidolite = **Lpd**) in S-C fabric configuration indicating reverse (top-to-SW/SSW) movement. S-surfaces defined by quartz ribbons with well-developed secondary subgrain fabrics. Tails of reaction softened feldspar adjacent to porphyroclasts, fine-grained white mica and chlorite define the C-shear surfaces. Quartz-feldspar orthomylonite (sample CJS/57).

(i) Antithetic high-angle normal microfaults developed in a fractured, bent K-feldspar porphyroclast (and in a nearby smaller plagioclase clast - **P**). Counter-clockwise rotation of the fragments and antithetic normal movement sense on individual microfaults, is consistent with reverse (top-to-SW/SSW) shearing. Quartz-feldspar protomylonite (sample CJS/30).

(j) Elongate quartz/epidote grains defining an secondary grain-shape fabric (**S**) oblique to the principal shear surfaces (**C**) reflecting reverse (top-to-SW/SSW) movement. C-surfaces are defined by an extremely fine-grained epidote/zoisite intergrowth. Quartz ultramylonite (sample CJS/56) from the Witvlei Shear Zone.

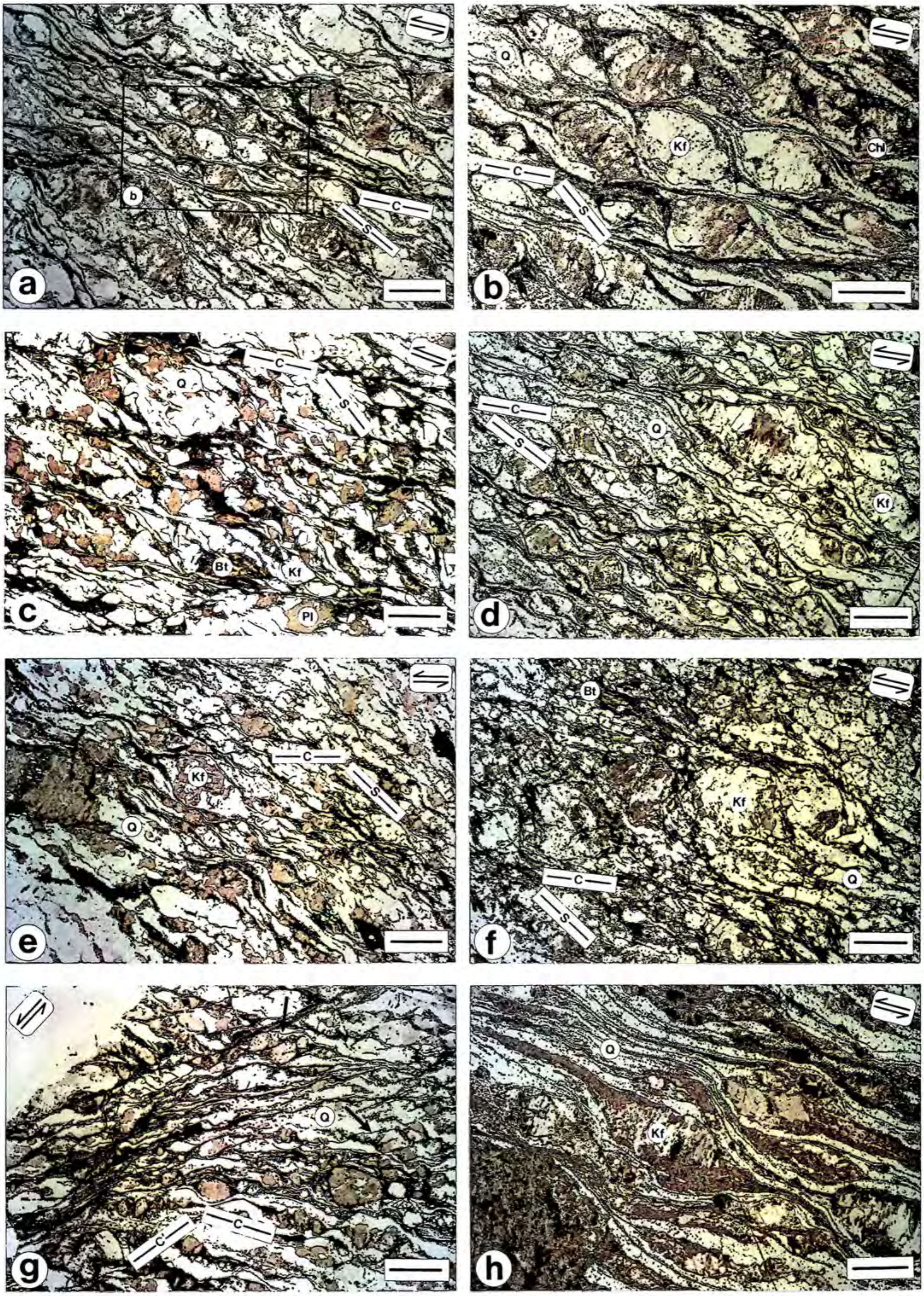

a
b
C
S
Q
Kf
Chl
Bt
Pl
c
d
e
f
g
h

Figure 23. (previous page) Photomicrographs of selected kinematic indicators preserved within mylonitic tectonites of the Rozynenbosch-Ganzenmond and Witvlei shear zones. All are XZ-sections, viewed towards the NW and maintaining the correct dip sense. Dip angles are not true. (a) to (h) and (k) are PPL; (i) and (j) are XPOL. Scale bars for (a), (c) to (i), and (k) = 1mm; (b) and (j) = 0.5mm.

S-C composite planar fabrics developed within quartz-feldspar orthomylonite (a - d) and protomylonite (e and f) from the RGSZ, indicating reverse (top-to-S) movement sense. Anastomosing quartz-ribbons and the subparallel elongation direction of σ_b feldspar porphyroclast aggregates define the S-surfaces. C-surfaces are darker reflecting a concentration of altered, recrystallized feldspar (derived from the tails of σ_b clasts), fine-grained secondary micas (commonly chlorite and white mica after biotite) and opaque mineral grains (derived from the breakdown of biotite). (a), (b) and (d) sample CJS/15, (c) sample CJS/17, (e) sample CJS/13, (f) sample RHK/602).

(b) Magnified view of a portion of (a) illustrating the typical clustered configuration of σ_b feldspar porphyroclast systems: Narrow polycrystalline quartz-ribbons (**Q**) wrap around lozenge-shaped feldspar (**Kf**) clasts and define the sigmoidal S-surfaces. Recrystallized material from the feldspar clasts is deflected along the more regular C-surfaces. Secondary chlorite (**Chl**) occasionally forms pressure-shadow "beards" adjacent to feldspar clasts.

In (f), a protomylonitic augen gneiss, the S and C fabrics are defined by anastomosing trains of recrystallized biotite-flakes which describe weak stair-stepping geometries, enclosing feldspar σ_b clasts and lozenge-shaped domains of quartz and feldspar.

(g) Brittle C' microfaults intersecting and overprinting weak S-C fabrics. Feldspar porphyroclasts are fractured and offset along closely-spaced C' planes (indicated by arrows). Limited ductile reorientation of quartz-ribbons occurs adjacent to the principal zone of microfaulting which crosses diagonally from top-right to bottom-left. The sense of movement on C' planes is the same as that on C-surfaces. Quartz-feldspar protomylonite (sample CJS/30), RGSZ.

(h) Flat geometry σ-type feldspar porphyroclasts enclosed by quartz-ribbons. The stair-stepping geometry of the highly-altered, recrystallized tails is consistent with reverse (top-to-S) movement. Quartz-feldspar orthomylonite, RGSZ (sample RHK/465).

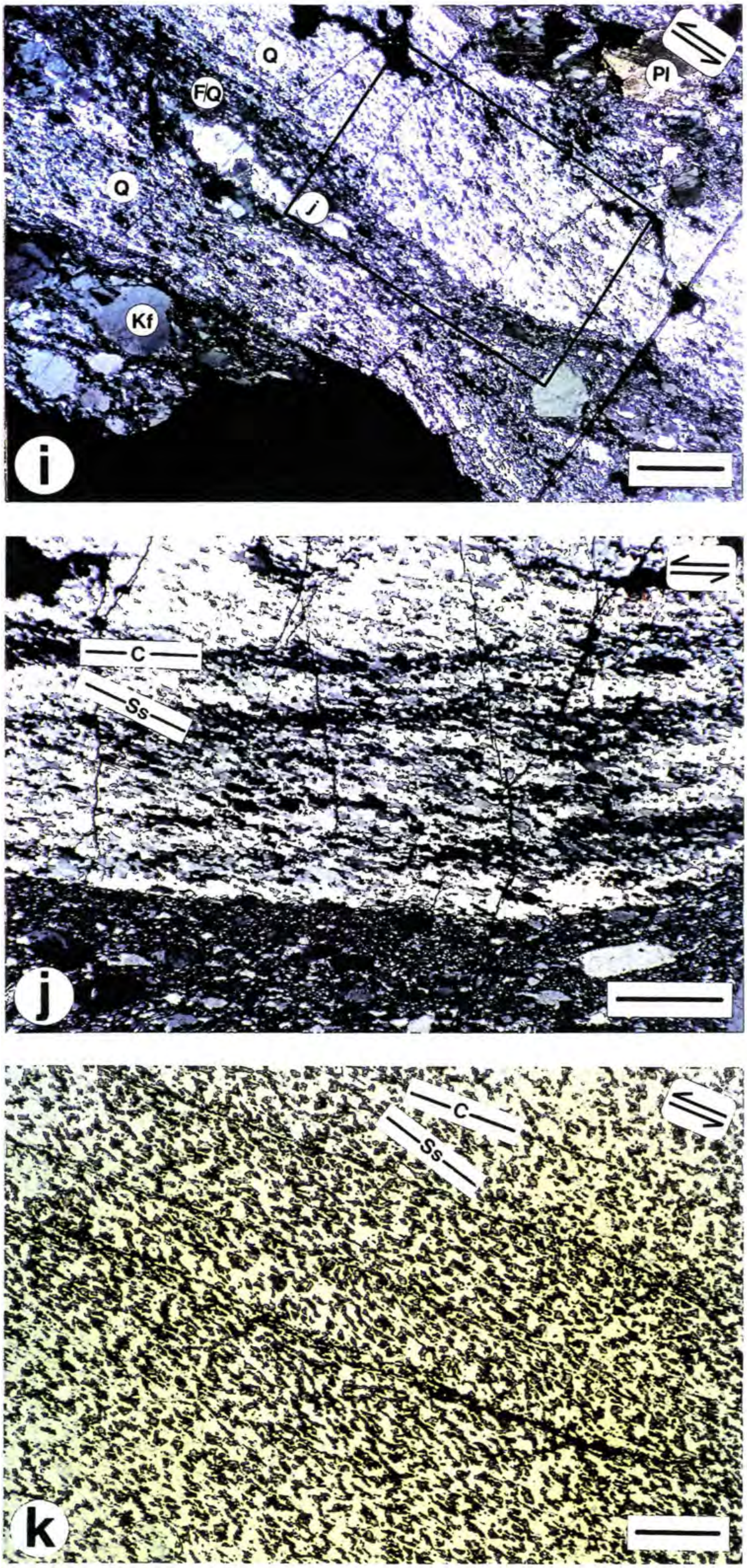
Q
F/Q
Q
j
Kf
Pl
i
C
Ss
j
C
Ss
k

Figure 23. (continued) (i) Alternating recrystallized quartzo-feldspathic domains (**F/Q**) and polycrystalline quartz-ribbons (**Q**) in a quartz-feldspar orthomylonite Deformed megacrysts of plagioclase (**Pl**) and K-feldspar (**Kf**) occur in the feldspathic domains (sample CJS/16, RGSZ).

(j) Magnified view of (i) showing a preferred alignment of elongate, dynamically recrystallized quartz grains and subgrains within a polycrystalline quartz-ribbon. This shape-fabric defines a secondary foliation (**S_s**) oblique to the principal shear foliation (**C**). Recrystallized deformation bands are defined by a subhorizontal extinction banding parallel to C. The obliquity of S_s with respect to C indicates reverse (top-to-S) movement sense.

(k) Preferred orientation of quartz and epidote grains defining an oblique secondary foliation (**S_s**) within a quartz ultramylonite. The obliquity of S_s with respect to the principal shear surfaces (C) indicates reverse (top-to-S) shear sense (sample CJS/56, WSZ).

6.5 Kinematic synthesis

Kinematic interpretations for each of the six sampling localities on the RGSZ and WSZ are summarized in stereograms A to F of Figure 20c (see also Fig. 21). The shear sense and relative Kinematic Confidence Index (KCI) for tectonite fabrics are shown by representative symbols at each sample station on the maps (see caption).

The orientation of L_M lineations, and shear sense determinations made from S-C composite planar fabrics, σ_b-type porphyroclast systems, mica-fish, oblique quartz grain/subgrain shape-fabrics, and the displacement sense of fractured feldspar clasts, indicate with a high-level of confidence that the principal shearing event on the RGSZ and WSZ was characterized by *reverse movement, with overthrusting directed towards the south and southwest.* In the north (localities A,B,C,D and E), movement was oblique with respect to the NE-dipping mylonite plane, with thrusting towards the south. Further to the southeast (locality F), movement occurred normal to the mylonite plane with SW-directed thrusting. The reason for this apparent disparity in movement direction between the northern and southern localities is unclear. Two possible explanations are:-

(1) The L_M lineation pattern described in section 6.3.1.1 may not be primary. Dispersion of the L_M lineation within the mylonite plane may have occurred by right-lateral shearing during D_4 (Harris, 1992). This model requires a N-trending primary orientation for L_M lineations, with later, clockwise rotation towards NE-trends. The influence of the D_4 strike-slip component may increase southwards within the HRTB, such that primary L_M trends are only preserved in the northern part of the belt.

(2) The two disparate kinematic vectors reflect end members of a progressive change in movement direction during a continuous thrusting event.

6.5.1 Characterization of physical conditions and timing of deformation

The RGSZ/WSZ sample set is dominated by quartzo-feldspathic tectonites with relatively simple synkinematic mineral assemblages, stable over a wide range of metamorphic conditions. Consequently no absolute P-T contraints on the conditions of deformation of the RGSZ/WSZ tectonites were established.

The ubiquitous presence of low-grade secondary minerals (chlorite + sericite + epidote + opaque oxides) along S and C surfaces and in pressure-shadow domains adjacent to feldspar porphyroclasts, is attributed to post-kinematic, low-temperature retrogression. Biotite mica fish are commonly partially pseudomorphed by white mica, chlorite or opaque oxides, with alteration occurring preferentially along cleavage planes. This indicates that biotite was stable at the time of thrusting and that mimetic replacement occurred at a later stage.

Within most RGSZ mylonites, quartz grains typically exhibit ragged boundaries, well-developed crystal substructure and undulatory extinction (Fig. 23j). This *suggests* that penetrative fabric development in RGSZ/WSZ tectonites was not accompanied, or followed by, significant latent heating and static recrystallization. Despite this, both plagioclase and K-feldspar within the tectonites exhibit widespread development of subgrains, neocrysts and recrystallized tails. This is consistent with a deformation mechanism of recrystallization - accommodated dislocation creep (White, 1975; Tullis and Yund, 1985, 1987), and is typical of feldspars deformed at middle to upper amphibolite facies (Simpson, 1985; Tullis and Yund, 1987). Voll (1976) indicates that temperatures of around 500°C permit recrystallization of feldspar. The presence of deformation and kink bands within feldspar grains, and of bent feldspar porphyroclasts (Fig. 22i), provides evidence for marked intracrystalline ductility, despite the widespread occurrence of cleavage controlled fracturing in feldspar grains. Mitra (1978) indicates that in quartzo-feldspathic rocks, feldspar remains relatively rigid down to about 18km depth (T = 450°C ± 50°C).

The data above suggest that penetrative microstructural and fabric development associated with early S/SW-directed thrusting on the RGSZ and WSZ, ocurred at relatively high-grade conditions (middle to upper amphibolite facies). Passive pseudomorphing and replacement of syn-kinematic fabrics by low-temperature secondary minerals occurred during uplift and exhumation of the HRTB. Retrogression may have been related to a high fluid flux during brittle reactivation of the HRTB. This supposition is sustained by the widespread occurrence of silicified breccias and cataclasites characterized by low-temperature hydrated assemblages (epidote ± chlorite ± calcite ± sericite).

Late reactivation of the RGSZ is indicated by the presence of semi-brittle to brittle C' microfaults, overprinting the early ductile mylonitic fabrics. Although the movement sense on C' microfaults is "synthetic" with respect to the C surfaces, their high-angle discordancy (C^C' = 50-75°) and brittle nature oppose a model of development within a common stress system. Instead, it is envisaged that the C' microfaults reflect localized reactivation of the RGSZ, coinciding with thermal relaxation during the D_4 strike-slip event.

6.6 Discussion

In summary, the variety of fault rocks and microstructures present along the RGSZ, reflects polyphase movements preferentially localized along a single strain softened zone.

The coexistence of ductile and brittle fault-rocks at one crustal level, and the textural overprint of brittle structures upon ductile, is consistent with a protracted movement history extending into the stage of uplift and unroofing of the HRTB. The RGSZ fault-rock suite may be explained by a sequence in which early ductile thrusting at mid-crustal levels (represented by high-temperature mylonite fabrics and microstructures), was followed by higher-level semi-brittle to brittle adjustments during uplift of the area through the ductile-brittle transition. Activity on the zone culminated with localized, polyphase, brittle deformation at a high crustal level (represented by cataclasite series fault products). Localized brittle deformation is possibly related to reactivation of the zone as a strike-slip fault late in the D_4 event.

The sequence of ductile to brittle fault rock products, without reversals in the mechanical response of the deforming rock, suggests that aseismic strain rates ($<10^{-10}$ s^{-1}: Sibson, 1986) dominated the passage of the area from deep-level through to the brittle-ductile transition. Late-stage cataclasis may have occurred at seismic strain rates ($>10^{-3}$ s^{-1}: Sibson, 1986), in the presence of sufficient fluid to lubricate the fault plane and prohibit the formation of pseudotachylite.

Chapter 7. - The Graafwater Shear System

7.1 Macrostructure

The Graafwater Shear System (GSS) comprises the two structurally lowermost mylonite zones of the HRTB. In the northwest it is represented by a single mylonite zone, but further south two distinct zones are recognized, and are referred to as the upper and lower Graafwater shear zones (UGSZ and LGSZ; Fig. 2). In recent literature (Joubert, 1986; Hartnady *et al.*, 1985; Stowe, 1986) the GSS has been proposed as the geoboundary between the Kakamas Terrane (Gordonia Subprovince) and the Garies Terrane (Bushmanland Subprovince; section 1.2).

The GSS mylonite zones have been refolded about N-trending F_3 fold axes in the north (Koegab synform and Pypklip dome), and ENE-trending F_3 fold axes in the south (Graafwater synform, Rietfontein antiform and synform, and the Poliesberg antiform and synform; Fig. 2). This change in the axial trend of F_3 folds across the HRTB is spatially related to the presence of right-lateral D_4 shear zones (Harris, 1988). Regional reorientation, stretching and tightening of F_3 folds occurred adjacent to the Rooidam Shear and the Pofadder Lineament. This is particularly noticeable in the ENE-trending Graafwater synform, whose broadly curved retort shape reflects regional bending, with elongation and passive tightening of the hinge region within the zone of extension centered on the Pofadder Lineament. The refolded nature of the GSS mylonite zones within the southern portion of the HRTB is clearly illustrated by the outcrop distribution on the maps of Figure 24. The degree of modification to the shape of the Graafwater synform is also seen to increase with proximity to the Pofadder Lineament in the southwest.

7.2 Sample localities

Twenty oriented samples of mylonitic and cataclastic rocks were collected from twelve sampling localities on the GSS, in the southern portion of the HRTB. The sample localities are indicated in Figure 24. Quartz-feldspar tectonites form the bulk of this sample set, but are supplemented by a few specimens of calc-silicate and amphibolitic mylonites. Independent kinematic analyses were performed, so that the influence of refolding on the kinematic interpretation could be assessed.

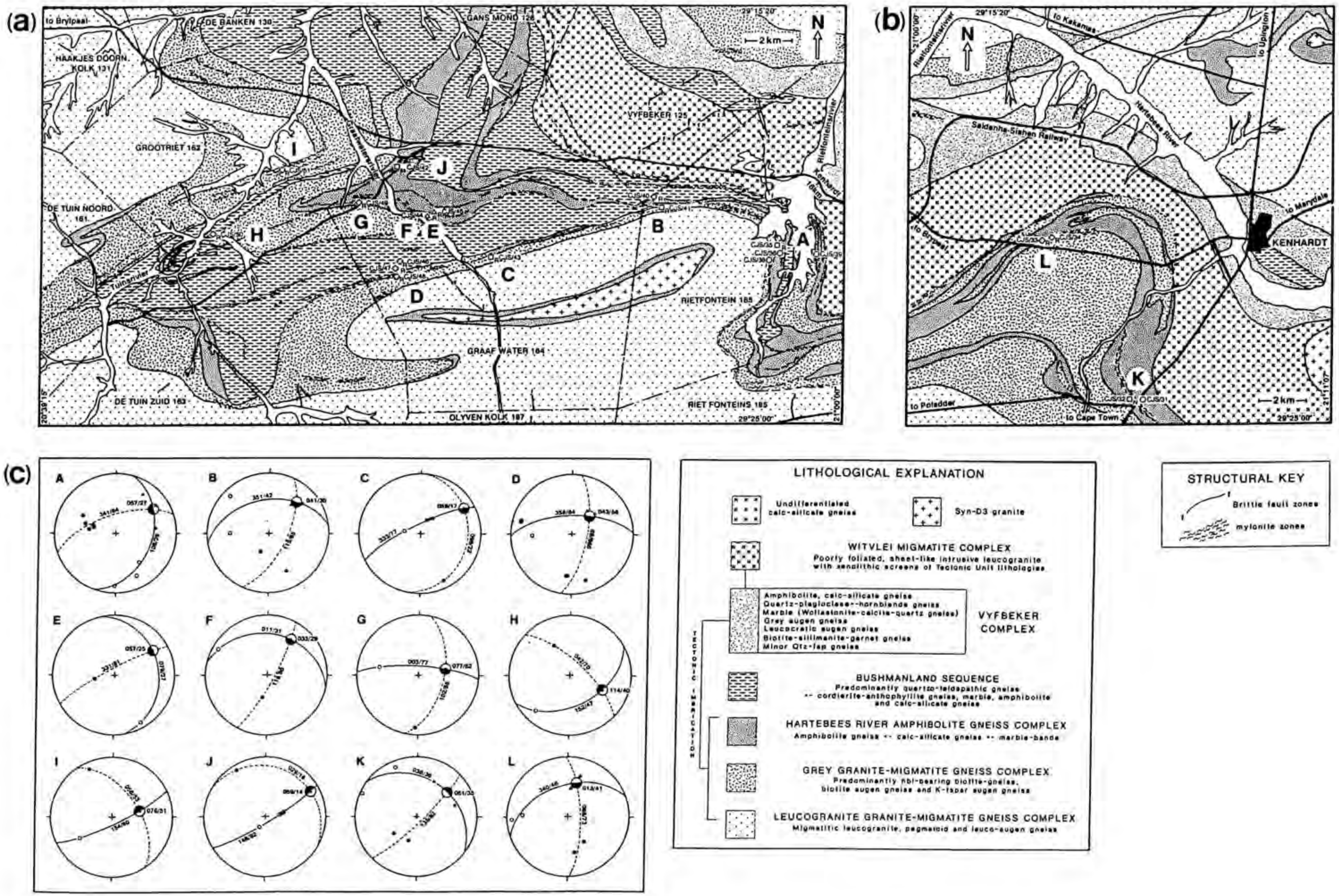
(a)
to Brylpaal
DE BANKEN 130
GANS MOND 126
HAAKJES DOORN KOLK 131
VYFBEKER 125
GROOTRIET 162
DE TUIN NOORD 161
Tuinsvlei
RIETFONTEIN 165
GRAAF WATER 164
DE TUIN ZUID 163
OLYVEN KOLK 187
RIET FONTEINS 165
29°15'20"
29°25'00"
2km
N
A
B
C
D
E
F
G
H
I
J
(b)
to Kakamas
to Upington
Saldanha-Sishen Railway
Hartebees River
to Marydale
KENHARDT
to Brytaal
to Pofadder
to Cape Town
L
K
29°15'20"
29°25'00"
2km
N
(c)
A
B
C
D
E
F
G
H
I
J
K
L
LITHOLOGICAL EXPLANATION
Undifferentiated calc-silicate gneiss
Syn-D3 granite
WITVLEI MIGMATITE COMPLEX
Poorly foliated, sheet-like intrusive leucogranite with xenolithic screens of Tectonic Unit lithologies
Amphibolite, calc-silicate gneiss
Quartz-plagioclase+-hornblende gneiss
Marble (Wollastonite-calcite-quartz gneiss)
Grey augen gneiss
Leucocratic augen gneiss
Biotite-sillimanite-garnet gneiss
Minor Qtz-fsp gneiss
VYFBEKER COMPLEX
TECTONIC IMBRICATION
BUSHMANLAND SEQUENCE
Predominantly quartzo-feldspathic gneiss +- cordierite-anthophyllite gneiss, marble, amphibolite and calc-silicate gneiss
HARTEBEES RIVER AMPHIBOLITE GNEISS COMPLEX
Amphibolite gneiss +- calc-silicate gneiss +- marble-bands
GREY GRANITE-MIGMATITE GNEISS COMPLEX
Predominantly hbl-bearing biotite-gneiss, biotite augen gneiss and K-fspar augen gneiss
LEUCOGRANITE GRANITE-MIGMATITE GNEISS COMPLEX
Migmatitic leucogranite, pegmatoid and leuco-augen gneiss
STRUCTURAL KEY
Brittle fault zones
mylonite zones

Figure 24. (previous page) (a and b) Lithotectonic maps of portions of the GSS, showing the twelve sampling localities (A to L). Map (a) modified after Harris (1992); map (b) interpretation from a LANDSAT-TM satellite image. Individual sample localities are labelled and indicated on the maps by KCI symbols:-

○ KCI = 0
△ KCI = 1
□ KCI = 2
◇ KCI = 3

subscript R = relative reverse movement sense
subscript N = relative normal movement sense
subscript ss = relative strike-slip movement sense

(c) Lower-hemisphere stereoprojections of fabric orientation and microstructural data for each of the sampling localities. Poles to S_M foliations and XZ sections are indicated by the filled and open circle symbols respectively. L_M lineations are indicated by triangles. Calculated kinematic vectors for relative dip-slip component indicated by large split-circle symbols: filled half marks down-dropped side. Shear-arrows indicate the sense of relative strike-slip translation.

7.3 Mesostructure

7.3.1 Mylonite zones and mylonite fabric elements

The mylonite zones of the GSS preserve some of the best developed mylonite series rocks seen in the HRTB. Tectonites displaying penetrative L-S fabrics are particularly well-developed within quartzo-feldspathic lithologies. Quartzo-feldspathic protoliths include biotite augen gneisses of the *Grey Granite-Migmatite Gneiss Complex*, and quartzo-feldspathic gneiss of the *Bushmanland Sequence*.

In outcrop the tectonites display a penetrative planar fabric (S_M), which is either an ortho/ultramylonitic fluxion banding or a protomylonitic augen foliation. Commonly, two or more composite planar fabrics (i.e. S-C or S-C-C') are developed, and in such cases, S_M usually approximates the C-surface. A strong mylonitic lineation (L_M) is ubiquitous in all mylonite series tectonites of the GSS, and is commonly defined by quartz-ribbons and streaks of micas within the plane of S_M. Within protomylonitic augen gneisses, L_M is defined by elongate rods of flattened feldspar and lenticular quartz ribbons. Relative fabric strength is usually $S \geq L$, except in the WSW where strong elongation within the zones of extension adjacent to the major D_4 shear zones, produces L>S fabrics (Harris, 1992; Fig. 25). These linear fabrics are very distinctive in the field, imparting a "streaky" appearance to the gneisses, and may be used to define areas in which modification of S_M and L_M fabrics has occurred.

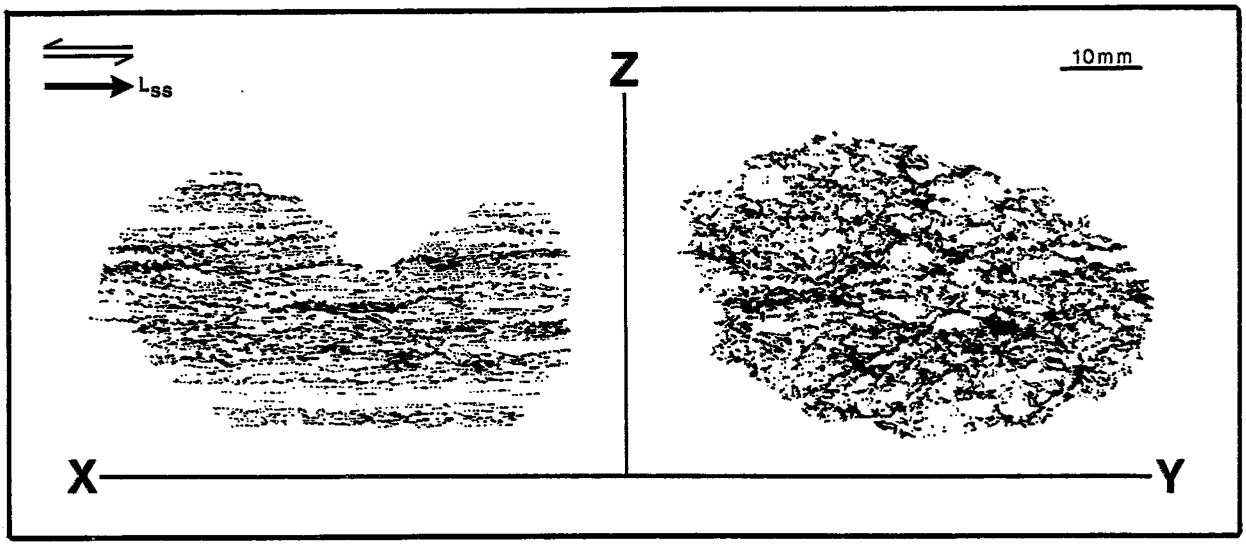

Figure 25. Sketch illustrating the different appearance of a strongly linear fabric in a banded biotite gneiss, in sections cut parallel to the lineation (XZ section) and normal to the lineation (YZ section). Within XZ sections considerable elongation has occurred parallel to L_{ss}, which is defined by elongate quartz-ribbons, flattened rods of feldspar, and a strong DPO within biotite-rich layers. In YZ sections (normal to L_{ss}) trains of biotite anastomose about ellipsoidal sections through flattened feldspar rods and lenticular quartz-ribbons. Weak S-C fabric relationships are evident in XZ sections, and these are consistent with left-lateral strike-slip movement parallel to L_{ss} (sample CJS/42 from the UGSZ on the northern limb of the Graafwater Synform).

7.3.1.1 Orientation of S_M fabrics

The orientation of GSS mylonitic fabric elements at each of the twelve sampling localities (A to L) are indicated stereographically in Figure 24.

The attitude of S_M is controlled by refolding of the mylonite zones about macroscopic and mesoscopic F_3 folds. Within the Graafwater synform, S_M fabrics within mylonite zones on the southern limb strike ENE to ESE and dip towards the NNW-NNE at 30-80° (localities B, C, D, F and G). Dips are relatively shallow along the eastern part of this limb, and become increasingly steep towards the synformal closure where considerable elongation and tightening-up has occurred (the ENE-dipping S_M of locality E is attributed to refolding of the mylonite zone about a minor F_3 fold). The mylonite zones on the northern limb are characterized by ENE-striking S_M fabrics, which dip steeply towards the SSE. Overturned S_M fabrics dipping to the NNW are encountered on the northern limb (localities H, I and J).

On the southwestern limb of the Rietfontein antiform (locality A), S_M dips towards the ESE at approximately 40°. On the northwestern limb of the Poliesberg antiform (locality L), S_M dips towards the NNW at 46°. In the Kenhardt road-cutting on the southeastern limb of the Poliesberg antiform, (locality K), S_M dips NE at 35°.

7.3.1.2 Orientation of L_M fabrics

L_M lineations within the southern GSS generally plunge obliquely within the plane of S_M towards the NE. Plunges are usually between 25° and 55°. Within the zones of extension adjacent to the Rooidam shear zone and Pofadder Lineament (localities C, G, I and J), the obliquity of L_M within the S_M plane increases, and plunges are shallower. Furthermore, within these zones the trend of L_M rotates clockwise towards E-ESE orientations.

This reorientation of L_M is attributed to regional clockwise rotation of linear and planar fabric elements during D_4 right-lateral shearing, coinciding with elongation and tightening in the nose of the Graafwater synform (Harris, 1992). This resulted in rotation of L_M towards the horizontal within a steepening mylonite foliation plane.

7.3.2 Demonstration of folding of the mylonite zones

Within the southern part of the GSS, the attitude of S_M is variable as a result of refolding of the mylonite zones about NE to ENE trending F_3 fold axes. This relationship is clearly illustrated in Figure 26 a and c, where S_M fabric data from the Graafwater synform and the Rietfontein antiform have been used to calculate the statistical F_3 fold axes for these structures. These computed fold axes are comparable with fold axes calculated by Harris (1992) using S_0 and S_1 fabric data.

7.3.3 Demonstration of coaxiality of F_3 and L_M

When the L_M fabric data from the Graafwater synform and Rietfontein antiform are plotted stereographically (Fig. 26 b and d), a close coincidence is observed between the mean L_M and the computed F_3 fold axes (Fig. 26 a and c). The disparity between the computed fold axes and mean L_M is 21°and 5° for the Graafwater synform and Rietfontein antiform respectively. This coaxial relationship between F_3 fold axes and the L_M lineation is fortunate, since it means that the primary orientation of L_M lineations (and hence the movement direction on the mylonite zones) will have been virtually unmodified by F_3 refolding.

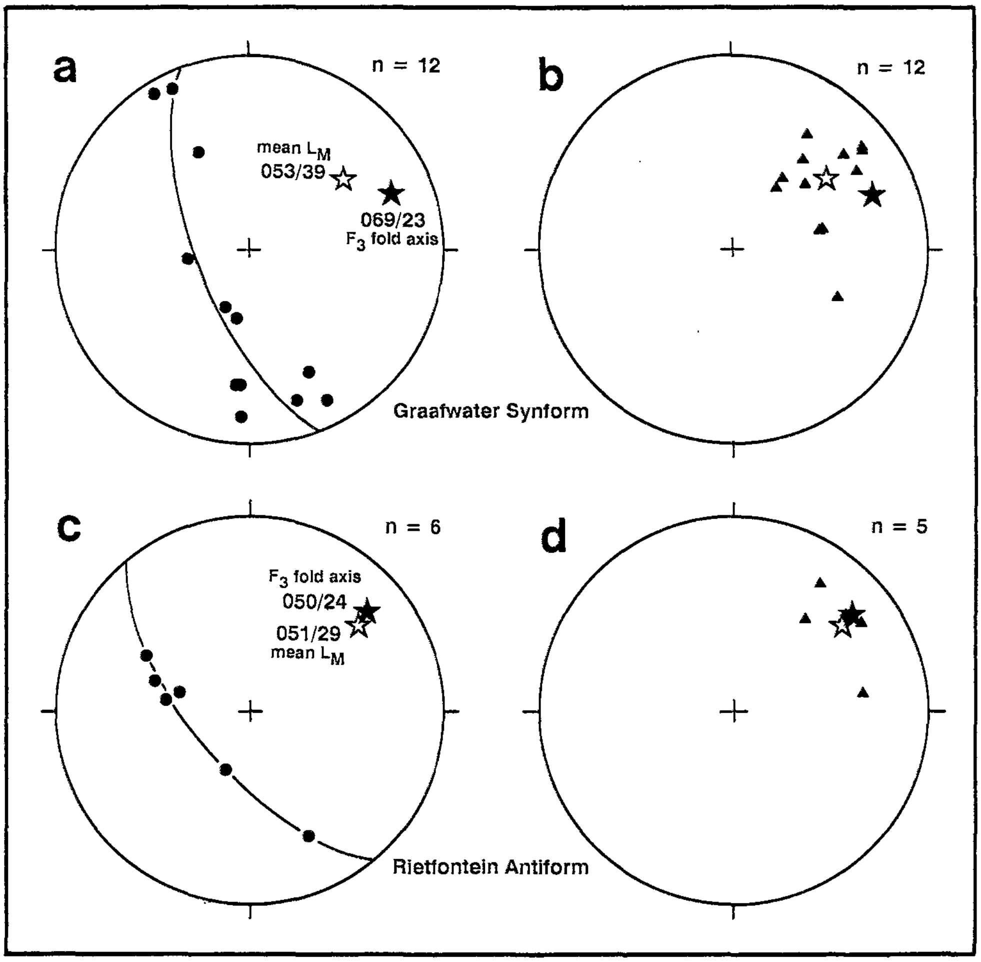

Figure 26. Mylonite fabric data for the Graafwater synform (a and b) and the Rietfontein antiform (c and d), demonstrating folding of the mylonite zones by F_3 folds, and the coaxial relationship between the calculated F_3 fold axes and the L_M lineation. Filled triangles and circles represent mylonite lineations (L_M) and poles to the mylonite foliation (S_M) respectively. Open stars represent the statistical F_3 fold axes, while filled stars denote the statistical mean L_M. Great-circles indicate computed best-fit girdles to the planar dispersion of S_M poles.

7.4 Microstructure

The following section documents the characteristic microstructures and microfabrics developed within tectonites of the GSS. An abridged inventory of textural development within the GSS sample set is catalogued in Table 5 of the Appendix. Selected sketches and photomicrographs of kinematically useful microstructures and fabrics are presented in Figures 27 and 28.

7.4.1 Mylonitic microfabrics and microstructures

Mylonitic rocks of the GSS are characterized by a wide variety of abundant asymmetrical microstructures and fabrics, which display remarkable consistency in terms of kinematic interpretation.

S-C-C' composite planar fabrics

Quartz-feldspar mylonites of the GSS are characterized by the development of S-C-C' composite planar microfabrics. Examples of typical S-C fabric configurations are illustrated in Figure 27 a, f-l, n and o; and Figure 28 b-d, f-i and l. Composite S-C-C' fabrics are illustrated in Figure 27q and Figure 28 a, b and e.

C-surfaces are characterized by intense dynamic recrystallization and grain-refinement. They are defined by reoriented polycrystalline ribbons of quartz, and microcrystalline intergrowths of highly-altered feldspar, secondary micas and opaque oxides. Asymmetrical microfolds are very common along the principal C-surfaces. S-surfaces are defined by anastomosing polycrystalline quartz-ribbons, which wrap about feldspar porphyroclast aggregates and lozenge-shaped domains of recrystallized quartz. They are sigmoidally deflected into C-planes with a consistent sense of curvature. The C-surfaces are characteristically darker than the S-surfaces in plane-polarised light. The mean angle between S and C planes is 27° ($S\hat{}C = 27.25° \pm 7.19°$; $n = 107$). Shallow-dipping, impersistently developed, ductile C' shear bands intersect and deflect both S and C fabrics with movement sense synthetic to that of C. The mean angle between C' and C planes is 20° ($C\hat{}C' = 19.81° \pm 4.5°$; $n = 32$).

Asymmetrical porphyroclast systems

Asymmetrical feldspar porphyroclast systems are the most common microstructural feature of GSS tectonites, clearly reflecting the ductility contrast between quartz and feldspar. Clusters of feldspar σ_b and to a lesser extent δ type porphyroclasts, dominate S-C orthomylonites of high clast-density (Fig. 27 f-l, n and o; and Fig. 28 a, b, f, h and i), while σ_a and δ types are widespread in matrix-dominated and ultramylonitic varieties (Fig. 27 c-e; and Fig. 28 c-e, g and m-o). This association reflects higher shear strain rates in ultramylonitic tectonites.

A common feature of δ-type porphyroclasts is the development of corrosion embayments at the rims of clasts, where the "roots" of recrystallizing tails have consumed reaction softened clast material (Fig. 27 c and d; and Fig. 28o).

Replacement of K-feldspar by quartz-plagioclase symplectite (myrmekite) is common along the two edges of σ-type porphyroclasts that face the local inferred incremental shortening direction (Fig. 28p). This deformation-induced reaction has been documented by previous workers (Hanmer, 1982; Simpson, 1983, 1985; Watts and Williams, 1983; Simpson and Wintsch, 1989), and its implications for the mylonitization process are discussed in section 7.5.1.

Mica-fish

Rare, relict clasts of biotite, commonly altered to chlorite or opaque oxides, assume mica-fish geometries with (001) cleavage planes tilted back approximately 20° against the inferred sense of shear (see Fig. 28 j and k). In general mica-fish are uncommon in quartz-feldspar mylonites of the GSS sample set. Biotite in orthomylonites usually occurs as an extremely fine-grained recrystallization product concentrated along shear surfaces, and in augen gneisses as tabular, wholly recrystallized grains with (001) parallel to S_M.

Asymmetrical microfolds

Asymmetrical, disharmonic folds are characteristically developed in polycrystalline quartz-ribbons within the flow plane of quartz-feldspar orthomylonites and ultramylonites. Examples are illustrated in Figure 27 i, m and n; and Figure 28 b, c, d and h. Various stages of shear fold development are represented. Folds initiate with fairly upright axial surfaces. With superposed simple shear the axial surfaces rotate, or bend, towards the flow plane. Concomitant thickening of hinge zones and attenuation / boudinage of overturned limbs, occurs in response to limb shearing. With progressive rotation and limb shearing, extreme fold asymmetry is achieved. Overturned limbs may become detached resulting in characteristically incomplete *fish-hook* folds (Fig. 28h). Axial surfaces and upper limbs attain sub-parallelism with the flow plane.

A highly asymmetric microscopic overfold, bearing morphological similarities to a megascopic Alpine fold nappe, is illustrated in Figure 27p. With continuous elongation of the fold during progressive simple shear, the axial surface has become arched, and drawn into parallelism with the flow plane in the frontal portion. Extreme attenuation of the overturned limb has resulted in detachment and replacement of the leading portion of the limb by a thrust surface (indicated by **a**). Reactivation of the upper limb as a thrust surface at a later stage, allowed several smaller, inclined to recumbent overfolds (indicated by **b**) to *ride-up* over the major overfold. These subordinate overfolds exhibit characteristic *fish-hook* geometries (indicated by **c**), with sheared-out lower limbs in contact with the thrust surface. Disrupted synformal fold components occur in the footwall of the the thrust surface (indicated by **d**). Complex development of *brow-digitations* (Hobbs *et al.*, 1976) in the hinge-regions of the inclined overfolds (indicated by **e**), attests to the heterogeneity of simple shear.

Quartz grain and subgrain shape-fabrics

Two varieties of quartz-ribbon fabrics occur within GSS S-C mylonites:-

1) Moderately elongated monocrystalline quartz-ribbons exhibiting undulose extinction and subparallel deformation bands.

2) Extremely elongated polycrystalline quartz-ribbons exhibiting considerable subgrain and neoblast development, and a tendency for grain-shape preferred alignments.

The former (type 1) may represent a coarser earlier microstructure, that is subsequently deformed and recrystallized to produce the latter higher strain variety (type 2). Both types of quartz-ribbon commonly host secondary fabrics useful for movement sense determination.

Elongate deformation bands are commonly inclined obliquely to the boundaries of monocrystalline ribbons subparallel to S_M, and define an early oblique secondary microfoliation. With progressive deformation and dynamic recrystallization, the deformation bands provide nucleation sites for subgrain development and neoblastesis. Fine recrystallization within the deformation bands produces a polycrystalline structure, commonly with an inclined grain/subgrain shape alignment defining an additional oblique secondary microfabric. At this late stage the recrystallized deformation bands are marked by a weak extinction banding. It is not uncommon for both secondary microfabric types to be preserved together. Figure 28k illustrates the development of asymmetric grain/subgrain shape-fabrics within oblique deformation band microfoliations. Law *et al.*, (1986), document similar quartz deformation microfabrics within quartz mylonites from the Assynt and Eriboll regions of the Moine thrust zone.

Quartz shape-fabrics are always potentially unreliable as kinematic indicators due to the ease with which they are reset by subsequent deformation events (Brunel, 1980; Simpson and Schmid, 1983; Simpson, 1986b; also see section 2.5.2.6). This is clearly illustrated in Figure 28 m and n, where the shear sense indicated by quartz microfabrics conflicts with that indicated by asymmetrical porphyroclast systems. The quality of kinematic interpretations of quartz microfabrics should always be tested by comparison with the shear sense derived from independent indicator fabrics.

Displaced, fractured feldspar porphyroclasts

Microfaulted feldspar clasts with offset components are relatively common in GSS mylonites. Figure 28i shows fractured components of a σ-type feldspar porphyroclast, synthetically offset along a low-angle, cissaillement-parallel microfault. Although these kinematically useful microstructures are widespread, they require cautious assessment, since local flow perturbations within high clast-density S-C mylonites, and complex reactivation of microfaults in rolling-clasts, may lead to misinterpretation. The reorientation of fragments of fractured clasts commonly creates voids which may be infilled by opaque oxides or by quartz exhibiting plastic strain features.

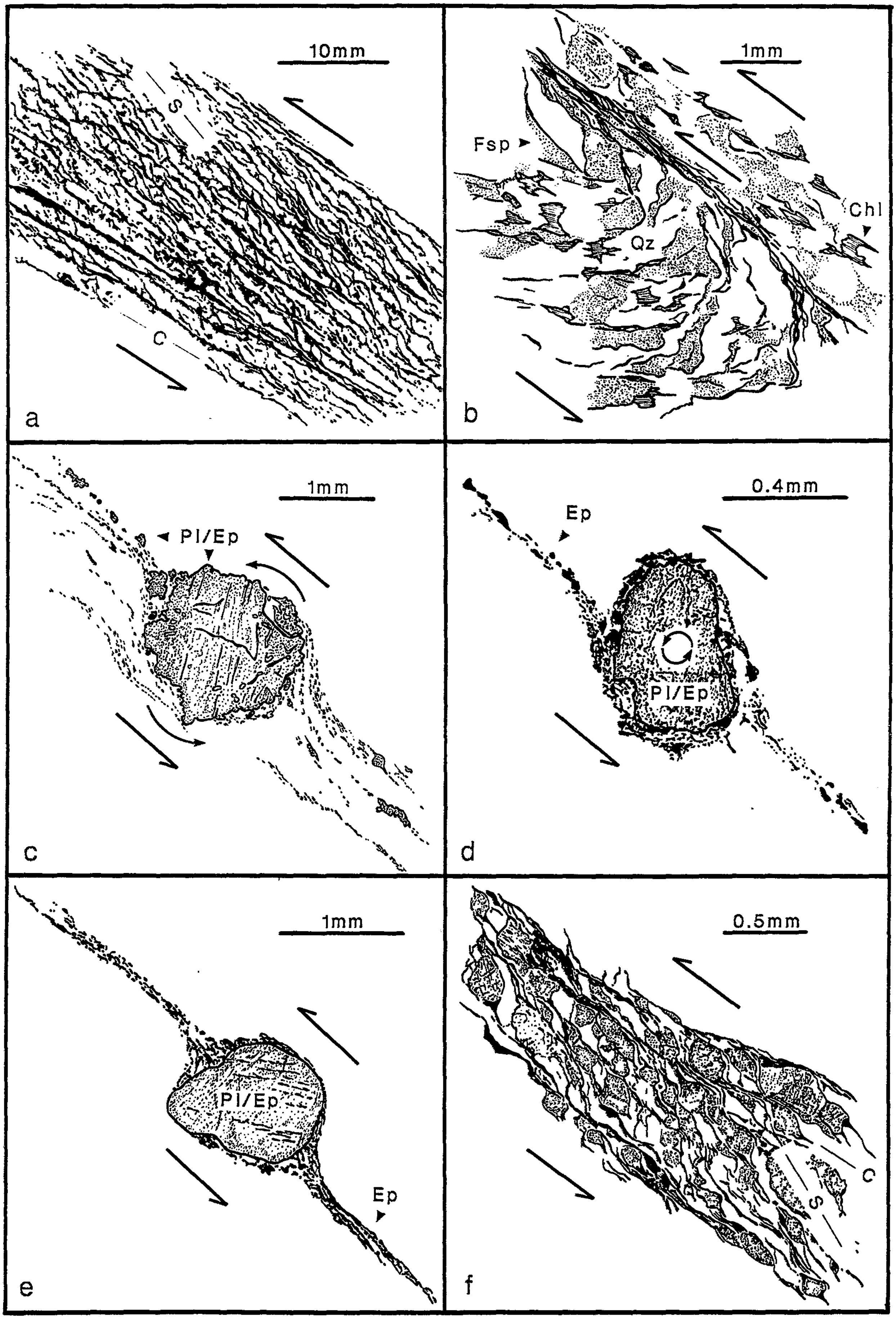
10mm
S
C
a
1mm
Fsp
Qz
Chl
b
1mm
Pl/Ep
c
0.4mm
Ep
Pl/Ep
d
1mm
Pl/Ep
Ep
e
0.5mm
C
S
f

Figure 27. (previous page) Examples of kinematic indicators within mylonitic rocks, Graafwater Shear System. All sketches made from XZ-sections. Look direction is variable and will be specified for each frame. Angle of dip approximate.

(a) S-C composite planar fabrics developed within quartz-feldspar orthomylonite. The C surfaces are only persistent within discrete bands (lower part of sketch), elsewhere they are discontinuous and poorly developed. Look direction is SW. Shear sense is reverse, top-to-S/SSW (sample CJS/34, Poliesberg antiform, LGSZ).

(b) Microscopic thrust surface developed within a quartz-feldspar protomylonite. The deformed protomylonitic fabric within the footwall defines a disrupted synformal ductile bend fold, consistent with reverse, top-to-S movement sense. The hangingwall protomylonitic fabric is undeformed and parallels the principal thrust surface. Look direction is W (sample CJS/33, Poliesberg antiform, LGSZ).

(c) and (d) Highly saussuritized δ-type plagioclase porphyroclast systems within calc-silicate ultramylonite. Corrosion embayments are locally developed at the rims of the clasts adjacent to the "roots" of the recrystallized tails. The tails are often completely epidotized. Look direction is NW. Reverse (anticlockwise, top-to-SW) vorticity is indicated (sample CJS/40, LGSZ, Maanhaarkop).

(e) Well-rounded, saussuritized σ-type plagioclase porphyroclast within calc-silicate ultramylonite. The recrystallized tails comprise fine-grained epidote with minor chlorite. Look direction is NW. Shear sense is reverse, top-to-SW (sample CJS/40, LGSZ, Maanhaarkop).

(f) S-C composite planar fabric within quartz-feldspar orthomylonite. Look-direction is W. Reverse, top-to-SW movement sense is indicated (sample CJS/46, LGSZ on Graafwater 106).

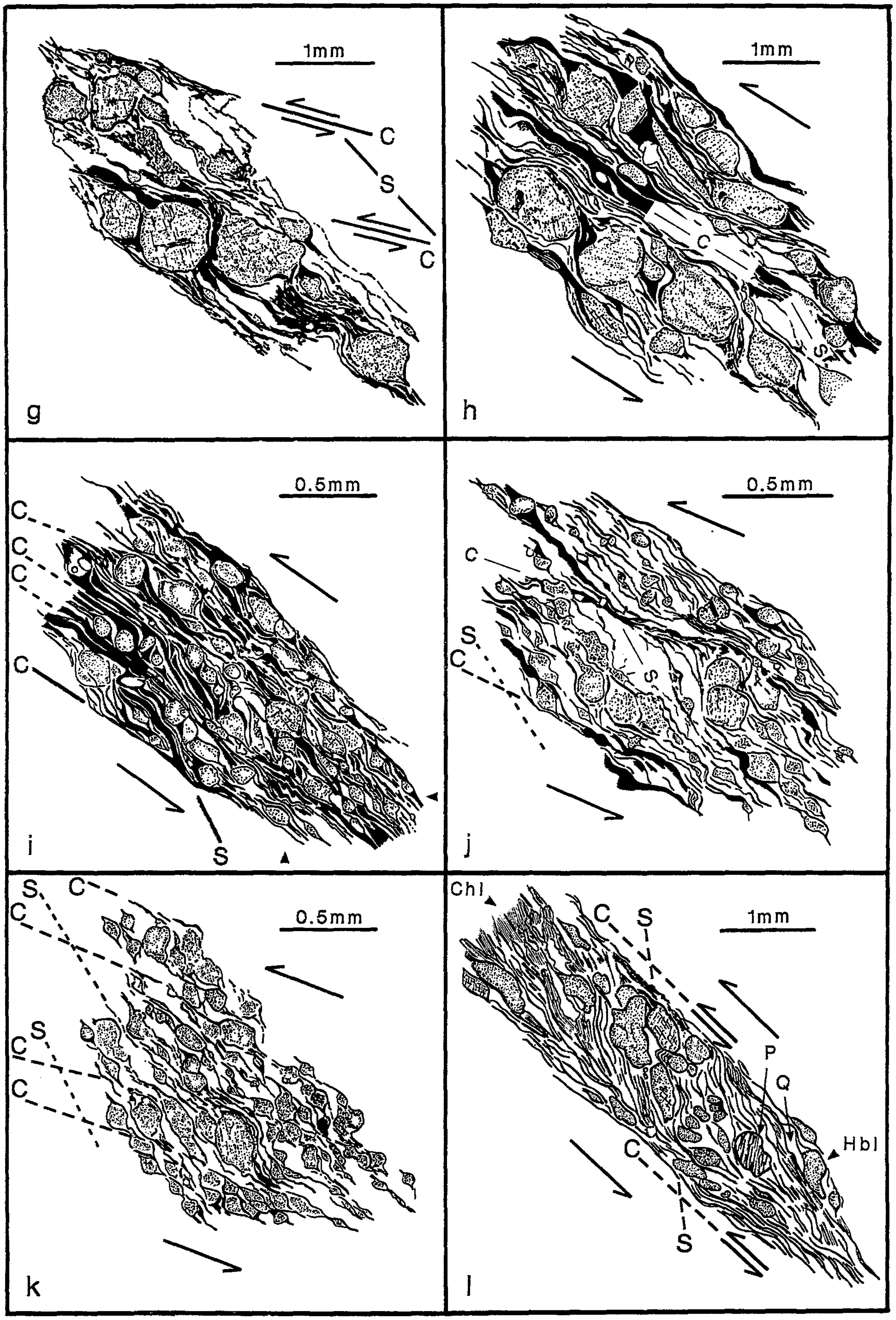
1mm
C
S
C
g
1mm
c
s
h
0.5mm
C
C
C
C
S
i
0.5mm
c
S
C
s
j
S
C
C
0.5mm
S
C
C
k
Chl
C
S
1mm
P
Q
Hbl
C
S
l

Figure 27. (continued) (g) to (k) S-C composite planar fabrics developed within quartz-feldspar orthomylonite from the LGSZ on Graafwater 106. Look direction is W. S-C fabric vergence relationships and the characteristic geometry of σ_b-type porphyroclast systems, indicate reverse, top-to-SW movement sense.
In (i), arrow-heads in the lower right corner indicate the X,Y positions of asymmetrically microfolded polycrystalline quartz-ribbons within the flow plane. Vergence of the microfolds is consistent with reverse, top-to-SW shear sense. The cissaillement surfaces marked in (k) are only poorly developed, but coincide with positions of concurrent inflection along the dominant S-surface sets.
(g) sample CJS/46; (h and i) sample CJS/47; (j and k) sample CJS/48.
(l) S-C type composite shear band fabrics developed within an orthomylonitic amphibolite. C-surfaces are defined by a DPO of fine-grained chlorite, sericite, quartz and epidote / clinozoisite. Elongate hornblende and plagioclase σ-type porphyroclast systems, the long-axes of polycrystalline, lenticular quartz-ribbons and a secondary chlorite (001) preferred orientation, define S-surfaces which curve sigmoidally into the principal shear planes (**C**). Secondary chlorite is common within the pressure shadow domains, adjacent to rigid porphyroclasts and in asymmetrical boudin-necks. Look direction is W. Shear sense is oblique reverse, top-to-WSW (sample CJS/49, UGSZ, southern limb of the Graafwater synform).

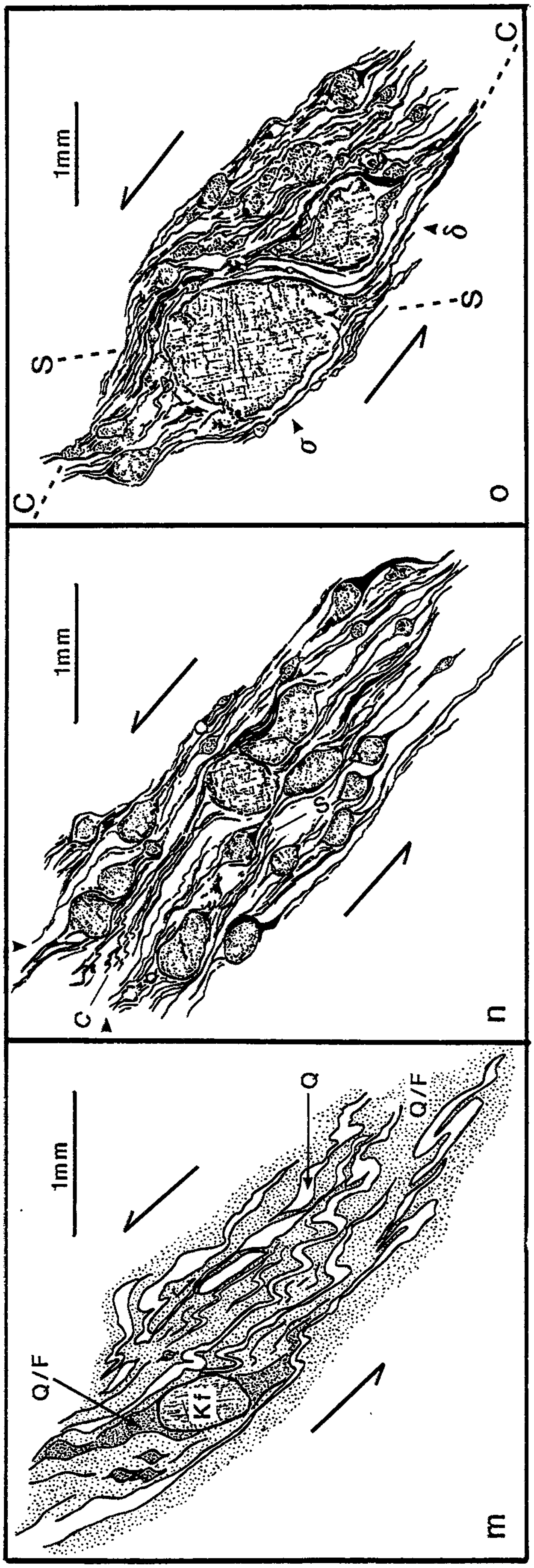
1mm
S
S
C
C
δ
σ
o
1mm
C
S
n
1mm
Q
Q/F
Q/F
Kf
m

Figure 27. (continued) (m) Asymmetrical, disharmonic microfolding of polycrystalline quartz-ribbons in ultramylonitic bands within a quartz-feldspar orthomylonite. Oblique reverse (top-to-WNW) shear sense is indicated by the vergence of asymmetrical microfolds, and the "stair-stepping" geometry of isolated σ-type K-feldspar porphyroclast systems (sample CJS/50, LGSZ, northern limb of Graafwater Synform).

(n) σ_b-type feldspar porphyroclast systems in S-C fabric configuration within a quartz-feldspar orthomylonite. Shear surfaces are defined by dark trains of microcrystalline altered feldspar, secondary micas and quartz. The arrow-heads in the top-left corner indicate the X,Y position of tiny asymmetrical microfolds developed within the fluxion banding. Look direction is NE. Shear sense is reverse, but highly oblique (top-to-ENE) (sample CJS/51, LGSZ, northern limb of the Graafwater Synform).

(o) σ-Type microcline porphyroclast system "stacked" against a smaller δ-type system in a S-C fabric configuration more commonly exhibited by σ_b-type porphyroclast associations. An aberrant perturbation in flow adjacent to the unusually large σ-type porphyroclast may have generated the vorticity required to cause the smaller neighbouring clast to rotate, resulting in a δ-type system. Quartz-feldspar orthomylonite (sample CJS/51) from the LGSZ on the northern limb of the Graafwater synform. Look direction is NE. Shear sense is reverse, but highly oblique (top-to-ENE).

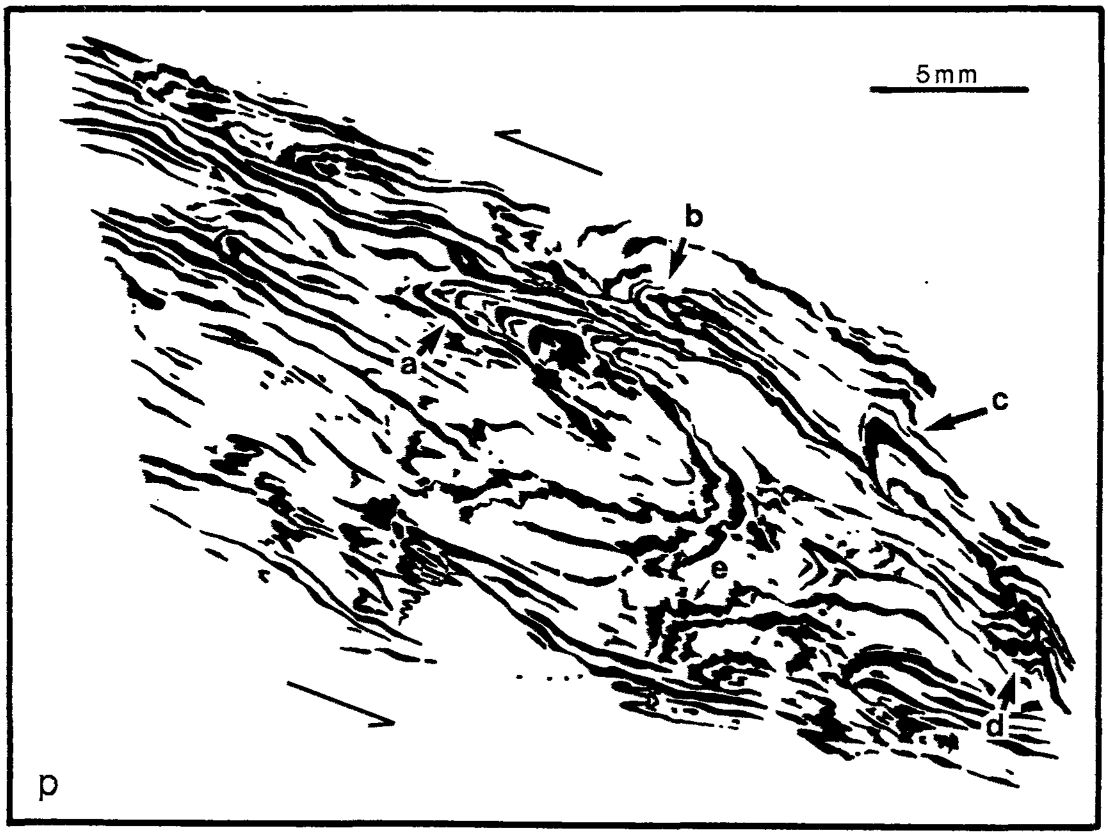
5mm
b
a
c
e
d
p

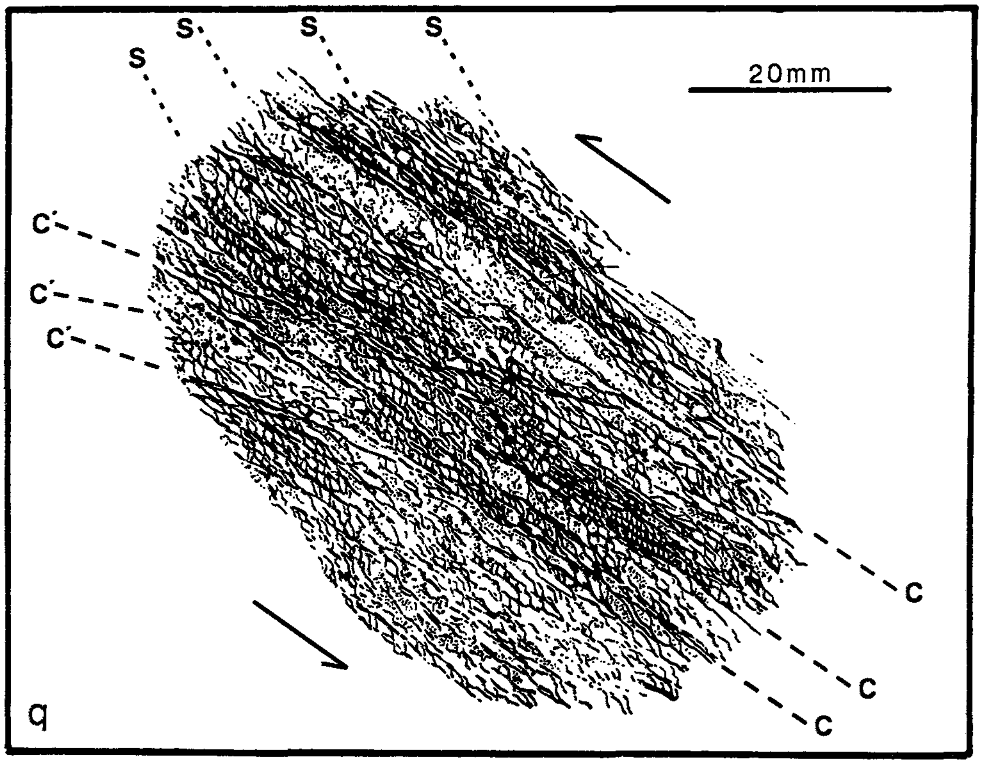
s
s
s
s
20mm
c'
c'
c'
c
c
c
q

Figure 27. (continued) (p) Highly asymmetrical microscopic overfold developed within a quartz-feldspar orthomylonite / ultramylonite. Sketch made from magnified xerox-copy of thin-section. Attention is drawn to the morphological similarities between these microscopic overfolds and megascopic Alpine fold nappes. For explanation of **a**, **b**, **c**, **d** and **e**, see section 7.4.1. Look direction is NE. Movement sense is oblique reverse, top-to-WNW (sample CJS/50, LGSZ, northern limb of the Graafwater synform).

(q) Composite S-C-C' planar fabrics within a quartz-feldspar orthomylonite. Sketch made from magnified xerox-copy of thin-section. Localised C' shear band surfaces disrupt and deflect both S and C surfaces. Look direction is W. Movement sense indicated by fabric vergence relationships is reverse, top-to-SW (sample CJS/47, LGSZ, southern limb of the Graafwater synform).

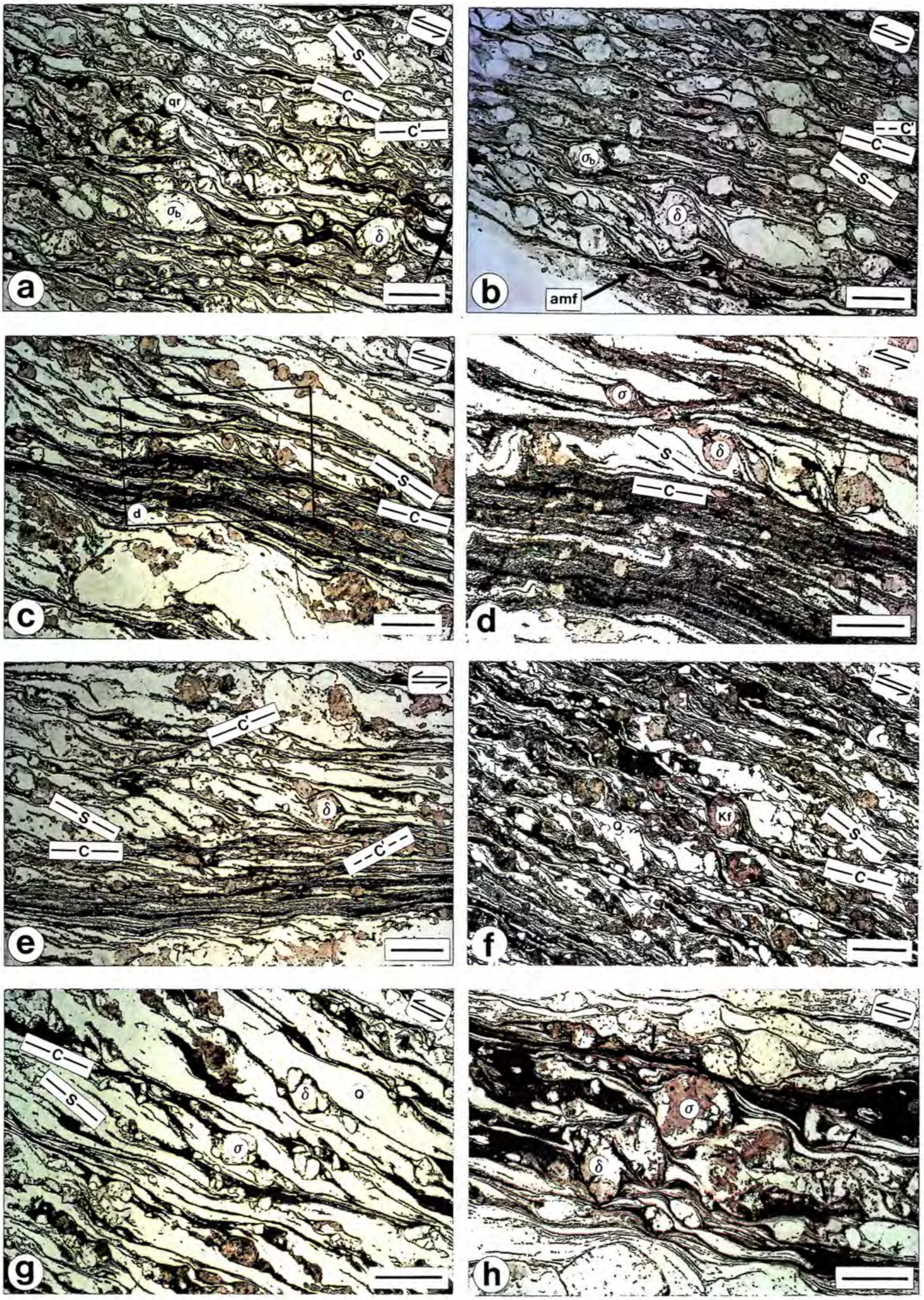
S
C
C'
qr
σb
δ
a
b
amf
d
c
σ
e
Kf
f
g
h

Figure 28. (previous page) Photomicrographs of typical microfabric development within mylonitic tectonites of the Graafwater Shear System, illustrating the range, abundance and consistency of kinematic indicators within this sample set. All are XZ-sections, maintaining the correct dip sense. Dip angles are not true. Scale bars for (a) to (c), (e) and (f) = 1mm; (d) and (g) to (p) = 0.5mm.

(a) and (b) High-ductility S-C-C' composite planar fabrics in a quartz-feldspar orthomylonite. Feldspar σ_b and δ porphyroclast aggregates are widespread, and asymmetrical microfolds occur along principal C-surfaces. Look-direction ENE. All independent indicators record oblique reverse (top-to-WSW) movement sense. PPL (sample CJS/51, LGSZ, northern limb of the Graafwater synform).

(c) S-C composite fabrics, σ and δ feldspar porphyroclast systems and asymmetrical microfolds within a quartz-feldspar orthomylonite. Look-direction is WSW. Movement sense is reverse (top-to-SSW). PPL (sample CJS/34, LGSZ, Poliesberg antiform).

(d) Magnified view of (c) showing asymmetrical microfolding of polycrystalline quartz-ribbons within the flow-plane, linked δ porphyroclasts in S-C fabric configuration, and occasional σ porphyroclasts. The prescribed movement sense is consistent for all of these indicators. PPL.

(e) S-C-C' composite planar fabrics within quartz-feldspar orthomylonite. Incipient C' shear bands appear as crenulations within the closely spaced C-surfaces towards the base of the photomicrograph. Look-direction is WSW. Movement sense is reverse (top-to-SSW). PPL (sample CJS/34), LGSZ, Poliesberg antiform).

(f) S-C fabrics and σ_b feldspar porphyroclasts within quartz-feldspar orthomylonite. Look-direction is W. Movement sense is oblique reverse (top-to-SW). PPL (sample CJS/48, LGSZ, southern limb of the Graafwater synform).

(g) σ And δ feldspar porphyroclast systems, and S-C composite planar fabrics in quartz-feldspar orthomylonite. Look-direction is WSW. Movement sense is reverse (top-to-SSW). PPL (sample CJS/34, LGSZ, Poliesberg antiform).

(h) Clustered δ and σ_b feldspar porphyroclasts in typical S-C fabric configuration in quartz-feldspar orthomylonite. Limited asymmetrical microfolding is visible within narrow quartz-ribbons (indicated by arrows). Note the fish-hook geometry of the top-right microfold. Look-direction is ENE. Movement sense is oblique reverse (top-to-WSW). PPL (sample CJS/51, LGSZ, northern limb Graafwater synform).

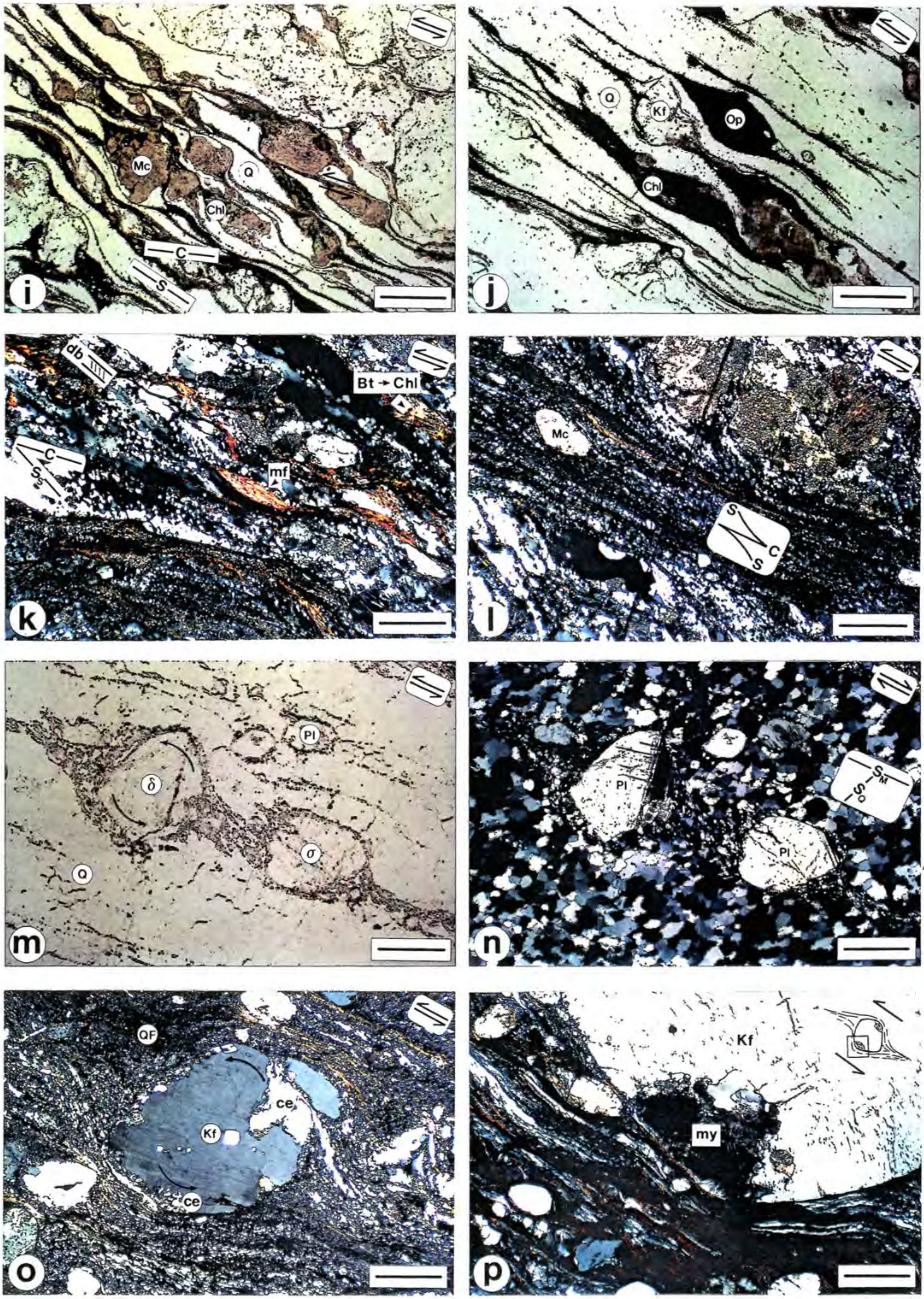
Mc
Q
Chl
C
S
i
Q
Kf
Op
Chl
j
db
Bt → Chl
C
S
S
mf
k
Mc
S
C
S
l
Pl
δ
σ
Q
m
Pl
Pl
S_M
S_Q
n
QF
ce
Kf
ce
o
Kf
my
p

Figure 28. (continued) (i) Clustered σ_b microcline porphyroclasts in S-C fabric configuration within quartz-feldspar orthomylonite. Note the synthetic offset along the low-angle microfault in the fractured feldspar porphyroclast on the right. Look-direction is WSW. Movement sense is reverse (top-to-SSW). PPL (sample CJS/34, LGSZ, Poliesberg antiform).

(j) Relict mica-fish, pseudomorphed by opaque oxides (**Op**), and K-feldspar σ-type porphyroclast within quartz-feldspar orthomylonite. Look-direction is WSW. Movement sense is reverse (top-to-SSW). PPL (sample CJS/34, LGSZ, Poliesberg antiform).

(k) Chloritic mica-fish (**mf** - after biotite) and secondary quartz grain/subgrain shape fabric ($\mathbf{S_s}$), oblique to the principal shear surface (**C**). An earlier quartz microfabric is defined by subparallel deformation bands (**db**) developed within relict quartz-ribbons. This fabric is also inclined to C, and records the same movement sense. Quartz grain-shape fabrics develop obliquely within recrystallized deformation bands. Look-direction is WSW. Movement sense is reverse (top-to-SSW). XPOL (quartz-feldspar orthomylonite, sample CJS/34, LGSZ, Poliesberg antiform).

(l) Sigmoidal deflection of S-fabrics defined by polycrystalline quartz-ribbons, into a principal shear surface (**C**) within quartz-feldspar orthomylonite. A microcline σ porphyroclast (**Mc**) is visible in the shear plane. Look-direction is WSW. Movement sense is reverse (top-to-SSW). XPOL (sample CJS/34, LGSZ, Poliesberg antiform).

(m) Linked σ and δ plagioclase porphyroclast systems within calc-silicate ultramylonite. Look-direction is WSW. Movement sense is oblique reverse (top-to-SW). PPL (sample CJS/40, LGSZ, Maanhaarkop).

(n) As for (m) but XPOL, illustrating a secondary quartz grain-shape fabric ($\mathbf{S_Q}$), inclined obliquely to the mylonite foliation (S_M). Oblique normal (top-to-NE) movement sense is indicated by this fabric, in discord with the reverse shear sense prescribed by the asymmetrical porphyroclast systems. Photomicrographs (m) and (n) serve to illustrate the potential unreliability of secondary quartz grain-shape fabrics as kinematic indicators .

(o) δ-Type K-feldspar porphyroclast system in a quartz-feldspar orthomylonite. Note the formation of subgrains and new grains within incipient corrosion embayments (**ce**), developed at the "roots" of the recrystallized tails. Look-direction is W. Movement sense is oblique reverse (top-to-SW). XPOL (sample CJS/47, LGSZ, southern limb of the Graafwater synform.

(p) Deformation-induced replacement of K-feldspar by myrmekite (**my**) on the edge of a σ-type porphyroclast, in quartz-feldspar orthomylonite. Inset schematically illustrates the distribution of myrmekite on the two sides of the clast that faced the local inferred incremental shortening direction. Look-direction is ENE. Movement sense is oblique reverse (top-to-WSW). XPOL (sample CJS/51, LGSZ, northern limb of the Graafwater synform).

7.5 Kinematic synthesis

Kinematic interpretations for each of the twelve sample localities within the GSS are summarized in stereograms A to L of Figure 24. The shear sense and relative Kinematic Confidence Index (KCI) for tectonite fabrics are shown by representative symbols at each sample station on the maps (see caption).

The orientation of the L_M lineation and movement sense determinations made from composite planar microfabrics, asymmetrical feldspar porphyroclast systems, mica-fish, oblique quartz microfabrics, and the displacement sense of microfaulted feldspar clasts, indicate with the highest level of confidence that penetrative fabric development within GSS tectonites is related to *reverse movement, with overthrusting directed towards the WSW/SW.* Extensional shear bands within a *single* amphibolite gneiss sample (CJS/32) indicate with a moderate degree of confidence (KCI = 2) that *top-to-NE, normal movement occurred on the LGSZ south of Kenhardt* (sample locality K, Fig. 24). This kinematic interpretation is in conflict with unequivocal mesoscopic evidence for SW-directed thrusting at the same locality: SW-vergent antiformal F_2 folds are observed, with refoliated forelimbs across which the S_1 gneissic foliation is deflected with consistent top-to-SW displacement sense. No mesoscopic evidence exists at this locality to suggest that extensional (top-to-NE) reactivation took place.

7.5.1 Modification of primary thrust vectors within the GSS

The orientation of S_M and L_M fabrics within the GSS are illustrated stereographically in Figure 29 a and b respectively. The dispersion of S_M poles along a great-circle having a pole plunging towards the ENE, reflects folding of the GSS mylonite zones about NE/ENE-plunging F_3 fold axes (see also Fig. 26). Due to the demonstrated coaxial relationship between F_3 fold axes and L_M lineations (section 7.3.3; Fig. 26), the calculated kinematic vectors are unmodified by F_3 cross-folding. Despite this, the L_M lineations are dispersed along a great-circle corresponding closely with the mean S_M foliation plane. This relationship indicates clockwise rotation of the L_M lineations within the S_M plane, from NNE-plunges towards ESE-plunges, during D_4 right-lateral transcurrent shearing (Harris, 1992). Consequently only the least rotated lineations are representative of primary thrust directions. The implications of regional modification of primary thrust vectors during D_4 shearing are discussed more fully in section 8.1.3.1.

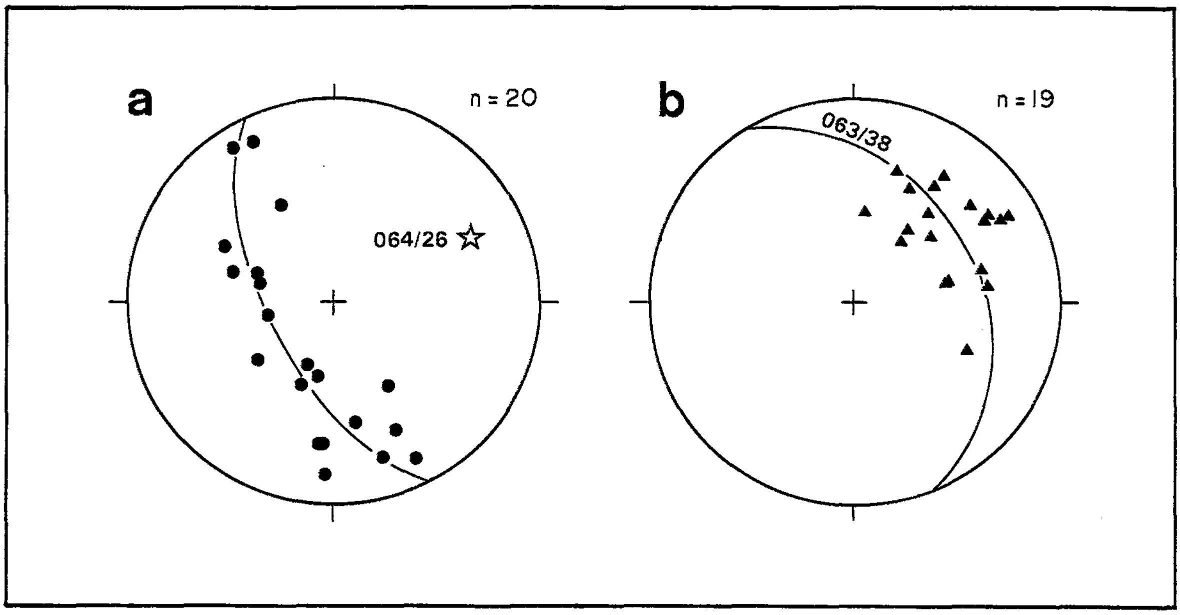

Figure 29. Equal-area lower-hemisphere stereograms illustrating the orientation of (a) S_M and (b) L_M fabrics in the GSS. L_M lineations and poles to S_M foliations are indicated by triangles and circles respectively. The star of (a) denotes the statistical mean for F_3 fold axes in the southern GSS. Great-circles indicate computed best-fit girdles to the planar dispersion of S_M poles and L_M lineations. See text for explanation.

7.5.2 Characterization of the physical conditions of mylonitization

7.5.2.1 Rheological constraints

Owing to the absence of diagnostic mineral assemblages within the quartzo-feldspathic dominated GSS sample set, a precise evaluation of the P-T conditions of shearing is difficult. Nevertheless, microstructural features of quartzo-feldspathic GSS tectonites are typical of high-grade mylonites, formed by full crystal-plastic processes in the ductile regime. Microfabrics are characterized by high ductility contrasts between quartz and feldspar, and significant grain-size dimunition by crystal-plastic processes.

Quartz is dynamically recrystallized resulting in rare elongate, monocrystalline ribbons and, more commonly, in exceptionally attenuated polycrystalline ribbons which are squeezed between feldspar porphyroclast clusters. The infilling of dilational fractures within feldspar by quartz exhibiting plastic strain features, is evidence for the extreme mobility of the quartzose matrix. Grain-size within polycrystalline ribbons is <0.1mm, which is thought to be the threshold requirement for superplasticity (Nicolas and Poirier, 1976; White, 1976, 1977). Superplastic flow in quartzite normally occurs by grain boundary sliding at temperatures above 400°C (Schmid *et al.*, 1977, Etheridge and Wilkie, 1979).

Feldspars exhibit both brittle and ductile deformation features. Extension cracking and microfaulting are common. Intracrystalline ductility of feldspars is indicated by lattice bending, mechanical twinning (Fig. 28n), and the widespread occurrence of kink bands, deformation bands and undulatory extinction (Fig. 28o). Initiation of ductile deformation of feldspars occurs at 450°C ± 50°C (Mitra, 1978).

Widespread dynamic recrystallization of both K-feldspar and plagioclase to fine-grained polygonal mosaics of new grains and subgrains, indicates deformation by recrystallization accommodated dislocation creep, the prevalent mechanism at middle to upper amphibolite facies (Simpson, 1985; Tullis and Yund, 1985, 1987). Recrystallization of feldspar is thought to occur at temperatures above 500°C (Voll, 1976). Fine-grained recrystallized aggregates are common in the mantles of K-feldspar porphyroclasts, and deformation-induced formation of myrmekite is widespread (see Fig. 28 o and p). Occurrences of strain-induced myrmekite within amphibolite grade mylonites are well-documented (Simpson, 1985; La Tour and Barnett, 1987; Gapais, 1989; Simpson and Wintsch, 1989).

The recovery state of GSS tectonites is variable, although most of the quartz-feldspar mylonites exhibit textures consistent with a lack of static annealing. Highly-attenuated polycrystalline quartz-ribbons exhibit serrated grain boundaries and internal polygonized substructure is rare. Grain-size is typically <0.1mm, indicating strong grain-size reduction by dynamic recrystallization without significant annealing grain growth. In mylonites with significant amounts of dispersed secondary minerals (e.g. opaques, phyllosilicates), this feature may be accounted for by inhibition of grain growth by grain-boundary pinning. Approximate equilibrium textures occur locally within monomineralic quartz lithons. Within the augen gneisses biotite is commonly wholly recrystallized, and occurs as strain-free tabular grains with (001) cleavage planes parallel to the margins of quartz-ribbons.

7.5.2.2 Paragenetic indicators

Within quartzo-feldspathic tectonites, replacement of primary brown biotite by green biotite, chlorite and opaque oxides is widespread. Early biotite mica-fish and pressure shadow wings are commonly partially, or wholly, pseudomorphed by chlorite or opaque oxides (Fig. 28 j and k). Shear surfaces are characterized by the break-down of feldspars to extremely fine-grained intergrowths of highly-altered feldspar, quartz, chlorite, sericite, epidote-group minerals and opaque oxides. Within calc-silicate tectonites, plagioclase porphyroclast systems are often partially, or totally saussuritized to fine-grained, *undistorted* intergrowths of epidote-group minerals and chlorite (Fig. 27 c, d and e). Alteration of hornblende to chlorite occurs frequently within amphibolitic tectonites. Mimetic alteration textures are consistent with post-kinematic, passive retrogression.

7.6 Discussion

Rheological data indicate that penetrative fabrics within GSS tectonites record high-temperature, ductile deformation at upper to middle amphibolite facies. These data are in discord with the apparently low annealing state of GSS tectonites which suggests that thrusting was accompanied, or followed by, uplift and cooling rather than static heating. However, alteration textures are not indicative of syn-kinematic retrogression and consequently do not support the second proposal. Furthermore, Harris (1992) has established that ductile reorientation of structures adjacent to the Pofadder Lineament during D_4 strike-slip shearing, occurred at temperatures in excess of 600°C, a finding which clearly conflicts with textural evidence suggesting that rapid-cooling succeeded D_2 thrusting on the GSS. This enigmatic relationship is explored more fully in section 8.1.4.3.

Extensive reworking of early, thrust-related ultramylonite fabrics and shear surfaces by cataclastic microstructures (samples CJS/33, CJS/35 and CJS/36; Table 5 of Appendix), within tectonites from the eastern limb of the Rietfontein anticline and northern limb of the Poliesberg antiform, is attributed to localized brittle reactivation of the GSS (*Graafwater splay*; Harris, 1992) during late-D_4 shearing.

Chapter 8. - Discussion and conclusions

8.1 Discussion

8.1.1 Overview

Microstructural data presented in Chapters 3 to 7 have clearly shown that movement histories of the principal shear zones within the HRTB are far more complex than previously envisaged. Despite the complex nature of movements and reactivations on individual shear zones, shared microstructural kinematic patterns occur which are best resolved by interpreting them as the result of multiple-phase shearing within a common kinematic framework. Moreover, syntectonic mineral assemblages and fabric relationships within the tectonites, constrain the PT-conditions of penetrative fabric development at the time of each shearing event. The recovery and annealing states of the mylonites provide insight into the thermotectonic evolution of individual shear zones, and of the HRTB as a whole. Rheological responses of, and contrasts between, individual mineral phases are diagnostic of specific deformation mechanisms, and thus constrain the tectonothermal regime active during penetrative fabric development within the shear zones. Regional NE to SW variation of the above criteria across the belt, reflect systematic changes in PT-conditions and strain regime through the structural section and provide insight into the crustal architecture of the HRTB. Section 8.2 proposes a kinematic model for the evolution of the HRTB based on the findings of this microstructural investigation.

8.1.2 Dip-slip movements within the HRTB

Unequivocal evidence for two principal dip-slip movement events is sustained by microstructural shear sense criteria preserved within tectonites from the principal shear zones of the HRTB.

Convincing evidence for *normal, top-to-NE, movement* occurs within tectonites from the Neusspruit Lineament, Kakamas Shear Zone and Hugosput Shear System, while *reverse, top-to-S/SW, movement* is conclusively recorded by tectonites of the Hugosput Shear System, Rozynenbosch-Ganzenmond Shear Zone, Witvlei Shear Zone and Graafwater Shear System. The possibility of a reverse movement component on the

Neusspruit Lineament is intimated by less reliable kinematic data. Mylonitic rocks within all these zones are characteristically dip-lineated, with rare strike- or highly-oblique lineated tectonites occurring locally along the Kakamas Shear Zone and Graafwater Shear System. This regionally consistent down-dip orientation of the principal mylonite elongation lineation suggests that transcurrent movements were not significant within the mylonite zones (section 8.1.3.5).

8.1.2.1 Relative timing of dip-slip movements

Harris (1987, 1992) demonstrated that the NW-trending, southwest-vergent mylonite zones of the southwestern HRTB are D_2 in age, since they rework the regionally penetrative D_1 fabrics. Based on the SW-vergence of F_2 shear-related folds, the deflection of S_1 foliations across the D_2 shear domains, and the transverse L_M lineation pattern within the belt, Harris (1987, 1988, 1992) regards the mylonite zones as ductile thrusts characterized by displacements towards the SW. Furthermore, Harris (1987, 1988) demonstrated refolding of the D_2 thrusts by a NE-trending F_3 fold component, and regional clockwise rotation of all earlier fabrics and structures in a broad belt adjacent to the Pofadder Lineament during a D_4 transcurrent shearing event (section 1.3.2).

The results of this investigation corroborate macroscopic evidence of SW-directed thrusting within the HRTB mylonite zones during D_2, but have in addition shown that not all down-dip lineated tectonites of the HRTB are temporally, metamorphically and kinematically compatible. Microstructural evidence has shown that despite the subparallelism of L_M lineations within shear zones across the HRTB, one cannot assume that these fabrics are the products of a single tectonic event.

Unequivocal evidence of the relative timing of thrusting and normal dip-slip shearing events in the HRTB is not forthcoming. However, rare transposition criteria and textural and paragenetic contrasts between syn-kinematic fabrics, allow temporal distinctions to be made with an acceptable degree of confidence.

1) At Neuspoort on the Neusspruit Lineament, cross-cutting extensional shear bands reflecting normal, SW-side up movement are observed disrupting fabrics within quartz mylonites which preserve evidence of early, top-to-SW reverse movement (section 3.4).

2) Within tectonites of the Neusspruit Lineament and HSS, microstructures and fabrics indicating normal, top-to-NE movement are frequently kinematically sensitive criteria (e.g. oblique quartz and mica (001) DPO microfabrics), which are likely to reflect the final increment of deformation on the zones (section 5.4). Had thrusting occurred after normal shearing these fabrics would almost certainly have been reset.

3) In mylonites of the HSS where evidence for both top-to-SW and top-to-NE shearing is preserved, development of thrust-fabrics has been shown to coincide with retrogression from granulite facies to upper-amphibolite facies (section 5.4.1), while *final-increment* normal-shearing fabrics are often defined by amphibolite facies or lower grade mineral assemblages (section 5.4.1).

4) Within the HSS reworking of the margins of the Hugosput Potassic Charnockite by *top-to-NE* shearing fabrics (Fig. 14), places additional constraints upon the timing of normal movements within the area. Based on presence of mylonitic fabrics within the Hugosput Charnockite, Harris (*pers. comm.*, 1990) proposed a pre- to syn-D_2 emplacement age for this granitoid body. The findings of this study have shown that the mylonitic fabrics within the charnockite reflect normal movement. Consequently emplacement need not have occurred pre-/syn-D_2 thrusting, but *may have occurred later* during normal movement. This proposal is sustained by the correlation of the Hugosput Charnockite with the *late- to post-tectonic* Friersdale Charnockitic Adamellite (Geringer *et al.*, 1988; Humphreys and Van Bever Donker, 1990). Isotopic age determinations of the Friersdale Charnockite have yielded a Rb/Sr isochron age of 1085 ± 130 Ma, and a composite zircon $^{207}Pb/^{208}Pb$ age of 1087 Ma (Barton and Burger, 1983). Assuming that these isotopically determined ages reflect magmatic crystallization, it is likely that top-to-NE shearing occurred sometime after 1100 Ma.

The tectogenetic significance of the omnipresent 1100 Ma age within a regional Namaqua context has important implications regarding the temporal correlation of deformation and metamorphic events. Many workers (e.g. Joubert, 1986; Waters, 1989, 1990) have correlated the 1100 Ma age with early Namaqua tectogenesis (D_2) and the so-called Namaqua "thermal event". However, Harris (1990, 1992) presented evidence suggesting that high-temperatures (>600°C) persisted well into D_4, a conclusion which strongly influences the interpretation of Rb/Sr whole-rock ages within the HRTB. The resetting of Rb/Sr radiometric clocks during or after D_4 is likely, in which case Rb/Sr ages probably reflect a minimum D_4 age rather than the D_2 age inferred by other workers (Harris, 1992). If this proposition is correct, the temporal correlation of extensional tectonism with 1100 Ma magmatic activity suggests that extensional tectonics within the northeastern HRTB may be related to the D_4 transtensional shearing event. In this respect, the U/Pb isotopic age of 1090 ± 20 Ma (Botha *et al.*, 1979) determined for the rift-related Koras Group lavas, has important implications for the *regional* significance of extensional tectonics within the Namaqua Province.

The above observations indicate superposition of extensional fabrics and structures upon thrust-related penetrative fabrics, strongly suggesting that the phase of normal, top-to-NE movement seen in the northeastern HRTB shear zones is *younger* than the widespread top-to-SW thrusting event. Furthermore normal, top-to-NE movement is likely to have occurred after regional granulite facies to upper amphibolite facies retrogression.

8.1.3 Regional synopsis

The results of this microstructural kinematic study are summarized in Figure 30. The direction and sense of movement of kinematically distinct shearing events are indicated on the map by means of arrow symbols. Solid arrows indicate early top-to-SW thrust movements, whilst open arrows represent later top-to-NE extensional movements. The arrow heads reflect the direction of hanging-wall translations. Several aspects of the map bear directly on the kinematic development of the HRTB and require further discussion.

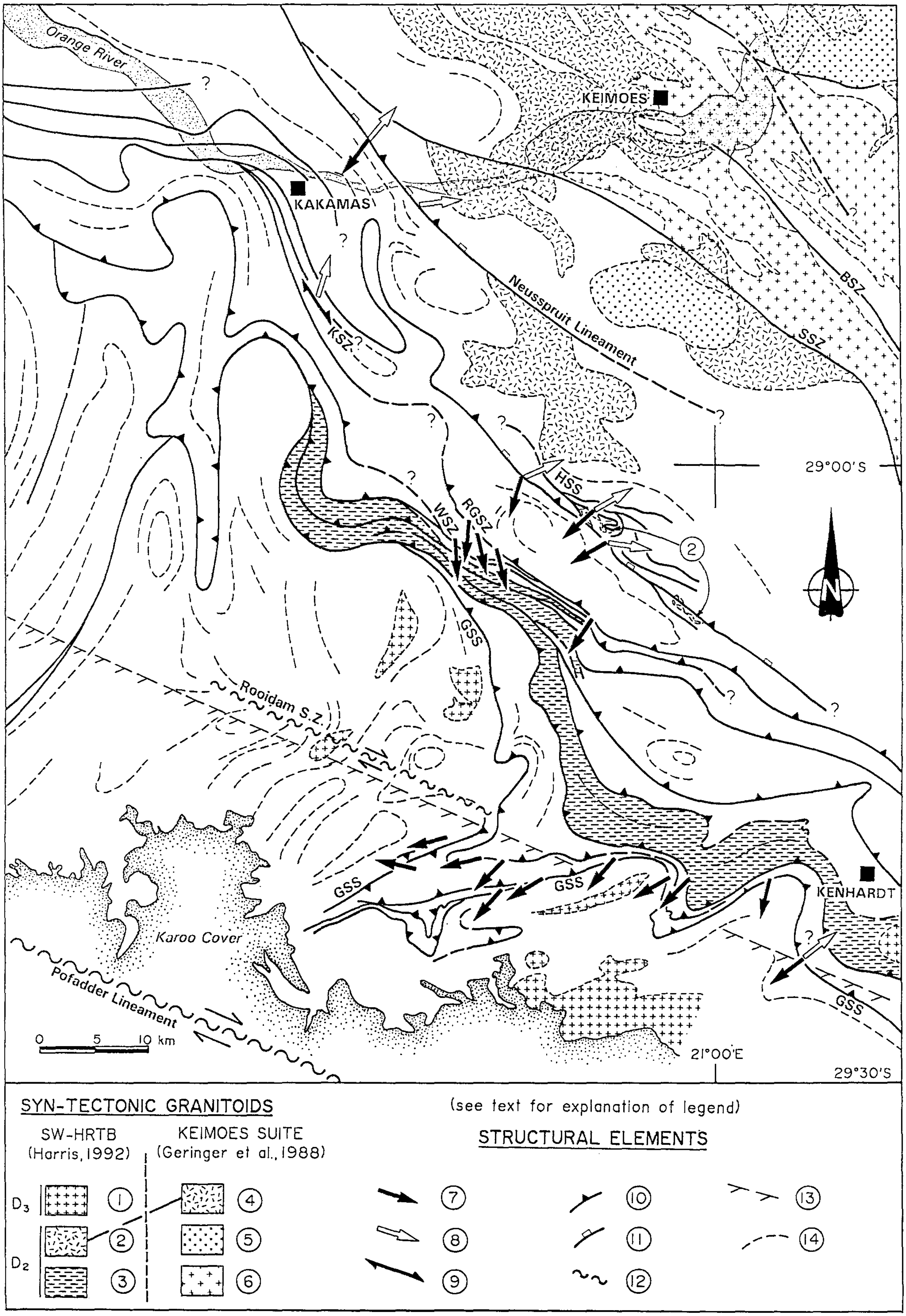
Orange River
KEIMOES
KAKAMAS
KSZ
Neusspruit Lineament
BSZ
SSZ
HSS
WSZ
RGSZ
GSS
29°00'S
Rooidam S.Z.
Karoo Cover
Pofadder Lineament
KENHARDT
0 5 10 km
21°00'E
29°30'S
SYN-TECTONIC GRANITOIDS
SW-HRTB
(Harris, 1992)
KEIMOES SUITE
(Geringer et al., 1988)
D3
D2
(see text for explanation of legend)
STRUCTURAL ELEMENTS

Figure 30. (previous page) Synoptic map of the HRTB showing the relationship between the distribution of syn- and post-tectonic granitoids, and the regional and temporal variation in kinematic vectors of the principal shear zones. Kinematic vectors are indicated by arrow symbols which reflect the direction of hanging-wall translations. For strike-slip movements the sense of shearing is indicated.
Syn-tectonic granitoids: (1) De Bakken, De Banken and Gifberg Granites; (2) Hugosput Potassic Charnockite; (3) Witvlei Migmatite Complex; (4) Friersdale Charnockitic Adamellite; (5) Keboes, Kanoneiland and Neilersdrif Granites; (6) Vaalputs Adamellite.
Structural elements: (7) thrust directions; (8) extensional movement directions; (9) strike-slip movement directions; (10) established thrust zone; (11) established zones of extensional reactivation; (12) D_4 shear zones (positions inferred from aeromagnetic data; after Harris, 1987, 1992); (13) Predicted northeastern limit of extensional modification of $L_{1/2}$ lineations by D_4 shearing on the Pofadder Lineament (corresponding to τ = 0.84; after Harris, 1992); (14) structural form lines.

8.1.3.1 Distribution and extent of extensional, top-to-NE shearing

Extensional (normal, top-to-NE) movements appear to be restricted to shear zones of the northeastern HRTB, while top-to-SW thrusting occurs throughout the belt. This spatial relationship suggests that normal dip-slip reactivation was confined to the northeastern shear zones. Furthermore, the intensity of extensional transposition diminishes towards the southwest. Along the Neusspruit Lineament and the KSZ, early thrust-related fabrics are almost totally obscured by extension-related refoliation and microstructural development. Extensional microstructures and fabrics are prevalent along the HSS, while evidence for normal movements on the RGSZ, WSZ and GSS is either insubstantial, ambiguous, or totally absent (with the possible exception of sample CJS/32, KCI=2, Fig. 24, locality K, GSS; see section 7.1). Consequently the southwestern limit of extensional reactivation appears to coincide with the HSS.

8.1.3.2 Evidence for inversion tectonics

The absence of purely extensional shear zones within the HRTB and widespread reworking of thrust fabrics by extensional fabrics, indicates that extension focussed upon, and was strongly influenced by pre-existing structural anisotropies produced during the early compressional phase. Close fabric control of normal faults by thrusts formed during shortening is common within orogenic zones that have undergone extensional collapse (Dewey, 1988).

8.1.3.3 Spatial and temporal distribution of syn- to post-tectonic granitoids

The spatial and temporal distribution of various syn- to post-tectonic granitoid "suites" within the HRTB is closely related to kinematically-similar domains bounded by shear zones.

1) The Witvlei Leucogranite and Migmatite Complex (Fig. 30; Harris, 1992), occurs between the LGSZ (Pypklip shear zone in the south) and the WSZ, a domain characterized by top-to-SW thrusting during D_2. The sheet-like leucogranite does not bear the regional D_1 fabrics and is only weakly-foliated near its thrust contacts (Harris, 1992; New, 1987), suggesting that it was emplaced during D_2 thrusting. The lack of internal fabric within the leucogranite sheet has been attributed to termination of thrusting prior to full-crystallization (New, 1987). However, the occurrence of narrow "paper" mylonite zones within the leucogranite (New, 1987), and minor thrust offsets of subordinate granite sheets, suggest that top-to-SSW shearing was still active after emplacement of the leucogranite.

2) The spatial distribution of the late- to post-tectonic (1.2-1.0 Ga) Keimoes Suite granitoids (Geringer *et al.*, 1988) is closely associated with shear zones that have been reactivated as normal dip-slip zones (e.g. Neusspruit Lineament, HSS; Fig. 30). Moreover, the southwestern limit of the Keimoes Suite coincides with the demonstrated southwestern limit of extensional reactivation within the HRTB (i.e. along the HSS). This spatial and temporal distribution of the Keimoes Suite granitoids suggests that their emplacement was facilitated by active extension in the northeastern HRTB late in the tectonic development of the belt. Intrusion of the Keimoes Suite granitoids into an extensional environment solves an enormous space problem, if one considers that these granitoids account for >30% of the presently exposed Kakamas Terrane.

8.1.3.4 Regional heterogeneity of thrusting trajectories

Although the general movement directions for the thrust event are broadly analogous, significant departures from the regional NE to SW trend are observed. The heterogeneous pattern of thrust trajectories is largely interpreted as the result of modification of the primary vectors by subsequent deformation episodes, although some anomalies may reflect primary variation in the regional displacement vector field.

1) Thrust vectors progressively rotate towards E-W trends within the southern part of the HRTB. Due to the demonstrated coaxial relationship between L_M lineations and F_3 fold axes (section 7.3.3), refolding of the lineation during D_3 is not a conceivable explanation for this anomaly. Harris (1988) demonstrated clockwise reorientation of F_3 folds (including the Graafwater Synform) by superimposed right-lateral D_4 shear strain in a broad belt alongside the Pofadder Lineament and the Rooidam Shear. Following from the coaxial relationship between F_3 fold axes and L_M lineations, it is implicit that the L_M lineations in the southern HRTB should exhibit a corresponding change in trend. Consequently, clockwise rotation of the thrust-related L_M lineations towards the D_4 shear-displacement vector (113°) adequately explains the apparent change in D_2 translation path observed in the southern HRTB. This hypothesis is supported by the girdle distribution of L_M lineations illustrated in Figure 29b (section 7.1.1), reflecting clockwise rotation of the lineations, from moderate N-plunges to more gentle ESE-plunges as the Pofadder Lineament is approached. This great-circle distribution is consistent with modification of the primary lineation trends by superimposed simple shear during D_4.

   Additionally, a shear strain analysis along the SE-segment of the Pofadder Lineament (Harris, 1990) determined that at distances less than 27km from the the Lineament (corresponding to areas in which τ > 0.84), L_1 lineations (and also L_2, since the two are subparallel; Harris, 1992) were rotated into the extensional field of the shear strain ellipse and underwent syn-shearing extensional modification. This relationship is supported by a fabric transition in the field from S>L to L>S tectonites. The NE-limit of D_4 extensional reworking is indicated in Figure 30, and corresponds closely with an abrupt transition in thrust trajectories. Furthermore subhorizontal L_M lineations and microstructural evidence of fabric reworking are encountered in some mylonite specimens (section 7.3.1 and Fig. 25).

2) Kinematic vectors determined for the northern RGSZ and WSZ indicate oblique, top-to-S or top-to-SE translations (Figs. 20, 21 and 30), in contrast to the typically orthogonal, top-to-SW thrusting characteristic of the HRTB. Two possible explanations are proposed in section 6.5. Another more speculative explanation may be contemplated when these oblique trajectories are considered in a regional framework. Although correlation of the KSZ with shear zones in the southern HRTB is uncertain, LANDSAT-TM satellite imagery suggests that it merges with either the HSS or RGSZ. Sub-horizontal L_{ss} lineations and microstructural criteria within tectonites from the Omkyk locality (section 4.2.2 and Fig. 12a), indicate a component of right-lateral strike-slip movement was active along the KSZ (section 4.3). If one assumes that this transcurrent translation represents a strike-slip component of oblique S-directed thrusting *during* D_2, a scenario may be envisaged in which relative oblique motion is partitioned into zones of thrusting and associated strike-slip shearing within the hanging-wall of the RGSZ. Similar movement partitioning has been widely described within zones of oblique convergence (e.g. Ridley, 1982, 1986; Mattauer, 1986; Lacassin, 1989; Pinet and Cobbold, 1992). Further to the south and deeper in the structural pile, oblique movement of the RGSZ hanging-wall may not have been resolved into pure thrust and pure strike-slip components, but instead resulted in oblique S-directed thrusting on the NW-striking segments of the RGSZ and WSZ. Analogous structural associations have been described by Brun and Berg (1982), Ellis (1986), and Ellis and Watkinson (1987). The above hypothesis is purely conjectural in that it assumes that the KSZ does not represent a D_4 right-lateral, strike-slip shear zone, and no attempt is made to account for external boundary conditions.

8.1.3.5 Relative orientation / evolution of L_M and S_M fabrics

The relative orientation of linear and planar mylonite fabric elements within HRTB shear zones is summarized in the triangular diagram of Figure 31. The gross pattern of consistently steep L_M rake-angles (>45°), and a corresponding increase of plunge of L_M with dip of S_M, is typical of frontal or oblique thrust ramps within orogenic belts characterized by orthogonal convergence. The pattern is also to a degree representative of extensional Cordilleran metamorphic core complexes, apart from the common occurrence of steeply-dipping planar fabrics.

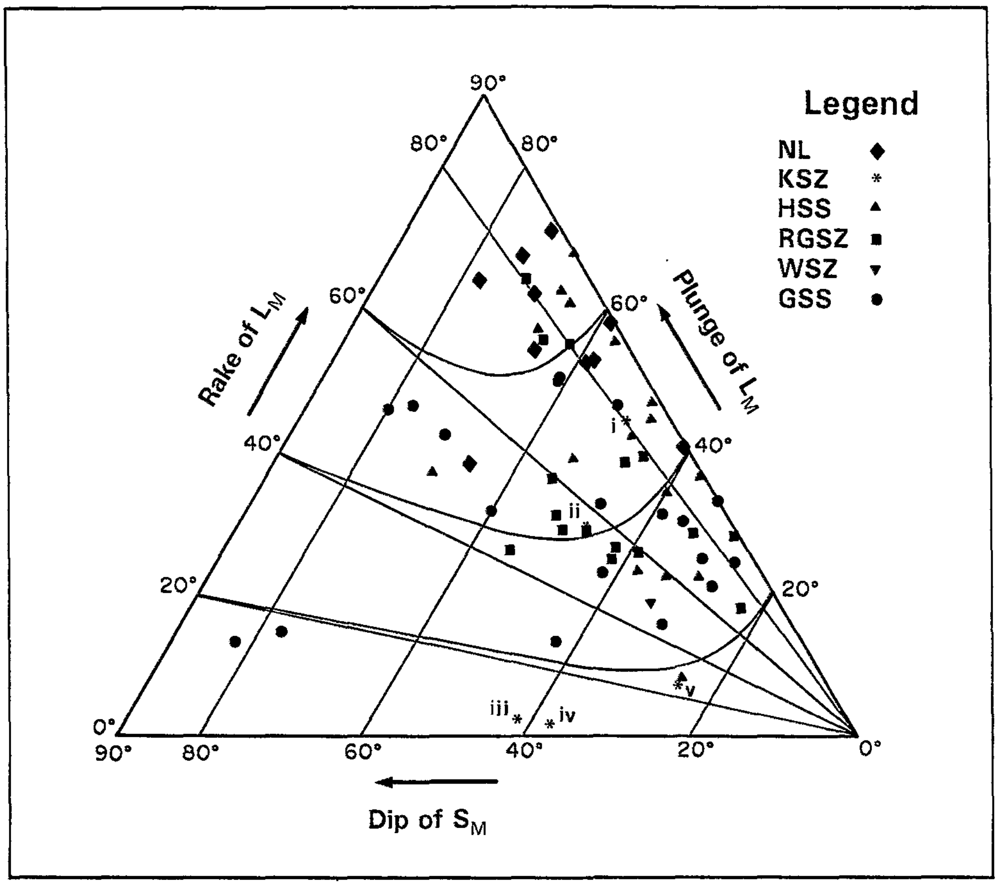

Figure 31. Triangular diagram (after Abalos, 1992) illustrating the relative orientation / evolution of the dip of S_M and the plunge/rake of L_M, within the principal shear zones of the HRTB. All mylonite fabric orientation data for this study are indicated, regardless of their kinematic or temporal distinctions. See section 8.1.3.5 for explanation.

Subhorizontal lineations and steep planar fabrics are characteristic of strike-slip zones, and occur infrequently within the HRTB. Fabric associations within transcurrent environments are expected to plot along the horizontal axis of the triangular plot, and particularly within the lower-left apex.

Consequently, only limited data from the GSS and KSZ are representative of strike-slip situations. Those from the GSS occur in the nose of the Graafwater synform, within the zone of extensional reworking adjacent to the Pofadder Lineament (Fig. 30) and are therefore explained as products of superimposed F_3 coaxial crossfolding and D_4 extension. During F_3 crossfolding of the thrust zone (GSS) the rake of L_M decreases due to a change in the strike of S_M resulting from rotation of S_M about the synformal Graafwater F_3 fold axis, while the trend and plunge of L_M remain constant due to the coaxiality of L_M and F_3 (Fig. 32). During D_4, L_M and S_M are rotated into the extensional field of the D_4 strain ellipse (at τ values > 0.83; Harris, 1992) and undergo pronounced strike-parallel stretching, further reducing the rake of L_M.

Only limited fabric data from the KSZ exhibit geometries (low rake\plunge of L_M, moderate dip of S_M) consistent with derivation by pure strike-parallel translation (Fig. 31). Although fabric orientation data from the KSZ are few, a progressive decrease in the rake of L_M (approximately 80° to 4°) at relatively constant S_M dip-angles (approximately 40° to 50°), suggests that relative "thrust-to-wrench" shear strain gradients may have existed through the structural section. The occurrence of increasingly strike-parallel lineations with depth in the structural section *(see addendum overleaf)*, might reflect progressive rotation of thrust-related, down-dip lineations towards the strike-slip vector in response to an intensifying "wrench" shear strain component. Consequently, the L_M-S_M pattern of Figure 31 potentially endorses the hypothesis of section 8.1.3.4, (2).

The considerable range in rake-angles of L_M illustrated in Figure 31 is attributed to F_3 refolding of the D_2 thrust zones (Fig. 32). The wide range in dip-angles of S_M in Figure 31 (approximately 20° to 80°) is ascribed to reorientation of the mylonite foliation plane on the limbs of F_3 folds (Fig. 32), and to progressive steepening of older, structurally-higher thrusts as break-forward thrusting proceeds in the foreland. This geometry may even reflect the primary morphology of the orogenic belt. Harris (1992) notes an increase in the average dip of the southern HRTB mylonite zones from the southwest to northeast, which he relates to the primary geometry of the thrust belt, in which thrusts root steeply into the hinterland and flatten-out progressively upwards and into the foreland.

ADDENDUM

with reference to paragraph 2 of page 164
and Fig. 31 of page 163

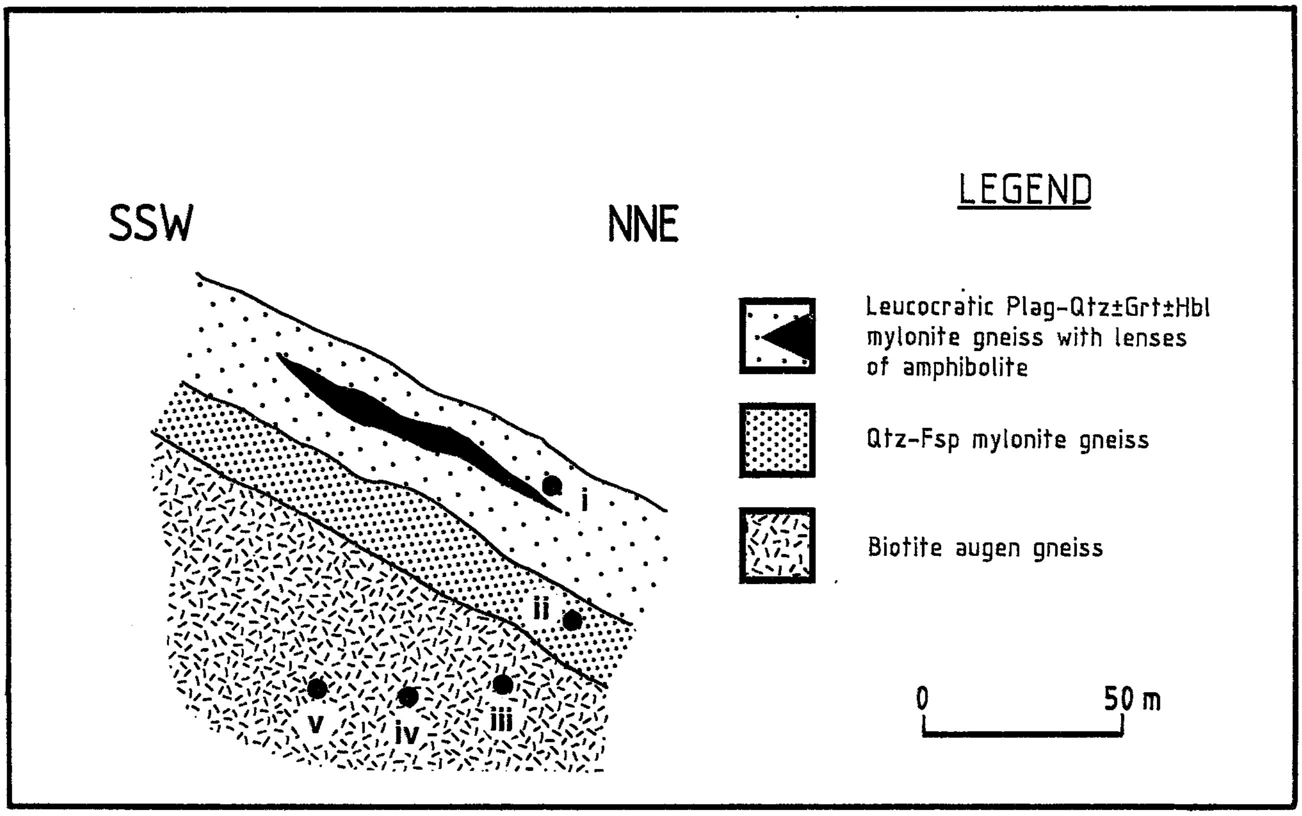

The diagram above represents a schematic cross-section through the KSZ at the Omkyk locality, showing the relative measurement positions within the structural sequence of mylonite fabric orientation data presented in Figure 31. Roman numerals i to v refer to labels adjacent to KSZ * symbols in Figure 31 and reflect increasing depth within the structural section. Examination of Figure 31 reveals that the KSZ L_M lineations become progressively strike-parallel with structural depth in accordance with the statement of paragraph 2, page 164.

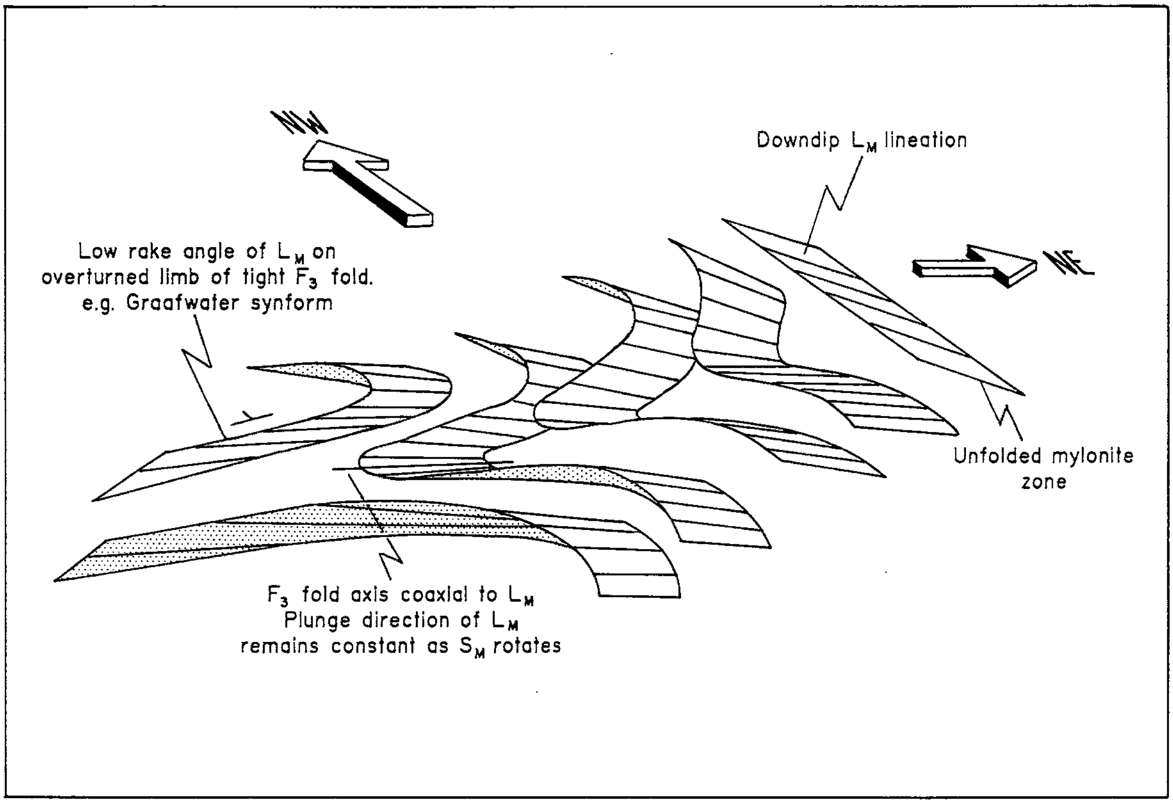

Figure 32. Schematic diagram illustrating the effects of coaxial F_3 cross-folding of an initially NW-striking, dip-lineated mylonite zone (after Fig. 36, p85 of Harris, 1992). A reduction in the rake angle of L_M in the S_M plane occurs through rotation of S_M about the F_3 fold axis. The orientation of L_M remains virtually unchanged due to the coaxial relationship between L_M lineations and F_3 fold axes.

Figure 33 illustrates the geometrical relationship between kinematically distinct L_M lineations within the HRTB. Reverse, top-to-SW lineations (Fig. 33a) show considerable scatter as a result of primary variations in, and secondary modification of, D_2 stretching trajectories. It is significant that the best-fit great-circle to thrust-related L_M lineations (025/49) coincides with the vector mean S_M plane (029/59), indicating dispersion of the lineations within the mylonite thrust plane (Fig. 33a). As discussed previously (sections 8.1.3.4), this great-circle dispersion pattern may be attributed to reworking of the D_2 mylonite zones during D_4. Although less well constrained by the data, normal, top-to-NE lineations (Fig. 33b) exhibit a similar great-circle dispersion (078/54) which lies relatively close to the vector mean S_M plane (048/58). This dispersion of normal lineations within the mylonite plane is significant since it implies a corresponding modification of these fabrics during D_4, indicating that extensional movements *preceded or accompanied* D_4 strike-slip shearing in the northeastern HRTB. Limited strike-slip lineations along the KSZ have a vector mean of 149/09 which differs significantly from the subhorizontal 113° strike-slip vector calculated for the Pofadder Lineament (Harris, 1990, 1992), suggesting that these kinematic vectors are not coeval.

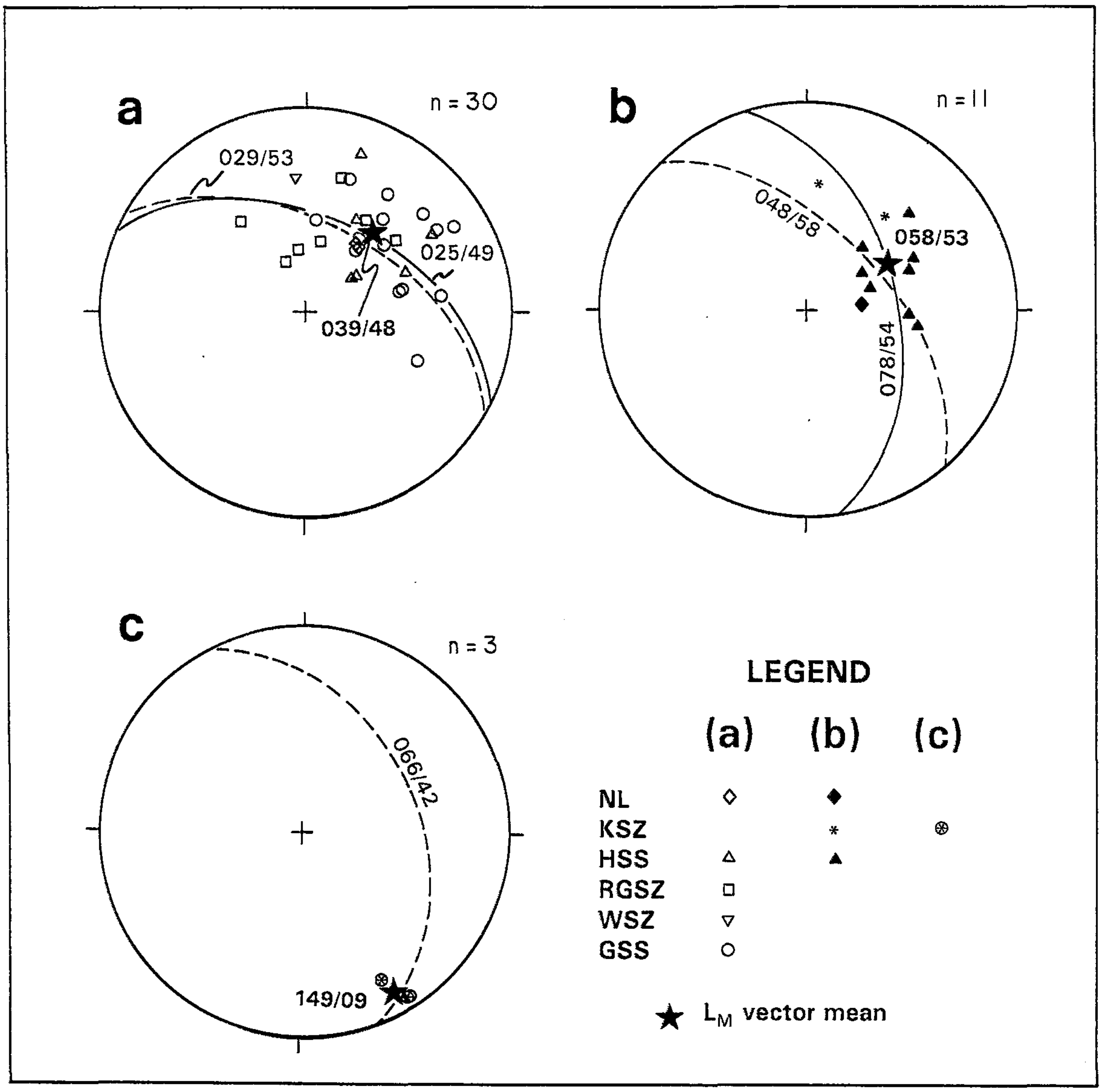

Figure 33. Equal area, lower-hemisphere stereoplots of (a) reverse, (b) normal, and (c) strike-slip mylonite elongation lineations within the principal shear zones of the HRTB. Only kinematically similar L_M data are included in each the stereoplots. The L_M vector mean of each population is indicated by a star symbol. Best-fit great-circles are superimposed where girdle distributions are evident. See text for explanation.

8.1.4 Thermotectonic contraints on the evolution of the HRTB

Syn-kinematic mineral assemblages, textural relationships and rheological contrasts between individual mineral species in tectonites of the HRTB, allow estimation of the strain-regime and P-T conditions operative at the time of penetrative fabric development within the HRTB shear zones. The degree of annealing / recovery exhibited by the mylonites gives insight into the timing of shearing relative to the thermal peak of the area. A polymetamorphic history is prescribed for metapelitic gneisses in the northeastern HRTB (Humphreys, 1991, 1992 *in prep.*). Correlation of these texturally distinct metamorphic events with shearing events determined for the HSS, gives additional insight into the structural and metamorphic evolution of this portion of the HRTB.

8.1.4.1 Syn-kinematic parageneses

Precise determination of the P-T conditions during each of the shearing events in the HRTB is made difficult by the predominance in the sample set of quartzo-feldspathic tectonites, having relatively simple mineral assemblages stable over a wide range of metamorphic conditions. Furthermore, without metamorphic data from the protolith wall rocks, accurate evaluation of retrogression fabrics is impossible. This point is particularly valid since shear zones act as important fluid channelways and therefore commonly host retrograde assemblages which are not necessarily representative of syn-shearing metamorphic conditions.

Within quartzo-feldspathic tectonites of the HRTB, syn-shearing fabrics and microstructures are commonly defined by secondary minerals including green biotite, chlorite, sericite, white-mica, epidote-group minerals and opaque oxides. Textural relationships indicate that these minerals formed at the expense of K-feldspar, plagioclase and biotite. Within calc-silicate tectonites, plagioclase typically breaks-down to epidote-group minerals ± chlorite, while in amphibolitic tectonites alteration of hornblende to chlorite is common.

Disequilibrium textures and the preservation of undistorted *soft assemblage* pseudomorphs (Barker, 1990) in ultramylonites, suggest that *low-temperature retrogression was post-kinematic and mimetic in nature:*

- Biotite mica-fish within quartzo-feldspathic mylonites from the RGSZ and GSS are commonly partially pseudomorphed by chlorite, indicating that biotite was stable at the time of thrusting and that low-grade alteration occurred at a later stage (e.g. Fig. 28k).

- Within calc-silicate ultramylonites from the GSS, plagioclase porphyroclast systems are frequently completely pseudomorphed by intergrowths of fine-grained epidote and chlorite (sample CJS/40). The preservation of a rigid porphyroclast shape by undeformed, yet mechanically incompetent aggregates indicates that saussuritization of the plagioclase clast occurred post-thrusting.

- Within normal shear sense phyllonitic mylonites from the HSS, oblique mica (001) fabrics are often defined by fine-grained biotites (Fig. 17 c and d), which show evidence of alteration to chlorite and opaque oxides along cleavage planes. This indicates that the oblique DPO of biotite, related to normal shearing, developed prior to retrograde alteration. The degree of pseudomorphing of biotite by chlorite varies considerably within microlithons across the domain of a thin-section. This probably reflects variable fluid infiltration and illustrates the important role of fluids in promoting reactions. It is interesting that complete pseudomorphing of biotite by chlorite is more common in HSS tectonites that exhibit a relatively high degree of annealing (e.g. Fig. 17 a and b), suggesting that static recrystallization was enhanced by the availibility of fluids.

- Pressure shadow "beards" of *coarse-grained, unstrained* chlorite ($\pm$ epidote) occur about highly-altered feldspar augen within normal shear sense tectonites from the Sonopeiland locality on the Neusspruit Lineament (Fig. 10a). This textural relationship is consistent with post-kinematic growth of secondary chlorite, indicating that retrogression is likely to have occurred after normal sense shearing.

- Localized disequilibrium textures within a metapelitic protomylonite (Fig. 17 g and h); section 5.4.1) from the HSS and a strike-lineated augen gneiss from the KSZ (Fig. 13 a and b; section 4.3.1), suggest that the development of penetrative thrust (top-to-SW) and strike-slip (right-lateral, SE-directed) fabrics occurred during high-temperature retrogression from granulite facies to upper amphibolite facies.

8.1.4.2 Rheological constraints

Fabrics and microstructures developed during both early thrusting and later normal-shearing events are typical of tectonites produced by high-temperature ductile deformation at mid-crustal levels (i.e. below the ductile-brittle transition). Textural observations indicate the predominance of thermally activated deformation mechanisms including recrystallization-accommodated dislocation creep in feldspar aggregates, formation of internal plastic deformation fabrics in feldspar, and superplasticity of quartz. Development of strain-induced myrmekite is widespread. All these features are consistent with deformation at middle to upper amphibolite facies and indicate temperatures in excess of about 500°C (Nicolas and Poirier, 1976; Voll, 1976; White, 1976, 1977; Schmid *et al.*, 1977; Mitra, 1978; Etheridge and Wilkie, 1979; Simpson, 1985; Tullis and Yund, 1985, 1987; Simpson and Wintsch, 1989).

8.1.4.3 Degree of annealing

Textures indicative of static recrystallization are more widespread within tectonites from the northeastern HRTB, than within those from the southern part of the belt. RGSZ, WSZ and GSS tectonites are characteristically fine-grained mylonites in which grain-size reduction occurred through dynamic recrystallization. Annealing textures are only locally encountered. In contrast the tectonites of the KSZ and Neusspruit Lineament are generally coarser grained, exhibiting equigranular polygonal or subpolygonal granoblastic textures indicative of extensive post-kinematic static recrystallization. Recovery within HSS tectonites is generally well-advanced, although their annealing states are highly variable.

The above data suggest that:-

1) D_2 thrusting in the southern HRTB occurred after the metamorphic thermal peak and was accompanied, or followed by uplift and cooling.

2) Within the northeastern HRTB, high-temperatures persisted through the later extensional shearing event.

The first hypothesis is in conflict with the conclusions of Harris (1990, 1992), who established that reorientation of structures adjacent to the Pofadder Lineament during D_4 must have occurred at elevated temperatures (>600°C). Direct evidence for high-temperatures during D_4 shearing include the stability of sillimanite defining the lineation in L>S tectonites adjacent to the Pofadder Lineament, and the local obliteration of the L>S fabric by granitic melt segregations (Harris, 1992). Indirect evidence is provided by the extremely wide zone of ductile stretching fabrics (approximately 50km) developed adjacent to the Lineament (Harris, *op. cit.*).

The strength of the above evidence demands an alternative explanation for the observed textural variation in HRTB tectonites. It is distinctly possible that the variable degree of annealing exhibited by HRTB tectonites is related to the spatial distribution of late- to post-tectonic granitoid bodies. Static recrystallization textures are widespread in tectonites from mylonite zones in close proximity to bodies of late granite and charnockite (Fig. 30), suggesting that the heat flux from these granitoids provided the thermal energy required for textural equilibration. Thus, tectonites from the northeastern mylonite zones generally exhibit a high degree of static recrystallization, on account of their close spatial association with the Keimoes Suite granitoids. This hypothesis is substantiated by textural transitions of hornfelsic (Grt-Crd-Sil) "kinzigites" into high-temperature mylonite zones at certain localities in the Kakamas Terrane (Waters, 1990).

Following from the above proposition, one might argue that annealed microtextures should be encountered within tectonites along those segments of the RGSZ, WSZ and GSS mylonite zones that are spatially associated with the syn-D_2 Witvlei leucogranite (migmatite) complex. However, evidence for significant static recrystallization is notably absent in these samples. This disparity is interpreted as the consequence of continued thrusting on these mylonite zones after emplacement and cooling of the sheeted leucogranite complex. Evidence in support of this interpretation include the occurrence of solid-state (D_2) deformation fabrics, both within the foliated margins of the larger granite sheets and within discrete "paper" mylonite zones (New, 1987), and common thrust offsets of subordinate granite sheets. It is proposed that the *lit-par-lit* style of intrusion of the leucogranite sheets (New, 1987; Harris, 1992), and the presence of large xenolithic screens of country rock (Harris, 1992), promoted relatively rapid cooling of the leucogranite complex, thus preventing annealing of mylonite textures developed during continuing thrusting.

8.1.4.4 Strain regime

Asymmetrical microstructures occur within reverse and normal shear sense mylonites of the HRTB which are interpreted as indicating dominant non-coaxial deformation during both thrusting and extensional shearing events. Mylonitic textures and microstructures including S-C fabrics, secondary shear bands, asymmetric porphyroclast systems, rolling-structures, mica-fish, asymmetrical pressure shadows, oblique grain and subgrain shape-fabrics, asymmetrical microfolds, and displacement and rotation of fractured rigid grains are all typical products of non-coaxial deformation regimes involving bulk, heterogeneous simple shear (e.g. Simpson, 1986).

The common occurrence of δ and Θ porphyroclast systems (rolling structures) within mylonites of the HSS and GSS may indicate that shear strain rates ($\dot{\gamma}$) were relatively high relative to recovery / recrystallization rates ($\dot{R}$) within these mylonite zones (Passchier and Simpson, 1986; Hooper and Hatcher, 1988; Hatcher and Hooper, 1992).

Within the mylonite zones of the southwestern HRTB (RGSZ, WSZ and GSS), thrust-related, mylonite microfabric elements are progressively better developed from NE to SW. This may reflect an *apparent* increase in ductile finite strain down the structural section which is expressed by a decrease in the angle between S and C surfaces (RGSZ: S^C = 32.68 ± 7.26°, n = 93; GSS: S^C = 27.25° ± 7.19°, n = 107), increased abundance of δ-type porphyroclast systems, increased superplasticity of quartz and intracrystalline plasticity in feldspars, and higher incidence of strain-induced myrmekite. It must be acknowledged that systematic variations of numerous other parameters including protolith mineralogy, temperature, prior deformation history, fluid pressure, confining pressure and deviatoric stress (Hatcher and Hooper, 1992) could conceivably explain these trends.

8.1.4.5 Implications of a metamorphic study in the northeastern HRTB

Although detailed metamorphic studies have not been undertaken in the southern HRTB, a recent investigation in the northeastern HRTB (northeast of the HSS) by Humphreys (1991, 1992 *in prep.*) indicate a polymetamorphic history for metapelitic gneisses in that area. Although the temporal correlation of metamorphic fabrics with specific deformation events is somewhat ambiguous, the sequence of metamorphic events proposed by Humphreys (1992 *in prep.*) gives insight into the tectonothermal evolution the northeastern HRTB. Furthermore, textural relationships within metapelitic tectonites from the HSS (this study) are analogous with disequilibrium textures described by Humphreys (*op. cit.*).

Humphreys (1992 *in prep.*) proposes an upper amphibolite facies, M_1 event at 750°C and 8kb, followed by decompression to 750-800°C and 5-6kb during a M_2 granulite facies event related to uplift during D_2 thrusting within the HRTB. Hydrous retrogression occurred during M_{4a}, in which biotite and sillimanite replaced cordierite and K-feldspar. M_{4a} rehydration was immediately followed by a reheating event (M_{4b}) and a second generation of garnet growth, implying an increase in pressure. Phase relationships (And → St) indicate lower temperatures and higher pressures during M_4 than during M_2. Humphreys (*op. cit.*) relates the higher pressures of M_{4b} to a period of post-orogenic extension accompanied by high-level granitoid emplacement, tentatively correlated with the D_4 deformation phase.

Disequilibrium textures within a metapelitic protomylonite from the HSS (section 5.3.3; Fig. 17 g and h), indicate that the break down of cordierite and K-feldspar to form sillimanite and biotite (± Mt ± Qtz) reflects hydrous-retrogression during D_2 thrusting. These textural relationships are identical to those described by Humphreys (1992 *in prep.*) as representative of the M_{4a} event, suggesting that this metamorphic event should be correlated with D_2, rather than D_4. Furthermore, hydrous retrogression would have been a natural consequence of the thrusting of high-grade rocks over lower-grade rocks along the HSS. Barker (1990) notes that emplacement of a hot slab over cooler rocks leads to convective circulation of fluids in the footwall block, promoting reactions within the thrust zone and bringing about retrogression at the base of the hangingwall block. Overthrusting would also result in reheating and recompression of the footwall block, possibly accounting for second generation garnet growth and the replacement of andalusite by sillimanite during M_{4b} (Humphreys, *op. cit.*). The apparent contradiction of attributing both early decompression (M_2) and subsequent recompression (M_4) to D_2 thrusting, may be resolved by a invoking a history of foreland-propogating, *in-sequence* (*sensu* McClay, 1992) thrusting, interrupted at a late stage by isolated *break-back, out-of-sequence thrusting* (*sensu* Morley, 1988; McClay, 1992; Nadeau and Hanmer, 1992) hindward of the HSS. Break-back thrusting may have reactivated an older "in-sequence" thrust, or cut-through the existing thrust stack (Morley, 1988).

Whilst favouring the above interpretation I do not discount the possibility that the M*4b* event (Humphreys, 1992 *in prep.*) reflects post-orogenic (D_4) extension coinciding with high-level granitoid intrusion. The results of this study clearly suggest that emplacement of the Keimoes Suite granitoids was facilitated by late extensional shearing in the northeastern HRTB (see (2) of section 8.1.3.3).

8.1.4.6 The significance of cataclastic rocks in the HRTB

The occurrence of cataclastic rocks and microstructures along the KSZ, RGSZ and GSS is evidence of the protracted history of movements along these shear zones. The consistent overprinting of cataclastic microstructures upon ductile, high-temperature mylonitic fabrics, frequently in association with pervasive low-grade (greenschist facies) alteration, is attributed to late brittle reactivation of these mylonite zones during uplift and exhumation of the HRTB. Although it cannot be proved conclusively, it is suggested that brecciation and cataclasis accompanied wrench-faulting late in the D_4 event, as the HRTB was uplifted through the *ductile-brittle transition zone* (Rutter, 1986). The superimposition of zones of brecciation, cataclasis and secondary alteration along older mylonite zones indicates that brittle deformation localized along pre-existing structural anisotropies. This strong strain partitioning probably reflects a ductility decrease during D_4, such that continuing strike-slip translations were compelled to exploit older structural discontinuities. No useful microstructural sense of shear criteria were encountered within specimens of cataclasite from the HRTB.

8.2 Conclusion

8.2.1 Model for the evolution of shear zones within the HRTB

Microstructural kinematic analysis of mylonitic rocks from the HRTB has indicated that two kinematically and temporally distinct ductile shearing events have affected the shear zones of this area. Despite the distinctiveness of these shearing events, they are best explained within a single integrated kinematic model. The model considers each shearing event as the kinematic response to changing tectonic boundary forces and internal gravitational forces within a evolving orogen. Although the kinematics of ductile deformation on the microscale form the foundation of the model, integration of these data with aspects of the regional geology is nonetheless essential. In particular the model explains the superimposition of extensional fabrics upon compressional fabrics, and the spatial association of extensional shearing fabrics with late- to post-tectonic bimodal magmatism in the Kakamas Terrane.

The inferred fan-like sectional profile of the Kakamas Terrane with double-vergent thrust structures "rooting" out of a steep, central, high-grade metamorphic and magmatic core (e.g. Stowe, 1983, 1986, 1988), is geometrically fundamental to the model and is illustrated schematically in the cross-sections of Figure 34. The HRTB represents a southwest vergent fold and thrust belt, separating the Kakamas Terrane and the Garies Terrane. Mylonite zones within the HRTB are relatively shallow dipping in the SW (foreland) and steepen-up towards the NE (hinterland). This geometry is typical of deep-level crystalline thrust systems found in the internal parts of mountain chains (e.g. Coward, 1983; Coward *et al.*, 1982, 1986; Hatcher and Williams, 1986; Mattauer, 1986). The mylonite zones are folded over the Graafwater Dome in the southwestern HRTB (Fig. 34a), indicating that the zones must have flattened out towards the southwest, where they "roofed" much the presently exposed northeastern margin of the Garies Terrane (Harris, 1992). Within the southern HRTB, no obvious metamorphic gradient is observed through the the thrust pile and upper amphibolite facies metamorphism is recorded by all the rocks in the study area south of the HSS. Across the HSS an abrupt inversion in metamorphic grade takes place, with upper amphibolite facies rocks occurring in the footwall and granulite facies rocks in the hangingwall (Humphreys, 1991, 1992 *in prep.*; Harris, 1992).

The model regards the northeastern Namaqua Tectonic Province as a collisional orogen that has gone through a later episode of extensional collapse. The kinematic significance of mylonite zones within the HRTB is explained in terms of a typical orogenic cycle, involving crustal thickening by thrusting during a compressional orogenic phase (Fig. 34a), followed by collapse of the thickened crust during an extensional *taphrogenic* phase (Fig. 34b). Extensional collapse of orogenically thickened crust is a feature of many orogens and has been extensively documented in recent years (e.g. Okulitch, 1984; Burchfiel and Royden, 1985; Malavieille, 1987; Dewey, 1988; Selverstone, 1988; Burg *et al.*, 1990; Echtler and Malavieille, 1990; Malavieille *et al.*, 1990; Jones *et al.*, 1992).

During the compressional orogenic phase (correlated with D_1 and D_2), NE-SW directed shortening resulted in SW-vergent folds and S/SW-directed thrusting within the HRTB. Penetrative, high-temperature mylonite fabrics developed along the thrust zones of the HRTB. Thrusting resulted in significant crustal thickening within the hinterland. In the northeastern HRTB, the effect of thrusting was to raise granulite facies rocks to their present structural level, where ambient upper amphibolite facies prevailed at that time. This is reflected by superposition of thrust-related, amphibolite facies protomylonitic textures over granulite facies assemblages within metapelitic gneisses along the HSS. Active foreland-vergent deformation concentrated on the youngest thrusts such that the older, higher thrusts were progressively steepened.

Figure 34. (overleaf) Schematic model explaining the movement histories of shear zones within the HRTB in terms of a typical orogenic cycle, involving crustal thickening by thrusting during a compressional orogenic phase (a), followed by collapse of the thickened crust during an extensional taphrogenic phase (b). F_T = tectonic boundary forces, F_G = internal gravitational forces. See text for further explanation.

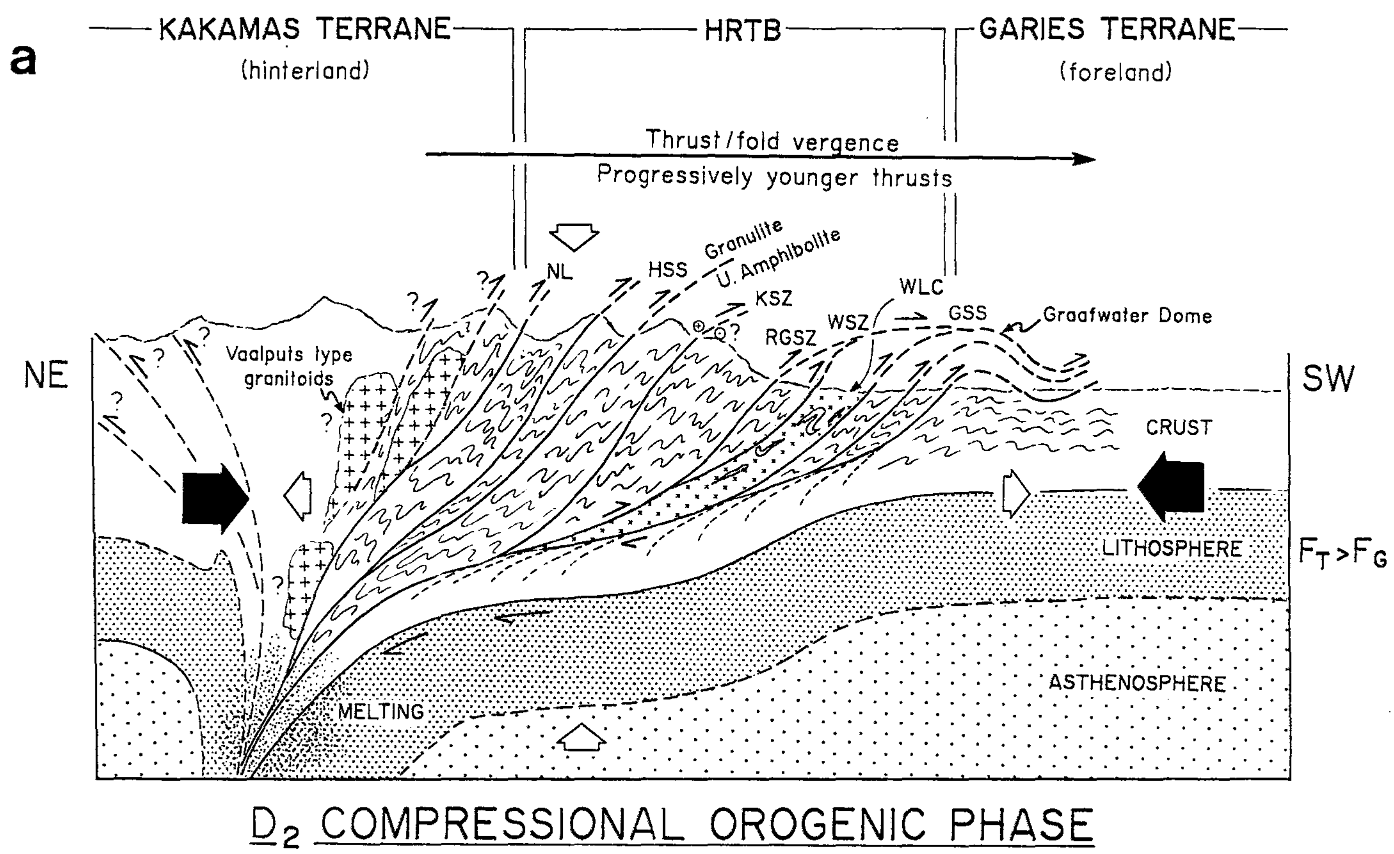
a
KAKAMAS TERRANE
(hinterland)
HRTB
GARIES TERRANE
(foreland)
Thrust/fold vergence
Progressively younger thrusts
NL
HSS
Granulite
U. Amphibolite
KSZ
RGSZ
WSZ
WLC
GSS
Graafwater Dome
Vaalputs type granitoids
NE
SW
CRUST
LITHOSPHERE
ASTHENOSPHERE
MELTING
F_T > F_G
D2 COMPRESSIONAL OROGENIC PHASE

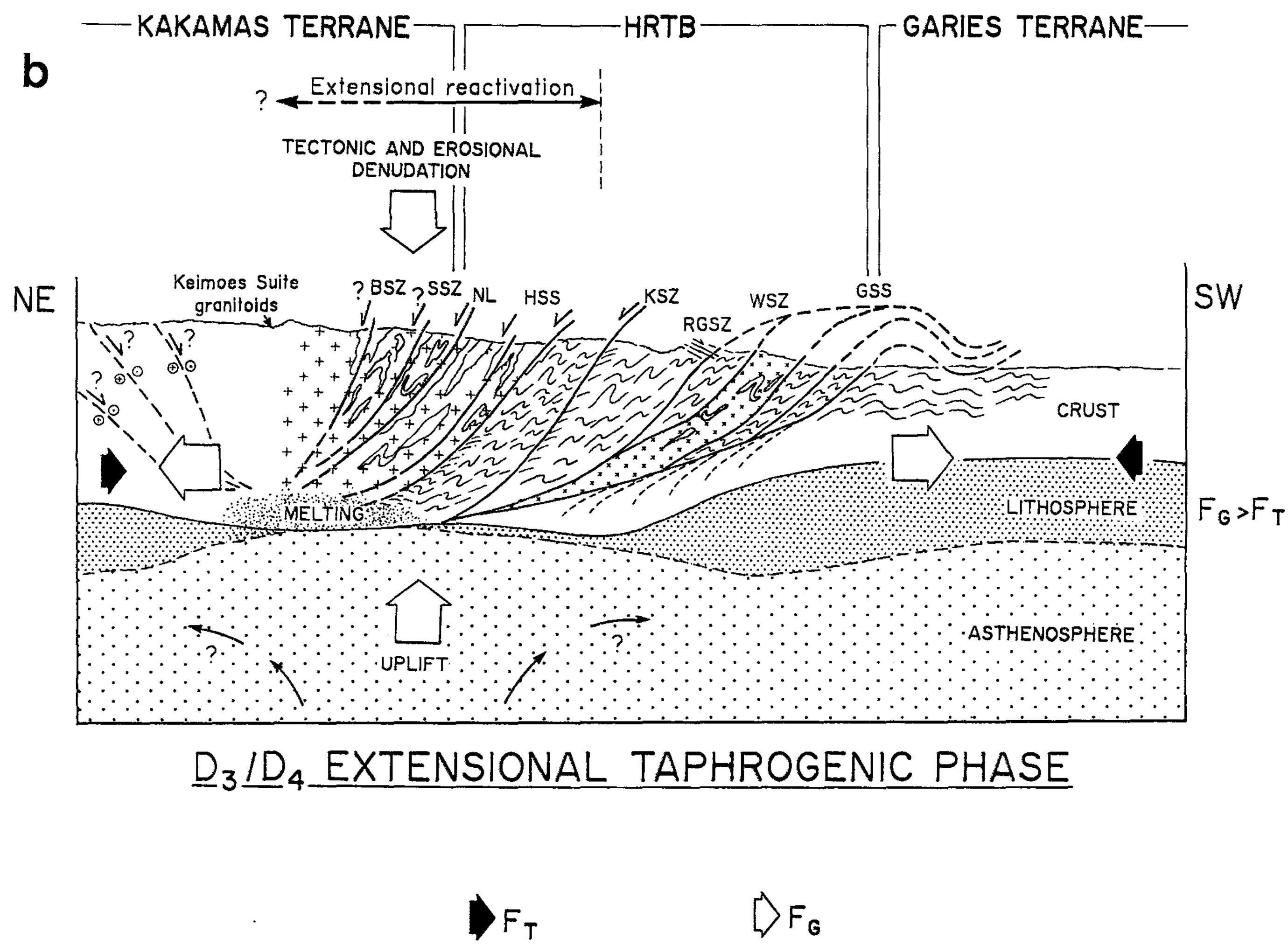
b
KAKAMAS TERRANE
HRTB
GARIES TERRANE
Extensional reactivation
TECTONIC AND EROSIONAL DENUDATION
Keimoes Suite granitoids
BSZ
SSZ
NL
HSS
KSZ
RGSZ
WSZ
GSS
NE
SW
CRUST
LITHOSPHERE
MELTING
ASTHENOSPHERE
UPLIFT
F_G > F_T
D3/D4 EXTENSIONAL TAPHROGENIC PHASE
F_T
F_G

Melting within the thickened lithospheric root generated synorogenic, anatectic melts, which intruded into active thrust planes and were emplaced at mid-crustal levels in a manner analogous to that described by Hollister and Crawford (1986). The syntectonic "Vaalputs type" granitoids and the syn-D_2 Witvlei Leucogranite Complex (WLC of Fig. 34a) are possible examples of these *surge-type* granitic melts. Analogous sheet granite and migmatite complexes have been described from the Himalayas (e.g. the Manaslu leucogranites; Le Fort, 1981) and the Lachlan Fold Belt of Australia (e.g. the Yarra granite; Tobisch and Paterson, 1990). Crustal thickening during the compressional phase occurred both by thrusting and by a magmatic influx at mid-crustal levels.

At some time during the waning stages of D_2 compressional deformation, the overthickened lower-continental lithospheric root in the Kakamas Terrane became gravitationally unstable and was catastrophically removed by convection (following models proposed by England, 1987 and Houseman *et al.*, 1981). Destruction of the lithospheric root resulted in rapid uplift and an abrupt increase in the geothermal gradient, which in turn promoted extensional collapse of the orogen, with related post-orogenic bimodal magmatism. Extensional collapse was restricted to the Kakamas Terrane and northeastern part of the HRTB (Fig 34b), where the greatest crustal thickening occurred. Extensional shearing localized along thrust zones produced in the earlier compressional phase, resulting in the superimposition of top-to-NE, normal shearing fabrics upon top-to-SSW, thrust fabrics, within mylonites of the Neusspruit Lineament, KSZ and HSS.

Extreme attenuation of the lithosphere during the extensional phase resulted in melting of the lower continental crust (Fig. 34b) and generation of significant volumes of late-orogenic bimodal magmas. Emplacement of these magmas at higher levels was facilitated by active extension along shear zones in the Kakamas Terrane and northeastern HRTB. Analogous examples of granitoid intrusion along active extensional shear zones have been documented by Hutton *et al.* (1990) and Malavieille *et al.* (1990). The close association between emplacement of the Keimoes Suite and extensional tectonism is demonstrated in the study area by the development of extensional shearing fabrics within the margins of the Hugosput Potassic Charnockite. Furthermore the observed southwestern limit of the Keimoes Suite coincides with the demonstrated limit of extensional reactivation within the HRTB (Fig. 34b).

The absence of equivocal evidence for extensional movements on shear zones in the southwestern HRTB (RGSZ, WSZ and GSS) suggests that this portion of the HRTB acted as a coherent block during normal-sense shearing in the NE-sector. Localized foreland-dipping, brittle to semi-brittle microfaults overprinting ductile thrust fabrics along the RGSZ (Fig. 34b), may represent microstructural evidence for late gravity slides related to continuing collapse of the orogenic topographic front.

It is suggested that the F_3 folds of the HRTB may refect the crustal response to *orogen-parallel* extension during the taphrogenic phase, in which lateral (NW-SE) gravitational escape was confined by external boundaries, resulting in NW-SE shortening and folding on NE-SW axes. Harris (1992) notes that the intensity of the F_3 fold phase decreases towards the northeast and becomes virtually imperceptible across the Witvlei sheet-granite / migmatite unit, suggesting that this unit may have acted as a zone of decoupling. An alternative hypothesis is that the NE-limit of F_3 folding coincides with an abrupt increase in crustal thickness, related to thrusting and magmatism during the compressional phase. The high mechanical strength of orogenically and magmatically thickened crust in the northeastern HRTB may have prevented the development of F_3 folds in this area.

8.2.2 Synopsis

The primary objective of this study has been fulfilled in that kinematically sensible movement histories have been determined for some of the principal mylonite zones of the HRTB. The precise orientation of kinematic vectors, and the sense and relative ages of movements on each of the shear zones have been convincingly established.

This investigation has authenticated macroscopic evidence for thrusting along the D_2 mylonite zones of the HRTB. Furthermore, the discovery of extensional reactivation of mylonite zones in the northeastern HRTB has fundamental importance to our present understanding of the tectonic evolution of the northeastern Namaqua Province. Normal movement along potential terrane boundaries has profound implications for attempts at stratigraphic reconstruction and the interpretation of the uplift history of the HRTB. In addition, the results of this study have demonstrated the

the complex movement histories of shear zones within high-grade metamorphic terrains. The integration of microstructural kinematic investigations with detailed thermobarometric and geochronological studies is essential in order to constrain P-T-time-displacement paths.

Although there is much more to learn about the reliability and stability of microstructures (e.g. Bell and Johnson, 1992), I believe that the techniques documented in this thesis are an accurate and valuable way to establish the kinematic significance of ductile shear zones in high-grade orogens. The results of this study clearly affirm the need for continued microstructural kinematic investigations of shear zones in the Namaqua Tectonic Province.

References

Abalos, B., 1992. Variscan shear zone deformation of late Precambrian basement in SW Iberia: implications for circum-Atlantic pre-Mesozoic tectonics. *J. Struct. Geol.*, **14**, 807-823.

Bard, J.P., 1986. *Microtextures of Igneous and Metamorphic Rocks*, Reidel, Dordrecht, 264p.

Barker, A.J., 1990. *Introduction to metamorphic textures and microstructures.* Chapman and Hall, New York, 170p.

Bartley, J.M. and Fletcher, J.M., 1990. Tertiary extension and contraction of lower-plate rocks in the Central Mojave Metamorphic Core Complex, southern California. *Tectonics,* **9**, 521-534.

Bartley, J.M. and Wernicke, B., 1984. The Snake Range decollement interpreted as a major extensional shear zone. *Tectonics,* **3**, 647-648.

Barton, E.S. and Burger, A.J., 1983. Reconnaissance isotopic investigations in the Namaqua Mobile Belt and implications for Proterozoic crustal evolution - Upington Geotraverse. *In:* Botha, B.J.V. (ed), *Namaqualand Metamorphic Complex*. Spec. Publ. geol. Soc. S. Afr., **10**, 173-191.

Behrmann, J.H. and Platt, J.P., 1982. Sense of nappe emplacement from quartz c-axis fabrics: An example from the Betic Cordillera, Spain. *Earth Planet. Sci. Lett.*, **59**, 208-215.

Bell, T.H., 1985. Deformation partitioning and porphyroblast rotation in metamorphic rocks: a radical reinterpretation. *J. Met. Geol.*, **3**, 109-118.

Bell, T.H., 1986. Foliation development and refraction in metamorphic rocks: reactivation due to shifting patterns of deformation partitioning. *J. Met. Geol.*, **4**, 421-444.

Bell, T.H., Duncan, A.C. and Simmons, J.V., 1989. Deformation partitioning, shear zone development and the role of undeformable objects. *Tectonophysics*, **158**, 163-171.

Bell, T.H. and Etheridge, M.A., 1973. Microstructures of mylonite and their descriptive terminology. *Lithos,* **6**, 337-348.

Bell, T.H., Forde, A. and Hayward, N., 1992. Do smoothly curving, spiral-shaped inclusion trails signify porphyroblast rotation? *Geology*, **20**, 59-62.

Bell, T.H. and Hayward, N., 1991. Episodic metamorphic reactions during orogenesis: the control of deformation partitioning on reaction sites and reaction duration. *J. Met. Geol.*, **9**, 619-640.

Bell, T.H. and Johnson, S.E., 1989. Porphyroblast inclusion trails: the key to orogenesis. *J. Met. Geol.*, **7**, 279-311.

Bell, T.H. and Johnson, S.E., 1990. Rotation of relatively large rigid objects during ductile deformation: Well-established fact or intuitive prejudice? *Austral. J. Earth Sci.*, **37**, 441-446.

Bell, T.H. and Johnson, S.E., 1992. Shear sense: a new approach that resolves conflicts between criteria in metamorphic rocks. *J. Met. Geol.*, **10**, 99-124.

Bell, T.H., Johnson, S.E., Davis, B., Forde, A., Hayward, N. and Wilkins, C., 1992. Porphyroblast inclusion-trail orientation data: *eppure non son girate! J. Met. Geol.,* **10**, 295-307.

Bell, T.H. and Rubenach, M.J., 1983. Sequential porphyroblast growth and crenulation development during progressive deformation. *Tectonophysics,* **92**, 171-194.

Bell, T.H., Rubenach, M.J. and Fleming, P.D., 1986. Porphyroblast nucleation, growth and dissolution in regional metamorphic rocks as a function of deformation partitioning during foliation development. *J. Met. Geol.*, **4**, 37-67.

Berthé, D., Choukroune, P. and Jegouzo, P., 1979. Orthogneiss, mylonite and non-coaxial deformation of granite: the example of the South Amorican Shear Zone. *J. Struct. Geol.*, **1**, 31-42.

Botha, B.J.V., Grobler, N.J. and Burger, A.J., 1979. New U-Pb age measurements on the Koras Group, Cape Province and its significance as a time reference horizon in eastern Namaqualand. *Trans. geol. Soc. S. Afr.,* **82**, 1-5.

Botha, B.J.V., Linström, W. and Smit, C.A., 1976. Stratigraphic correlation between the Kheis and Matsap Formations and their relation to the Namaqualand Metamorphic Complex. *Trans. geol. Soc. S. Afr.,* **79**, 304-311.

Bouchez, J-L., 1977. Plastic deformation of quartzites at low temperature in an area of natural strain gradient (Angers, France). *Tectonophysics,* **39**, 25-50.

Brown, R.L. and Murphy, D.C., 1982. Kinematic interpretation of mylonitic rocks in part of the Columbia River Fault Zone, Susways Terrane, British Columbia. *Can. J. Earth Sci.,* **19**, 456-465.

Brown, E.H. and Talbot, J.L., 1989. Orogen-parallel extension in the north Cascades crystalline core, Washington. *Tectonics,* **8**, 1105-1114.

Brunel, M., 1980. Quartz fabrics in shear zone mylonites: Evidence for a major imprint due to late strain increments. *Tectonophysics,* **64**, T33-T44.

Brunel, M., 1986. Ductile thrusting in the Himalayas: shear sense criteria and stretching lineations. *Tectonics,* **5**, 247-265.

Brun, J-P. and Burg, J-P., 1982. Combined thrusting and wrenching in the Ibero-Armorican arc: a corner effect during continental collision. *Earth Planet. Sci. Let.,* **61**, 319-332.

Brun, J-P. and Burg, J-P., 1985. Strain trajectories above the Main Central Thrust (Himalaya) in southern Tibet. *Nature,* **313**, 388-390.

Bryant, B. and Reed, J.C., 1969. Significance of lineation and minor folds near major thrust faults in the southern Appalachians and British and Norwegian Caledonides. *Geol. Mag.,* **106**, 412-429.

Burchfiel, B.C. and Royden, L.H., 1985. North-south extension within the convergent Himalayan region. *Geology,* **13**, 679-682.

Burg, J-P., Ivanov, Z., Ricou, L-E. and Klain, D.D.L., 1990. Implications of shear-sense criteria for the tectonic evolution of the Central Rhodope massif, southern Bulgaria. *Geology,* **18**, 451-454.

Carreras, J., Estrada, A. and White, S.H., 1977. The effects of folding of the c-axis fabrics of a quartz mylonite. *Tectonophysics*, **39**, 3-24.

Carlson, K.A., Van Der Pluijm, B.A. and Hanmer, S., 1990. Marble mylonites of the Bancroft shear zone: Evidence for extension in the Canadian Grenville. *Bull. geol. Soc. Am.*, **102**, 174-181.

Cashman, K.V. and Ferry, J.M., 1988. Crystal size distribution (CSD) in rocks and the kinetics and dynamics of crystallization: III Metamorphic crystallization. *Contrib. Mineral. Petrol.*, **99**, 401-415.

Cashman, P.H., 1990. Evidence for extensional deformation during a collisional orogeny, Rombak Window, North Norway. *Tectonics*, **9**, 859-886.

Charlesworth, H.A.K., Langenberg, C.W. and Ramsden, J., 1976. Determining axes, axial planes, and sections of macroscopic folds using computer-based methods. *Can. J. Earth Sci.*, **13**, 54-65.

Clifford, T.N., Gronow, J., Rex, D.C. and Burger, A.J., 1975. Geochronological and petrogenetic studies of high-grade metamorphic rocks and intrusives in Namaqualand, South Africa. *J. Petrol.*, **16**, 154-188.

Clifford, T.N., Stumpfl, E.F., Burger, A.J., McCarthy, T.S. and Rex, D.C., 1981. Mineral-chemical and isotopic studies of Namaqualand granulites, South Africa: a Grenville analogue. *Contrib. Mineral. Petrol.*, **77**, 225-250.

Cluzel, D., Lee, B-J. and Cadet, J-P., 1991. Indosinian dextral ductile fault system and synkinematic plutonism in the southwest of the Ogcheon belt (South Korea). *Tectonophysics*, **194**, 131-151.

Cobbold, P.R., 1977. Description and origin of banded deformation structures. II Rheology and the growth of banded perturbations. *Can. J. Earth Sci.*, **14**, 2510-2523.

Cornell, D.H., Hawkesworth, C.J., Van Calsteren, P. and Scott, W.D., 1986. Sm-Nd study of Precambrian crustal development in the Prieska-Copperton region, Cape Province. *Trans. geol. Soc. S. Afr.*, **89**, 17-28.

Coward, M.P., 1983. Thrust tectonics, thin skinned or thick skinned, and the continuation of thrusts to deep in the crust. *J. Struct. Geol.*, **5**, 113-123.

Coward, M.P., Jan, M.Q., Rex, D., Tarney, J., Thirlwall, M. and Windley, B.F., 1982, Geotectonic framework of the Himalaya of N. Pakistan. *J. geol. Soc. Lond.*, **139**, 299-308.

Coward, M.P. and Potgieter, R., 1983. Thrust zones and shear zones of the margin of the Namaqua metamorphic belt, South Africa. *Trans. geol. Soc. S. Afr.*, **82**, 287-303.

Coward, M.P. and Ries, A.C., 1986. *Collision Tectonics*, Spec. Publ. geol. Soc. Lond., **19**, 415p.

Coward, M.P., Windley, B.F., Broughton, R.D., Luff, I.W., Petterson, M.G., Pudsey, C.J., Rex, D.C. and Asif Khan, M., 1986. Collision tectonics in the NW Himalayas. *In:* Coward, M.P. and Ries, A.C. (eds), *Collision Tectonics*, Spec. Publ. geol. Soc. Lond., 203-219.

Crespo-Blanc, A., 1992. Structure and kinematics of a sinistral transpressive suture between the Ossa-Moreno and South Portuguese Zones, South Iberian Massif. *J. geol. Soc. Lond.*, **149**, 384-401.

Culshaw, N., 1987. Microstructure, c-axis pattern, microstrain and kinematics of some S-C mylonites in Grenville gneiss. *J. Struct. Geol.*, **9**, 299-311.

Davidson, D.M., 1983. Strain analysis of deformed granitic rocks (Helikian) Muskoka district, Ontario. *J. Struct. Geol.*, **4**, 181-195.

Davis, G.H., 1983. Shear-zone model for the origin of metamorphic core complexes. *Geology*, **11**, 342-347.

Davis, G.H., 1987. A shear zone model for the structural evolution of metamorphic core complexes in southeastern Arizona. *In:* Coward, M.P., Dewey, J.F. and Hancock, P.L. (eds), *Continental Extensional Tectonics*. Spec. Publ. geol. Soc. Lond., **28**, 247-266.

Davis, G.H., Gardulski, A.F. and Lister, G.S., 1987. Shear zone origin of quartzite mylonite and mylonitic pegmatite in the Coyote Mountains metamorphic core complex, Arizona. *J. Struct. Geol.*, **9**, 289-298.

Davis, G.A., Lister, G.S. and Reynolds, S.J., 1986. Structural evolution of the Whipple and South Mountains shear zones, southwestern United States. *Geology*, **14**, 7-10.

Dennis, A. and Secor, D., 1987. A model for the development of crenulations in shear zones with applications from the Southern Appalachian Piedmont. *J. Struct. Geol.*, **9**, 809-817.

De Saint Blanquat, M., Lardeaux, J.M. and Brunel, M., 1990. Petrological arguments for high-temperature extensional deformation in the Pyrenean Variscan crust (Saint Barthélémy Massif, Ariège, France). *Tectonophysics*, **177**, 245-262.

Dewey, J.F., 1988. Extensional collapse of orogens. *Tectonics*, **7**, 1123-1139.

Dietrich, D. and Durney, D.W., 1986. Change in direction of overthrust shear in the Helvetic nappes of western Switzerland. *J. Struct. Geol.*, **8**, 389-398.

Dover, J.H., 1990. Problems with terrane terminology - Causes and effects. *Geology*, **18(6)**, 487-488.

Dunnet, D., 1969. A technique of finite strain analysis using elliptical particles. *Tectonophysics*, **7**, 117-136.

Dunnet, D. and Siddans, A.W.B., 1971. Non-random sedimentary fabrics and their modification by strain. *Tectonophysics*, **12**, 307-325.

Echtler, H. and Malavieille, J., 1990. Extensional tectonics, basement uplift and Stephano-Permian collapse basin in a late Variscan metamorphic core complex (Montagne Noire, Southern Massif Central). *Tectonophysics*, **177**, 125-138.

Edelman, S.H., Angang, L. and Hatcher, R.D., 1987. The Brevard zone in south Carolina and adjacent areas: an Alleghanian orogen-scale dextral shear zone reactivated as a thrust fault. *J. Geol.*, **95**, 793-806.

Eisbacher, G.H., 1970. Deformation mechanisms of mylonitic rocks and fractured granites in Cobequid Mountains, Nova Scotia, Canada. *Bull. geol. Soc. Am.*, **81**, 2009-2020.

Elliot, D., 1970. Determination of finite strain and initial shape from deformed elliptical objects. *Bull. geol. Soc. Am.*, **81**, 2221-2236.

Ellis, M.A., 1986. Structural morphology and associated strain in the central Cordillera (British Columbia and Washington): Evidence of oblique tectonics. *Geology*, **14**, 647-650.

Ellis, M.A. and Watkinson, A.J., 1987, Orogen parallel extension and oblique tectonics: The relation between stretching lineations and relative plate motions. *Geology*, **15**, 1022-1026.

England, P.C., 1987. Diffuse continental deformation, length scales, rates and metamorphic evolution. *Phil. Trans. Roy. Soc. Lond.*, **A321**, 3-22.

Erdmer, P., 1985. An examination of the cataclastic fabrics and structures of parts of Nitsulin, Anvil and Simpson allochtons, central Yukon: test of the arc-continent collision model. *J. Struct. Geol.*, **7**, 57-72.

Escher, A. and Watterson, J., 1974. Stretching fabrics, folds and crustal shortening. *Tectonophysics*, **22**, 223-231.

Etchecopar, A. and Malavieille, J., 1987. Computer models of pressure shadows: a method for strain measurement and shear sense determination. *J. Struct. Geol.*, **9**, 667-677.

Etchecopar, A. and Vasseur, G., 1987. A 3-D kinematic model of fabric development in polycrystalline aggregates: comparisons with experimental and natural examples. *J. Struct. Geol.*, **9**, 705-717.

Etheridge, M.A. and Wilkie, J.C., 1979. Grain size reduction, grain boundary sliding and the flow strength of mylonites. *Tectonophysics*, **58**, 159-178.

Evans, D.J. and White, S.H., 1984. Microstructural and fabric studies from the rocks of the Moine Nappe, Eriboll, northwest Scotland. *J. Struct. Geol.*, **6**, 369-389.

Faure, M., 1985. Microtectonic evidence for eastward ductile shear in the Jurassic orogen of S.W. Japan. *J. Struct. Geol.*, **7**, 175-186.

Fry, N., 1979. Random point distributions and strain measurement in rocks. *Tectonophysics*, **60**, 89-105.

Gapais, D., 1989. Shear structures within deformed granites: Mechanical and thermal indicators. *Geology*, **17**, 1144-1147.

Geringer, G.J., 1973. *Die geologie van die Argeiese gesteentes en jongere formasies in die gebied wes van Upington met spesiale verwysing na die verskillende granietvoorkomste.* Ph.D. thesis (unpubl.), Univ. Orange Free State, Bloemfontein, 203p.

Geringer, G.J., 1979. The origin and tectonic setting of amphibolites in part of the Namaqua metamorphic belt, South Africa. *Trans. geol. Soc. S. Afr.*, **82**, 287-303.

Geringer, G.J., Botha, B.J.V. and Slabbert, M.J., 1988. The Keimoes Suite - a composite granitoid batholith along the eastern margin of the Namaqua mobile belt, South Africa. *S. Afr. J. Geol.*, **91**, 465-476.

Gibson, R.G., 1990. Nucleation and growth of retrograde shear zones: an example from the Needle Mountains, Colorado, U.S.A. *J. Struct. Geol.*, **12**, 339-350.

Guérin, G., Brun, J-P. and Van Den Driessche, J., 1990. Kinematics of pre-Miocene ductile deformation in the Santa Catalina Core Complex and adjacent regions. *Tectonics*, **9(6)**, 1305-1326.

Hanmer, S.K., 1982. Microstructure and geochemistry of plagioclase and microcline in naturally deformed granite. *J. Struct. Geol.*, **4**, 197-214.

Hanna, S.S. and Fry, N., 1979. A comparison of methods of strain determination in rocks from southwest Dyfed (Pembrokeshire) and adjacent areas. *J. Struct. Geol.*, **1(2)**, 155-162.

Hansen, V.L., 1989. Structural and kinematic evolution of the Teslin suture zone, Yukon: record of an ancient transpressional margin. *J. Struct. Geol.*, **11(6)**, 717-733.

Hansen, V.L., 1990. Yukon-Tanana terrane: A partial acquittal. *Geology*, **18**, 365-369.

Hansen, V.L., 1992a. Backflow and margin-parallel shear within an ancient subduction complex. *Geology*, **20**, 71-74.

Hansen, V.L., 1992b. P-T evolution of the Teslin suture zone and Cassiar tectonites, Yukon, Canada: evidence for A- and B-type subduction. *J. Met. Geol.*, **10**, 239-263.

Harland, W.B., 1971. Tectonic transpression in Caledonian Spitsbergen. *Geol. Mag.*, **108**, 27-42.

Harris, L.B. and Cobbold, P.R., 1984. Development of conjugate shear bands during bulk simple shearing. *J. Struct. Geol.*, **7**, 37-44.

Harris, R.W., 1987. Primary versus secondary features of accreted terranes: Implications for tectonostratigraphic analysis in the Namaqua Province. *Proceedings of the Alex L. du Toit Golden Jubilee Conference on Tectonostratigraphic Terrane Analysis*, Precambr. Res. Unit, Univ. Cape Town, 46-48.

Harris, R.W., 1988. Examination of dextral transpression as a model for the evolution of thrusts and late folds in Eastern Namaqualand. *S. Afr. J. Geol.*, **91**, 329-336.

Harris, R.W., 1990. Shear strain analysis along the southeastern segment of the Pofadder Lineament. *Abstracts Geocongress '90*, Geological Society of South Africa, Cape Town, 214-217.

Harris, R.W., 1992. *A structural analysis of the Hartbees River Thrust Belt, with special emphasis on the nature and origin of the change in structural patterns across the boundary between the Bushmanland and Gordonia Subprovinces.* Unpubl. Ph.D thesis, Dept. of Geology, University of Cape Town, 285p.

Hartnady, C.J.H., Joubert, P. and Stowe, C.W., 1985. Proterozoic crustal evolution in southwestern Africa. *Episodes*, **8**, 236-244.

Hatcher, R.D., 1978. Eastern Piedmont fault system: Speculations on its extent; Reply. *Geology*, **6**, 580-582.

Hatcher, R.D. and Hooper, R.J., 1992. Evolution of crystalline thrust sheets in the internal parts of mountain chains. *In:* McClay, K.R. (ed), *Thrust Tectonics*, Chapman and Hall, London, 217-233.

Hatcher, R.D. and Williams, R.T., 1986. Mechanical model for single thrust sheets Part I: Crystalline thrust sheets and their relationships to the mechanical/thermal behaviour of orogenic belts. *Bull. geol. Soc. Am.*, **97**, 975-985.

Hayward, N., 1992. Microstructural analysis of the classical spiral garnet porphyroblasts of south-east Vermont: evidence for non-rotation. *J. Met. Geol.*, **10**, 567-587.

Higgins, M.W., 1971. Cataclastic rocks. *Prof. Paper U.S. geol. Surv.*, **687**, 1-97.

Hobbs, B.E., Means, W.D. and Williams, P.F., 1976. *An Outline of Structural Geology*, John Wiley & Sons, Toronto, 571p.

Holdaway, M.J. and Lee, S.M., 1977. Fe-Mg cordierite stability in high grade pelitic rocks based on experimental, theoretical and natural observations. *Contrib. Mineral. Petrol.*, **63**, 175-198.

Hollister, C.S. and Crawford, M.L., 1986. Melt-enhanced deformation: a major tectonic process. *Geology*, **14**, 558-561.

Hooper, R.J. and Hatcher, R.D., 1988. Mylonites from the Towaliga fault zone, central Georgia: products of heterogeneous non-coaxial deformation. *Tectonophysics*, **152**, 1-17.

Houseman, G.A., McKenzie, D.P. and Molnar, P., 1981. Convective instability of a thickened boundary layer and its relevance for the thermal evolution of continental convergent belts. *J. Geophys. Res.*, **86**, 6155-6135.

Hudson, T.L., 1987. Suspect philosophy? *Geology*, **15**, 1177.

Humphreys, H.C., 1990. The extent and significance of low-pressure amphibolite facies metamorphism in the Gordonia Subprovince. *Abtracts Geocongress '90*, Geological Society of South Africa, Cape Town, 265-268.

Humphreys, H.C., 1991. *The tectonothermal evolution of the eastern Namaqua Province deduced from the petrology and reaction history of metapelites.* Unpubl. Ph.D thesis, Dept. of Geology, University of Cape Town, 433p.

Humphreys, H.C. (1992 in prep.) Polymetamorphic evolution of cordierite gneisses within a Proterozoic thrust belt, eastern Namaqua Province, South Africa.

Humphreys, H.C. and Swartz, H.G., 1988. Pressure-temperature determinations and garnet profiles in metapelites from the central Areachap Group, south of Upington. *Abstracts Geocongress '88*, Geological Society of South Africa, Cape Town, 295-298.

Humphreys, H.C. and Van Bever Donker, J.M., 1990. Early Namaqua low-pressure metamorphism, deformation and porphyroblast growth in the Zeevoorby staurolite schist, South Africa. *J. Met. Geol.*, **8**, 159-170.

Hutton, D.H.W., Dempster, T.J., Brown, P.E. and Becker, S.D., 1990. A new mechanism of granite emplacement: intrusion in active extensional shear zones. *Nature*, **343**, 452-455.

Jamieson, R.A. and Strong, D.F., 1981. A metasomatic mylonite zone within the ophiolite aureole, St Anthony Complex, Newfoundland. *Am. J. Sci.*, **281**, 264-281.

Jegouzo, P., 1980. The South Armorican shear zone. *J. Struct. Geol.*, **2**, 39-47.

Johnson, E., 1990. Lack of porphyroblast rotation in the Otago schists, New Zealand: implications for crenulation cleavage development, folding and deformation partitioning. *J. Met. Geol.*, **8**, 13-30.

Jones, C.E., Tarney, J., Baker, J.H. and Gerouki, F., 1992. Tertiary granitoids of Rhodope, northern Greece: magmatism related to extensional collapse of the Hellenic Orogen? *Tectonophysics*, **210**, 295-314.

Joubert, P., 1974a. Wrench-fault tectonics in the Namaqualand metamorphic complex. *Bull. Precambr. Research Unit, Univ Cape Town,* **15**, 17-28.

Joubert, P., 1974b. The gneisses of Namaqualand and their deformation. *Trans. geol. Soc. S. Afr.,* **77**, 339-345.

Joubert, P., 1978. The fault pattern south of Kakamas - an example of convergent wrench fault tectonics. *In:* Verwoerd, W.J. (ed), *Mineralization in Metamorphic Terranes*, Spec. Publ. geol. Soc. S. Afr., **4**, 215-222.

Joubert, P., 1986. Namaqualand - a model of Proterozoic accretion?. *Trans. geol. Soc. S. Afr.,* **89**, 79-96.

Kelley, S.P. and Powell, D., 1985. Relationships between marginal thrusting and movement on major internal shear zones in the Northern Highland Caledonides, Scotland. *J. Struct. Geol.,* **7**, 161-174.

Lacassin, R., 1987. Kinematics of ductile shearing from outcrop to crustal scale in the Monte Rosa Nappe, western Alps. *Tectonics,* **6**, 69-88.

Lacassin, R., 1989. Plate-scale kinematics and compatibility of crustal shear zones in the Alps. *In:* Coward, M.P., Dietrich, D. and Park, R.G. (eds) *Alpine Tectonics*, Spec. Publ. geol. Soc. Lond., **45**, 339-352.

Lagarde, J-L. and Michard, A., 1986. Stretching normal to the regional thrust displacement in a thrust-wrench shear zone, Rehamna Massif, Morocco. *J. Struct. Geol.,* **8**, 483-492.

Lapworth, C., 1885. The Highland controversy in British history: Its causes, course, and consequences. *Nature,* **32**, 558-559.

La Tour, T.E. and Barnett, R.L., 1987. Mineralogical changes accompanying mylonitization in the Bitteroot dome of the Idaho Batholith: implications for timing of deformation. *Bull. geol. Soc. Am.,* **98**, 356-363.

Law, R.D., Casey, M. and Knipe, R.J., 1986. Kinematic and tectonic significance of microstructures and crystallographic fabrics within quartz mylonites from the Assynt and Loch Eriboll regions of the Moine thrust zone, NW Scotland. *Trans. R. Soc. Edinburgh. Earth. Sci.,* **77**, 99-125.

Law, R.D., Knipe, R.J. and Dayan, H., 1984. Strain path partitioning within thrust sheets: microstructural and petrofabric evidence from the Moine thrust zone at Loch Eriboll, northwestern Scotland. *J. Struct. Geol.,* **6**, 477-497.

Law, R.D., Schmid, S.M. and Wheeler, J., 1990. Simple shear deformation and quartz crystallographic fabrics: a possible natural example from the Torridon area of NW Scotland. *J. Struct. Geol.,* **12**, 29-45.

Lee, J., Miller, E.L. and Sutter, J.F., 1987. Ductile strain and metamorphism in an extensional tectonic setting: a case study from the northern Snake Range, Nevada, U.S.A. *In:* Coward, M.P., Dewey, J.F. and Hancock, P.L., (Eds), *Continental Extensional Tectonics*, Spec. Publ. geol. Soc. Lond., **28**, 267-298.

Le Fort, P., 1981. Manaslu leucogranites: A collision signature of the Himalaya. A model for its genesis and emplacement. *J. Geophys. Res.,* **86**, 10545-10568.

Lisle, R.J., 1977. Estimation of tectonic strain ratio from the mean shape of deformed elliptical markers. *Geol. Mijnb.,* **56**, 140-144.

Lisle, R.J., 1979. Strain analysis using deformed pebbles: influence of initial pebble shape. *Tectonophysics*, **60**, 263-277.

Lisle, R.J., Rondeel, H.E., Doorn, D., Brugge, J. and Van De Gaag, P., 1983. Estimation of viscosity contrast and finite strain from deformed elliptical inclusions. *J. Struct. Geol.*, **5**, 603-609.

Lister, G.S. and Davis, G.A., 1989. The origin of metamorphic core complexes and detachment faults formed during Tertiary continental extension in the northern Colorado River region, U.S.A.. *J. Struct. Geol.*, 11, 65-94.

Lister, G.S. and Dornsiepen, U.F., 1982. Fabric transitions in the Saxony granulite terrain. *J. Struct. Geol.*, **4**, 81-92.

Lister, G.S. and Hobbs, B.E., 1980. The simulation of fabric development during plastic deformation and its application to quartzite: the influence of deformation history. *J. Struct. Geol.*, **2**, 355-370.

Lister, G.S. and Price, G.P., 1978. Fabric development in a quartz-feldspar mylonite. *Tectonophysics*, **49**, 37-78.

Lister, G.S. and Snoke, A.W., 1984. S-C mylonites. *J. Struct. Geol.*, **6**, 617-638.

Lister, G.S. and Williams, P.F., 1979. Fabric development in shear zones: theoretical controls and observed phenomena. *J. Struct. Geol.*, 1, 283-297.

Lister, G.S., Williams, P.F., Zwart, H.J. and Lisle, R.J., 1977. Fabrics, microstructures and microtectonics. *Tectonophysics*, **39**, 499.

Maclaren, A.H., 1984. *The geology of the area east of Pofadder with emphasis on shearing associated with the Pofadder Lineament, north west Cape.*, MSc thesis (unpubl.), Univ. Cape Town, 123p.

Maddock, R.H., 1983. Melt origin of fault-generated pseudotachylites demonstrated by textures. *Geology*, 11, 105-108.

Maiver, C.K., 1987. Shear criteria in the Grenville Province, Ontario, Canada. *J. Struct. Geol.*, **9**, 531-539.

Malavieille, J., 1987. Kinematics of compressional and extensional ductile shearing deformation in a metamorphic core complex of the northeastern Basin and Range. *J. Struct. Geol.*, **9**, 541-554.

Malavieille, J. and Etchecopar, A., 1981. Ductile shear deformation of quartzite in an Alpine crustal sheet (Ambin massif). *Tectonophysics*, **78**, 65-71.

Malavieille, J., Guilot, P., Costa, S., Lardeaux, J.M. and Gardien, V., 1990. Collapse of the thickened Variscan crust in the French Massif Central: Mont Pilat extensional shear zone and St. Etienne Late Carboniferous Basin. *Tectonophysics*, **177**, 139-149.

Mattauer, M., 1986. Intracontinental subduction, crust-mantle décollement and crustal-stacking wedge in the Himalayas and other collision belts. *In:* Coward, M.P. and Ries, A.C. (eds), *Collision Tectonics*, Spec. Publ. geol. Soc. Lond., **19**, 37-50.

Mattauer, M., Faure, M. and Malavielle, J., 1981. Transverse lineation and large scale structures related to Alpine obduction in Corsica. *J. Struct. Geol.*, **3**, 401-409.

Matthews, P.E., Bond, R.A.B. and van den Berg, J.J., 1974. An algebraic method of strain analysis using elliptical markers. *Tectonophysics*, **24**, 31-67.

Mawer, C.K., 1987. Shear criteria in the Grenville Province, Ontario, Canada. *J. Struct. Geol.*, **9**, 531-539.

Mawer, C. and White, J., 1987. Sense of displacement on the Cobequid-Chedabucto fault system, Nova Scotia, Canada. *Can. J. Earth. Sci.*, **24**, 217-223.

McClay, K.R., 1992. Glossary of thrust tectonic terms. *In:* McClay, K.R. (ed), *Thrust Tectonics*, Chapman and Hall, London, 447p.

Meneilly, A.W. and Storey, B.C., 1986. Ductile thrusting within subduction complex rocks on Signy Island, South Orkney Islands. *J. Struct. Geol.*, **8**, 457-472.

Merle, O., Cobbold, P.R. and Schmid, S., 1989. Tertiary kinematics in the Lepontine dome. *In:* Coward, M.P., Dietrich, D. and Park, R.G. (eds), *Alpine Tectonics*, Spec. Publ. geol. Soc. Lond., **45**, 113-134.

Miller, E.L., Gans, P.B. and Garing, J., 1983. The Snake range decollement: an exhumed mid-Tertiary brittle-ductile transition. *Tectonics*, **2**, 239-263.

Mitra, G., 1978. Microscopic deformation mechanisms and flow laws in quartzites within the South Mountain anticline. *J. Geol.*, **86**, 129-152.

Monsen, S.A. and Aalto, K.R., 1980. Petrology, structure and regional tectonics of South Fork Mountain Schist, Pine Ridge Summit, northern California. *Bull. geol. Soc. Am.*, **91**, 369-373.

Moore, J.M., 1989. A comparative study of metamorphosed supracrustal rocks from the Western Namaqualand Metamorphic Complex. *Bull. Precambr. Res. Unit, Univ. Cape Town*, **37**, 370p.

Morley, C.K., 1988. Out-of-sequence thrusts. *Tectonics*, **7**, 539-561.

Nadeau, L. and Hanmer, 1992. Deep-crustal break-back stacking and slow exhumation of the continental footwall beneath a thrusted marginal basin, Grenville orogen, Canada. *Tectonophysics*, **210**, 215-233.

New, M., 1987., *A petrographic and kinematic analysis of a section across the Hartebees Thrust Belt, Namaqua Province.* Unpubl. B.Sc. Hons. project, Dept. of Geology, Univ. Cape Town, 90p.

Nicolas, A., Bouchez., J-L., Boudier, F. and Mercier,J.C., 1971. Textures, structures and fabrics due to solid state flow in some European Lherzolites. *Tectonophysics*, **12**, 55-85.

Nicolas, A. and Poirier, J-P., 1976. *Crystalline plasticity and solid state flow in metamorphic rocks.* Wiley, New York, 444p.

Odling, N.E., 1984. Strain analysis and strain path modelling in the Loch Tollie gneisses, Gairloch, NW Scotland. *J. Struct. Geol.*, **6**, 543-562.

Okulitch, A.V., 1984. The role of the Shuswap Metamorphic Complex in Cordilleran tectonism: a review. *Can. J. Earth Sci.*, **21**, 1171-1193.

Olesen, N.O., 1982. Heterogeneous strain of a phyllite as revealed by porphyroblast-matrix relationships. *J. Struct. Geol.*, **4**, 481-490.

Passchier, C.W., 1983. The reliability of asymmetric c-axis fabrics of quartz to determine sense of vorticity. *Tectonophysics,* **99**, T9-T18.

Passchier, C.W., 1988. Analysis of deformation paths in shear zones. *Geol. Rundshau,* **77**, 309-318.

Passchier, C.W. and Simpson, C., 1986. Porphyroclast systems as kinematic indicators. *J. Struct. Geol.,* **8**, 831-843.

Passchier, C.W., Trouw, R.A.J., Zwart, H.J. and Vissers, R.L.M., 1992. Porphyroblast rotation: *eppur si muove? J. Met. Geol.*, **10**, 283-294.

Paterson, S.R., 1983. A comparison of methods used in measuring finite strains from ellipsoidal objects. *J. Struct. Geol.*, **5**, 611-618.

Peach, C.J. and Lisle, R.J., 1979. A Fortran IV program for the analysis of tectonic strain using deformed elliptical markers. *Comput. Geosci.*, **5**, 325-334.

Pinet, N. and Cobbold, P.R., 1992. Experimental insights into the partitioning of motion within zones of oblique subduction. *Tectonophysics*, **206**, 371-388.

Platt, J.P., 1979. Extensional crenulation cleavage. *J. Struct. Geol.*, **1**, 95.

Platt, J.P., 1984. Secondary cleavages in ductile shear zones. *J. Struct. Geol.,* **6**, 439-442.

Platt, J.P., Lister, G.S., Cunningham, P., Weston, P., Peel, F., Baudin, T. and Dondey, H., 1989. Thrusting and backthrusting in the Briançonnais domain of the western Alps. *In:* Coward, M.P., Dietrich, D. and Park, R.G. (eds), *Alpine Tectonics*, Spec. Publ. geol. Soc. Lond., **45**, 135-152.

Platt, J.P. and Vissers, R.L.M., 1980. Extensional features in anisotropic rocks. *J. Struct. Geol.,* **2**, 397-410.

Poldervaart, A. and Von Backström, J.W., 1949. Study of an area at Kakamas. *Trans. geol. Soc. S. Afr.,* **52**, 433-495.

Ponce de Leon, M.I. and Choukroune, P., 1980. Shear zones in the Iberian Arc. *J. Struct. Geol.*, **2**, 63-68.

Potter, P.E. and Pettijohn, F.J., 1977. *Paleocurrents and Basin Analysis.* Springer-Verlag, Berlin, 296p.

Powell, D. and Treagus, J.E., 1967. On the geometry of S-shaped inclusion trails in garnet porphyroblasts. *Mineral. Mag.,* **36**, 453-456.

Powell, D. and Treagus, J.E., 1970. Rotational fabrics in metamorphic minerals. *Mineral. Mag.,* **37**, 801-814.

Pretorius, D.A., 1974. The structural boundary between the Kaapvaal and Sonama Provinces. *Econ. geol. Res. Unit, Univ. Witwatersrand, Inf. Circ.*, **88**, 27p.

Ralser, S., 1990. Shear zones developed in an experimentally deformed quartz mylonite. *J. Struct. Geol.*, **12**, 1033-1045.

Ramsay, J.G., 1967. *Folding and Fracturing of Rocks.* McGraw Hill, New York, 568p.

Ramsay, J.G., 1980. Shear zone geometry: A review. *J. Struct. Geol.,* **2**, 83-99.

Ramsay, J.G. and Graham, R.H., 1970. Strain variation in shear belts. *Can. J. Earth. Sci.*, **7**, 786-813.

Ramsay, J.G. and Huber, M.I., 1983. *The techniques of modern structural geology, vol. 1: strain analysis.* Academic Press, London, 307p.

Ratschbacher, L., 1986. Kinematics of Austro-Alpine cover nappes: changing translation path due to transpression. *Tectonophysics,* **125**, 335-356.

Rattey, P.R. and Sanderson, D.J., 1982. Patterns of folding within thrust sheets: examples from the Variscan of Southwest England. *Tectonophysics,* **88**, 247-267.

Reynolds, S.J. and Lister, G.S., 1990. Folding of mylonitic zones in Cordilleran metamorphic core complexes: evidence from near the mylonitic front. *Geology,* **18**, 216-219.

Rhodes, S. and Gayer, R.A., 1977. Non-cylindrical folds, linear structures in the X-direction and mylonite development during translation of the Caledonian Kalak Nappe Complex of Finmark. *Geol. Mag.,* **114**, 329-408.

Ridley, J., 1982. Arcuate lineation trends in a deep level, ductile thrust belt, Syros, Greece. *Tectonophysics,* **88**, 347-360.

Ridley, J., 1986. Parallel stretching lineations and fold axes oblique to a shear displacement direction - a model and observations. *J. Struct. Geol.,* **8**, 647-653.

Rosenfeld, J.L., 1970. Rotated garnets in metamorphic rocks. *Geol. Soc. Am. Spec. Pap.,* **129**, 102p.

Ross, J.V., 1973. Mylonitic rocks and flattened garnets in the southern Okanagan of British Columbia. *Can. J. Earth. Sci.,* **10**, 1-17.

Rutter, E.M., 1986. On the nomenclature of mode of failure in rocks. *Tectonophysics,* **122**, 381-387.

South African Committee for Stratigraphy (SACS), 1980. *Stratigraphy of South Africa. Part 1 (Comp. Kent, L.E.), Lithostratigraphy of the Republic of South Africa, South West Africa/Namibia, and the Republics of Bophutatswana, Transkei and Venda.* Handb. geol. Surv. S. Afr., **8**, 690p.

Sanderson, D.J. and Marchini, W.R.D., 1984. Transpression. *J. Struct. Geol.,* **6**, 449-458.

Schmid, S.M., Boland, J.N. and Paterson, M.S., 1977. Superplastic flow in fine-grained limestone. *Tectonophysics,* **43**, 245-280.

Schmid, S.M., Casey, M. and Starkey, J., 1981. The microfabric of calcite tectonites from the Helvetic nappes (Swiss Alps). *In:* McClay, K.R. and Price, N.J., (eds), *Thrust and Nappe Tectonics*, Geol. Soc. Spec. Publ., **9**, 151-158.

Schoneveld, C., 1977. A study of typical inclusion patterns in strongly paracrystalline-rotated garnets. *Tectonophysics,* **39**, 453-471.

Schulmann, K., 1990. Fabric and kinematic study of the Bítes orthogneiss (southwestern Maravia): Result of large-scale northeastward shearing parallel to the Moldanubian / Moravian boundary. *Tectonophysics,* **177**, 229-244.

Selverstone, J., 1988. Evidence for east-west crustal extension in the eastern Alps: implications for the unroofing history of the Tauern Window. *Tectonics,* **7**, 87-105.

Sengör, A.M.C., 1991. Plate tectonics and orogenic research after 25 years: synopsis of a Tethyan perspective. *Tectonophysics,* **187**, 315-344.

Shackleton, R.M. and Ries, A.C., 1984. The relation between regionally consistent stretching lineations and plate motions. *J. Struct. Geol.,* **6**, 147-157.

Shimamoto, T., 1989. The origin of S-C mylonites and a new fault-zone model. *J. Struct. Geol.,* **11**, 51-64.

Shimamoto, T. and Ikeda, Y., 1976. A simple algebraic method for strain estimation for deformed ellipsoidal objects - I. Basic theory. *Tectonophysics,* **36**, 315-337.

Sibson, R.H., 1977. Fault rocks and fault mechanisms. *J. geol. Soc. Lond.,* **133**, 191-213.

Sibson, R.H., 1983. Continental fault structure and the shallow earthquake source. *J. geol. Soc. Lond.,* **140**, 741-767.

Sibson, R.H., 1986. Earthquakes and rock deformation in crustal fault zones. *Ann. Rev. Earth Planet. Sci.,* **14**, 149-175.

Simpson, C., 1983. Strain and shape fabric variations associated with ductile shear zones. *J. Struct. Geol.,* **5**, 61-72.

Simpson, C., 1984. Borrego Springs - Santa Rosa mylonite zone: a late Cretaceous west directed thrust in southern California. *Geology,* **12**, 8-11.

Simpson, C., 1985. Deformation of granitic rocks across the brittle-ductile transition. *J. Struct. Geol.,* **7**, 503-511.

Simpson, C., 1986a. Fabric development in brittle-to-ductile shear zones. *Pure & Appl. Geophys.,* **124**, 269-288.

Simpson, C., 1986b. Determination of movement sense in mylonites. *J. geol. Educ.,* **34**, 246-261.

Simpson, C. and Schmid, S.M., 1983. Microstructural indicators of sense of shear in shear zones. *Bull. geol. Soc. Am.,* **94**, 1281-1288.

Simpson, C. and Wintsch, R.P., 1989. Evidence for deformation-induced K-feldspar replacement by myrmekite. *J. Met. Geol.,* **7**, 261-275.

Spry, A., 1963. The origin and significance of snowball structure in garnet. *J. Petrol.,* **4**, 211-222.

Stowe, C.W., 1979. The Upington geotraverse National Geodynamics Project - 1979 progress report and outline of the macrostructure. *Precambr. Res. Unit, Univ. Cape Town, 16th ann. Rep., 1978,* 20-34.

Stowe, C.W., 1980. Preliminary report on geodynamics in the Upington geotraverse. *Precambr. Res. Unit, Univ. Cape Town, 17th ann. Rep., 1980,* 24-48.

Stowe, C.W., 1983. The Upington geotraverse and its implication for Craton Margin Tectonics. *In:* Botha, B.J.V. (ed), *Namaqualand Metamorphic Complex,* Spec. Publ. geol. Soc. S. Afr., **10**, 147-171.

Stowe, C.W., 1984. Explanation of the Upington Geotraverse Section, South Africa. *In:* Rast, N. and DeLaney, S.M. (eds), *Profiles of Orogenic Belts,* Int. Geodynamics Series, Amer. Geophys. Union, **10**, 35-44.

Stowe, C.W., 1986. Synthesis and interpretation of structures along the north-eastern boundary of the Namaqua Tectonic Province, South Africa. *Trans. geol. Soc. S. Afr.,* **89**, 185-198.

Stowe, C.W., 1988. *The Namaqua Province: a mid-Proterozoic zone of microcontinental collision?* African Crustal Evolution - Lecture **3**.1 (unpublished), Univ. Cape Town, 9p.

Sylvester, A.G. and Smith, R.R., 1976. Tectonic transpression and basement-controlled deformation in the San Andreas Fault Zone, Salton Trough, California. *Bull. Am. Assoc. Pet. Geol.*, **60**, 2081-2102.

Takagi, H., 1986. Implications of mylonitic microstructures for the geotectonic evolution of the Median Tectonic Line, central Japan. *J. Struct. Geol.,* **8**, 3-14.

Thompson, A.B., 1982. Dehydration melting of pelitic rocks and the generation of H_2O-undersaturated granitic liquids. *Am. J. Sci.,* **282**, 1576-1595.

Tobisch, O.T. and Paterson, S.R., 1990. The Yarra granite: An intradeformational pluton associated with ductile thrusting, Lachlan Fold Belt, southeastern Australia. *Bull. geol. Soc. Am.*, **102**, 693-703.

Toogood, D.J., 1976. Structural and metamorphic evolution of a gneiss terrane in the Namaqua Belt near Onseepkans, South West Africa. *Bull. Precambr. Res. Unit, Univ. Cape Town,* **76**, 189p.

Tullis, J., Snoke, A.W. and Todd, V.R., 1982. Significance and petrogenesis of mylonitic rocks. *Geology*, **10**, 227-230.

Tullis, J. and Yund, R.A., 1977. Experimental deformation of dry Westerly Granite. *J. Geophys. Res.,* **82**, 5705-5718.

Tullis, J. and Yund, R.A., 1985. Dynamic recrystallization of feldspar - A mechanism for ductile shear zone deformation. *Geology,* **13**, 238-241.

Tullis, J. and Yund, R.A., 1987. Transition from cataclastic flow to dislocation creep of feldspar: Mechanisms and microstructures. *Geology,* **15**, 606-609.

Tulloch, A.J., 1989. The Paparoa metamorphic core complex, New Zealand: Cretaceous extension associated with fragmentation of the Pacific margin of Gondwana. *Tectonophysics,* **8**, 1217-1234.

Vajner, V., 1974a. The tectonic development of the Namaqua Mobile Belt and its foreland inparts of the Northern Cape. *Bull. Precambr. Res. Unit, Univ. Cape Town,* **14**, 201p.

Vajner, V., 1974b. The Upington Geotraverse - first progress report. *Ann. Rep. Precambr. Res. Unit, Univ. Cape Town,* **12**, 8-11.

Vajner, V., 1974c. Preliminary report on the geology and structure of parts of the Namaqua Foreland in the Upington area. *Ann. Rep. Precambr. Res. Unit, Univ. Cape Town,* **12**, 11-19.

Vajner, V., 1975. Crustal evolution of the Namaqua mobile belt and its foreland in parts of the northern Cape. *Bull. Precambr. Res. Unit, Univ. Cape Town,* **15**, 1-15.

Vajner, V., 1978. The Jannelsepan Formation. *Ann. Rep. Precambr. Res. Unit, Univ. Cape Town,* **14-15**, 26-40.

Vajner, V. and Jackson, M.P.A., 1974. Brief report on a field trip to the area between Kakamas, Kenhardt, Marydale and Upington. *Ann. Rep. Precambr. Res. Unit, Univ. Cape Town,* **10-11**, 56-57.

Van Bever Donker, J.M., 1978. An estimation of strain rate on a major shear zone in the Kakamas-Keimoes area, Northern Cape. *Ann. Rep. Precambr. Res. Unit, Univ. Cape Town,* **14**, 41-47.

Van Bever Donker, J.M., 1980. Structural and metamorphic evolution of an area around Kakamas and Keimoes, Cape Province, South Africa. *Bull. Precambr. Res. Unit, Univ. Cape Town,* **28**, 165p.

Van Bever Donker, J.M., 1983. The Neusspruit Lineament, Upington Geotraverse, possible boundary between the Namaqualand Metamorphic Complex and the Namaqua Front. *Spec. Publ. geol. Soc. S. Afr.,* **10**, 193-198.

Van Den Driessche, J. and Brun, J-P., 1987. Rolling structures at large shear strain. *J. Struct. Geol.,* **9**, 691-704.

Van Zyl, C.Z., 1981. Structural and metamorphic evolution in the transitional zone between craton and mobile belt, Upington geotraverse. *Bull. Precambr. Res. Unit, Univ. Cape Town,* **31**, 243p.

Vauchez, A., 1987. The development of discrete shear-zones in a granite: stress, strain and changes in deformation mechanisms. *Tectonophysics,* **133**, 137-156.

Vauchez, A. and Brunel, M., 1988. Polygenetic evolution and longitudinal transport within the Henderson mylonite gneiss, North Carolina (southern Appalachians, Piedmont). *Geology,* **16**, 1011-1014.

Vernon, R.H., 1988. Microstructural evidence of rotation and non-rotation of mica porphyroblasts. *J. Met. Geol.,* **6**, 595-601.

Vernon, R.H., Williams, V.A. and D'Arcy, W.F., 1983. Grain size reduction and foliation development in a granite batholith. *Tectonophysics,* **92**, 123-146.

Visser, D.J.L. (compiler), 1984. *1:1 000 000 Geological Map of the Republic of South Africa and the Kingdoms of Lesotho and Swaziland.* Geol. Surv. S. Afr., Pretoria.

Vissers, R.L.M., 1989. Asymmetric quartz c-axis fabrics and flow vorticity: a study using rotated garnets. *J. Struct. Geol.,* **11**, 231-244.

Voll, G., 1976. Recrystallization of quartz, biotite, and feldspars from Erstfeld to the Leventina Nappe, Swiss Alps, and its geological significance. *Schweizerische Mineralogische und Petrographische Mitteilungen,* **65**, 641-647.

Von Backström, J.W., 1964. The geology of an area around Keimoes, Cape Province, with special reference to phacoliths of charnockitic adamellite-porphyry. *Mem. geol. Surv. S. Afr.,* **53**, 218p.

Von Veh, M.W. and Hartnady, C.J.H., 1983. A Fortran 77 program for acquiring axial ratios, long axis orientations and centroid positions of elliptical strain markers. *Computers and Geosciences,* **12**, 339-347.

Walther, J.V. and Wood, B.J., 1984. Rate and mechanism in prograde metamorphism. *Contrib. Mineral. Petrol.,* **88**, 246-259.

Waters, A.C. and Campbell, C.D., 1935. Mylonites and the San Andreas Fault Zone. *Am. J. Sci.*, **174**, 473-503.

Waters, D.J., 1989. Metamorphic evidence for the heating and cooling path of Namaqualand granulites. *In:* Daly, J.S., Cliff, R.A. and Yardley, B.W.D. (eds), *Evolution of Metamorphic Belts*, Spec. Publ. geol. Soc. Lond., **43**, 357-363.

Waters, D.J., 1990. Thermal history and tectonic setting of the Namaqualand granulites, southern Africa: Clues to Proterozoic crustal development. *In:* Vielzeuf, D. and Vidal, Ph. (eds), *Granulites and Crustal Evolution*, Kluwer Academic Publishers, Netherlands, 243-256.

Watts, M.J. and Williams, G.D., 1979. Fault rocks as indicators of progressive shear deformation in the Guingamp region, Brittany. *J. Struct. Geol.*, 1, 323-332.

Watts, M.J. and Williams, G.D., 1983. Strain geometry, microstructure and mineral chemistry in metagabbro shear zones: a study of softening mechanisms during progressive mylonitization. *J. Struct. Geol.*, **5**, 507-518.

Weijermars, R. and Rondeel, H.E., 1984. Shear band foliation as an indicator of sense of shear: Field observations in central Spain. *Geology*, **12**, 603-606.

Wenk, H.R., 1978. Are pseudotachylites products of fracture or fusion? *Geology*, **6**, 507-511.

Wenk, H.R., Takeshita, T., Bechler, E., Erskine, B.G. and Matthies, S., 1987. Pure shear and simple shear calcite textures: Comparison of experimental, theoretical and natural data. *J. Struct. Geol.*, **9**, 731-745.

Wheeler, J., 1987. The determination of true shear senses from the deflection of passive markers in shear zones. *J. geol. Soc. Lond.*, **144**, 73-77.

White, J.C. and White, S.H., 1983. Semi-brittle deformation within the Alpine Fault Zone, New Zealand. *J. Struct. Geol.*, **5**, 679-689.

White, S.H., 1973. Syntectonic recrystallization and texture development in quartz. *Nature*, **244**, 276-278.

White, S.H., 1975. Tectonic deformation and recrystallization of plagioclase. *Contrib. Mineral. Petrol.*, **50**, 287-304.

White, S.H., 1976. The effects of strain on microstructures, fabrics and deformation mechanisms in quartzites. *Phil. Trans. R. Soc. Lond.*, **283**, 69-86.

White, S.H., 1977. Geological significance of recovery and recrystallization processes in quartz. *Tectonophysics*, **39**, 143-170.

White, S.H., 1982. Fault rocks of the Moine Thrust Zone: a guide to their nomenclature. *Textures and Microstructures*, **5**, 33-61.

White, S.H., Burrows, S.E., Carreras, J., Shaw, N.D. and Humphreys, F.J., 1980. On mylonites in ductile shear zones. *J. Struct. Geol.*, **2**, 175-187.

Wilcox, R.E., Harding, T.P. and Seely, D.R., 1973. Basic wrench tectonics. *Bull. Am. Ass. Petrol. Geol.*, **57**, 74-96.

Williams, D.G., 1978. Rotation of contempory folds into the X-direction during overthrust processes in Laksefjord, Finmark. *Tectonophysics*, **48**, 29-40.

Wintsch, R.P. and Andrews, M.S., 1988. Deformation induced growth of sillimanite: stress minerals revised *J. Geol.*, **96**, 143-161.

Wise, D.U., Dunn, D.E., Engelder, J.T., Geiser, P.A., Hatcher, R.D., Kish, S.A., Odom, A.L. and Schamel, S., 1984. Fault related rocks: Suggestions for terminology. *Geology*, **12**, 391-394.

Woodcock, N.H., 1977. Specification of fabric shapes using an eigenvalue method. *Bull. geol. Soc. Am.*, **88**, 1231-1236.

Zeck, H.P., 1974. Cataclasites, hemiclasites, holoclasites, blastoditto and myloblastites - Cataclastic rocks. *Am. J. Sci.*, **274**, 1064-1073.

Appendix

Explanation of abbreviations used in the microstructural summary tables:

LITH. CLASSIFICATION - lithological classification

FABRIC ORN. - Fabric orientation (dip-direction/dip for planar fabrics, trend/plunge for linear fabrics

BSS - Bulk shear sense for sample (a single sample may record several movement events of different shear sense

ISS - Indicator shear sense (shear sense of individual microstructural indicator types)

R = reverse shear sense
N = normal shear sense
D = right-lateral (dextral strike-slip) shear sense
B = both normal and reverse shear sense

KCI - Kinematic Confidence Index:

0 = no kinematic interpretation possible
1 = potentially ambiguous interpretation
2 = moderately reliable interpretation
3 = trustworthy interpretation

FIG. - Figure number reference

% P.CLAST - percentage porphyroclasts

S_M - mylonite foliation
L_M - mylonite elongation lineation
L_{ds} - dip-slip elongation lineation
L_{ss} - strike-slip elongation lineation
S_s - shear surface
p.clasts - porphyroclasts
p.blasts - porphyroblasts
plag - plagioclase feldspar
fspar - feldspar
epid - epidote
2° - secondary
displ. - displacement
rot. - rotation
fract. - fractured
DPO - dimensional preferred orientation
conc. - concentration
f. grained - fine grained

TABLE 1. NEUSSPRUIT LINEAMENT - MICROSTRUCTURAL SUMMARY

SAMPLE	LITH. CLASSIFICATION	FABRIC ORN.	BSS	KCI	INDICATOR TYPE	ISS	FIG.	MATRIX GRAIN SIZE	% P.CLAST	GENERAL
Neuspoort Locality										
CJS/1	mylonitic feldspathic quartzite	S_M: 052/59 L_M: 034/56	R	2	oblique 2° Qtz grain / subgrain shape fabric.	R	9	0.3mm (long axis)	0	Coarsely recrystallized Qtz-ribbons; Significant Qtz crystal substructure: deformation bands / lamellae, undulatory extinction; Feldspars typically plastically deformed.
CJS/2	mylonitic feldspathic quartzite	S_M: 052/58 L_M: 037/56	R	2	oblique 2° Qtz grain / subgrain shape fabric.	R	9	0.3mm (long axis)	0	Coarsely recrystallized Qtz-ribbons; Significant Qtz crystal substructure: deformation bands / lamellae, undulatory extinction; Feldspars typically plastically deformed.
CJS/3	Mt amphibolite gneiss	S_M: 038/41 L_M: 038/41	0	0	weakly asymmetric Qtz-Fsp pressure shadows about Mt porphyroblasts.	B		0.1mm - 0.6mm (long axis)	10	Shear sense of pressure shadows ambiguous; Strong elongation of amphibole and Mt aggregates parallel to L_M:- Amphibole shape aspect (XZ) = 6.9 Mt shape aspect (XZ) = 2.6
Sonopeiland Locality										
CJS/4	amphibolite gneiss	S_M: 080/74 L_M: 102/68	0	0	None			0.1mm - 0.3mm	0	No p.clasts/blasts; Strong elongation of amphiboles parallel to L_M:- Amphibole shape aspect (XZ) = 4.1
CJS/5	calc-silicate gneiss	S_M: 047/70 L_M: 071/66	0	0	None			0.1mm - 0.3mm	0	No asymmetric microstructures; Compositional banding defined by calc-silicate minerals.
CJS/6	calc-silicate orthomylonite	S_M: 035/90 L_M: 220/90	N	3	σ_b-type Grt p.blasts; σ_a-type Grt p.blasts; asymmetric Fsp-Cte pressure shadows about Grt p.blasts.	N N N	10(a)	0.2mm - 0.4mm	25	Grt p.blasts are syn-kinematic; Fluxion banding defined by compositional layering of calc-silicate minerals.
CJS/7	epidotized calc-silicate gneiss	S_M: 049/78 L_M: 105/70	0	0	None			0.3mm - 0.5mm (Qtz)	0	Retrograde calc-silicate rock containing epidote, sphene, chlorite, saussuritized plagioclase and Qtz.
CJS/8	altered feldspathic augen gneiss	S_M: 052/67	N	1	σ_b-type fspar p.clasts; σ_a-type fspar p.clasts; asymmetric Chl pressure shadows about plagioclase p.clasts.	N N N	10(b)	Pervasive alteration of matrix	30	Extensive saussuritization of plagioclase; Sheaves of Chl wrap around fspar p.clasts and define the augen foliation; Mt occurs in pressure shadows about fspar augen; Discordant fractures infilled by epidote.
CJS/52	Qtz-Fsp mylonite gneiss	S_M: 059/58 L_M: 059/57	0	0	None			0.1mm - 0.3mm	0	Pervasive recovery and extensive annealing growth of neocrysts; Relict recrystallized Qtz-ribbons; Equigranular polygonal texture within variable grain size domains.

TABLE 1. (CONTINUED)

SAMPLE	LITH. CLASSIFICATION	FABRIC ORN.	BSS	KCI	INDICATOR TYPE	ISS	FIG.	MATRIX GRAIN SIZE	% P.CLAST	GENERAL
CJS/53	Qtz-Fsp mylonite gneiss	S_M: 055/66 L_M: 090/62	0	0	None			0.1mm - 0.3mm	0	Pervasive recovery and extensive annealing growth of neocrysts; Relict recrystallized Qtz-ribbons; Equigranular polygonal texture within variable grain size domains.
CJS/54	Qtz-Fsp mylonite gneiss	S_M: 052/72 L_M: 049/75	0	0	None			0.1mm - 0.3mm	0	Pervasive recovery and extensive annealing growth of neocrysts; Relict recrystallized Qtz-ribbons; Equigranular polygonal texture within variable grain size domains.
CJS/55	Qtz-Fsp mylonite gneiss	S_M: 054/66 L_M: 115/45	0	0	None			0.1mm - 0.3mm	0	Pervasive recovery and extensive annealing growth of neocrysts; Relict recrystallized Qtz-ribbons; Equigranular polygonal texture within variable grain size domains.

TABLE 2. KAKAMAS SHEAR ZONE - MICROSTRUCTURAL SUMMARY

SAMPLE	LITH. CLASSIFICATION	FABRIC ORN.	BSS	KCI	INDICATOR TYPE	ISS	FIG.	MATRIX GRAIN SIZE	% P.CLAST	GENERAL
KSZ	silicified microbreccia	Random fabrics	0	0	None			<0.1mm	70	Coherent, unfoliated rock with chaotic substructure; Clasts of mylonite and reworked cataclasite; Microfractures infilled by coarse vein Qtz or epidote; Hydrothermal alteration and pervasive silicification.
CJS/9	Qtz-Fsp mylonite gneiss	S_M: 042/50 L_{ds}: 036/39	N	1	obliquity of Qtz sub-grain shape fabric; σ-type p.clasts.	R N		0.3mm - 0.8mm (long axis)	<10	Almost no annealing but dynamic recrystallization pervasive; Significant Qtz crystal substructure.
CJS/10	Qtz-Fsp mylonite gneiss	S_M: 048/47 L_{ds}: 004/36	N	2	σ-type p.clasts.	N	13(b)	0.2mm	<10	Recovery and annealing extensive; Matrix has granoblastic polygonal texture.
CJS/11A	biotite augen gneiss	S_M: 060/42 L_{ss}: 147/04	D	2	asymmetric Qtz-fspar augen.	D		variable	10-15	Considerable extension parallel to L_{ss}; Early augen microstructures extensively recrystallized and modified by annealing overgrowths; Myrmekite occurs along megacryst margins.
CJS/11B	biotite augen gneiss	S_M: 057/38 L_{ss}: 147/04	D	2	asymmetric Qtz-fspar augen.	D		variable	10-15	Considerable extension parallel to L_{ss}; Early augen microstructures extensively recrystallized and modified by annealing overgrowths; Myrmekite occurs along megacryst margins.
CJS/12	biotite augen gneiss	S_M: 079/45 L_{ss}: 152/19	D	2	asymmetric Qtz-Fsp pressure shadows about fspar p.clasts.	D	13(a)	<0.1mm - 0.6mm	10	Considerable extension parallel to L_{ss}; Early augen microstructures extensively recrystallized and modified by annealing overgrowths; Myrmekite occurs along megacryst margins; Metastable granulite assemblages retrograding to amphibolite facies assemblages along the margins of neosome material: Crd + Grt → Sil + Bt.

TABLE 3. HUGOSPUT SHEAR SYSTEM - MICROSTUCTURAL SUMMARY

SAMPLE	LITH. CLASSIFICATION	FABRIC ORN.	BSS	KCI	INDICATOR TYPE	ISS	FIG.	MATRIX GRAIN SIZE	% P.CLAST	GENERAL
Northern Area										
CJS/58	Qtz-Fsp ribbon orthomylonite	S_M: 090/48 L_M: 093/50	N	2	σ_a-type fspar p.clasts; δ-type fspar p.clasts.	N N	15(a) 15(b) 16(a) 16(b)	0.2mm	10	Qtz-ribbon aggregates; Compositional fluxion banding; Core and mantle structures on fspar p.clasts; Mt and Chl in pressure shadow tails; Myrmekite lobes along Kfs p.clast rims.
CJS/59	Qtz-Fsp ribbon orthomylonite	S_M: 083/25 L_M: 018/16	R	1	σ_a-type fspar p.clasts; δ-type fspar p.clasts.	R R	 15(d)	0.3mm	10-20	Qtz-ribbon aggregates; Core and mantle structures on fspar p.clasts; Myrmekite lobes along Kfs p.clast rims; Significant recovery and annealing.
CJS/60	Qtz-Fsp ribbon orthomylonite	S_M: 087/38 L_M: 045/30	N	3	σ_a-type fspar p.clasts; σ_b-type fspar p.clasts; δ-type fspar p.clasts; complex σ-δ type fspar p.clasts; shear band foliation (S-C) geometry.	N N N N N	15(f) 15(e) 15(c)	0.1mm - 0.3mm	10-20	Well developed fluxion foliation; Qtz-ribbon aggregates; Fspar p.clast systems "armoured" by Qtz-ribbons; Mt and Chl concentrates along shear planes; Significant recovery and annealing.
Central Area										
CJS/18	Qtz-Fsp ultramylonite	S_M: 044/57 L_M: 041/56	N	2	σ_a-type fspar p.clasts; δ-type fspar p.clasts; overturned fspar p.clast systems; oblique Chl (001) 2°-fabric; oblique Mt DPO 2°-fabric.	N N N N N	 15(i)	<0.1mm	<10	Compositional fluxion banding; Penetrative 2° Chl (001) foliation; Concentration of Chl and Mt parallel to flow plane; Occasional Qtz-ribbon aggregates; Core and mantle structures on fspar p.clasts; P.clasts sometimes completely recrystallized to coarse-grained aggregates; Inclusion inhibition of annealing grain growth.
CJS/19	Qtz-Fsp orthomylonite	S_M: 045/40 L_M: 062/42	N	2	σ_a-type fspar p.clasts; σ_b-type fspar p.clasts; δ-type fspar p.clasts; weak S-C fabric geometries; asymmetric pressure shadow tails.	N N N N	15(g) 15(h) 15(g,h)	0.1mm - 0.3mm	30	Numerous small fspar augen; Coarsely-recrystallized Qtz-ribbon aggregrates; Pinning of Qtz-ribbon margins by opaque impurities; Mt trains parallel to flow plane, and in low strain domains in pressure shadow tails and in boudin-necks between p.clasts; Recovery and annealing advanced.

TABLE 3. (CONTINUED)

SAMPLE	LITH. CLASSIFICATION	FABRIC ORN.	BSS	KCI	INDICATOR TYPE	ISS	FIG.	MATRIX GRAIN SIZE	% P.CLAST	GENERAL
CJS/20	Qtz-Fsp ultramylonite	S_M: 030/54 L_M: 067/46	N R	1 2	σ_a-type fspar p.clasts; σ_b-type fspar p.clasts; δ-type fspar p.clasts; tailess θ-type fspar p.clasts; oblique Chl (001) 2°-fabric; antithetic stacking opaque minerals.	R R R R N N	15(k) 15(j)	<0.1mm	<10	Compositional fluxion banding; Coarsely-recrystallized Qtz-ribbon aggregates (0.3mm - 0.4mm); Qtz-ribbons usually severely attenuated; Core-mantle structures in fspar p.clasts; Fspar p.clasts "armoured" by enveloping Qtz-ribbons; Mt trains parallel to flow plane; σ-type systems have flat geometries; Penetrative 2° Chl (001) foliation; Inclusion-inhibition of matrix grain-growth.
CJS/21	Qtz-Fsp ultramylonite	S_M: 068/67 L_M: 053/65	R	2	σ_a-type fspar p.clasts; σ_b-type fspar p.clasts; δ-type fspar p.clasts; complex σ-δ type fspar p.clasts.	R R R R	 15(l)	<0.1mm	10-20	Ultramylonite compositional fluxion banding; Highly attenuated, coarsely recrystallized Qtz-ribbon aggregates; Bent twin-lamellae within fspar p.clasts; Trains of mica and opaques parallel to flow plane; P.clast systems are weakly asymmetric (flat-geometries); P.clasts "armoured" by enveloping Qtz-ribbons.
CJS/22	Qtz-Fsp ultramylonite	S_M: 020/47 L_M: 027/46	R	1	σ_b-type fspar p.clasts; weak shear band foliation.	R R		<0.1mm (QF-domains)	<10	Complete annealing texture within recrystallized quartz-lenses; Average grain size within Qtz-lenses is 0.1mm - 0.2mm; QF-domains are very finely recrystallized; Intense grain-refinement defines C′-surfaces; Extremely weak shear bands occur antithetic to C′-surfaces.
CJS/23	Qtz-Fsp orthomylonite	S_M: 023/67 L_M: 055/64	N	3	σ_a-type fspar p.clasts; σ_b-type fspar p.clasts; δ-type fspar p.clasts; weak S-C fabric relationships.	N N N N		0.1mm - 0.3mm	20-30	σ_b-Type fspar p.clasts common; Core and mantle structures with fspar p.clasts; Coarsely-recrystallized Qtz-ribbons (0.2mm - 0.4mm) elongated parallel to flow plane; Qtz-ribbon aggregates envelop and "armour" fspar p.clasts; Bt trains parallel to flow plane.

TABLE 3. (CONTINUED)

SAMPLE	LITH. CLASSIFICATION	FABRIC ORN.	BSS	KCI	INDICATOR TYPE	ISS	FIG.	MATRIX GRAIN SIZE	% P.CLAST	GENERAL
CJS/24	Crd-Kfs-Qtz protomylonite (± Sil ± Bt ± Mt)	S_M: 051/68 L_M: 051/68	R	1	σ-type Crd p.clasts.	R		variable	>60	Protomylonite foliation defined by fractured Kfs-Crd domains interspersed with lenses of ductiley deformed quartz; Microshears defined by fibrolitic sillimanite (± biotite) disrupt Kfs-Crd domains; Grain-scale tension fractures infilled by Mt occur within Crd-Kfs domains, at 90° to the protomylonitic microshears; Microshears anastomose around Crd p.clasts; Crd p.clasts rimmed by fibrolite, and have fibrolitic/biotite tails; Pinitization along healed microfractures in Crd p.clasts; Inclusion trails of prismatic sillimanite within Crd p.clasts; Conjugate sets of deformed twins within Crd p.clasts.
CJS/25	Qtz ultramylonite	S_M: 055/65 L_M: 068/64	N	2	oblique Bt (001) 2°-fabric.	N		0.1mm - 0.3mm	0	Mylonite foliation defined by trains of biotite; Matrix has equigranular polygonal texture typical of pervasive recovery and annealing.
CJS/61	calc-silicate gneiss	S_M: 012/37 L_M: 011/36	0	0	None			0.3mm - 1.2mm	0	Altered relicts of early tectonite fabric occur as scattered "islands" within completely annealed, polygonized aggregate; 120° triple junctions of grain boundaries; Extensive static recrystallization and grain growth.
Southern Area										
CJS/26	Qtz-Fsp ortho/ultramylonite	S_M: 030/70 L_M: 100/45	N	3	σ-type fspar p.clasts; δ-type fspar p.clasts; oblique Bt (001) 2°-fabric; oblique Mt DPO 2°-fabric; tailess θ-type fspar p.clasts.	N N N N N	 15(m) 16(c,d) 15(o) 15(p) 16(e)	<0.1mm	10-20	Penetrative oblique 2° foliation defined by Bt and opaques; Fspar p.clasts exhibit deformation twins (twin planes frequently bent); Qtz-ribbons occur infrequently; σ-, δ-, and tailess θ-type p.clast systems dominate; Deflection of mica preferred orientation around p.clast systems; Many p.clasts are extremely elongate (shape aspects >5:1); Elongate p.clasts generally aligned with long-axes parallel to flow plane, but some occur as δ- and θ-type "rolling structures"; Clast-matrix interfaces generally sharp.

TABLE 3. (CONTINUED)

SAMPLE	LITH. CLASSIFICATION	FABRIC ORN.	BSS	KCI	INDICATOR TYPE	ISS	FIG.	MATRIX GRAIN SIZE	% P.CLAST	GENERAL
CJS/27	Qtz-Fsp orthomylonite	S_M: 084/30 L_M: 058/28	R	3	stair-stepping σ-type p.clasts; σ_a-type fspar p.clasts; σ_b-type fspar p.clasts; rare δ-type fspar p.clasts; S-C fabric geometry; rotation of fract. fspar grains.	R R R R R R	 15(r) 15(q) 16(f)	<0.1mm - 0.4mm	30-40	Well-developed porphyroclastic mylonite fluxion foliation; Completely annealed Qtz-ribbon aggregates wrap-around σ_b-type p.clast systems in weak S-C fabric configurations; Well-developed core and mantle structures exhibited by fspar p.clasts; Extensive recrystallization of feldspathic domains; Brittle fractures in fspar p.clasts infilled by Mt; Trains of Mt grains parallel to flow plane.
CJS/28	annealed Qtz ultramylonite	S_M: 133/34 L_M: 097/28 S_M: 057/48 L_M: 073/46	0	0	None			<0.1mm - 0.2mm	0	No asymmetric microstructures; Ultramylonite composed of composite equigranular, foliation-parallel Qtz-ribbons separated by linear trains of opaque impurities; Qtz exhibits equigranular polygonal textures, consistent with pervasive static recrystallization.

TABLE 4. ROZYNENBOSCH-GANZENMOND SHEAR ZONE - MICROSTRUCTURAL SUMMARY

SAMPLE	LITH. CLASSIFICATION	FABRIC ORN.	BSS	KCI	INDICATOR TYPE	ISS	FIG.	MATRIX GRAIN SIZE	% P.CLAST	GENERAL
CJS/13	Qtz-fspar protomylonite	S_M: 010/29 L_M: 014/30	R	2	S-C shear band fabrics; σ_b-type fspar p.clasts; rot. of fract. fspar grains.	R R R	22(a),23(e) 22(a)	variable	≈50	Concentration of Chl (after Bt) and fine-grained Mt along shear band surfaces; Intense mechanical twinning in Kfs aggregates; Microfractures in Kfs aggregates/grains infilled by Mt; Ribbon-like Qtz aggregates.
CJS/14	Qtz-fspar protomylonite	S_M: 039/39 L_M: ?	R	2	brittle C' shear band fabrics;	R		variable	60-70	Chl concentrated along shear band surfaces; Elongate aggregates of Kfs with microfractures normal to elongation direction (infilled by Mt); Mechanical twinning in Kfs; Ribbon-like Qtz aggregates with advanced crystal substructure.
CJS/15	Qtz-fspar S-C orthomylonite	S_M: 011/55 L_M: 326/44	R	3	S-C fabric geometry; σ_b-type fspar p.clasts; oblique 2° Qtz subgrain fabrics; fine-grained white mica fish; displ. of fract. fspar grains.	R R R R R	22(b) 23(a,b,d) 22(b) 23(a,b,d)	<0.1mm	50-60	Conc. of f.grained Chl, white mica and Mt along shear plane surfaces; Ribbon-like Qtz aggregates with advanced crystal substructure; Mechanical twinning in Kfs (twin planes frequently bent); Microstructures in Kfs p.clasts frequently infilled by Mt.
CJS/16	Qtz-fspar S-C proto/orthomylonite	S_M: 320/66 L_M: 353/64	R	3	S-C fabric geometry; C'-type brittle shear band foliation; σ_b-type fspar p.clasts; intense 2°Qtz subgrain fabrics; Displ. of fract. fspar grains.	R R R R R	22(d),23(j) 22(e) 22(d) 23(i,j) 22(e)	<0.1mm	50-60	Highly recrystallized Qtz-ribbons; Intense quartz crystal-substructure; Fspar p.clasts intensely fractured with fractures often infilled by antitaxial Qtz fibres; Bent twin planes in plag. p.clasts; Intense mechanical twinning in Kfs p.clasts; F.grained white mica and recrystallized fspar conc. along shear plane surfaces.
CJS/17	Qtz-fspar S-C orthomylonite	S_M: 008/72 L_M: 340/68	R	3	S-C fabric geometry; σ_b-type fspar p.clasts; 2° Qtz subgrain fabrics.	R R R	22(f),26(c) 22(f),26(c)	<0.1mm	40-50	Highly recrystallized Qtz-rich matrix with little annealing; Bent and fractured mechanically twinned fspar p.clasts; Conc. of Chl and f.grained white mica along shear plane surfaces; Chl-growth in pressure shadow domains adjacent to fspar p.clasts.

TABLE 4. (CONTINUED)

SAMPLE	LITH. CLASSIFICATION	FABRIC ORN.	BSS	KCI	INDICATOR TYPE	ISS	FIG.	MATRIX GRAIN SIZE	% P.CLAST	GENERAL
CJS/29	Qtz-Pl-Hbl-Diop-Sph calc-silicate gneiss	S_M: 033/45 L_M: 050/43	R	1	weak 2° Qtz subgrain fabrics.	R		0.4mm - 1.0mm	0	Elongate Qtz-ribbons with well developed crystal substructure; Elongate fspar aggregates, frequently microfractured at a high angle to S_M; Cross-cutting calcite-infilled fractures.
CJS/30	Qtz-fspar protomylonite	S_M: 032/62 L_M: 011/60	R	2	brittle C'-type shear band foliation; very weak S-C fabric geometry; weakly developed σ_b-type fspar p.clasts; 2° Qtz subgrain fabrics; displ. of fract. fspar grains; Chl (after Bt) mica fish.	R R R R R	23(g) 23(g) 23(g) 22(i) 23(g)	<0.1mm	variable (≈50)	Conc. of Chl (after Bt) and finely-recrystallized altered fspar along shear plane surfaces; Elongate fspar-rich domains exhibiting intense crushing; Fspars exhibit kink bands, bent twin planes, deformation bands, healed fractures, extension cracks, and undulatory extinction.
CJS/57	Qtz-fspar proto/orthomylonite	S_M: 056/47 L_M: 031/45	R	3	weak S-C fabric geometry; σ_b-type fspar p.clasts; mica fish; displ. of fract. fspar grains; 2° Qtz subgrain/grain fabrics.	R R R R R	22(h) 22(h) 22(h)	<0.4mm	40-50	Matrix comprises elongate ribbon Qtz with significant crystal substructure (v. little recovery and no annealing); Occasional white mica fish in assoc. with σ_b-type fspar p.clasts; Conc. of finely recrystallized, highly altered fspar, white mica and Chl along shear plane surfaces.
RHK/600	quartzo-feldspathic gneiss		R	1	limited 2° Qtz subgrain fabrics.	R		variable	0	Minor mylonitic foliation developed; Grain size reduction accompanying dynamic recrystallization; Little recovery or annealing; Mortar textures developed.
RHK/601	Qtz-fspar-Bt protomylonite		R	2	weak S-C fabric relationships; σ_b-type fspar p.clasts; asymmetric retort-shaped feldspar augen; asymmetric p.shadows about Mt grains; Bt mica fish.	R R R R		variable	≈60	Fspar p.clasts commonly rimmed by fine-grained neocrysts; S-surfaces defined by subparallel alignment of Qtz-grains, and biotite (001) preferred orientation; C'-surfaces defined by concentrations of dynamically recrystallized fspar and trains of biotite.

×

TABLE 4. (CONTINUED)

SAMPLE	LITH. CLASSIFICATION	FABRIC ORN.	BSS	KCI	INDICATOR TYPE	ISS	FIG.	MATRIX GRAIN SIZE	% P.CLAST	GENERAL
RHK/602	protomylonitic Qtz-fspar-Bt augen gneiss		R	2	weak S-C fabric relationships; σ_b-type fspar p.clasts; asymmetric Bt pressure shadows about fspar augen; limited 2° Qtz subgrain fabrics.	R R R R	22(g),23(f) 22(g),23(f) 22(g),23(f)	0.3mm (variable)	≈30	S and C surfaces, and the augen foliation defined by trains of Bt-flakes with weak stair-stepping geometry; Feldspar augen exhibit myrmekitic intergrowths.
RHK/603	Qtz-fspar microbreccia		0	0	None					Coherent rock with choatic substructure arising from brittle reworking of Qtz-fspar orthomylonite; Larger clasts of mylonite tend to fracture and shatter parallel to their elongation direction; Rotation of fragments and extension microfracturing normal to their length, indicate cataclastic flow within the breccia matrix; Microfractures infilled by Ep, Chl, and Cte.
RHK/465	Qtz-fspar orthomylonite		R	3	σ_a-type fspar p.clasts; σ_b-type fspar p.clasts; 2° Qtz subgrain fabrics; displ. of fract. fspar grains.	R R R R	23(h)	fspar: <0.1mm Qtz: 0.1mm - 0.2mm	30-40	Qtz-ribbons comprising equigranular polygonal neocrysts alternate with highly-altered fspar-rich compositional layers; Conc. of Chl, recrystallized altered fspar and fine-grained opaques along shear plane surfaces; Fspar p.clasts have well developed mantles of fine-grained neocrysts.

WITVLEI SHEAR ZONE - MICROSTRUCTURAL SUMMARY

TABLE 4. (CONTINUED)

SAMPLE	LITH. CLASSIFICATION	FABRIC ORN.	BSS	KCI	INDICATOR TYPE	ISS	FIG.	MATRIX GRAIN SIZE	% P.CLAST	GENERAL
CJS/56	Qtz-epidote ultramylonite	S_M: 033/39 L_M: 356/32	R	2	2° Qtz grain shape/subgrain fabrics; 2° epidote grain shape fabric.	R R	22(k),23(k) 22(k),23(k)	0.1mm - 0.4mm	0	Principal S_M foliation defined by compositional variations in the amount of interstitial Ep, and by conc. of extremely fine-grained Ep parallel to the flow plane; Qtz exhibits significant crystal substructure including subgrains, deformation bands, deformation lamellae and strong undulatory extinction.

TABLE 5. GRAAFWATER SHEAR SYSTEM - MICROSTRUCTURAL SUMMARY

SAMPLE	LITH. CLASSIFICATION	FABRIC ORN.	BSS	KCI	INDICATOR TYPE	ISS	FIG.	MATRIX GRAIN SIZE	% P.CLAST	GENERAL
CJS/31	quartzo-feldspathic gneiss	S_M: 052/39 L_M: 074/35	O	O	None			0.1mm - 1.5mm (variable)	0	Crude DPO of Qtz and fspar defines gneissic foliation; Recrystallization is poorly advanced.
CJS/32	amphibolite gneiss	S_M: 019/36 L_M: 025/35	N	2	shear band foliation; σ-type plagioclase p.clasts.	N N		variable	<10	Asymmetrical microstructures more evident in hand specimen than in thin section; Shear band surfaces are spaced at 5-10mm intervals.
CJS/33	Qtz-fspar protomylonite	S_M: 350/52 L_M: 006/51	R	3	sense of rotation of ductile bend folds; S-C fabric geometry; microstructural imbricate zones; σ_b-type p.clasts.	R R R R	27(b)	undeveloped	N/A	Micro-thrust surfaces with deformed footwall containing isolated synclinal ductile bend folds; Ductile shear surfaces show evidence of brittle reactivation.
CJS/34	Qtz-fspar orthomylonite	S_M: 328/42 L_M: 017/30	R	3	S-C-C' composite fabrics; oblique 2° Qtz subgrain fabrics; σ_a-type fspar p.clasts; σ_b-type fspar p.clasts; displ. of fract. fspar grains; δ-type fspar p.clast systems; vergence of asymmetrical microfolds; rare Bt/Chl mica fish.	R R R R R R R R	27(a) 28(c,d,g,i,l) 28(k,l) 28(c,d,g,j,l) 28(i) 28(i) 28(c,d,e,g) 28(c,d) 28(j,k)	<0.1mm	30-40	C-surfaces defined by fine-grained altered fspar, Bt/Chl intergrowths, and trains of opaque mineral grains; S-shear plane anastomose sigmoidally about σ-type p.clasts, and isolate lozenge-shaped domains of recrystallized quartz which display strong secondary grain-shape fabrics; Feldspar p.clasts are commonly fractured, and internal microfaults of all types are present; Asymmetrically microfolded Qtz-ribbons, often displaying attenuated short-limbs, are common along principal cissaillement surfaces.
CJS/35	interlaced Qtz-fspar cataclasite and protomylonite with ultramylonitic bands	S_M: 109/33 L_M: 083/34	R	2	localized S-C fabric geometry; oblique 2° Qtz subgrain fabrics; displ. of fract. fspar grains; localized C'-shear bands; occasional σ_b-type fspar p.clasts.	R R R R R		highly variable	highly variable	Range from brittle to ductile fault rock products within a single thin section; Feldspathic domains exhibit textures consistent with comminution by crushing and fragmentation (cataclasis), while grain-refinement in quartz-rich domains has occurred through recrystallization and neomineralization; Where overprinting criteria are present, the sequence of development is ultramylonite → cataclasite; Two generations of transposed shear band foliations are present.

TABLE 5. (CONTINUED)

SAMPLE	LITH. CLASSIFICATION	FABRIC ORN.	BSS	KCI	INDICATOR TYPE	ISS	FIG.	MATRIX GRAIN SIZE	% P.CLAST	GENERAL
CJS/36	silicified Qtz-fspar microbreccia	S_M: 107/43 L_M: 034/22	O	O	None			≪0.1mm	20-30	Chaotic and unfoliated internal structure; Clasts are generally angular to subangular in shape and range in size from 0.1mm to 1mm; Pervasive alteration of extremely fine-grained matrix; Secondary minerals include epidote, clinozoisite and chlorite; Cross cutting veins of epidote-group minerals.
CJS/38	biotite augen gneiss	S_M: 118/51	O	O	None			variable	variable	Poikiloblastic garnets and myrmekitic intergrowths are characteristic; Augen foliation defined by fspar compostional layering and Qtz-ribbons; Linear fabric (evident in thin section) defined by feldspar rods, indicates that elongation was strike parallel.
CJS/39	Mt-bearing calc-silicate gneiss	S_M: 104/31 L_M: 055/21	O	O	None			0.3mm - 0.7mm	<10	Calc-silicate gneiss with idiomorphic Mt-porphyroblasts exhibiting symmetrical plagioclase pressure shadows; "Matrix" is granoblastic, and the gneissic foliation is defined by a biotite DPO.
CJS/40	saussuritized calc-silicate ultramylonite	S_M: 023/28 L_M: 049/25	R N	3 1	σ_a-type plag/epidote p.clasts; σ_b-type plag/epidote p.clasts; δ-type plag/epidote p.clasts; vergence of asymmetrical microfolds; S-C fabric geometry; 2° Qtz grain-shape fabrics.	R R R R R N	27(e) 28(m,n) 27(c,d) 28(m,n) 28(n)	0.1mm	<10	Plag. p.clasts generally well rounded, and often partially or wholly pseudomorphed by epidote/chlorite; Asymmetrical microfolds occur in recrystallized plag/epidote layers, and commonly display disrupted short limbs.
CJS/41	Qtz-fspar protomylonite	S_M: 335/60 L_M: 038/40	R N	2 2	conjugate shear bands; secondary shear band foliation; 2° Qtz grain-shape fabrics; displ. & rot. of fract. fspar clasts; σ-type fspar p.clasts.	B R B B B		<0.1mm	45-55	Qtz highly recrystallized into a polycrystalline, highly-strained matrix; Differential movement along multiple (conjugate) shear band surfaces has resulted in isolation of rhombic domains of opposing shear sense; Use of rotated and displaced clast fragments as shear sense indicators is complicated by interference from neighbouring clasts (due to high clast density).

TABLE 5. (CONTINUED)

SAMPLE	LITH. CLASSIFICATION	FABRIC ORN.	BSS	KCI	INDICATOR TYPE	ISS	FIG.	MATRIX GRAIN SIZE	% P.CLAST	GENERAL
CJS/42	protomylonite biotite augen gneiss (L>S tectonite)	S_s: 148/82 L_{ss}: 059/14	D	2	weak S-C fabric geometry; 2° Qtz subgrain shape fabrics.	D D	25	>0.3mm (variable)	0	Considerable elongation parallel to L_{ss} (subparallel to strike); L_{ss} defined by flattened rods of feldspar, elongate Qtz-ribbons and a biotite DPO; In sections normal to L_{ss} (YZ), trains of biotite anastomose around ellipsoidal sections through flattened feldspar rods (whose axes of flattening define S_s); In XZ-sections, retort shaped Qtz-lenses enclosed by biotite trains, and exhibiting oblique secondary subgrain fabrics, define the S-surfaces which are sigmoidally deflected into C-surfaces (defined by narrow zones of recrystallization, grain refinement, and biotite enrichment).
CJS/43	Qtz-fspar protomylonite	S_M: 333/77 L_M: 059/17	R	2	intense Qtz subgrain shape fabrics; incipient S-C fabric; very weak σ_b-type fspar p.clasts.	 R R R		variable	N/A	Qtz matrix composes highly strained and recrystallized polycrystalline ribbons with ragged margins; Larger monocrystalline Qtz-ribbons exhibit undulatory extinction and deformation bands; These Qtz-ribbons attain aspect ratios in excess of 20:1; Feldspar p.clast development is limited; Isolated, incipent C-surfaces defined by chlorite enrichment (after biotite).
CJS/44	orthomylonitic amphibolite	S_M: 011/31 L_M: 033/29	R	1	2° amphibole grain-shape fabric.	 R		0.3mm long axis	0	Strongly foliated and highly recrystallized amphibole rock; Plagioclase highly altered; Average hornblende shape aspect = 4.32.
CJS/45	protomylonitic Qtz-fspar augen gneiss	S_M: 079/27 L_M: 057/25	R	1	sigmoidal deflection of Qtz subgrain fabrics into discrete shear surfaces; weak S-C fabric geometry.	 R B		highly variable	0	Strain localized in Qtz/Bt rich microlithons - resulting microstucture is one of anastomosing shear surfaces enclosing fractured fspar grains; Biotite grains are bent and kinked; Deformation induced myrmekitization is widespread.
CJS/46	Qtz-fspar S-C proto/orthomylonite	S_M: 343/71 L_M: 048/48	R	3	S-C fabric; σ_b-type pspar p.clasts; 2° Qtz grain/subgrain shape fabrics; displ. of fract. fspar grains.	R R R R	27(f,g) 27(f,g)	0.1mm - 0.3mm	50-60	Qtz is extensively recrystallized into ragged ribbons with well developed substructure; C-surfaces defined by zones of intensely recrystallized Qtz and fspar; S-surfaces defined by retort-shaped lenses of polycrystalline Qtz and the elongation direction of σ_b-type p.clasts.

TABLE 5. (CONTINUED)

SAMPLE	LITH. CLASSIFICATION	FABRIC ORN.	BSS	KCI	INDICATOR TYPE	ISS	FIG.	MATRIX GRAIN SIZE	% P.CLAST	GENERAL
CJS/47	Qtz-fspar S-C orthomylonite	S_M: 005/61 L_M: 036/58	R	3	S-C-C' composite planar fabrics; σ_a-type fspar p.clasts; σ_b-type fspar p.clasts; δ-type fspar p.clasts; vergence of asymmetrical microfolds; 2° Qtz grain/subgrain shape fabrics.	 R R R R R R	 27(h,i,q) 27(h,i) 27(h,i) 28(o) 27(i)	<0.1mm - 0.2mm	40	C-surfaces comprise zones of intense recrystallization and grain refinement, defined by highly altered, microcrystalline intergrowths of fspar, Qtz, micas and opaques; Weak C'shear band fabric development; S-surfaces defined by retort-shaped lenses of polycrystalline Qtz, and the elongation direction of σ_b-type p.clasts; Asymmetrical microfolds are developed in polycrystalline Qtz-ribbons within the flow plane.
CJS/48	Qtz-fspar S-C orthomylonite	S_M: 006/61 L_M: 035/52	R	3	S-C fabric; C'-type shear band foliation; σ_a-type fspar p.clasts; σ_b-type fspar p.clasts; rare δ-type fspar p.clasts; vergence of asymmetrical microfolds; 2° Qtz grain/subgrain shape fabrics; displ. of fract. fspar clasts.	R R R R R R R R	27(j,k),28(f) 27(j,k),28(f) 27(j,k)	<0.1mm - 0.2mm	35-45	C-surfaces comprise zones of intense recrystallization and grain refinement, defined by highly altered, microcrystalline intergrowths of fspar, Qtz, micas, epidote group minerals, and opaques; S-surfaces defined by retort-shaped lenses of polycrystalline Qtz, and the elongation direction of σ_b-type p.clasts; Secondary C' shear band surfaces disrupt and deflect S- and C-surfaces; Asymmetrical microfolds are developed in polycrystalline Qtz-ribbons within the flow plane; Plag. p.clasts frequently partially or wholly saussuritized.
CJS/49	orthomylonitic amphibolite	S_M: 003/77 L_M: 077/52	R	3	weak shear band foliation geometry; crude σ-type Hbl p.clasts; rare σ-type plag./epid. p.clasts; 2° Qtz grain/subgrain shape fabrics; asymmetrical boudinage of Hbl grains.	 R R R R R	 27(l) 27(l) 27(l)	<0.1mm - 0.3mm	15-20	Shear band surfaces defined by DPO of fine-grained Chl, sericite, Qtz, and epid./zoisite; A minimum of two sets of shear band foliation are superimposed, with characteristic sigmoidal deflection of earlier foliation sets; Quartz matrix has recrystallized into polycrystalline lenticular ribbons with well-developed crystal substructure; Plag. p.clasts extensively saussuritized; Chl occurs in pressure shadow domains adjacent to Hbl p.clasts, and in asymmetrical boudin-necks.

TABLE 5. (CONTINUED)

SAMPLE	LITH. CLASSIFICATION	FABRIC ORN.	BSS	KCI	INDICATOR TYPE	ISS	FIG.	MATRIX GRAIN SIZE	% P.CLAST	GENERAL
CJS/50	Qtz-fspar S-C orthomylonite with ultramylonite bands	S_M: 152/47 L_M: 114/40	R	3	S-C-C′ composite shear band fabrics; σ_a-type fspar p.clasts; σ_b-type fspar p.clasts; vergence of asymmetrical microfolds; 2° Qtz grain/subgrain shape fabrics; displ. of fract. fspar clasts.	R R R R R R	 27(m) 27(m,p) 	0.1mm (o.myl) $\leqslant$0.1mm (u.myl)	30 (o.myl) <10 (u.myl)	Alternating orthomylonite and ultramylonite bands exhibiting intense Qtz-subgrain fabrics, refolded into highly asymmetrical recumbent overfolds ("micro-nappes"); Cataclastic crush-zones occur within monomineralic feldspathic layers.
CJS/51	Qtz-fspar S-C orthomylonite	S_M: 154/80 L_M: 076/51	R	3	S-C-C′ composite shear band fabrics; σ_a-type fspar p.clasts; σ_b-type fspar p.clasts; δ-type fspar p.clasts; 2° Qtz grain/subgrain shape fabrics; displ. of fract. fspar clasts; vergence of asymmetrical microfolds; asymm. boudinage fspar bands.	R R R R R R R R	27(n,o) 28(a,b,h) 27(n,o) 28(a,b,p) 27(n,o) 28(a,b,h) 27(o) 28(a,b,h) 27(n) 28(b,h) 	$\leqslant$0.1mm	40	Extremely well developed S-C-C′ composite fabrics; Extreme grain-size dimunition and substructure development within Qtz-rich matrix; Asymmetrical microfolding of polycrystalline Qtz-ribbons; Shear band fabrics defined by dark trains of microcrystalline altered feldspar, secondary micas and quartz; Asymmetrical boudinage observed within feldspathic bands; Myrmekite developed on sides of p.clasts facing the inferred incremental shortening direction.